Neuroprotection in Neurodegenerative Disease: From Basic Science to Clinical Applications

Guest Editors: Marta C. Monteiro, Michael D. Coleman, Eric J. Hill, Rui D. Prediger, and Cristiane S. F. Maia

Neuroprotection in Neurodegenerative Disease: From Basic Science to Clinical Applications

Neuroprotection in Neurodegenerative Disease: From Basic Science to Clinical Applications

Guest Editors: Marta C. Monteiro, Michael D. Coleman, Eric J. Hill, Rui D. Prediger, and Cristiane S. F. Maia

Editorial Board

Contents

Editorial
Neuroprotection in Neurodegenerative Disease: From Basic Science to Clinical Applications

Marta C. Monteiro,[1] Michael D. Coleman,[2] Eric J. Hill,[2] Rui D. Prediger,[3] and Cristiane S. F. Maia[1]

[1]*Faculty of Pharmacy, Center of Health Sciences, Universidade Federal do Pará (UFPA), Belém, PA, Brazil*
[2]*Mechanisms of Drug Toxicity Group, School of Life and Health Sciences, Aston University, Aston Triangle, Birmingham B4 7ET, UK*
[3]*Department of Pharmacology, Center of Biological Sciences, Universidade Federal de Santa Catarina (UFSC), Florianópolis, SC, Brazil*

Correspondence should be addressed to Marta C. Monteiro; martachagas2@yahoo.com.br

The limitations of current pharmacological treatments of neurodegenerative disease have led to the extensive investigation of novel compounds and nonpharmacological approaches to modify the course of these conditions, whilst reducing drug side effects. The definition of neuroprotection is complex and involves both preventing cell death and restoring function to damaged neurons, as well as restoring neuronal numbers. The development of drugs to slow or prevent the progression of neurodegenerative diseases might logically evolve from an improved understanding of the etiology and pathogenesis of these diseases. There have certainly been major advances in these areas over the past few years and the prospect for the introduction of "neuroprotective" therapies is much improved over previous years.

In this context, there is growing recognition that neuroinflammatory mechanisms might contribute to the cascade of events leading to neuronal degeneration observed in Alzheimer's disease (AD), Parkinson's disease (PD), stroke, and many other neurodegenerative diseases. Postmortem studies and experimental models have revealed an increase in activated glial cells and in concentrations of certain cytokines and interleukins in brain areas such as the hippocampus, cerebral cortex, substantia nigra, and striatum, which are all affected in neurodegenerative diseases. Therefore, the study of the role of neuroinflammatory mechanisms in the pathophysiology of neurodegenerative diseases and the potential of anti-inflammatory strategies for neuroprotection has also attracted the interest of many authors.

Lima and colleagues explored the patterns of microglial activation, astrocytosis, oligodendrocyte damage, myelin impairment, and Nogo-A immunoreactivity between 3 and 30 days after experimental striatal stroke in adult rats induced by microinjections of endothelin-1 (ET-1). They established the temporal evolution of these neuropathological events, which will be very relevant to future studies of neuroprotective drugs targeting neuroinflammation and white matter damage.

In the study by N. Lins et al., the authors investigated behavioral impairments and neuroinflammatory markers following the interaction between an intranasal arbovirus infection and the intrahippocampal injection of ME7 prion strain in C57BL/6. They observed that virus infection exacerbates the microglial inflammatory response to a greater degree in prion-infected mice, but this response was not correlated with hippocampal-dependent behavioral deficits.

Besides its regulatory effects in the light-dark cycle, melatonin is a hormone with neuroprotective, anti-inflammatory, and antioxidant properties. J. M. Mack and colleagues reviewed the literature about the potential role of the melatoninergic system in the pathogenesis and treatment of PD. The data available so far indicates that PD is associated with impaired brain expression of melatonin and its receptors MT1 and MT2. Exogenous melatonin treatment presented an outstanding neuroprotective effect in animal models of PD induced by different toxins. Melatonin might also potentially improve nonmotor symptoms commonly experienced by PD

patients such as sleep and anxiety disorders, depression, and memory dysfunction.

Another important hormone is 17β-estradiol (E2), which, in addition to its multiple actions throughout the body and brain, exerts neuroprotective effects in both acute and chronic neurodegenerative diseases such as cerebral ischemia, traumatic brain injury, AD, and PD. R. Thakkar and colleagues investigated whether 17β-estradiol (E2), acting via the estrogen receptor coregulator PELP1, can exert anti-inflammatory effects in the ovariectomized rat and mouse hippocampus to regulate NLRP3 inflammasome activation after global cerebral ischemia (GCI). The authors showed that rats subjected to GCI had significantly higher NLRP3 inflammasome activation in the hippocampus compared to the sham animals that did not undergo ischemia. In addition, E2 treatment suppresses both expression and activation of the NLRP3 inflammasome at both days 1 and 3 after injury. PELP1 together with upstream inducers of NLRP3 inflammasome activation (P2X7 and TXNIP) was essential for the anti-inflammatory effect of E2 to regulate the NLRP3 inflammasome after GCI. These findings showed a new insight into the anti-inflammatory effect of E2 in the brain, suggesting that the NLRP3 inflammasome is a potential therapeutic target and E2 analogues or NLRP3 inflammasome selective inhibitors may have efficacy in the treatment of some neurodegenerative disorders, such as GCI.

Calcium is a second messenger and plays an important role in regulating a great variety of neuronal functions, such as release of neurotransmitters, synaptic plasticity, neuronal excitation, and gene transcription. Indeed, changes of intracellular free Ca^{2+} concentration ($[Ca2+]i$) may directly alter neuronal excitability. X. Liu and colleagues explored Ca^{2+} status as part of their investigation into the cardiovascular effects of H2S, which were due to decreased oxidative stress, via inhibition of NADPH oxidase activity in the rostral ventrolateral medulla (RVLM) of spontaneously hypertensive rats (SHR). The molecular mechanisms involved in this neuromodulator effect of H2S are not clear, although the effects, both exogenous and endogenous, of H2S in primarily cultured medullary neurons elevate $[Ca2+]_i$ levels, mainly by increasing the calcium influx and mobilizing intracellular Ca^{2+} stores from ER from primarily cultured rat medullary neurons.

In HIV-associated neurocognitive disorders (HAND), the HIV-1 transactivator protein (Tat) activated from HIV-1-infected cells and cell membranes may lead to disruption of tight junctions (TJs) associated with astrocytes along the blood-brain barrier (BBB), which increase the permeability of this barrier and can lead to HAND. Y. Chen and colleagues investigated the relationship between occludin and amyloid-beta ($A\beta$) transfer receptors in human cerebral microvascular endothelial cells (hCMEC/D3) in the context of HIV-1-related pathology. The authors showed that HIV-1 Tat and the Rho inhibitor hydroxyfasudil (HF) had no significant effect on hCMEC/D3 cell viability. However, the HF significantly inhibited HIV-1 Tat-induced occludin dysfunction and regulated LRP1 and RAGE expression in hCMEC/D3 cells. Thereby, they suggested a potential protective role for HF in HIV-1 Tat-mediated BBB destruction and $A\beta$ accumulation,

revealing a new therapeutic strategy for reducing the $A\beta$ burden in HAND.

Natural products have emerged as a source for potential agents, which might ameliorate CNS neurodegeneration. Whilst the antioxidant properties of the bee-derived plant resin propolis have been extensively reported, its effects on the behavioral/cognitive functions have been poorly described. C. C. S. D. M. Da Silveira et al. examined the neurobehavioral effects of yellow propolis, related to anxiety, depression, and spontaneous locomotor activity in rats. The authors also investigated mnemonic activity as well as antioxidant properties of the extract, since both behavioral and cognitive disorders may manifest themselves in the course of the neurodegenerative diseases as symptoms or comorbidities. The authors concluded that yellow propolis elicits antioxidant activity associated with anxiolytic, antidepressant, and cognitive enhancer properties. Therefore, yellow propolis shows some promise product from natural sources in the therapy of the central nervous system disorders, as neurodegenerative diseases.

It is well documented that oxidative stress plays a pivotal role in neurodegenerative diseases pathology, particularly with AD. Another feature related to AD is the occurrence of dementia, in which the cholinergic neuronal enzymatic activity [i.e., acetylcholinesterase (AChE) and butyrylcholinesterase (BuChE)] is involved in the optimal impulse transmission at cholinergic synapses. The AChE/BuChE upregulation promotes excessive degradation of the neurotransmitter acetylcholine in the synaptic terminals, which leads to cognitive dysfunctions. In fact, the treatment of AD symptoms related to cognitive decline is based on anticholinesterase activity modulation. D. Załuski and R. Kuźniewski investigated the biological activity of the 12 extracts of *Eleutherococcus* species related to both neurodegenerative mechanisms (i.e., oxidative stress and increased cholinesterase activity). Their results indicated that bioactive compounds from *Eleutherococcus* species are a promising source for the protection or treatment of neurodegenerative diseases, since the extracts were able to inhibit both AChE and BuChE avoiding feedback loop, allied to the antioxidant activity that in turn may ameliorate the cognitive dysfunction and reduce the oxidative damage, respectively.

Whilst it is clear from the studies included in this special issue that many advances have been made in basic research directed at improving the symptoms of neurodegenerative diseases, there are many key issues still to be overcome. Firstly, we remain ignorant of the genesis of the major neurodegenerative diseases in individuals, although the study of gene expression in human groups who are highly susceptible to AD such as those with Down's syndrome is a notable exception. Secondly, this special issue also illustrates that the mechanisms at play in neurodegenerative diseases are clearly multifactorial in terms of their impact on CNS functionality, with contributions from the immune system, antioxidant status, changes in gene expression, and epigenetic impacts on enzymatic function. Often, a single targeted therapeutic intervention will successfully repair a particular issue such as anti-inflammatory and antioxidant status, only for this apparent advance to have little or no impact on the genesis

and progress of the neurodegenerative condition. Thirdly, there also remains the issue of suitability of appropriate models employed for the assessment of possible therapeutic initiatives. Whilst there are several animal models for various human neurodegenerative conditions, their record in providing relevant agents which are then successful in clinical trials has been problematic and in vitro models are very much in their infancy.

Overall, it is imperative that we continue to progress in our search for appropriate models, either in vivo or in vitro, which can adequately and faithfully assess integrated therapeutic initiatives, which can do much more than can be done at the moment, that is, simply treating the symptoms of these conditions and managing an inevitable decline. It is necessary to devise treatment regimens, which not only halt the progress of these conditions, but also one day prevent their appearance and even restore full function in those who have been afflicted by them. The progress reported in this special edition suggests that, in the future, achieving these aims might be a distant prospect but not an unattainable one.

Marta C. Monteiro
Michael D. Coleman
Eric J. Hill
Rui D. Prediger
Cristiane S. F. Maia

Research Article

Age and Environment Influences on Mouse Prion Disease Progression: Behavioral Changes and Morphometry and Stereology of Hippocampal Astrocytes

J. Bento-Torres,[1] L. L. Sobral,[2] R. R. Reis,[3] R. B. de Oliveira,[1] D. C. Anthony,[4] P. F. C. Vasconcelos,[5] and Cristovam Wanderley Picanço Diniz[1]

[1]*Laboratório de Investigações em Neurodegeneração e Infecção, Hospital Universitário, João de Barros Barreto, Instituto de Ciências Biológicas, Universidade Federal do Pará, Belém, PA, Brazil*
[2]*Universidade do Estado do Pará, Centro de Ciências da Saúde, Belém, PA, Brazil*
[3]*Vertebrate Embryology Laboratory, Biomedical Sciences Institute, Health Sciences Center, Federal University of Rio de Janeiro, Rio de Janeiro, RJ, Brazil*
[4]*Lab of Experimental Neuropathology, Department of Pharmacology, University of Oxford, Oxford, UK*
[5]*Departamento de Arbovirologia e Febres Hemorrágicas, Instituto Evandro Chagas, Ananindeua, PA, Brazil*

Correspondence should be addressed to Cristovam Wanderley Picanço Diniz; cwpdiniz@gmail.com

Because enriched environment (EE) and exercise increase and aging decreases immune response, we hypothesized that environmental enrichment and aging will, respectively, delay and increase prion disease progression. Mice dorsal striatum received bilateral stereotaxic intracerebral injections of normal or ME7 prion infected mouse brain homogenates. After behavior analysis, animals were euthanized and their brains processed for astrocyte GFAP immunolabeling. Our analysis related to the environmental influence are limited to young adult mice, whereas age influence refers to aged mice raised on standard cages. Burrowing activity began to reduce in ME7-SE two weeks before ME7-EE, while no changes were apparent in ME7 aged mice (ME7-A). Object placement recognition was impaired in ME7-SE, NBH-A, and ME7-A but normal in all other groups. Object identity recognition was impaired in ME7-A. Cluster analysis revealed two morphological families of astrocytes in NBH-SE animals, three in NBH-A and ME7-A, and four in NBH-EE, ME7-SE, and ME7-EE. As compared with control groups, astrocytes from DG and CA3 prion-diseased animals show significant numerical and morphological differences and environmental enrichment did not reverse these changes but induced different morphological changes in GFAP+ hippocampal astroglia. We suggest that environmental enrichment and aging delayed hippocampal-dependent behavioral and neuropathological signs of disease progression.

1. Introduction

Prion diseases are fatal neurodegenerative diseases characterized by accumulation of prion misfolded (PrP$^{\text{sc}}$) protein, gliosis, synaptic dysfunction, and, at late stages, neuronal loss [1–5]. This sequence of events shares the neuropathological features of chronic neurodegeneration in Alzheimer's disease (AD) and is well reproduced in the ME7 murine young adult model of prion disease [6–8]. Previous studies in murine model of prion disease identified as disease progresses an increase in immunoreactivity of GFAP (glial fibrillary acidic protein), a selective marker for astrocytes [9]. The contribution of astrocytes in young adult scrapie pathogenesis at the cellular and molecular levels has been recently investigated and resulted in a better understanding of disease progression mechanisms [10]. Prion disease is caused by a conformational change of the normal membrane bound glycoprotein PrPc (cellular prion protein) into a insoluble infectious form PrPSc (scrapie isoform) [11]. A close relationship between PrPSc and enhanced glial fibrillary acidic protein (GFAP) immunoreactivity at different stages of the disease has been identified [3, 12], giving morphological evidence of specific

astrocytic involvement in the progression of prion disease. In addition, a recent analysis of the hippocampal proteome in ME7 prion disease in correlation with behavioral and cellular dysfunctions at different time points has revealed a predominant astrocytic signature with four upregulated proteins, including GFAP, selectively expressed in astrocytes [4].

Prion pathogenesis is, however, dramatically slowed in aged mice when compared with young animals [13, 14]. Indeed, aged infected mice show significantly less disease-specific pathological markers such as gliosis, vacuolation, and PrP^{sc} and less pronounced upregulation of disease-associated inflammatory and stress-response genes [15]. These findings suggest that an immune senescent system may contribute to slowing down neuropathological and behavioral changes. A healthy, young, fully responsive immune system, therefore, may be necessary to generate the whole spectrum of prion disease features in rapid progression.

Previous reports demonstrated beneficial effects of environmental enrichment on neurodegenerative disease progression in experimental models including Huntington's disease [16–18], transgenic mice coexpressing familial AD-linked APP and PS1 variants [19], MPTP and 6-OHDA Parkinson's disease models [20, 21], and amyotrophic lateral sclerosis mouse model expressing the human SOD1(G93A) gene mutation [22]. However, no previous study has investigated the possible beneficial effects of EE on prion disease outcomes.

Both environmental changes and aging influence astrocytic plasticity [23–26], which seems to be a key element of the host protective system in prion progression [3, 4, 27]. For this reason, we evaluated possible correlations between behavioral changes related to prion disease progression and number and morphology of astrocytes in both young adult and aged prion-diseased mice. Because we previously demonstrated in albino Swiss mice model of prion disease that astrocytes from the polymorphic layer of dentate gyrus exhibit intense reactive astrocytosis earlier than all other layers of dentate gyrus and that this change was associated with axonal degeneration of mossy fiber, we thought polymorphic layer and CA3 (target of mossy fibers) may exhibit the earliest astroglial pathology of the hippocampal formation of albino Swiss mouse model of prion disease. In addition, to the selected areas for morphometry and stereological analysis of astrocytes, we have chosen a time window for astrocytes reconstructions when stereological data showed no change in the number of neuronal cell bodies [27].

Stereological analysis and microscopic three-dimensional reconstruction combine unbiased systematic sampling approach to count cells [28] and detailed morphological description of objects of interest [29]. This combination increases resolution of quantitative neuropathology and offers an integrative analysis of morphology and numeric cell changes using hardware and software readily available. Indeed, these new analytic tools in correlation with clinical outcomes in different time windows may provide reliable detailed quantitative information about subtle or profound changes in abnormal conditions that may help to understand pathogenesis [30, 31]. Here we used this unbiased meticulous approach to investigate influences of age and environment on morphology and numbers of astrocytes of hippocampus in a murine model of prion disease.

2. Methods

All procedures were approved by the institutional Animal Care Committee of the University Hospital of the Federal University of Pará under the Protocol Number 1701/05. All animals were handled in accordance with the "Guidelines for the Use of Animals in Research" and followed the legal requirements of the Brazilian Council of Experimental Animal Research (CONCEA). A total of 33 albino Swiss female mice at ages 6 (young) and 18 (aged; A) months were used. Adult males could not be used because of aggression levels [32]. Females were housed in EE or standard environment (SE) cages for 5 weeks, followed by surgeries for intracerebral injection of ME7-infected or normal brain homogenates (NBH). After recovery from anesthesia, all animals were returned to their preoperative housing and tested weekly for burrowing activity. At 18th week after injection (wai), all mice were subjected to the object recognition test and then euthanized and perfused.

2.1. Housing, Food, and Welfare. EE animals (n = 12; 6 ME7, 6 NBH) were housed in plastic cages ($32 \times 39 \times 16.5$ cm) equipped with wheels for voluntary running, tunnels, and various plastic, metal, or cardboard objects that were exchanged and/or placed at different positions once a week to stimulate exploratory activity. SE mice (n = 21; 5 NBH, 6 ME7; 4 NBH-A, 6 ME7-A) were kept in a similar type of cage but with minimal environmental stimulation. Both cage types were lined with autoclaved rice straw, which was exchanged at least weekly. Animals had free access to food (containing 23 g protein/100 g) and water and were maintained on a room with minimum noise exposure, at $23 \pm 2°C$, 12 h light/dark cycle and light period was used for behavioral tests. Because we have not investigated possible environmental influence on aged mice prion disease progression, no data from aged mice raised on enriched cages are exhibited.

2.2. Intracerebral Inoculation. After the 5-week cage acclimation, animals were weighed and i.p. anesthetized with 2,2,2-tribromoethanol (Sigma-Aldrich, USA) (250 mg/kg body weight) for stereotaxic surgery (Insight Equipment) for bilateral intracerebral inoculation of 1 μL of normal (NBH) or ME7-infected brain homogenates. ME7 tissue was obtained from mice with clinical signs of prion terminal illness and kindly provided by Professor V. H. Perry (Centre for Biological Sciences, University of Southampton, Southampton, UK). Because integrity of hippocampal formation would be essential to guarantee fine details of astrocytes three-dimensional reconstruction and mechanical damage induced by injections needle could induce reactive astrogliosis around the tract, we decided to select dorsal striatum as the target area of injections. Thus, injections were made on the following coordinates: +1 mm bregma, ±1.5 mm from midline, and 3.0 mm deep [33]. Two openings were made with the aid of a drill to enable bilateral striatal injections (10% w/v in phosphate
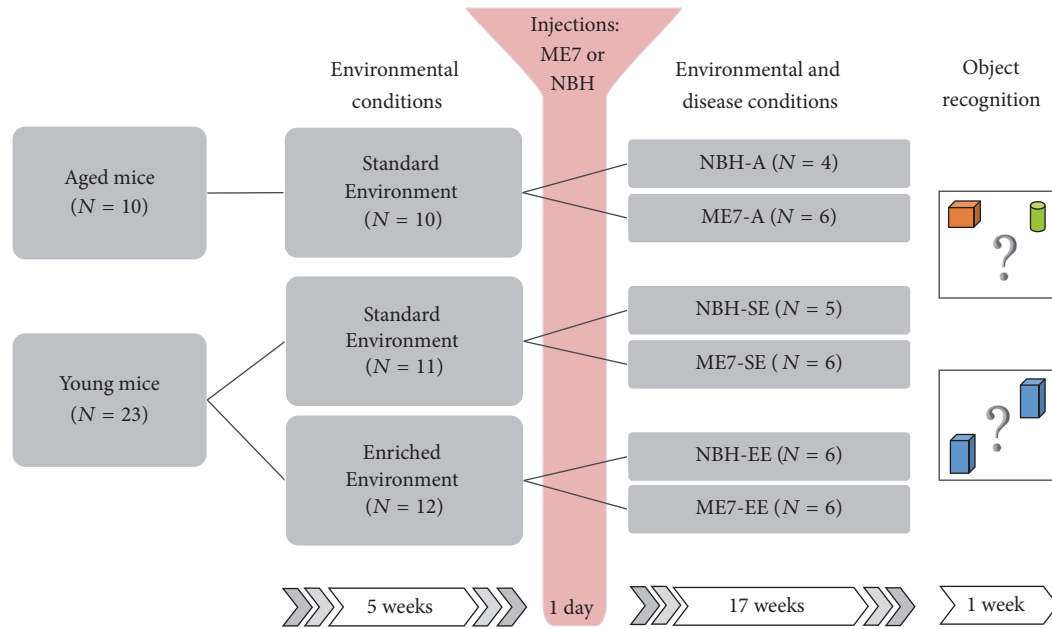
FIGURE 1: Experimental timeline. Young adult (6 months old) and aged (18 months old) female albino Swiss mice were maintained for 5 weeks either in enriched or in standard cages and then subjected to injections of normal or ME7 infected brain homogenates and returned to their original cages. After 17 weeks after injections they were submitted to placement and identity object recognition tests, euthanized, and had their brains processed for selective GFAP, PrPSc, and IBA1 immunolabeling.

buffered saline (PBS)) of NBH or ME7-infected homogenates. After injection, the needle (Hamilton 10 μL) was held in place for 3 minutes to avoid solution backflow, after which it was slowly withdrawn. The scalp was then sutured and the animal put into a cage for recovery. After recovery, animals were returned to their original cages. Ultimately, the numbers for treatment and control groups were as follows: NBH-SE = 5; NBH-EE = 6; ME7-SE = 6; ME7-EE = 6; NBH-A = 4; and ME7-A = 6. As noted, at 18 wai, all animals were perfused for brain tissue analysis. Figure 1 is a graphic representation of the experimental timeline.

2.3. Behavior Assessment

2.3.1. Burrowing. Burrowing is the most sensitive test to indicate earlier signs of hippocampal prion-induced dysfunction [34]. In this test a tube with food pellets is placed in the cage of a single mouse and almost all mice spontaneously remove pellets out of the tube. It is expected that a normal mouse will burrow many times its own weight in food pellets in two hours [35]. Weekly for a 4-hour testing period (from 09:00 to 11:00 hours), each animal was individually placed in a plastic cage (32 cm × 39 cm × 16.5 cm) containing a cylindrical PVC tube (20 cm length, 7.2 cm diameter) filled with 250 g of normal diet food pellets. The open end of the tube was supported 3 cm above the floor. After the testing period, the remaining food in the cylinders was weighed, and the animals were returned to their collective cages [34]. Burrowing measurements started at week 3 after injection and finished at 18 weeks.

2.3.2. Placement and Object Identity Recognition. We used one-trial object placement recognition [36] and one-trial identity recognition tests [37]. All mice were subjected to both tests.

The apparatus for these tests consisted of an open box (30 × 30 × 40 cm) made of painted white wood. The floor was painted with black lines to form nine squares (10 × 10 cm), and the luminance at the center of the cage floor was 2.4 cd/m^2. One meter above the open field, a video camera connected to a computer recorded each training session for later analysis by Any-Maze software (Stöelting). Detailed protocols and the rationale for test choices are discussed elsewhere [38]. In brief, behavioral tests were performed after 12 days, with 7 days to become accustomed to handling, 3 days for open field habituation, and 2 days for object habituation, with testing on the 13th day.

For handling, mice were daily picked up by the tail and released into the center of the open field. After 1 min of open field exposure, the animals were removed from the open field and placed back into their home cages. For open field habituation, mice were placed daily in the arena, free of objects, for 5 minutes to explore the open field. To achieve object habituation, mice were exposed to two identical objects placed at the corners of the arena for 5 minutes, three times, with 50 minutes in between. These objects were not used on the test days. Finally, on test day, memory tests were administered once for each mouse.

To minimize the influence of natural preferences for particular objects or materials, we chose objects of the same material, with different geometries that could be easily

discriminated, and similar access for interaction [39]. All objects were made of plastic with different shapes, heights, and colors. Before each mouse entered in the arena, the box and objects were cleaned with 75% ethanol to minimize distinguishing olfactory cues.

On the testing day, in a first trial, mice were exposed for 5 minutes to two identical objects (samples) and, in a second trial of 5 minutes, to two dissimilar objects, one a familiar object (from the sample session) and the other a new distinct object. The intertrial interval was 50 minutes. Most mice were expected to spend more time with the novel than the familiar object. Similarly, the next day, animals were subjected to the one-trial placement recognition test. In this test, mice were exposed for 5 minutes in the first trial to two identical objects. After an intertrial interval of 50 minutes, mice were exposed for 5 minutes to the same objects, one stationary and one displaced. The expectation was that, after the intertrial interval, most mice would spend more time with the displaced than the stationary object.

We measured the time of exploration on each object, expressed as a proportion (percentage) of the total time of exploration. Possible significant differences were also detected with the two-tailed t-tests for dependent groups [40].

2.4. Perfusion and Histology.

At week 18 after injection, when ME7-Y mice show typical behavioral signs of preclinical disease, including a significant reduction in burrowing activity and increase in locomotor exploratory activity [35], they were weighed, i.p. anesthetized with 2,2,2-tribromoethanol (Sigma-Aldrich, USA) (250 mg/kg body weight), and perfused transcardially with heparinized 0.9% saline solution (5000 IU/L), followed by 4% paraformaldehyde in 0.1 M phosphate buffer (pH 7.2–7.4). After perfusion, the brains were removed and sectioned in a vibratome (Micron) on the horizontal plane (70 μm thick); see detailed histological procedures elsewhere [27]. Serial anatomical series of sections (1 : 6) were collected and subjected to immunohistochemical analysis, as described below.

2.4.1. Immunohistochemistry for GFAP and Iba1.

The morphology and number of astrocytes were assessed using the primary antibody to GFAP (Millipore© # MAB360) and Iba1 (Wako© # 019-19741). Brain sections from both diseased and control animals were selected randomly and systematically, taking one in every six slices of 70 μm. The sections were washed in 0.1 M phosphate buffer, pH 7.2–7.4, and pretreated for 60 minutes in 0.2 M boric acid solution, pH 9.0, at 70°C for antigenic recovery. After being washed with PBS-5% Triton, sections were transferred for 15 minutes to a solution of 0.3% hydrogen peroxide in 0.1 M phosphate buffer, pH 7.2–7.4. After washing sections in PBS, we followed the protocol for the Mouse-on-Mouse Kit (Vector Laboratories), using anti-GFAP or anti-Iba1 primary antibodies at 1 : 400 in 0.1 M PBS, pH 7.2–7.4.

Finally, sections were washed in PBS and incubated in ABC (Avidin-Biotin Complex Vector Laboratories) for 30 minutes. The DAB/nickel/glucose oxidase/diaminobenzidine protocol was used to reveal GFAP and Iba1 binding sites

[41]. Sections were mounted on gelatinized slides, left to dry at room temperature, and subsequently counterstained with cresyl violet, dehydrated in alcohol (70, 80, 90, and 100%), and cleared in xylenes before being covered with Entellan (Merck) and cover slips for further analysis.

2.4.2. Protease-Resistant PrP^c Immunolabeling.

Sections immunoreacted to detect PrP protease resistance were pretreated in formic acid 85%, for 30 minutes, incubated in trypsin 0.05% at room temperature for 10 minutes, and then transferred to a solution of 0.1 M citrate buffer, pH 6.0, at 90°C for 1 hour. Sections were rinsed in 0.1 M PBS-Triton X-100 (5%). After a wash in PBS, the sections were subjected to the Mouse-on-Mouse (MOM) Blocking Kit (Vector Laboratories, Burlingame, CA, USA) protocol, as follows: MOM IgG blocking for one hour, primary antibody exposure for 72 hours (ABCAM, mouse monoclonal [8H4] to Prion protein PrP, 1 : 2500) diluted in 0.1 M PBS, and washes in 0.1 M PBS three times for 5 minutes, followed by MOM Biotinylated Anti-Mouse IgG Reagent for 12 hours. Sections were treated with 0.3% hydrogen peroxide in 0.1 M phosphate buffer, pH 7.2–7.4, then transferred to ABC solution for 1 hour, and washed again before incubation in acetate buffer 0.2 M, pH 6.0, for 5 minutes and revealed in GND solution (diaminobenzidine 0.5 mg/mL, ammonium nickel chloride 0.6 mg/mL, and glucose oxidase). All steps were carried out under gentle and constant agitation.

2.5. Stereology.

The quantitative analysis of the number of objects of interest in regions of interest in infected mice or controls from the different environmental conditions was performed using the optical fractionator method [42]. The regions of interest were the CA3 stratum radiatum and the polymorphic layer of the dentate gyrus (DG) of the dorsal hippocampal formation. Their boundaries were defined using a 4x objective optical microscope (Nikon Eclipse 80i, Japan) equipped with a motorized stage to control the X, Y, and Z coordinates with help of a stage controller (MAC6000, Ludl Electronic Products, Hawthorne, NY, USA). This system was coupled to a computer containing the Stereo Investigator program (MBF Bioscience, Williston, VT, USA), which recorded the three-dimensional coordinates and stored the stereological data. A 100x objective was used to count and reconstruct astrocytes. The stereological parameters for counting astrocytes were dissector 12, guard 1, and counting probe 80–60 for the CA3 and DG regions, with a sample grid 130–100 for CA3 and 100–80 for DG.

Astrocyte cell body volume was obtained during the counting procedures using an optical fractionator. The satellite probe "nucleator," when run in parallel with the optical fractionator, allows each cell to have the same probability of being selected regardless of shape, orientation, or size [43]. The analysis consisted of the superposition of six radial lines (the number of lines configured according to interest) that crossed the cell body in the center of the point marked by counting the optical fractionator. The user identified the point at which each radial line intersected the edge of the cell body, and the spreadsheet program provided the results for volume, area, and the coefficient of error.
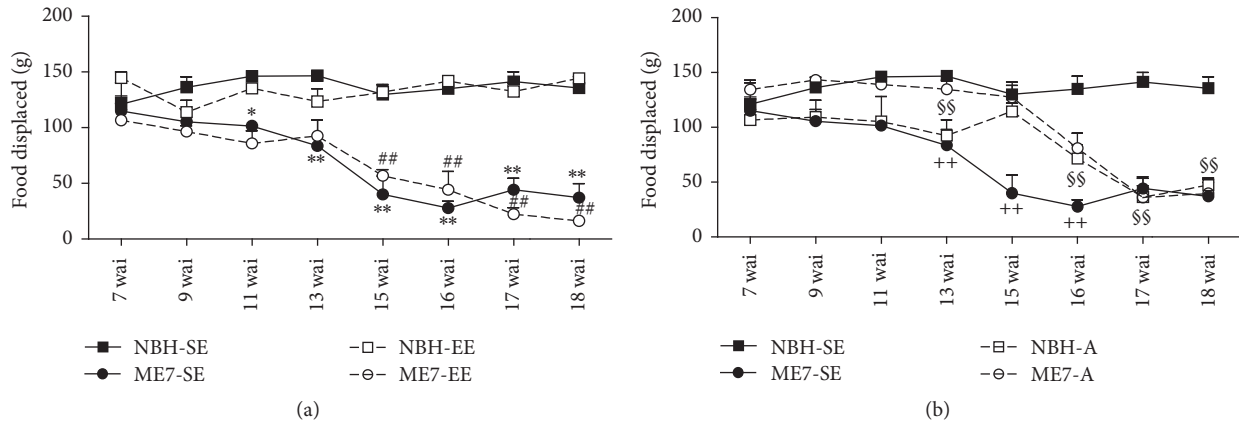
FIGURE 2: Burrowing activity. (a) Amount of burrowed food in the ME7-SE group compared to NBH-SE controls. Note significant reduction at 11 wai in ME7-SE compared with NBH-SE and at 15 wai in ME7-EE compared with NBH-EE. (b) ME7-SE young mice were different from ME7-A mice between 13 and 16 wai, and NBH-A showed a reduction in burrowing activity at 16 wai. (* $p < 0.05$, ** $p < 0.01$ versus NBH-SE; ## $p < 0.01$ versus NBH-EE; ++ $p < 0.01$ versus ME7-A; §§ $p < 0.01$ versus NBH-SE; Two-way repeated measures Bonferroni posttests).

2.6. Three-Dimensional Reconstruction of Astrocytes. For three-dimensional reconstruction of astrocytes, we used dedicated software (Neurolucida, Microbrightfield, Williston, VT, USA) to store the coordinates of points of interest. To avoid ambiguity in the identification of objects of interest and provide greater accuracy in the reconstruction, the 4.0x objective was replaced by a high-power objective, the Plan Fluor 100x (NA 1.3; DF $= 0.2 \mu M$, Nikon, Japan). A total of 171 astrocytes were reconstructed, 12 to 14 for each animal, all from the DG polymorphic layer.

We adopted a random and systematic sample procedure in the same sections analyzed by the optical fractionator, as has been suggested [44]. Astrocytes were selected from boxes of $70 \times 70 \mu$m, separated from each other by 200μm intervals. Only astrocytes located within the box boundaries were selected for analysis. In rare exceptions, when no cells inside the box met the standard immunostaining and integrity requirements of the branches, astrocytes were chosen that were located near the edge of the box. We applied correction for shrinkage related to histological processing for all experimental groups but only for the Z-axis, with an assumption of 75% shrinkage, as previously suggested [45].

To assess morphological changes in astrocytes associated with murine prion disease, we measured and compared 14 morphological parameters of astrocytes reconstructed from the DG polymorphic layer of NBH and ME7-infected animals. Thus, each reconstructed astrocyte was the subject of multiple measures. Detailed descriptions of these 14 parameters (segment length, μm; total number of endings; segment surface area, μm^2; segment volume, μm^3; segments/mm; fractal dimension, k-dim; branch node total; segment number; complexity; tree number; soma area, μm^2; soma perimeter, μm; convex hull, μm^3) can be found elsewhere [46].

2.7. Statistical Analysis. The results from the Stereo Investigator, Neurolucida, and Any-Maze program were statistically analyzed using BioEstat 5.3 and GraphPad Prism software [47], applying parametric tests and multivariate analyses to establish differences or similarities among groups. A $p < 0.05$ was considered to indicate significance. The results are presented as arithmetic means and standard error values.

3. Results

3.1. Behavioral Changes. Our findings related to the environmental influence on prion disease progression are limited to young mice whereas those related to age influence are limited to mice raised on standard cages. ME7-SE but not ME7-A mice showed typical behavioral changes with disease progression [37]; however, as compared to young mice from standard cages, ME7-EE young animals seemed to exhibit slower disease progression. Figure 2 shows the amount of burrowed food as a function of time progression. Two-way repeated measures ANOVA revealed significant interaction between infection and temporal progression (Figure 2(a), $F = 6.39$, $p < 0.0001$; and Figure 2(b), $F = 5.71$, $p < 0.0001$). EE influenced burrowing activity of prion-diseased mice; indeed, compared to NBH control groups, the amount of burrowed food in ME7-SE infected animals dropped significantly at 11 wai, but ME7-EE mice showed significant reduction only at 15 wai (Figure 2(a)). However, one-way repeated measures ANOVA revealed significant differences in burrowing between 7 and 15 wai for both ME7-SE and ME7-EE animals. No change in burrowed food was seen in control groups (NBH-SE and NBH-EE).

In contrast with young adult ME7-SE mice which show significant differences in burrowing activity, two-way repeated measurements ANOVA showed that aged mice ME7-A group did not differ in burrowing activity from age-matched controls (NBH-A). However, significant differences between ME7-A and ME7-SE at 13, 15, and 16 wai and between NBH-A and NBH-SE at 13, 16, 17, and 18 wai were found as an effect of aging (Figure 2(b)). One-way repeated measures ANOVA revealed significant differences between 7 and 16 up to 18 wai in ME7-A and between 7 and 17 up to 18 wai in NBH-A. For detailed statistical data,

Place

(a)

Identity

(b)
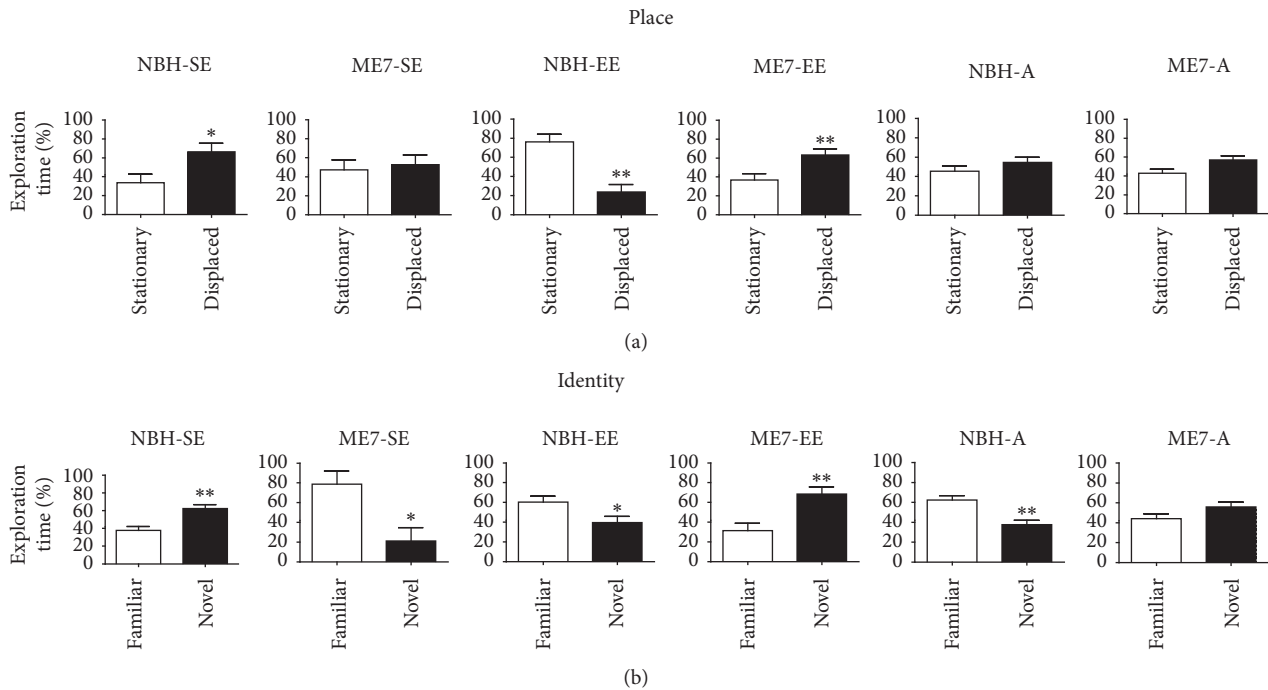
FIGURE 3: Object recognition impairments. At 17 wai, all mice were tested on object recognition tasks to recognize placement and identity of objects. (a) ME7-SE, NBH-A, and ME7-A did not distinguish displaced from stationary objects. All other groups succeeded in this task. (b) In the object identity recognition task, except for ME7-A, all groups recognized the identity of the objects ($^*p < 0.05$, $^{**}p < 0.01$; two-tailed t-tests).

see Table S1 in Supplementary Material available online at https://doi.org/10.1155/2017/4504925.

Taken together, our findings suggest that prion-diseased young adult mice progressively reduced burrowing activity starting at 11 wai and that EE postponed this decrease by about 4 weeks, whereas aged mice, independently of infection, reduced significantly burrowing activity without significant differences in the amount of burrowed food between NBH-A and ME7-A individuals.

3.1.1. Spatial Memory and Object Identity Recognition. Figure 3 shows that significant differences were identified between time spent on exploration of displaced and stationary objects in the object placement test (Figure 3(a)). Significant differences between the amount of time spent on the exploration of familiar and novel objects were used as an indicator of object recognition in the object identity test (Figure 3(b)). Note that, on average, ME7-SE, NBH-A, and ME7-A could not distinguish displaced from stationary objects. All other groups succeeded in this task. However, all groups except ME7-A recognized the identity of the objects (Figure 3(b)), suggesting that the disease and aging first impair spatial memory task performance. At least in this time window, prion-diseased mice had their object identity recognition preserved. Although control aged mice could not distinguish between stationary and displaced objects, they distinguished between familiar and novel objects, whereas prion-diseased aged mice lost those abilities. For statistical details, see supplementary Table S2.

3.2. Prion Disease Pathology and Astrocytes Morphology at 18 wai. Stereological estimation and three-dimensional morphometric analysis of astrocytes were used to detect reactive astrocytosis in prion-diseased mice. At 18 wai histological signs of prion disease appeared in areas of injection, stereological, and morphometrical analyses, including PrPSc deposition, inflammatory microglial response, vacuolation (Figure 4), and reactive astrogliosis (Figure 5).

Reactive astrocytosis is clearly evident in prion-diseased young mice (ME7-SE and ME7-EE) but not in prion-injected aged mice (ME7-A). As compared to young mice, astrocytes from aged groups (NBH-A and ME7-A) are shrunk (Figure 5).

We compared control and ME7-infected animals from different environments or different ages to detect potential alterations in astrocytes (Figures 6 and 8).

Figure 6 shows in young adult mice the environment ($F = 10.02$; $p = 0.011$) and disease ($F = 6.02$; $p = 0.036$) and influences on the total number of astrocytes in the DG polymorphic layer and stratum radiatum of CA3 (environment, $F = 5.23$; $p = 0.045$), with specific comparisons between groups given in Supplementary Table S1.

In the polymorphic layer, ME7-SE mice had higher number of astrocytes than NBH-SE animals (5342 ± 227.5 versus 3912 ± 376.3) whereas nonsignificant differences were detected in the comparisons between ME7-EE and NBH-EE (Figure 6(a)). However, as compared with SE, EE increased the number of astrocytes in the polymorphic layer in controls (NBH-EE versus NBH-SE). In the stratum radiatum of CA3, aged mice showed a significantly higher number of astrocytes than young adults (Figure 6(b)).

PrPsc Iba1
NBH-SE   ME7-SE   NBH-SE   ME7-SE
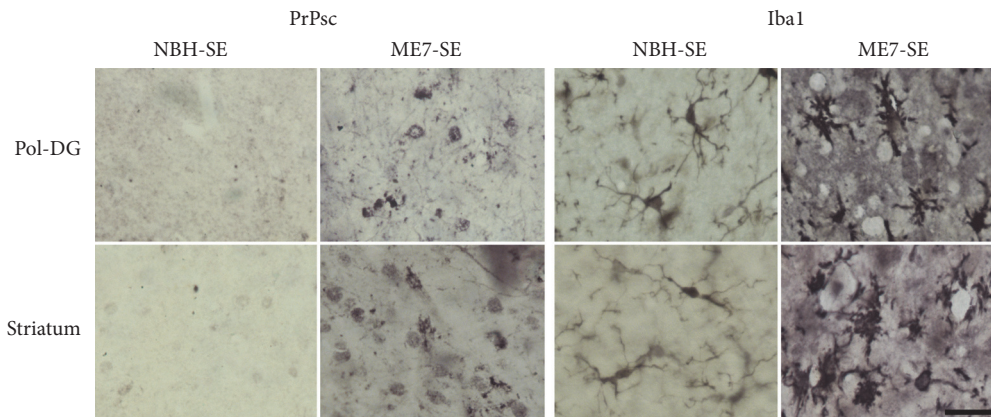
FIGURE 4: Photomicrographs from PrPSc and Iba1 immunolabeled sections from the polymorphic layer of dentate gyrus and striatum to illustrate mouse prion disease associated histological changes. Note PrPSc deposits and morphological activated microglia and vacuolation in ME7-SE. Scale bar: 25 μm.

SE   EE   A
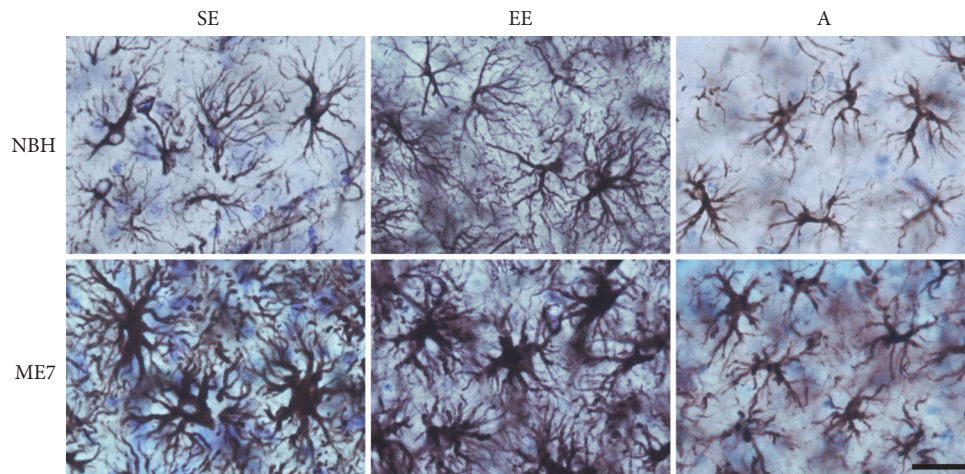
FIGURE 5: Photomicrographs from control and prion-diseased mice at 18 wai to illustrate morphological astrocytic changes in the stratum radiatum of CA3 from young and aged adults from standard and enriched environments. Scale bar: 25 μm.

Different from the polymorphic layer, the stratum radiatum of CA3 of ME7-EE showed a higher number of astrocytes than that of ME7-SE mice whereas nonsignificant differences were detected in the comparisons between ME7-SE and NBH-SE or ME7-A and NBH-A animals (Figure 6(a)). The disease condition increased astrocyte cell body volume in ME7-SE and ME7-EE groups in the DG polymorphic layer and stratum radiatum of the CA3 (Figures 6(c) and 6(d)). However, EE reduced this hypertrophic effect on cell body astrocytes of ME7-EE group in the stratum radiatum of CA3. Prion disease did not produce volume changes in cell bodies in aged mice (ME7-A versus NBH-A); coherently, as compared with young infected mice cell body volumes from aged infected mice are smaller (ME7-A versus ME7-SE) (Figure 6(d)). A significant interaction between disease and environment ($F = 11.77$; $p = 0.006$) and between disease and age ($F = 62.02$; $p < 0.0001$) was found in CA3 astrocytes cell body volumes. See Supplementary Table S3 for more details.

Figure 7 shows graphic representations of astrocyte morphological changes on astrocyte three-dimensional reconstructions of the polymorphic layer at 18 wai. The total volume of branches was influenced by prion disease ($F_{(1,10)} = 245.1$; $p < 0.0001$), EE ($F_{(1,10)} = 5.19$; $p = 0.046$), and aging ($F_{(1,11)} = 49.36$; $p < 0.0001$) with significant interactions between these variables (prion and environment: $F_{(1,10)} = 10.91$; $p = 0.008$; prion and aging: $F_{(1,11)} = 53.10$; $p < 0.0001$). In contrast, the surface area of branches was affected only by prion disease independent of environmental condition ($F_{(1,10)} = 96.74$; $p < 0.0001$) and by aging ($F_{(1,11)} = 22.72$; $p = 0.0006$), with a significant interaction between prion disease and aging ($F_{(1,11)} = 44.76$; $p < 0.0001$). The total length of branches was influenced by prion disease ($F_{(1,11)} = 5.039$; $p = 0.046$) and aging ($F_{(1,10)} = 23.21$; $p = 0.0005$). In agreement, two-way ANOVA Bonferroni posttests (Table S3) revealed, as compared with NBH-SE and NBH-EE, significantly higher branch volumes in the ME7-SE and ME7-EE animals. ME7-EE and ME7-A groups showed reduced branch volumes compared to ME7-SE animals (Figure 7(a)). As compared with NBH-SE and ME7-A groups, ME7-SE showed an increase in the surface of the

(a)

(b)

(c)

(d)
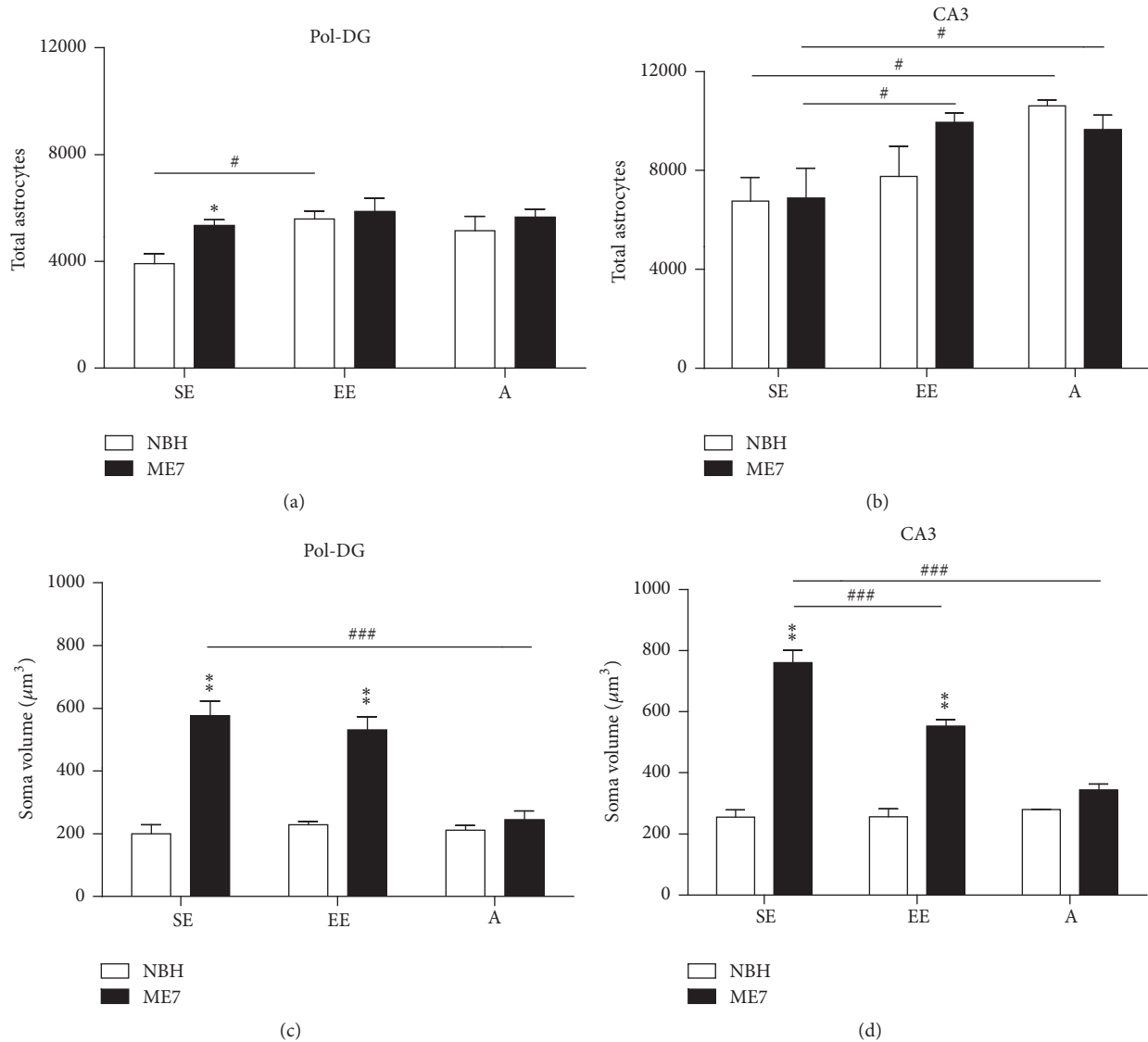
FIGURE 6: Astrocyte number and cell body volume changes. (a) In the polymorphic layer, ME7-SE mice showed higher number of astrocytes than NBH-SE animals. AS compared with NBH-SE, an increased number of astrocytes is observed in NBH-EE. (b) In the stratum radiatum of CA3, NBH-A and ME7-A mice showed higher number of astrocytes than NBH-SE and ME7-SE animals, respectively. In contrast to the polymorphic layer, stratum radiatum of CA3 of ME7-EE showed a higher number of astrocytes than that of ME7-SE mice. (c) and (d) show prion disease influence on the cell body volumes of astrocytes in the DG polymorphic layer and stratum radiatum of the CA3, respectively. ME7-SE and ME7-EE showed significant soma hypertrophy in astrocytes from DG and CA3 compared with their respective controls. However, ME7-A cell body volume was smaller than ME7-SE in the polymorphic layer and stratum radiatum of CA3 layers. In the stratum radiatum of CA3, the cell body volume of astrocytes from ME7-EE mice was smaller than that of ME7-SE animals ($^{*,\#}p < 0.05$; $^{**}p < 0.01$; $^{\#\#\#}p < 0.001$ Bonferroni posttests).

branches. Similarly, as compared with NBH-EE, an increase in the branch surface area was found in ME7-EE mice. A similar increase in branch surface areas was also found in NBH-EE in comparison with NBH-SE (Figure 7(c)). On average, the branches of the ME7-SE group were significantly longer than those from the NBH-SE and ME7-A groups.

Differences in branch volumes between NBH and ME7 started at the first-order branches and persisted until the sixth order in SE groups but only until the fourth order in EE animals (Figure 7(b)). Prion disease also seemed to

affect the surface of more distal branches of the SE group (fourth order) compared to the EE group (third order) (Figure 7(d)). Although no differences were observed in the total length of these branches, the first- and second-order branches were longer in ME7-EE in comparison with NBH-EE mice (Figure 7(f)). For more details, see supplementary Table S3.

Figure 8 shows graphical models of three-dimensional reconstructions of astrocytes of the polymorphic layer of the DG with correspondent dendrograms, to compare astrocytes
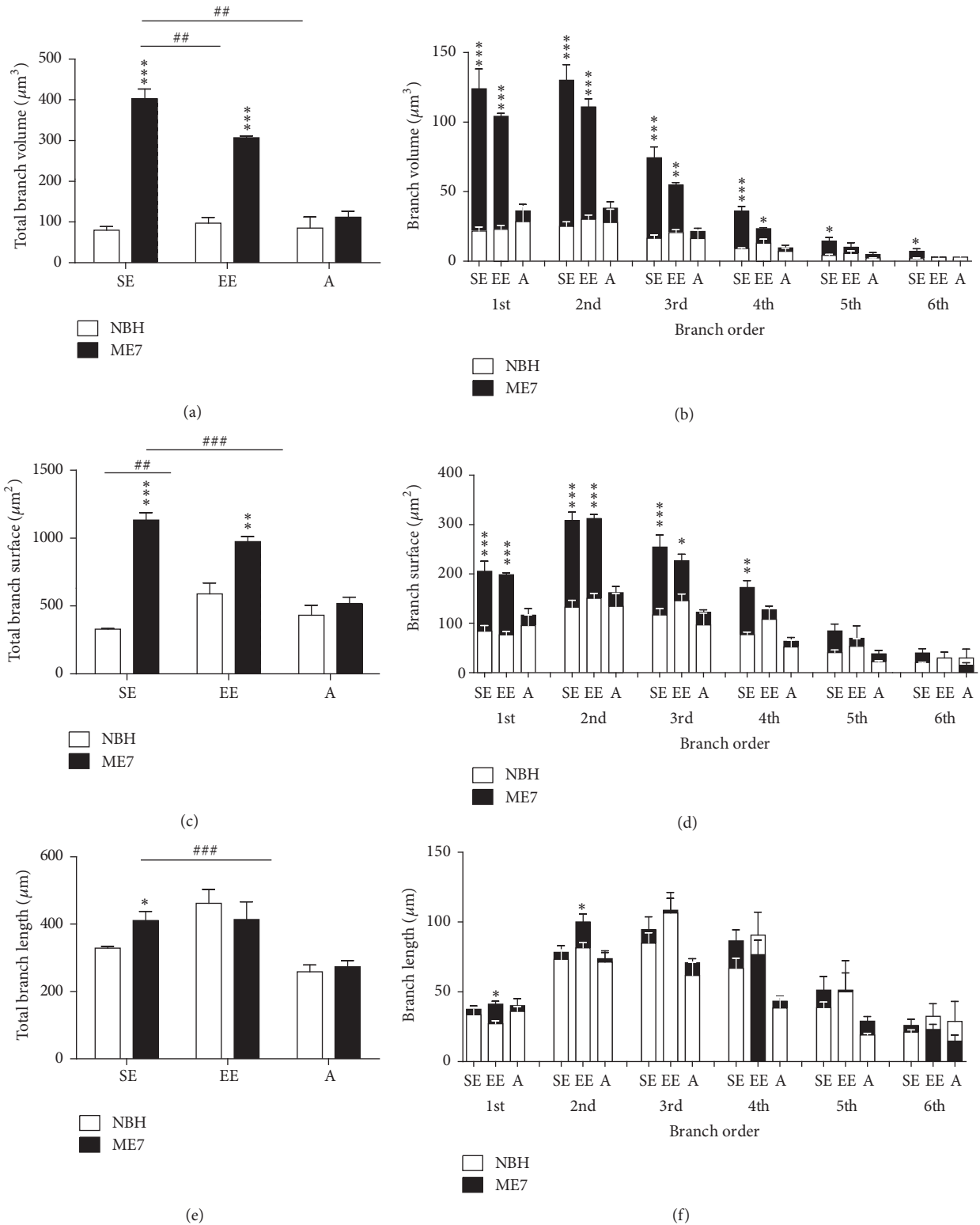
FIGURE 7: Astrocyte morphometry. (a) ME7-SE and ME7-EE mice showed significantly higher branch volumes compared to NBH-SE and NBH-EE animals, respectively. ME7-EE and ME7-A groups had reduced branch volumes versus ME7-SE mice. (c) Prion disease also increased the surface area of astrocyte branches compared with NBH-SE and ME7-A groups. An increase in branch surface area also was seen in ME7-EE versus NBH-EE mice and in NBH-EE versus NBH-SE animals. (e) ME7-SE astrocytes showed significantly longer branches than NBH-SE and ME7-A astrocytes. (b, d) Total volume and total surface area in ME7-SE mice were found in the 1st, 2nd, 3rd, 4th, 5th, and 6th branch orders whereas, in EE animals, effects on surface area were limited to branches from the 1st to 3rd orders, and volume differences were limited to between the 1st and 4th orders. (f) 1st and 2nd branch orders from ME7-EE were significantly longer than the corresponding branches of ME7-SE. Nonsignificant alterations were detected in aged mice ($^{*}p < 0.05$; $^{**,\#\#}p < 0.01$; $^{***,\#\#\#}p < 0.001$ Bonferroni posttests).

(a)   (b)
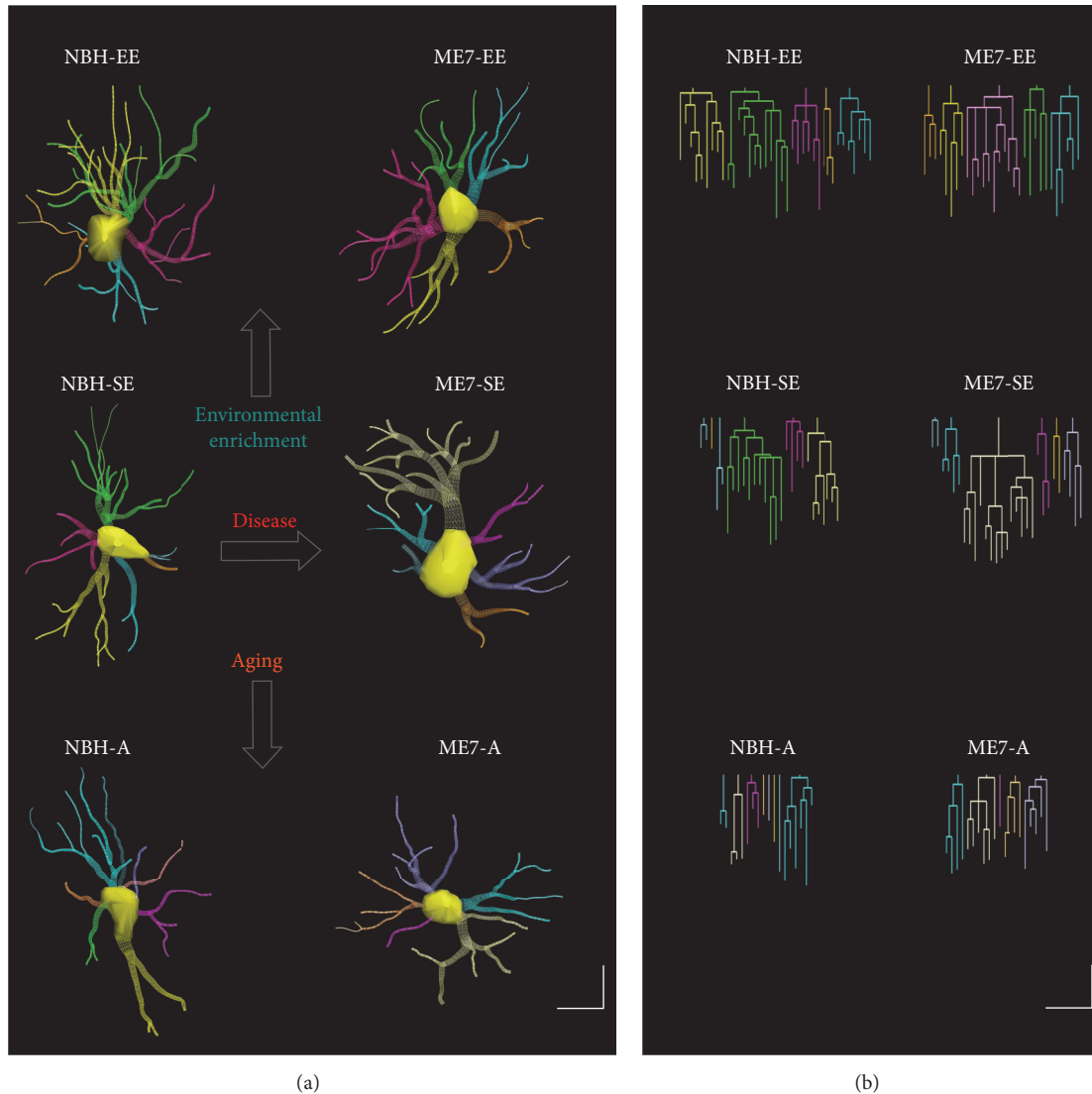
FIGURE 8: Three-dimensional reconstructions of astrocytes of the DG polymorphic layer at 18 wai (a) with corresponding dendrograms (b) in prion-diseased mice and age-matched controls. Note that aging seemed to shrink astrocyte arbors and that prion disease seemed to be associated with thicker astrocyte processes and larger cell bodies. EE was associated with an increase in the number of branches and a reduction in the prion disease-induced hypertrophy. Linear dendrogram of each astrocyte arbor with the length of each branch segment is displayed to scale as vertical lines and sister branches is horizontally displaced. Arrows indicate changes induced by each variable (environment, infection, and age). Dendrogram was plotted and analyzed with Neuroexplorer (MicroBrightField). Branches of the same parental (primary branch) trunk are shown in one color. Scale bar: 10 μm.

from prion-diseased mice at 18 wai with those of control mice to measure possible influences of environment and age on astrocyte morphology. To illustrate morphological changes, the mean values of multiple measurements of branches and soma astrocytes were previously estimated, and the selected reconstructions exhibited metric features close to the mean values of the mean astrocyte of each experimental group. Note that, as compared to control mice, prion-diseased animals show a remarkable increase in the soma and branch volumes of astrocytes.

Figure 9 shows graphic representations of convex-hull analysis applied to the reconstructed astrocytes from the DG polymorphic layer at 18 wai. As compared with NBH-SE mice,

EE increased by as much as 91% the total tree field volume of the astrocytes (NBH-EE versus NBH-EE = 4778.95 ± 110.85 versus 2500.77±306.17; $t = 2.74$, $p < 0.05$; two-way ANOVA, $F_{(1,9)} = 6.14$; $p = 0.035$).

Figure 10 shows graphical representations of cluster analysis of all reconstructed astrocytes ($n = 269$) to test the hypothesis that astrocytes from prion-diseased mice (ME7-SE, ME7-EE, and ME7-A) are morphologically distinct from control mice astrocytes (NBH-SE, NBH-EE, and NBH-A). Branch length, number of branch nodes, and soma area were the morphological features that most contributed to the cluster formation of young adult groups (Figure 10(a)). A canonical graphic representation of the discriminant analysis
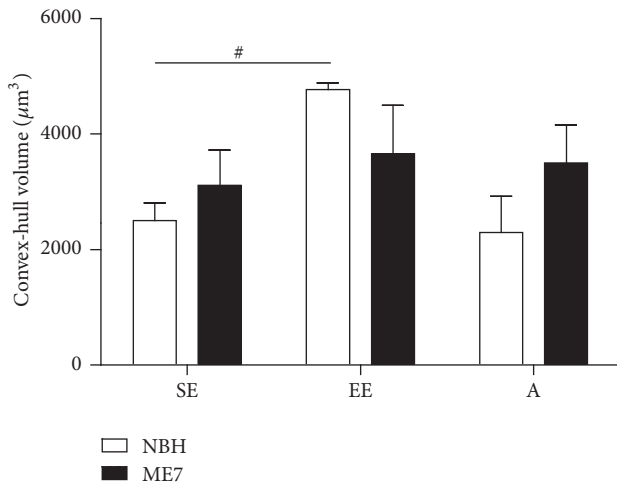
FIGURE 9: Graphic representations of convex-hull analysis showing that EE increased by as much as 91% the total tree field volume of the astrocytes from NBH-EE as compared with NBH-SE mice ($^{\#}p <$ 0.05; Bonferroni posttest).

based on these morphological features revealed significant interception between ME7 astrocytes and between NBH-SE and NBH-EE mice. Except for one individual from NBH-EE, included in the zone of interception of ME7-SE and ME7-EE, no other interceptions were observed between NBH and ME7 individuals (Figure 10(c)). Significant logarithmic correlation ($R^2 = 0.63$, $F = 285.05$, and $p < 0.00001$) was detected between branch volumes and soma area, suggesting an interdependence between these morphological features (Figure 10(d)). Tree surface, soma area, branch length, branch nodes, and tree volume were the morphological features that most contributed to the cluster formation of aged groups (Figure 10(b)). A canonical graphic representation of the discriminant analysis revealed significant interception between ME7-A, NBH-A, and NBH-SE astrocytes, with significant differences in Mahalanobis centroid distance ($F_{(7,177)} = 69.89$, $p < 0.0001$) from the ME7-SE astrocytes (Figure 10(e)).

Figure 11 shows graphical representations of cluster analysis of each experimental group (NBH-SE, NBH-EE, ME7-SE, ME7-EE, NBH-A, and ME7-A) to test the hypothesis of occurrence of astrocyte morphological families inside each group. Discriminant analysis and two-tailed t-tests of morphometric features indicate the morphometric features that most contribute to cluster formation and distinguish astrocytes from different morphological families. Note that astrocytes from ME7 groups tended to have larger somas and thicker branches than astrocytes from control groups. Control groups from the SE animals exhibited only two morphological families of astrocytes whereas EE mice showed four distinct morphological families. A third family was found in NBH-EE, showing larger astrocyte trees (surface area) than the other three families. ME7 groups showed in general larger soma and branch surfaces than control mice, distributed into four different families where astrocyte families exhibited larger surface area than control mice astrocyte families. In addition, two of these astrocyte families

from ME7 mice exhibited significantly higher values for branch surface areas than all NBH families. Different from ME7-SE, the ME7-EE group showed only one family with higher surface area than the control NBH-EE group. Aged groups also had three morphometrically distinct families of astrocytes, and the NBH-A group had the family with the lower surface area. Branch surfaces (all groups), soma area (ME7 groups), and branch length (EE and NBH-A groups) were the morphometric features that most contributed to cluster formation.

Astrocyte morphological changes in prion-diseased young adult and aged mice are illustrated in Figure 12. Cluster analysis and canonical distribution of discriminant analysis revealed a clear distinction between NBH and ME7 young adults. Branch volume was the morphometric feature that most contributed to the cluster formation. However, ME7-A and NBH-EE control mice could not be distinguished from one another, suggesting that prion disease in aged mice did not change astrocyte morphology in the same proportion as it did in younger mice. Soma volumes estimated by the nucleator method were linearly correlated with branch surfaces and volumes ($R^2 = 0.83$; $F_{(1,19)} = 94.92$; $p < 0.00001$), suggesting interdependence between these variables.

4. Discussion

The neuropathology of prion disease has been widely investigated in experimental models, contributing new understanding about cellular and molecular mechanisms of chronic neurodegeneration. However, most of previous contributions to understand neuropathology and clinical signs and subjacent neuropathology of prion disease were done at late stages of the disease [5] when motor impairments and posture changes are evident [48, 49]. Before clinical signs (used to define the incubation period), preclinical signs may be apparent including reduction in burrowing activity, anhedonia, and significant increase of open field activity [50]. Burrowing is by far the most sensitive task to detect early hippocampal dysfunction in mouse prion disease which coincides with preclinical stage onset [34]. In this study, we combined three-dimensional reconstruction and an unbiased stereology sampling approach to quantify morphological changes of astrocytes in young and aged diseased animals in the preclinical stage (18 wai) to investigate the hypothesis that EE would slow prion disease progression. Our findings from the DG and CA3 revealed that astrocytes from prion-diseased animals show numerical and morphological differences when compared to control animals. The DG polymorphic layer is targeted by reactive astrocytosis in ME7 groups, showing an increase in cell body volume and number of astrocytes, while in CA3, prion-induced changes were limited to cell body hypertrophy defined as significant increase in the volume of soma. The three-dimensional morphometric analysis of astrocytes from the polymorphic layer of infected animals also revealed significant hypertrophy of proximal and distal segments and significant changes in the branching pattern of astrocytes. EE control animals showed significant changes in morphology of astrocytes from the polymorphic layer
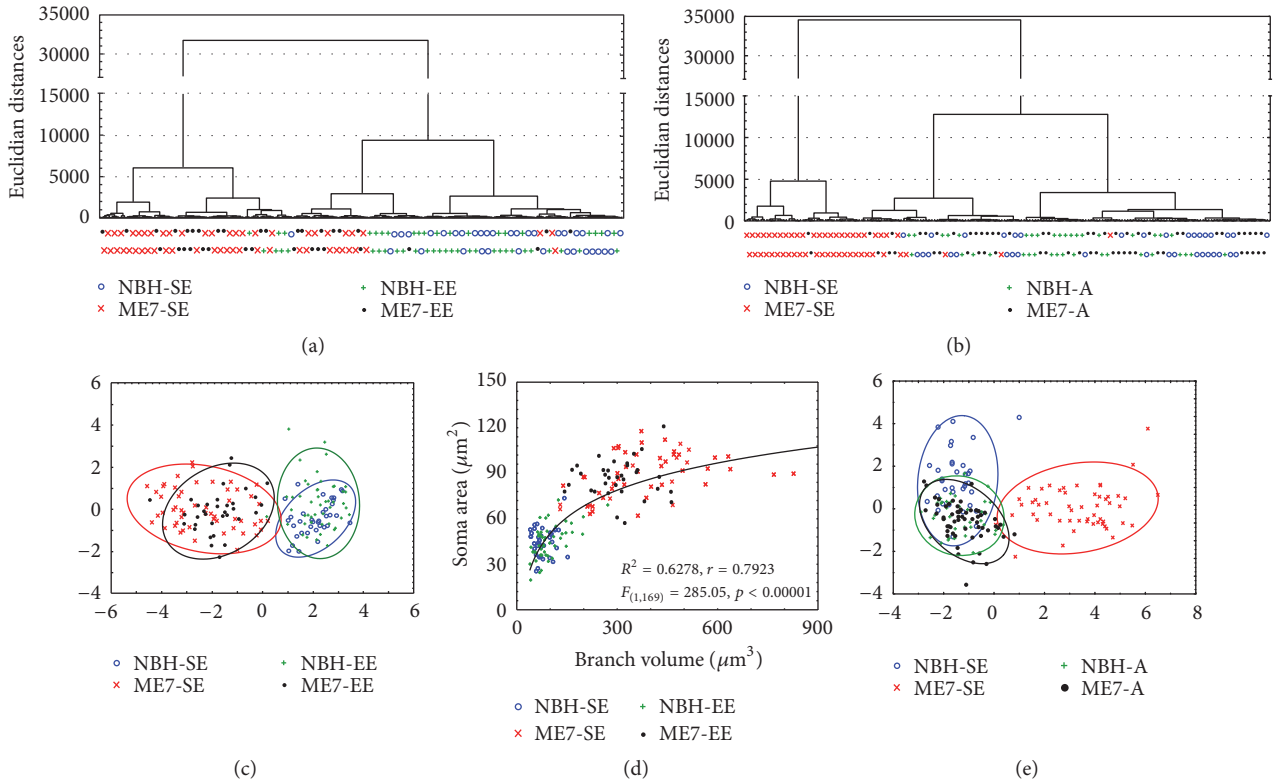
FIGURE 10: Graphic representation of results of multivariate statistical analysis of morphometric features of all reconstructed astrocytes ($n = 269$). (a) Dendrogram illustrating astrocyte morphological phenotypes of the DG polymorphic layer from infected and control adults. Branch length, nodes, and soma area were the morphological features that most contributed to cluster formation in young adult groups. (b) Dendrogram illustrating astrocyte morphological phenotypes of the DG polymorphic layer from infected and control aged mice. Tree surface, soma area, branch length, branch nodes, and tree volumes were the morphological features that most contributed to the cluster formation of SE young adults and aged groups. (c) Canonical distribution of the discriminant analysis of morphological phenotypes of the polymorphic layer from both control and infected adult mice. Canonical analysis based on these morphological features revealed significant Mahalanobis distance between ME7 and NBH astrocytes and (e) between ME7-SE and all others. (d) Significant logarithmic correlation was detected between branch volumes and soma area, suggesting an interdependence between these morphological features.

by increasing the number of branches and the volume of parenchyma covered by astrocyte trees. In addition, EE was associated with increased number and GFAP immunostaining of astrocytes. As compared with prion-diseased SE animals, infected EE mice showed a reduction in the increase in CA3 astrocytic cell bodies, mimicking the effects of EE on astrocyte process volume and spatial distribution in the polymorphic layer of infected animals. In the CA3, aged mice also showed a higher number of astrocytes and significant cell body atrophy in the DG polymorphic layer and CA3. The branches of astrocytes were not significantly altered in aged mice, and prion disease did not affect their morphology. Multivariate statistical methods revealed morphologically distinct subtypes of astrocytes in each experimental group, but the molecular mechanisms and functional implications of such changes remain to be investigated. In the present report we found that ME7-SE, NBH-A, and ME7-A failed to recognize object placement and only ME7-A failed to recognize object identity at 18 wai. The one-trial object recognition task involves memory of a familiar object in parallel with the detection and encoding of a novel object. It has been largely suggested that novelty preference concept should be

used to interpret identity and placement object recognition in many relevant studies, including mice and rats [37, 39, 40, 51]. Indeed, a normal mouse when exposed to a familiar object alongside a novel object frequently spends more time exploring the novel than the familiar object and this has been indicated that a memory of the familiar object is available [38]. However, our findings indicate that NBH-EE spent more time in the stationary object than in displaced object and in the object recognition identity test ME7-SE, NBH-EE, and NBH-A spent more time in the familiar object than the new object.

Because these results are unexpected outcomes for this type of tests previous reports suggest they could be associated with neophobia and anxiety-like behavior [52, 53]. However, the validity of this concept has been recently questioned and the novelty preference model and novelty-bias hypothesis proposed to account for object recognition memory have been reexamined [38, 54]. In addition, neophobia as an explanation of rodents preference for familiar objects has been questioned [54]. To minimize neophobic behavior, we applied in the present report the object recognition protocol described elsewhere [39] in which animals are handling for 7
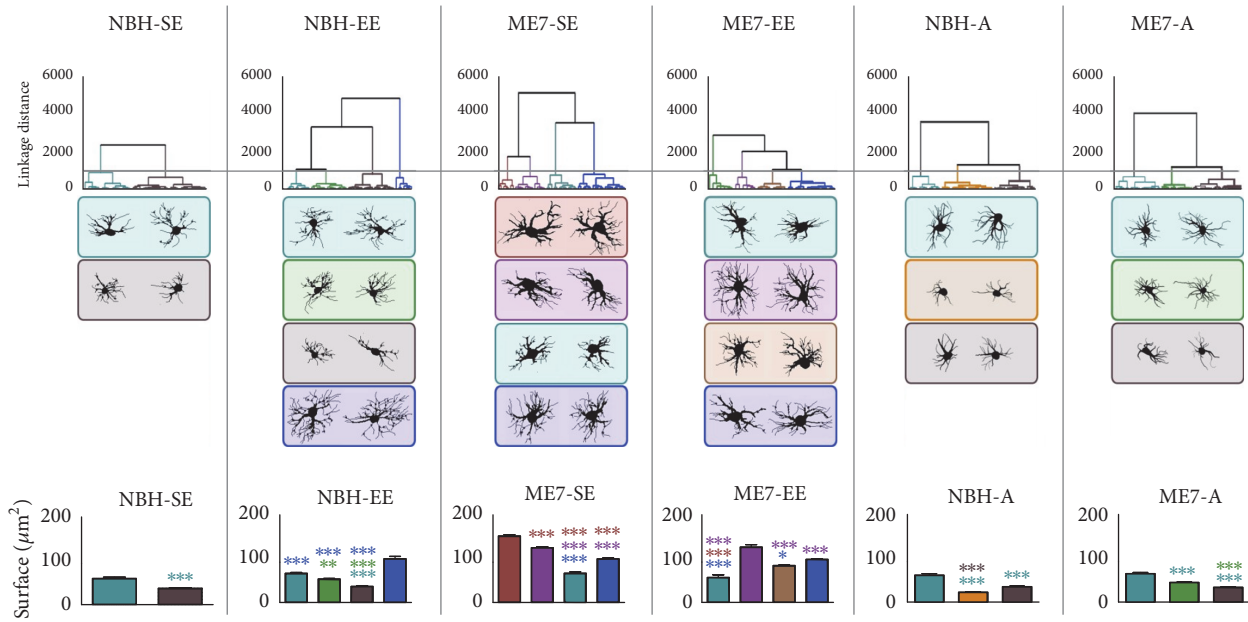
FIGURE 11: Hierarchical cluster analysis of morphological features of astrocytes from the polymorphic layer limited to each experimental group. Astrocytes associated with SE exhibited only two morphological families, whereas those from EE animals showed four distinct morphological families. Astrocytes from ME7 groups were distributed into four different families with a larger surface area, and two of these astrocyte families exhibited significantly higher values for branch surface areas than all NBH families. Aged groups showed three astrocyte families. NBH-A formed a family with smaller surface area, suggesting that SE and aging, acting together, shrank astrocytes trees. In contrast, prion disease increased it. Branch surfaces (from all groups), soma area (from ME7 groups), and branch length (from EE and NBH-A groups) were the morphometric features that most contributed to cluster formation. ($^*P < 0.05$; $^{**}P < 0.01$; $^{***}P < 0.001$, Bonferroni posttests).
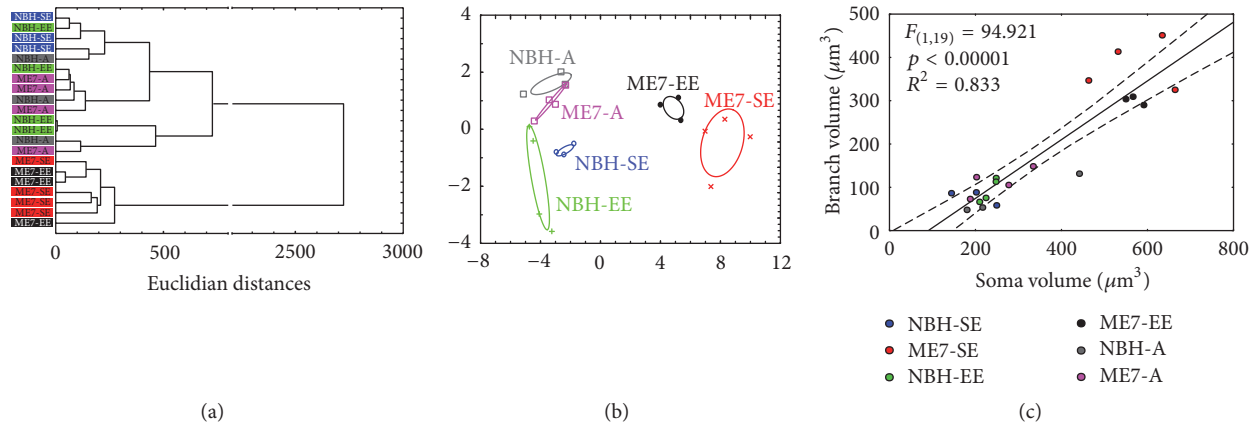
FIGURE 12: Astrocyte morphological changes in prion-diseased adult and aged mice. (a) Cluster analysis and (b) canonical distribution of discriminant analysis. Note the clear distinction between NBH and ME7 young adults in both cluster and discriminant canonical analysis. Branch volume was the morphometric feature that most contributed to the cluster formation. However, ME7-A and NBH-EE control mice occupy the same cluster in the dendrogram, suggesting that prion disease in aged mice did not alter astrocyte morphology as it did in adult mice. (c) Soma volumes estimated by the nucleator method are linearly correlated with branch and volumes.

consecutive days and then introduced to the test apparatus for several sessions of habituation (5 days) without and with objects before the start of the object recognition test. If we succeeded in our attempts to reduce neophobia, it remains a temptation to speculate that significant differences between times spent in the objects (either novel or familiar) are not a consequence of neophobia and do require object recognition (to recognize familiar object) or the absence

of familiarity (to identify new object). In both cases the ability to recognize familiar objects or detect novelty should be intact. Another important issue is related to the fact that aged infected mice did not distinguish object identity. Is this impairment related to prion disease or is this a consequence of aging? Because control aged mice distinguish object identity, it may be possible that prion disease could be associated with this deficit. However, because both normal

and prion-diseased aged mice reduced at the same time window burrowing activity it is reasonable to suggest they may have both hippocampal dysfunction [34]. Whether or not these hippocampal dysfunctions have the same cause remains to be investigated.

4.1. Astrocytic Changes in Albino Swiss Mouse Model of Prion Disease. Astrocytes exhibit typical morphological changes when they are reactive, and the main feature of these changes is an increase in GFAP expression; to our knowledge, this study is the first to describe morphological changes in astrocytic three-dimensional reconstruction in an experimental mouse model of prion disease using a stereological sampling approach to select astrocytes for reconstruction. A single quantification of the total number of astrocytes in experimental models of prion disease by stereological methods was performed previously [27], and the majority of available data are limited to two-dimensional quantification and qualitative analysis. Our previous results [27] and present findings revealed a significant increase in GFAP-immunolabeled astrocytes in the DG polymorphic layer at 18 wai with ME7-infected brain homogenate in both hippocampal formation and dorsal striatum. Although previous findings indicated increased GFAP synthesis as the main protein affected over the time course of prion disease [4], no significant numerical increase in astrocytes was detected by studying cells with double staining for Ki67 and GFAP at 21 wai with ME7-infected brain homogenate in the hippocampus. It remains to be investigated if these differences in GFAP results are related to the adoption of distinct experimental models or technical procedures.

In response to CNS inflammation astrocytes may adopt neurotoxic or neuroprotective functional phenotypes [55]. In the present report the cluster analysis based on surface area (discriminant variable) suggested that astrocytes from polymorphic layer of dentate gyrus of young adult ME7 infected groups include 4 morphological distinct families. The highest values of surface area indicating thicker astrocytes branches correspond to an increase in GFAP expression. Because pro- and anti-inflammatory gene expression induces an increase in glial fibrillary acidic protein expression we do not know, limited to morphological phenotypic analysis, in what direction (neurotoxic or neuroprotective) astrocytic functional polarization is oriented for [56]. Similarly control animals from enriched environment showed two more astrocytic families than controls from standard environment. Although it is reasonable to suggest that environmental enrichment may induce neuroprotective phenotypes, morphological analysis alone is not enough to confirm this hypothesis.

4.2. Relations among Prion Disease and Reactive Astrocytosis in the DG, EE, and Cognitive Function. In homeostatic conditions, the memory formation of recent events is entirely dependent on DG. Indeed, the dendrites of the granular neurons of the DG are the main target of the entorhinal-to-DG projection, and placement of these synapses in the DG molecular layer is the first step in episodic memory formation [57]. The integrity of the DG but not the CA1 is essential to the discrimination of similar objects in different contexts [58]. Given this functional architecture, it is reasonable to propose that astrocyte changes associated with the DG in sick animals may contribute directly to breaking the homeostatic balance of the neuronal microenvironment, alter synaptic function, and compromise the neurogenesis of the subgranular layer. In fact, from the data gathered in this study, it becomes apparent that behavioral changes worsen over the time course of the disease and that this worsening is evident from the performance on hippocampal-dependent tasks. The first signs of hippocampal-dependent sickness that are behavior dependent are observed in burrowing activity tests, nest building, and consumption of glucose, all arising around 12 wai, while motor changes such as open field exploration and muscle strength show signs of change around 18 wai [35]. Our results show that the ME7 injection in the dorsal striatum did not change the temporal course of the disease compared to prion disease induced by hippocampus injection. Injection in both places showed clear hippocampal degeneration and corresponding changes in burrowing activity at 11 wai for SE mice and at 15 wai for EE mice. Previous studies have shown that, regardless of the route of inoculation of the prion agent, the hippocampus is one of the main targets of chronic neurodegeneration associated with the disease [59, 60], and the burrowing test is sensitive and specific to hippocampal damage [34, 61]. As far as we know, our results are the first to demonstrate a spatial memory decline in object recognition associated with reactive astrogliosis in a murine model of prion disease. We are also the first to demonstrate a reduction in the rate of prion disease progression in EE mice.

Physical exercise and multisensory stimulation have been applied as effective nonpharmacological interventions to decrease the rapidity of AD progression. EE is widely used in experimental models in many neurodegenerative diseases, resulting in a growing number of publications investigating the cellular and molecular mechanisms underlying the neuroprotective effects it may confer [14, 15]. Because previous studies have not been conducted to investigate the impact of EE in prion disease, we are left with the comparison with other experimental models using transgenic mice models for AD maintained in EE [16, 17]. In AD (PDAPP-J20) model, EE decreases the volume of GFAP-immunolabeled astrocytes [38]. Similarly, these findings were later confirmed in another transgenic mouse model of AD (3xTg-AD) which showed that mice from EE had a significant decrease in the surface and volume of cell bodies and branches of astrocytes [62]. Our findings are in line with both observations.

In addition, our findings expand previous results and contribute to the understanding of astroglial morphological plasticity in healthy animals exposed to an EE. Indeed; we investigated previously whether aging and environmental-related influences on learning and memory were correlated with astroglial changes in the DG [23]. We demonstrated that episodic-like memory was absent in mice raised in impoverished conditions but was preserved in both young and aged EE mice and these results were associated with a laminar-dependent increased number of astrocytes in both aging and EE. Thus, impoverished conditions seem to be

associated with abnormal cognitive development and an altered laminar distribution of astrocytes in the DG [23].

Therefore, we earlier suggested that astrocytosis in different conditions may arise from different astrocyte phenotypes. Here, we expanded our previous results, which were limited to the molecular layer of the DG, to the polymorphic layer, where we also found an increased number of astrocytes, increased number of branches, and increased volume of the neuropil covered individually by each astrocyte. These results can be compared to those of Viola et al. (2009), in which the two-dimensional reconstruction of astrocytes from the stratum radiatum of CA1 showed increased branching after 8 weeks of EE [25].

Similarly, Sampedro-Piquero et al. [26] demonstrated that improvement in cognitive performance in older EE mice may be related to an increase in GFAP selective immunoreactivity for astrocytes in the DG and CA3 and by increasing the length, number of intersections, and branching nodes of astrocytes of the DG, CA1, and CA3. Moreover, Beauquis and collaborators [62] used confocal microscopy and immunostaining for GFAP to show that CA1 astrocytes increased the branching pattern after 3 months of EE. In pathological conditions, astrocytes from EE animals started to produce neurotrophic factors such as BDNF and GDNF [63] and altered the immune response by promoting neuroprotective cytokine modulation.

Taken together, our results demonstrate for the first time in an albino Swiss mouse ME7 model of prion disease that EE produces reduction in the rate of cognitive decline measured with hippocampal-dependent tasks which was associated decreased reactive astrocytosis. However, in the present report, whereas most young mice revealed both preclinical and neuropathological signs of prion disease, aged mice failed to develop these features. Thus, in contrast to old age, young age may be a risk factor for infectious prion disease following exposure to prion agent [15]. Our findings confirm and expand other reports demonstrating that, in contrast to adult young mice, which succumbed to clinical prion disease, no aged mice exposed to prion agent developed clinical disease [13, 14]. Different though from previous descriptions demonstrating that both aged and young mice infected with scrapie agent directly into the brain were fully susceptible to disease and developed clinical scrapie with similar incubation periods [13], our findings did not reproduce these results. Indeed, in contrast with young adult mice, which showed the full spectrum of clinical and neuropathological signs of prion disease, at least until 18 wai, when all animals were euthanized, neither clinical nor neuropathological features of prion disease were found in ME7-infected aged mice. Because we used the same amount of the same infected ME7 brain homogenate, injected in the same stereotaxic coordinates, it is difficult to explain why albino Swiss aged mice did not become ill. Previous comparisons between prion disease models using albino Swiss mice and C57BL6 revealed that, on average, early behavioral changes in albino Swiss mice start 4 weeks later than in C57BL6 animals [27], so it may be possible that strain differences contributed to these contrasting results. Thus, our data suggest that when the ME7 agent is delivered directly to the brain of albino Swiss mice,

host age can have a significant influence on the onset of clinical disease.

4.3. Technical Limitations. Based on morphological analysis of 3 selective astroglial markers (anti-GFAP, anti-glutamine synthetase, and anti-S-100ß) an emerging view that "astrocytes" constitute a heterogeneous population even within a given region became apparent [64]. Thus, the present report limited to GFAP-immunolabeled astrocytes may show only part of the potential morphological and numerical changes in mouse prion disease model, under influence of age and environmental changes. With such clear limitation in mind, it is worth recalling that previous studies, using stereology, have shown that age [23, 65] and environment [23] appear to induce changes in GFAP-immunolabeled astrocytes in the dentate gyrus. In addition, an enriched environment promoted changes in the astrocytes morphological phenotypes which appeared longer and more ramified [25, 26], stimulating neurogenesis and glycogenesis [66], increasing the network of GFAP-immunolabeled cells [63].

Previous reports using different animal lineages, different histological procedures, and counting methods revealed contradictory results related to the influences of age and environment on the number and morphology of astrocytes [23, 24, 26, 63]. To minimize most sources of nonbiological variation, we standardized all methodological procedures as previously suggested [42, 65]. In addition, due to mechanical factors associated with the vibratome sectioning and further dehydration procedure, a nonuniform shrinkage in the z-axis of the sections is obtained [67]. Thus, estimates of modifications in the x/y dimensions during tissue processing cannot be linearly extrapolated to the z dimension. These methodological constraints impose limitations that should be taken into consideration when analyzing the present data. However, it is important to note that an indication of a severe shrinkage in z-axis is the curling of branches, implying that individual processes did not shrink at the same rate as the slice in which they are located. This pattern was not observed in the reconstructed cells of our study. It was recently demonstrated that the final thickness in the Z-axis is approximately 25% of the cut thickness after dehydration and clearing [45] and therefore we applied 75% shrinkage correction along the z-axis and no corrections to the x/y dimensions. Finally, because microscopic 3D analysis is limited to a small fraction of the whole area of interest, sampling limitation is inevitable. However, as previously described [68], our morphometric analysis of astrocytes combined stereological sampling approach and three-dimensional reconstruction to guarantee that all regions of the areas of interest had the same probability to contribute to the sample of astrocytes three-dimensionally reconstructed.

5. Conclusion

Overall, our findings revealed the beneficial effects of EE in slowing prion disease progression and reducing neuropathological and behavioral outcomes. Moreover, they confirm previous results suggesting that host age is an important barrier to the full-spectrum manifestation of the clinical and

neuropathological features of prion disease. Prion disease neuropathological features have been suggested to be similar to those of AD, but it is important to highlight that, in contrast to AD, a chronic neurodegenerative disorder of the elderly, prion disease does not appear to express its full severity in aged immune systems.

Abbreviations

A: Aged
EE: Enriched environment
GFAP: Glial fibrillary acidic protein
Iba1: Ionized calcium-binding adapter molecule 1
ME7:   Prion strain
NBH: Normal brain homogenate
SE: Standard environment
wai: Weeks after inoculation.

Competing Interests

The authors declare that they have no competing interests.

Acknowledgments

References

[1] B. Caughey and G. S. Baron, "Prions and their partners in crime," *Nature*, vol. 443, no. 7113, pp. 803–810, 2006.

[2] M. Caleo, L. Restani, E. Vannini et al., "The role of activity in synaptic degeneration in a protein misfolding disease, prion disease," *PLoS ONE*, vol. 7, no. 7, Article ID e41182, 2012.

[3] R. S. Hernández, R. Sarasa, A. Toledano, J. J. Badiola, and M. Monzón, "Morphological approach to assess the involvement of astrocytes in prion propagation," *Cell and Tissue Research*, vol. 358, no. 1, pp. 57–63, 2014.

[4] A. A. Asuni, B. Gray, J. Bailey, P. Skipp, V. H. Perry, and V. O'Connor, "Analysis of the hippocampal proteome in ME7 prion disease reveals a predominant astrocytic signature and highlights the brain-restricted production of clusterin in chronic neurodegeneration," *Journal of Biological Chemistry*, vol. 289, no. 7, pp. 4532–4545, 2014.

[5] C. Cunningham, R. Deacon, H. Wells et al., "Synaptic changes characterize early behavioural signs in the ME7 model of murine prion disease," *European Journal of Neuroscience*, vol. 17, no. 10, pp. 2147–2155, 2003.

[6] A. A. Asuni, V. H. Perry, and V. O'Connor, "Change in tau phosphorylation associated with neurodegeneration in the ME7 model of prion disease," *Biochemical Society Transactions*, vol. 38, no. 2, pp. 545–551, 2010.

[7] B. C. Gray, Z. Siskova, V. H. Perry, and V. O'Connor, "Selective presynaptic degeneration in the synaptopathy associated with ME7-induced hippocampal pathology," *Neurobiology of Disease*, vol. 35, no. 1, pp. 63–74, 2009.

[8] R.-H. Yin, L. Tan, T. Jiang, and J.-T. Yu, "Prion-like mechanisms in alzheimer's disease," *Current Alzheimer Research*, vol. 11, no. 8, pp. 755–764, 2014.

[9] B. C. Gray, P. Skipp, V. M. O'Connor, and V. H. Perry, "Increased expression of glial fibrillary acidic protein fragments and μ-calpain activation within the hippocampus of prion-infected mice," *Biochemical Society Transactions*, vol. 34, part 1, pp. 51–54, 2006.

[10] G. S. Victoria, A. Arkhipenko, S. Zhu, S. Syan, and C. Zurzolo, "Astrocyte-to-neuron intercellular prion transfer is mediated by cell-cell contact," *Scientific Reports*, vol. 6, Article ID 20762, 2016.

[11] S. B. Prusiner, "Molecular biology and pathogenesis of prion diseases," *Trends in Biochemical Sciences*, vol. 21, no. 12, pp. 482–487, 1996.

[12] J. F. Diedrich, P. E. Bendheim, Y. S. Kim, R. I. Carp, and A. T. Haase, "Scrapie-associated prion protein accumulates in astrocytes during scrapie infection," *Proceedings of the National Academy of Sciences of the United States of America*, vol. 88, no. 2, pp. 375–379, 1991.

[13] K. L. Brown and N. A. Mabbott, "Evidence of subclinical prion disease in aged mice following exposure to bovine spongiform encephalopathy," *Journal of General Virology*, vol. 95, no. 1, pp. 231–243, 2014.

[14] K. L. Brown, G. J. Wathne, J. Sales, M. E. Bruce, and N. A. Mabbott, "The effects of host age on follicular dendritic cell status dramatically impair scrapie agent neuroinvasion in aged mice," *Journal of Immunology*, vol. 183, no. 8, pp. 5199–5207, 2009.

[15] D. Avrahami and R. Gabizon, "Age-related alterations affect the susceptibility of mice to prion infection," *Neurobiology of Aging*, vol. 32, no. 11, pp. 2006–2015, 2011.

[16] A. Van Dellen, C. Blakemore, R. Deacon, D. York, and A. J. Hannan, "Delaying the onset of Huntington's in mice," *Nature*, vol. 404, no. 6779, pp. 721–722, 2000.

[17] E. Hockly, P. M. Cordery, B. Woodman et al., "Environmental enrichment slows disease progression in R6/2 Huntington's disease mice," *Annals of Neurology*, vol. 51, no. 2, pp. 235–242, 2002.

[18] T. L. Spires, H. E. Grote, N. K. Varshney et al., "Environmental enrichment rescues protein deficits in a mouse model of huntington's disease, indicating a possible disease mechanism," *Journal of Neuroscience*, vol. 24, no. 9, pp. 2270–2276, 2004.

[19] O. Lazarov, J. Robinson, Y.-P. Tang et al., "Environmental enrichment reduces Aβ levels and amyloid deposition in transgenic mice," *Cell*, vol. 120, no. 5, pp. 701–713, 2005.

[20] C. J. Faherty, K. Raviie Shepherd, A. Herasimtschuk, and R. J. Smeyne, "Environmental enrichment in adulthood eliminates neuronal death in experimental Parkinsonism," *Molecular Brain Research*, vol. 134, no. 1, pp. 170–179, 2005.

[21] N. M. Jadavji, B. Kolb, and G. A. Metz, "Enriched environment improves motor function in intact and unilateral dopamine-depleted rats," *Neuroscience*, vol. 140, no. 4, pp. 1127–1138, 2006.

[22] N. C. Stam, J. Nithianantharajah, M. L. Howard, J. D. Atkin, S. S. Cheema, and A. J. Hannan, "Sex-specific behavioural effects of environmental enrichment in a transgenic mouse model of amyotrophic lateral sclerosis," *European Journal of Neuroscience*, vol. 28, no. 4, pp. 717–723, 2008.

[23] D. G. Diniz, C. A. R. Foro, C. M. D. Rego et al., "Environmental impoverishment and aging alter object recognition, spatial learning, and dentate gyrus astrocytes," *European Journal of Neuroscience*, vol. 32, no. 3, pp. 509–519, 2010.

[24] M. Soffié, K. Hahn, E. Terao, and F. Eclancher, "Behavioural and glial changes in old rats following environmental enrichment," *Behavioural Brain Research*, vol. 101, no. 1, pp. 37–49, 1999.

[25] G. G. Viola, L. Rodrigues, J. C. Américo et al., "Morphological changes in hippocampal astrocytes induced by environmental enrichment in mice," *Brain Research*, vol. 1274, pp. 47–54, 2009.

[26] P. Sampedro-Piquero, P. De Bartolo, L. Petrosini, C. Zancada-Menendez, J. L. Arias, and A. Begega, "Astrocytic plasticity as a possible mediator of the cognitive improvements after environmental enrichment in aged rats," *Neurobiology of Learning and Memory*, vol. 114, pp. 16–25, 2014.

[27] R. Borner, J. Bento-Torres, D. R. V. Souza et al., "Early behavioral changes and quantitative analysis of neuropathological features in murine prion disease: stereological analysis in the albino Swiss mice model," *Prion*, vol. 5, no. 3, pp. 215–227, 2011.

[28] M. J. West, "Stereological methods for estimating the total number of neurons and synapses: issues of precision and bias," *Trends in Neurosciences*, vol. 22, no. 2, pp. 51–61, 1999.

[29] M. A. M. Lemmens, H. W. M. Steinbusch, B. P. F. Rutten, and C. Schmitz, "Advanced microscopy techniques for quantitative analysis in neuromorphology and neuropathology research: current status and requirements for the future," *Journal of Chemical Neuroanatomy*, vol. 40, no. 3, pp. 199–209, 2010.

[30] M. J. West, C. H. Kawas, W. F. Stewart, G. L. Rudow, and J. C. Troncoso, "Hippocampal neurons in pre-clinical Alzheimer's disease," *Neurobiology of Aging*, vol. 25, no. 9, pp. 1205–1212, 2004.

[31] D. Goti, S. M. Katzen, J. Mez et al., "A mutant ataxin-3 putative-cleavage fragment in brains of Machado-Joseph disease patients and transgenic mice is cytotoxic above a critical concentration," *Journal of Neuroscience*, vol. 24, no. 45, pp. 10266–10279, 2004.

[32] P. van Loo, L. F. van Zutphen, and V. Baumans, "Male management: coping with aggression problems in male laboratory mice," *Laboratory Animals*, vol. 37, pp. 300–313, 2003.

[33] G. Paxinos and K. Franklin, *The Mouse Brain in Stereotaxic Coordinates*, Academic Press, London, UK, 2001.

[34] R. M. J. Deacon, J. M. Raley, V. H. Perry, and J. N. P. Rawlins, "Burrowing into prion disease," *NeuroReport*, vol. 12, no. 9, pp. 2053–2057, 2001.

[35] C. Cunningham, "Mouse behavioral studies and what they can teach us about prion diseses," in *Neurodegeneration and Prion Disese*, D. Brown, Ed., pp. 111–137, Springer Science + Business Media, New York, NY, USA, 2005.

[36] A. Ennaceur, N. Neave, and J. P. Aggleton, "Spontaneous object recognition and object location memory in rats: the effects of lesions in the cingulate cortices, the medial prefrontal cortex, the cingulum bundle and the fornix," *Experimental Brain Research*, vol. 113, no. 3, pp. 509–519, 1997.

[37] A. Ennaceur and J. Delacour, "A new one-trial test for neurobiological studies of memory in rats. 1: behavioral data," *Behavioural Brain Research*, vol. 31, no. 1, pp. 47–59, 1988.

[38] A. Ennaceur, "One-trial object recognition in rats and mice: methodological and theoretical issues," *Behavioural Brain Research*, vol. 215, no. 2, pp. 244–254, 2010.

[39] E. Dere, J. P. Huston, and M. A. De Souza Silva, "Episodic-like memory in mice: simultaneous assessment of object, place and temporal order memory," *Brain Research Protocols*, vol. 16, no. 1–3, pp. 10–19, 2005.

[40] S. L. Dix and J. P. Aggleton, "Extending the spontaneous preference test of recognition: evidence of object-location and object-context recognition," *Behavioural Brain Research*, vol. 99, no. 2, pp. 191–200, 1999.

[41] S. Shu, G. Ju, and L. Fan, "The glucose oxidase-DAB-nickel method in peroxidase histochemistry of the nervous system," *Neuroscience Letters*, vol. 85, no. 2, pp. 169–171, 1988.

[42] M. J. West, L. Slomianka, and H. J. G. Gundersen, "Unbiased stereological estimation of the total number of neurons in the subdivisions of the rat hippocampus using the optical fractionator," *The Anatomical Record*, vol. 231, no. 4, pp. 482–497, 1991.

[43] H. J. G. Gundersen, P. Bagger, T. F. Bendtsen et al., "The new stereological tools: disector, fractionator, nucleator and point sampled intercepts and their use in pathological research and diagnosis," *APMIS*, vol. 96, no. 10, pp. 857–881, 1988.

[44] A. A. de Sousa, R. R. dos Reis, C. M. de Lima et al., "Three-dimensional morphometric analysis of microglial changes in a mouse model of virus encephalitis: age and environmental influences," *European Journal of Neuroscience*, vol. 42, no. 4, pp. 2036–2050, 2015.

[45] C. N. Carlo and C. F. Stevens, "Analysis of differential shrinkage in frozen brain sections and its implications for the use of guard zones in stereology," *Journal of Comparative Neurology*, vol. 519, no. 14, pp. 2803–2810, 2011.

[46] MicroBright Field I, Ed., *Neurolucida. 2.01 ed*, MicroBright Field, Colchester, UK, 2000, http://www.microbrightfield.com/.

[47] M. Ayres, J. Ayres, D. Ayres et al., *BioEstat 5.0: Aplicações Estatísticas nas Áreas das Ciências Biológicas e Médicas*, Sociedade Civil Mamirauá, Brasília CNPq, Belém, Brazil, 2007.

[48] A. J. Hunter, M. P. Caulfield, and R. H. Kimberlin, "Learning ability of mice infected with different strains of scrapie," *Physiology and Behavior*, vol. 36, no. 6, pp. 1089–1092, 1986.

[49] S. Kempster, M. E. Collins, R. Deacon, and N. Edington, "Impaired motor coordination on static rods in BSE-infected mice," *Behavioural Brain Research*, vol. 154, no. 1, pp. 291–295, 2004.

[50] K. Guenther, R. M. J. Deacon, V. H. Perry, and J. N. P. Rawlins, "Early behavioural changes in scrapie-affected mice and the influence of dapsone," *European Journal of Neuroscience*, vol. 14, no. 2, pp. 401–409, 2001.

[51] A. Vogel-Ciernia and M. A. Wood, "Examining object location and object recognition memory in mice," *Current Protocols in Neuroscience*, vol. 69, no. 8.31, pp. 1–17, 2014.

[52] M. D. Walker and G. Mason, "Female C57BL/6 mice show consistent individual differences in spontaneous interaction with environmental enrichment that are predicted by neophobia," *Behavioural Brain Research*, vol. 224, no. 1, pp. 207–212, 2011.

[53] R. Stryjek, K. Modlińska, and W. Pisula, "Species specific behavioural patterns (digging and swimming) and reaction to novel objects in wild type, Wistar, Sprague-Dawley and Brown Norway rats," *PLoS ONE*, vol. 7, no. 7, Article ID e40642, 2012.

[54] A. Ennaceur, S. Michalikova, and P. L. Chazot, "Do rats really express neophobia towards novel objects? Experimental evidence from exposure to novelty and to an object recognition task in an open space and an enclosed space," *Behavioural Brain Research*, vol. 197, no. 2, pp. 417–434, 2009.

[55] M. K. Jha, W.-H. Lee, and K. Suk, "Functional polarization of neuroglia: implications in neuroinflammation and neurological disorders," *Biochemical Pharmacology*, vol. 103, pp. 1–16, 2016.

[56] E. Jang, J.-H. Kim, S. Lee et al., "Phenotypic polarization of activated astrocytes: the critical role of lipocalin-2 in the classical inflammatory activation of astrocytes," *Journal of Immunology*, vol. 191, no. 10, pp. 5204–5219, 2013.

[57] D. G. Amaral, H. E. Scharfman, and P. Lavenex, "The dentate gyrus: fundamental neuroanatomical organization (dentate gyrus for dummies)," *Progress in Brain Research*, vol. 163, pp. 3–22, 2007.

[58] J. B. Aimone, W. Deng, and F. H. Gage, "Resolving new memories: a critical look at the dentate gyrus, adult neurogenesis, and pattern separation," *Neuron*, vol. 70, no. 4, pp. 589–596, 2011.

[59] M. Russelakis-Carneiro, S. Betmouni, and V. H. Perry, "Inflammatory response and retinal ganglion cell degeneration following intraocular injection of ME7," *Neuropathology and Applied Neurobiology*, vol. 25, no. 3, pp. 196–206, 1999.

[60] R. H. Kimberlin, S. Cole, and C. A. Walker, "Pathogenesis of scrapie is faster when infection is intraspinal instead of intracerebral," *Microbial Pathogenesis*, vol. 2, no. 6, pp. 405–415, 1987.

[61] P. Jirkof, "Burrowing and nest building behavior as indicators of well-being in mice," *Journal of Neuroscience Methods*, vol. 234, pp. 139–146, 2014.

[62] J. Beauquis, P. Pavía, C. Pomilio et al., "Environmental enrichment prevents astroglial pathological changes in the hippocampus of APP transgenic mice, model of Alzheimer's disease," *Experimental Neurology*, vol. 239, no. 1, pp. 28–37, 2013.

[63] L. L. Williamson, A. Chao, and S. D. Bilbo, "Environmental enrichment alters glial antigen expression and neuroimmune function in the adult rat hippocampus," *Brain, Behavior, and Immunity*, vol. 26, no. 3, pp. 500–510, 2012.

[64] J. J. Rodríguez, C.-Y. Yeh, S. Terzieva, M. Olabarria, M. Kulijewicz-Nawrot, and A. Verkhratsky, "Complex and region-specific changes in astroglial markers in the aging brain," *Neurobiology of Aging*, vol. 35, no. 1, pp. 15–23, 2014.

[65] P. R. Mouton, J. M. Long, D.-L. Lei et al., "Age and gender effects on microglia and astrocyte numbers in brains of mice," *Brain Research*, vol. 956, no. 1, pp. 30–35, 2002.

[66] E. S. Yamada, D. W. Marshak, L. C. L. Silveira, and V. A. Casagrande, "Morphology of P and M retinal ganglion cells of the bush baby," *Vision Research*, vol. 38, no. 21, pp. 3345–3352, 1998.

[67] M. Hosseini-Sharifabad and J. R. Nyengaard, "Design-based estimation of neuronal number and individual neuronal volume in the rat hippocampus," *Journal of Neuroscience Methods*, vol. 162, no. 1-2, pp. 206–214, 2007.

[68] D. G. Diniz, M. A. de Oliveira, C. M. de Lima et al., "Age, environment, object recognition and morphological diversity of GFAP-immunolabeled astrocytes," *Behavioral and Brain Functions*, vol. 12, article 28, 2016.

Research Article

Neurodegeneration and Glial Response after Acute Striatal Stroke: Histological Basis for Neuroprotective Studies

**Rafael R. Lima,[1] Luana N. S. Santana,[1] Rafael M. Fernandes,[1]
Elder M. Nascimento,[2] Ana Carolina A. Oliveira,[1] Luanna M. P. Fernandes,[1]
Enio Mauricio N. dos Santos,[1] Patrycy Assis N. Tavares,[2] Ijair Rogério dos Santos,[2]
Adriano Gimarães-Santos,[2] and Walace Gomes-Leal[2]**

[1]*Institute of Biological Sciences, Laboratory of Functional and Structural Biology, Federal University of Pará,
  66075-900 Belém, PA, Brazil*
[2]*Institute of Biological Sciences, Laboratory of Experimental Neuroprotection and Neuroregeneration,
  Federal University of Pará, 66075-900 Belém, PA, Brazil*

Correspondence should be addressed to Rafael R. Lima; rafalima@ufpa.br

Stroke is a leading cause of death and neurological disability worldwide and striatal ischemic stroke is frequent in humans due to obstruction of middle cerebral artery. Several pathological events underlie damage progression and a comprehensive description of the pathological features following experimental stroke in both acute and chronic survival times is a necessary step for further functional studies. Here, we explored the patterns of microglial activation, astrocytosis, oligodendrocyte damage, myelin impairment, and Nogo-A immunoreactivity between 3 and 30 postlesion days (PLDs) after experimental striatal stroke in adult rats induced by microinjections of endothelin-1 (ET-1). The focal ischemia induced tissue loss concomitant with intense microglia activation between 3 and 14 PLDs (maximum at 7 PLDs), decreasing afterward. Astrocytosis was maximum around 7 PLDs. Oligodendrocyte damage and Nogo-A upregulation were higher at 3 PLDs. Myelin impairment was maximum between 7 and 14 PLDs. Nogo-A expression was higher in the first week in comparison to control. The results add important histopathological features of ET-1 induced stroke in subacute and chronic survival times. In addition, the establishment of the temporal evolution of these neuropathological events is an important step for future studies seeking suitable neuroprotective drugs targeting neuroinflammation and white matter damage.

1. Introduction

Stroke is a devastating condition and a leading cause of death and functional disability worldwide [1, 2]. This central nervous system (CNS) disorder is characterized by obstruction of blood vessels (ischemic stroke) or their rupture (hemorrhagic stroke) leading to metabolic collapse and a multitude of secondary mechanisms, including excitotoxicity, inflammation, metabolic acidosis, apoptosis, periinfarct depolarization, and oxidative stress [1, 2].

Following stroke an intense inflammatory response takes place, characterized by recruitment of neutrophils [3, 4], microglial activation [3, 5–7], and astrocytosis [8, 9].

Microglia activation plays both beneficial and detrimental actions following experimental stroke [5, 10, 11]. Inhibition of microglial activation with minocycline induces conspicuous neuroprotection following focal ischemia [12–14], but other experimental reports suggest that microglia may be also beneficial following stroke [10, 15–17].

Astrocytes are activated following both acute [18, 19] and chronic [20] neural disorders. These glial cells play both detrimental and beneficial actions following stroke and spinal cord injury (SCI) [21]. Astrocyte activation may contribute to ischemic damage in the hippocampus by activation of N-methyl-D-aspartate (NMDA) extrasynaptic receptors, a phenomenon involving calcium signaling [19]. On the other

hand, astrocytes seem to mediate endogenous neuroprotection following stroke, a phenomenon involving activation of a glial-specific purinergic receptor, P2Y(1)R, and inositol 1,4,5 trisphosphate IP(3)/Ca^{2++} signaling [22].

Following stroke and SCI, neuroplasticity is inhibited by white matter- (WM-) associated proteins, including Nogo-A and proteoglycans [23]. Chondroitin sulfate proteoglycans (CSPS) are associated with astrocytosis and contribute to inhibition of axonal regeneration following stroke and SCI [24]. Nogo-A is an oligodendrocyte-associated protein and a major inhibitor of axonal sprouting [25, 26]. CSPS degradation with chondroitinase ABC enhances axonal sprouting following SCI [27, 28] and stroke [29, 30]. Similar findings have been found using a neutralizing antibody against Nogo-A [31–34].

In our previous investigations, we have described the patterns of microglial activation [3, 4, 12, 35], astrocytosis [18], and WM damage [3, 4, 35, 36] using experimental models of stroke, excitotoxicity, and SCI. Nevertheless, the pathological events were described up to 7 days from the disease onset. It has been suggested that WM damage with concomitant neuroinflammation is a long-lasting phenomenon even following human stroke [37]. In addition, it has been reported that the expression of Nogo-A is associated with inhibition of neuroplasticity following experimental stroke [31, 32].

Middle cerebral artery occlusion (MCAO) is a common pathological event in human stroke in which striatum and parietal cortex are damaged [37]. A comprehensive descriptive study on the basic neuropathology in both acute and chronic survival times following experimental striatal stroke is a fundamental step for future investigations seeking for neuroprotective and neuroregenerative therapies. In this study, we describe the patterns of microglia activation, astrocytosis, oligodendrocyte damage, Nogo-A immunoreactivity, and myelin impairment from 3 days to 30 days following focal ischemia induced by microinjections of endothelin-1 (ET-1) into the rat striatum.

2. Material and Methods

2.1. Experimental Animals. Male adult Wistar rats (290–300 g) were obtained from the Central Animal Facility in the Federal University of Pará. All animals were housed under standard conditions with food and water available *ad libitum*.

2.2. Ethics Statement. All procedures were approved by the Ethics Committee on Experimental Animals of the Federal University of Pará (CEPAE-UFPA), under license BIO 038-12. All experimental procedures followed the Principles of laboratory animal care (NIH Publication number 86-23, revised 1985). All efforts were made to avoid animal suffering and distress.

2.3. Stroke Model. Animals were deeply anesthetized with an intraperitoneal injection of a mixture of ketamine hydrochloride (90 mg/kg, i.p.) and xylazine hydrochloride (10 mg/kg, i.p.) and positioned in a stereotaxic apparatus after abolishment of their corneal reflex. After craniotomy, 80 pMol of ET-1 (Sigma-Aldrich, USA) in 1 μL of sterile saline was injected into the rat striatum ($N = 5$ per survival time) over a period of 2 min using a glass capillary micropipette. The pipette was left in place for 3 min before being slowly withdrawn. Control animals were injected with the same volume of sterile saline ($N = 12$). We used the following stereotaxic coordinates for the injection (in millimeters relative to bregma): 2.5 mm lateral; 1.2 mm posterior; and 4.5 mm below from the pial surface. After surgery, animals were allowed to rest in their cages (maximum 4 animals per cage) with water and food *ad libitum* until postlesion days (PLDs) 3, 7, 14, and 30. This stroke model was established in our previous reports [3, 13]. The mortality rate is less than 5% in this stroke model.

2.4. Perfusion and Histological Procedures. Following the described survival times, animals were deeply anesthetized with ketamine hydrochloride (90 mg/kg, i.p.) and xylazine hydrochloride (10 mg/kg, i.p.) and transcardially perfused with heparinized 0.9% phosphate-buffered saline (PBS) followed by 4% paraformaldehyde in 0.2 M phosphate buffer. Surgical manipulation was performed only after both corneal and the paw withdraw reflexes were abolished. Brains were removed from the skull, post-fixed for 24 h in the same fixative, and cryoprotected in increasing concentrations of sucrose–glycerol solutions over 7 days. The brains were then frozen in TissueTek and sectioned in order to obtain 20 and 50 μm coronal sections using a cryostat (Carl Zeiss/Micron, Germany). Sections were mounted onto gelatinized slides and air-dried for 24 h. Slides were stored in a freezer at −20°C for posterior histopathological analysis.

2.5. Gross Histopathology and Immunohistochemistry. The ischemic lesion area was visualized in coronal sections (50 μm thick) stained with cresyl violet. The site of ET-1 injection was recognized by tissue pallor associated with loss of cell bodies as described in our previous studies [3, 13, 38].

To analyze microglial activation, we resorted to standard immunohistochemical procedures. Activated microglia/macrophages were labeled using the antibody anti-rat CD68 (clone ED1, 1 : 500, Serotec, UK), which binds to an epitope on the lysosomal membrane of activated macrophages/microglia [38–40], rabbit anti-Iba1 (1 : 1000, WAKO), an antibody that recognizes a calcium binding protein present in the cytoplasm of microglia [41–43], and mouse anti-MHC-II (1 : 100, Serotec), an antibody that recognizes the major histocompatibility complex class II molecule [7].

Based on previous reports showing that pathological oligodendrocytes become Tau-1 positive after brain trauma and ischemia [44], we used the mouse anti-Tau-1 antibody (1 : 500, Chemicon, USA) to label dephosphorylated epitopes on damaged oligodendrocytes. Normal oligodendrocytes were labeled by mouse anti-Nogo-A (1 : 100, BD Transduction Lab, USA), an antibody that recognizes Nogo-A in the rat brain [45]. Myelin impairment was evaluated using an antibody against mouse anti-myelin basic protein (MBP), an important component of the compact myelin (1 : 100, Serotec, UK) [35].

Astrocytes were immunolabeled with an antibody rabbit antiglial fibrillary acid protein (GFAP, 1 : 1000, DAKO, UK), a classical astrocyte marker [18, 46, 47].

2.6. Immunolabeling Protocol. The slide-mounted sections were removed from the freezer, kept in an oven at 37°C for 30 minutes, and rinsed in 0.1 M phosphate buffer saline (PBS) for 5 min. To improve labeling intensity, sections were treated with 0.2 M boric acid (pH 9.0) previously heated to 65°C for 25 min. This temperature was maintained constant over the treatment period. Sections were allowed to cool down for about 20 min and incubated under constant agitation in 1% hydrogen peroxide solution in methanol for 20 min. Sections were then rinsed in 0.05% PBS/Tween (Sigma-Aldrich, USA) solution for 5 min for three times and incubated with 10% normal goat (GFAP, Iba-1) or horse (CD68, MBP, MHC-II, and Tau-1, Nogo-A) serum in PBS for 1 h.

Without further rinsing, sections were then incubated overnight with primary antibody in PBS, rinsed in PBS/Tween solution for 5 min (3 times), and incubated with biotinylated goat anti-rabbit (GFAP and Iba-1) or horse anti-mouse (ED1, MBP, MHC-II, Tau-1, Nogo-A) secondary antibodies (Vector Laboratories, USA) diluted at 1 : 200 or 1 : 100 in PBS, respectively, for 2 h. As a negative control, normal sera, rather the primary antibody, were used in some sections. Sections were rinsed again for 5 min (three times) and incubated in the avidin-biotin-peroxidase complex (ABC Kit, Vector Laboratories, USA) for 2 h. Sections were rinsed four times (5 min each) and revealed with DAB. After DAB reaction, sections were rinsed two times (5 min each) in 0.1 PB, dehydrated, and coverslipped with Entellan (Merck, Germany).

2.7. Qualitative Analysis. All sections stained with the different histological methods were surveyed by light microscopy (Nikon Eclipse E200). Illustrative images from all experimental groups were obtained using a digital camera attached to the microscope (Nikon Eclipse, 50i) using the software Moticam 2500®.

2.8. Quantitative Analysis. We used coronal sections containing the damaged striatum located at 1.2 mm posterior to bregma to count the number of activated macrophages/microglia (CD68+ cells), MHC-II+ cells, pathological oligodendrocytes (Tau-1+ cells), Nogo-A+ cells, and astrocytes (GFAP+ cells) per field. Adjacent 20 μm sections anterior and posterior to the lesion site were used for immunohistochemistry and cell bodies were counted over 1.5 mm from the lesion site. The counting field was defined as a square 0.25 mm wide grid (objective, ×40) in the eyepiece of a microscope. In the ×40 objective, this grid corresponds to an area of 0.0625 mm^2. We counted 9 fields located at the dorsal striatum per section and 3 sections/animal ($N = 5$ animals per group) for all experimental groups (Figure 1).

For quantitative analysis of MBP immunolabeling, photomicrographs were segmented by Color Deconvolution plugin (Gabriel Landini, http://www.dentistry.bham.ac.uk/landinig/software/software.html) from ImageJ software version 1.33-1.34 (NIMH, NIH, Bethesda, MD, USA, https://imagej.nih.gov/ij/). After image segmentation, area values (μm) and percentual fraction of DAB staining on sections were measured [48, 49]. We evaluated 5 sections/animal ($N = 5$ animals per group). Average values were expressed as mean ± S.E.M.

2.9. Statistical Analysis. Means and standard errors were calculated for all groups of data. Comparisons between different groups were assessed by analysis of variance (ANOVA) with Tukey *post hoc* test (one-way ANOVA-Tukey). Statistical significance was accepted at $p < 0.05$. All statistical analyses were performed using the Graphpad Prism 5.0 software.

3. Results

3.1. Focal Ischemia Induced by ET-1 Microinjections into the Rat Striatum. ET-1 microinjections caused a focal ischemic damage characterized by tissue pallor, edema, intense inflammatory response, and loss of cell bodies (Figures 2(c)–2(j)). The tissue damage evolved from 1 day PLD with maximum infiltration of inflammatory cells between 3 and 7 PLDs (Figures 2(c)–2(f)). Mononuclear cells were present at 14 PLDs (Figures 2(g) and 2(h)), but there was a conspicuous decrease in their presence at 30 PLDs (Figures 2(i) and 2(j)). Control animals injected with sterile saline did not present these histopathological findings (Figures 2(a) and 2(b)).

3.2. ET-1 Microinjections Induce Progressive Astrocyte Activation in the Ischemic Striatum. In vehicle animals, astrocytes presented their normal morphology with nonhypertrophic cell bodies and a ramified pattern of their branches (Figures 3(a) and 3(b)). In ischemic animals, there was a progressive astrocyte activation starting from 3 PLDs (Figures 3(c) and 3(d)), with peak between 7 (Figures 3(e) and 3(f)) and 14 PLDs (Figures 3(g) and 3(h)) and clear reduction at 30 PLDs (Figures 3(i) and 3(j)). This activation was characterized by increased cell body volume and ramifications, mainly at 7 (Figures 3(e) and 3(f)) and 14 PLDs (Figures 3(g) and 3(h)).

One-way ANOVA revealed significant changes in the variance of the number of GFAP+ cells ($F_4 = 28.55$; $p < 0.0001$). There was a decrease in the number of GFAP+ cells at 3 PLDs (129.2 ± 5.65) compared to vehicle animals (163.2 ± 6.13; $p < 0.05$). A further decrease occurred from 3 PLDs to 7 (85.00 ± 6.06; $p < 0.001$) and 14 PLDs (78.20 ± 6.93; $p < 0.001$) PLDs. There was a rise in the number of GFAP+ cells at 30 PLDs (113.2 ± 7.38) compared to 7 and 14 PLDs.

3.3. Microinjections of ET-1 Induce Microglia Activation up to 30 Days after Focal Ischemia. Microglial activation was investigated using immunohistochemistry for 3 antibodies: Iba1, CD68, and MHC-II. In control animals, microglia displayed a ramified morphology with small Iba1+ cell bodies, which are characteristic features of resting microglia (Figures 4(a) and 4(b)). After focal ischemia, there was a progressive activation of microglia from 3 PLDs up to 14 PLDs (Figures 4(c)–4(h)). At 30 PLDs, microglia displayed morphological features of resting microglia (Figures 4(i) and 4(j)). The peak of microglia activation was around 7 PLDs (Figures 4(e) and 4(f)).

The Iba1 immunohistochemistry revealed the evolution of the morphological activation of microglia in ischemic animals. At 3 PLDs, there was a decrease in ramified Iba1+ cells in the ischemic site, with increase in amoeboid and

(a)

(b)

(c)
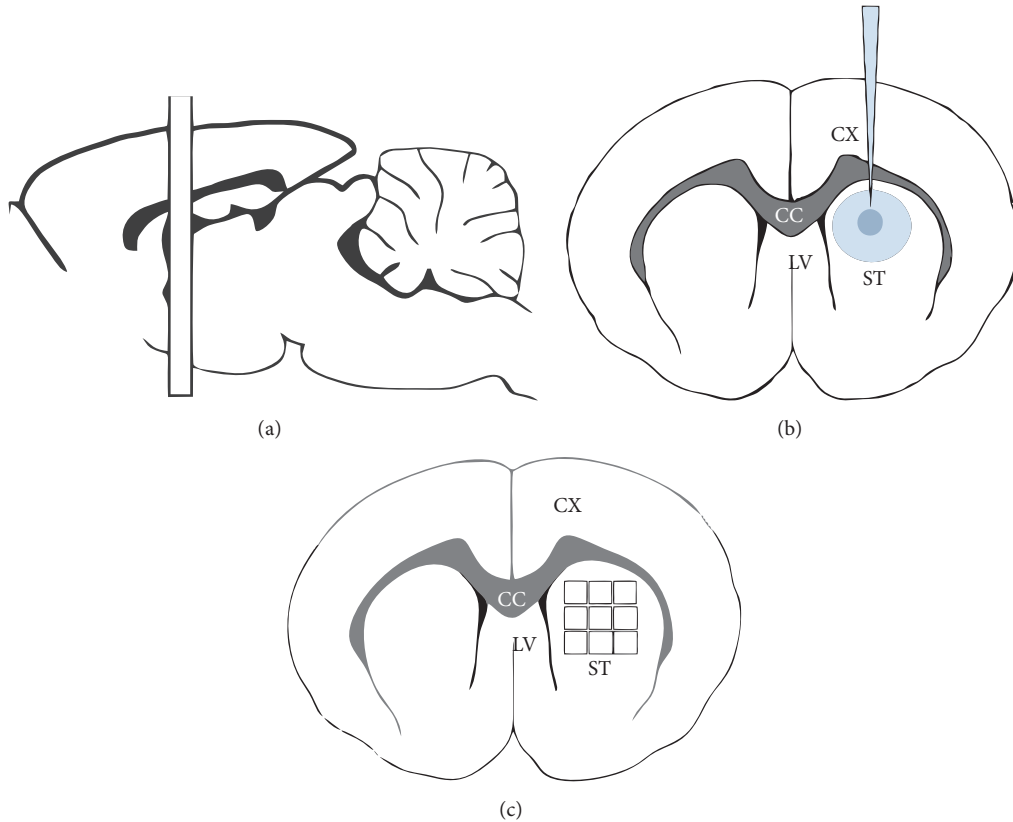
FIGURE 1: Schematic diagram illustrating the striatal injection site of ET-1 and the counting method. Drawing of a parasagittal section depicting the sectioning location (a), illustration of the ET-1 injection site in a coronal section drawing (b), and the location of the counting fields in the rat striatum (c). The squares in (c) are in scale to the counting fields they represent. CX = cortex; CC = corpus callosum; ST = striatum; LV = lateral ventricle.

round Iba1+ cells (Figures 4(c) and 4(d)). The amount of round Iba1+ cells (phagocytes) dramatically increased at the ischemic core at 7 days PLDs (Figures 4(e) and 4(f)). There was a progressive decrease in microglia activation at 14 (Figures 4(g) and 4(h)) and 30 PLDs (Figures 4(i) and 4(j)). At this later PLD, ramified Iba1+ cells were again observed in the ischemic site, despite the presence of some round and amoeboid microglia (Figures 4(i) and 4(j)).

To quantitatively describe the temporal evolution of microglia activation following striatal ischemia, we counted the number of CD68+ cells between 3 and 30 PLDs (Figure 5(k)). The temporal immunoreactivity of CD68+ cells followed that described using the anti-Iba1 antibody (Figures 5(i) and 5(j)). One-way ANOVA revealed significant changes in the variance of the number of CD68+ cells ($F_4 = 96.35$; $p < 0.0001$). The average number of CD68+ cells was 6.44 ± 0.29 cells/field in vehicle animals (Figures 5(a), 5(b), and 5(k)). Subsequent Tukey's *post hoc* comparisons indicated that this number increased to 209.70 ± 13.90, 266.40 ± 9.8, and 218.40 ± 1.69 cells/field at 3, 7, and 14 PLDs, respectively, ($p < 0.001$, Figure 5(k)). There was a considerable decrease in the number of CD68+ cells at 30 PLDs (140.70 ± 7.14; $p < 0.001$), but it remained elevated in comparison to control animals (6.44 ± 0.29; $p < 0.001$, Figures 5(i)–5(k)).

After ET-1 microinjections, there was a progressive expression of MHC-II in the ischemic striatum. The temporal profile of MHC-II expression was similar to those described with Iba1 and CD68, with maximum number of cells at 7 PLDs (Figures 5(l)–5(u) and 5(v)). MHC-II+ cells displayed morphology of activated round microglia (Figures 5(n)–5(u)). The average number of MHC-II+ cells was 5.77 ± 1.06 cells/field in control animals (Figure 5(v)).

One-way ANOVA revealed significant changes in the variance of the number of MHC-II+ cells ($F_4 = 153.1$; $p < 0.0001$). *Post hoc* comparisons indicated that there was a progressive increase in the number of MHC-II+ cells per field at 3 and 7 PLDs, (201.26 ± 1.54; 236.57 ± 14.58; $p < 0.001$, Figure 5(v)). These numbers decreased at 14 and 30 PLDs, respectively (86.20 ± 2.69; 73.20 ± 1.98, $p < 0.001$, Figure 5(v)). All ischemic groups statistically differed from control animals. There was no statistical difference between 14 and 30 PLDs ($p > 0.05$, ANOVA-Tukey).

3.4. Microinjections of ET-1 Induced Progressive Impairment of MBP Immunoreactivity in the Ischemic Striatum. The immunolabeling of the myelin sheath was performed using an anti-MBP antibody [35]. One-way ANOVA revealed significant changes in the variance of the values for MBP
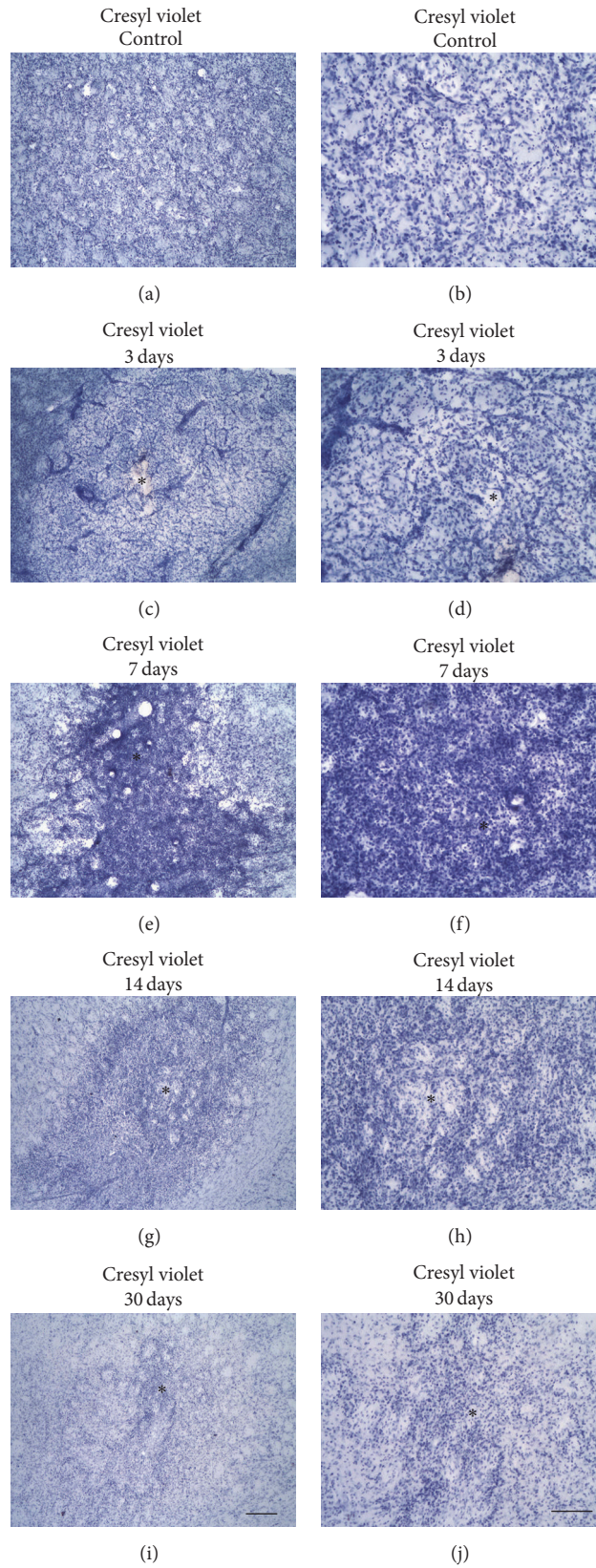
Figure 2: Gross histopathology after ET-1 microinjections revealed by cresyl violet staining. Control animal injected with sterile saline (a-b) or ischemic animals injected with ET-1 at 3 (c-d), 7 (e-f), 14 (g-h), and 30 (i-j) PLDs. Asterisks are in the lesion epicenter. Scale bars: (a), (c), (e), (g), and (i) (200 μm) and (b), (d), (f), (h), and (j) (100 μm).
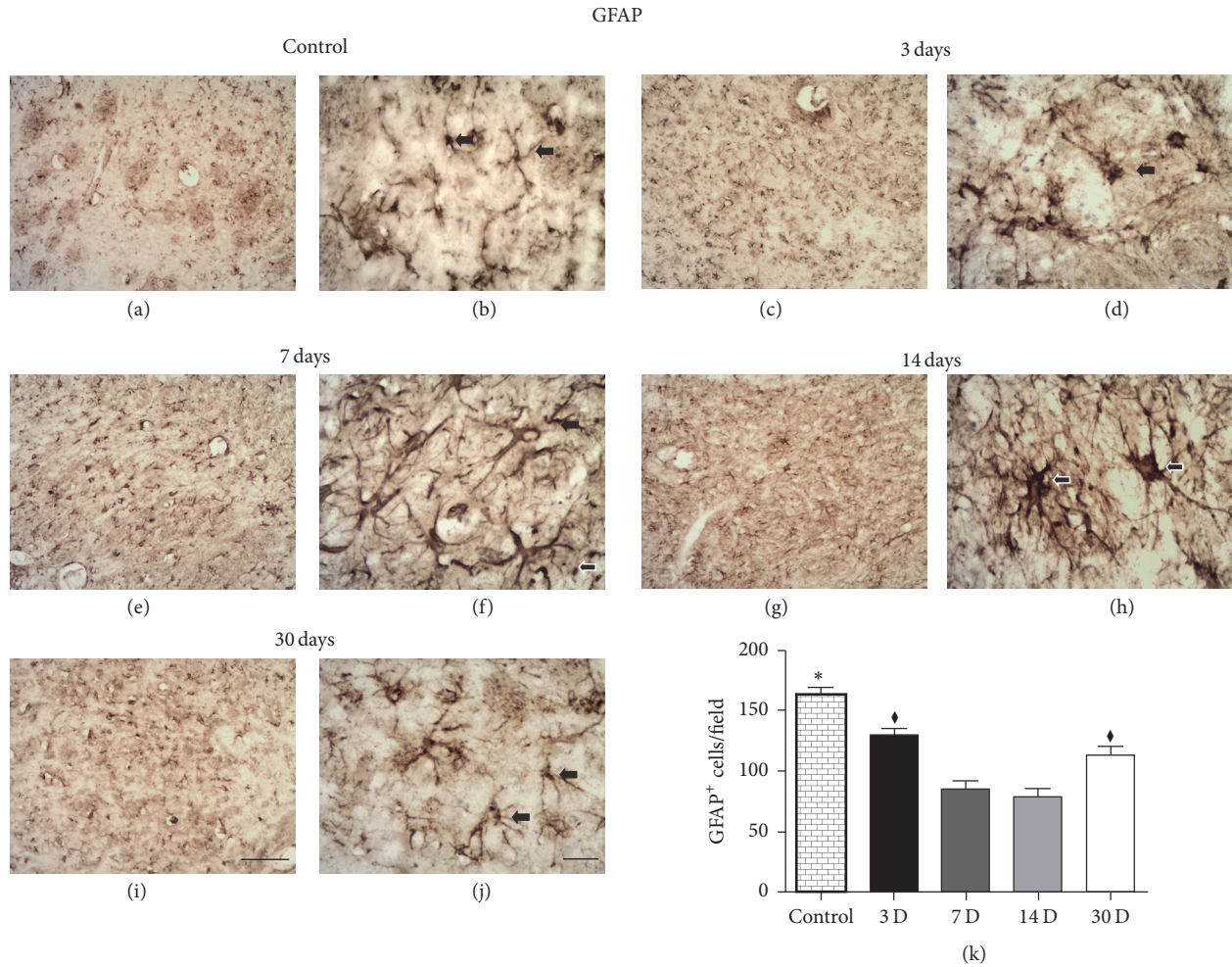
FIGURE 3: Progressive astrocyte activation after striatal focal ischemia. Control animal injected with sterile saline (a-b) or ischemic animals injected with ET-1 at 3 (c-d), 7 (e-f), 14 (g-h), and 30 (i-j) PLDs. Maximum astrocyte activation occurred around 7 and 14 PLDs. The cell density was smaller at 7 and 14 PLDs. $^{*}p < 0.05$ compared to others groups; $^{\blacklozenge}p < 0.05$ compared to 7 and 14 PLDs. Arrows point to astrocytes in the higher power images. Scale bars: (a), (c), (e), (g), and (i) (100 μm) and (b), (d), (f), (h), and (j) (20 μm).

immunoreactivity in the striatum of ischemic animals ($F_4 = 28.97$; $p < 0.0001$). Subsequent Tukey's *post hoc* comparisons indicated that there was a progressive impairment of MBP immunoreactivity after focal ischemia in the rat striatum from 3 days (12.67 ± 0.59; $p < 0.05$, Figure 6(b)) up to 30 days (9.71 ± 0.54; $p < 0.001$, Figure 6(e)) PLDs. The loss of MBP immunoreactivity was maximum at 7 (8.01 ± 0.57; $p < 0.001$, Figure 6(c)) and 14 PLDs (8.17 ± 0.46; $p < 0.001$, Figure 6(d)), but myelin impairment could be also observed at 30 PLDs (Figure 6(e)).

3.5. Microinjections of ET-1 Induce Oligodendrocytes Damage after Striatal Ischemia. It has been shown that Tau-1 is a marker of pathological oligodendrocytes after acute damage to CNS [44, 50, 51]. Control animals expressed a small amount (3.773 ± 1.095/field) of Tau-1+ cells in the striatum (Figures 7(a), 7(b), and 7(k)). Ischemic damage induced a considerable increase in Tau-1 immunoreactivity in the acute phase after focal ischemia (Figure 7). One-way ANOVA revealed significant changes in the variance of the number

of Tau-1+ cells in the striatum of ischemic animals ($F_4 = 153.1$; $p < 0.0001$). Subsequent Tukey's *post hoc* comparisons indicated that the number of Tau-1+ cells/field was 33.56 ± 1.51 at 3 PLDs ($p < 0.001$, Figures 7(c), 7(d), and 7(k)). This number decreased to 14.80 ± 1.49, 2.59 ± 0.55, and 1.46 ± 0.22 at 7, 14, and 30 PLDs compared to 3 PLDs ($p < 0.001$, Figure 7(k)).

3.6. The ET-1-Induced Striatal Ischemic Damage Results in Progressive Increase in Nogo-A Immunoreactivity. Nogo-A is an oligodendrocyte-associated protein involved in the inhibition of axonal growth after acute CNS damage [31, 34]. One-way ANOVA revealed significant chances in the variance of the number of Nogo-A+ cells in the striatum of ischemic animals ($F_4 = 206.2$; $p < 0.0001$). Subsequent Tukey's *post hoc* comparisons indicated that microinjections of ET-1 induced progressive increase in the number of Nogo-A+ cells with peak around 3 PLDs (267.59 ± 5.69; $p < 0.001$), with subsequent decrease at 7 (193.8 ± 3.980; $p < 0.001$), 14 (137.9 ± 137.9; $p < 0.001$), and 30 (112.8 ± 3.39; $p < 0.001$)
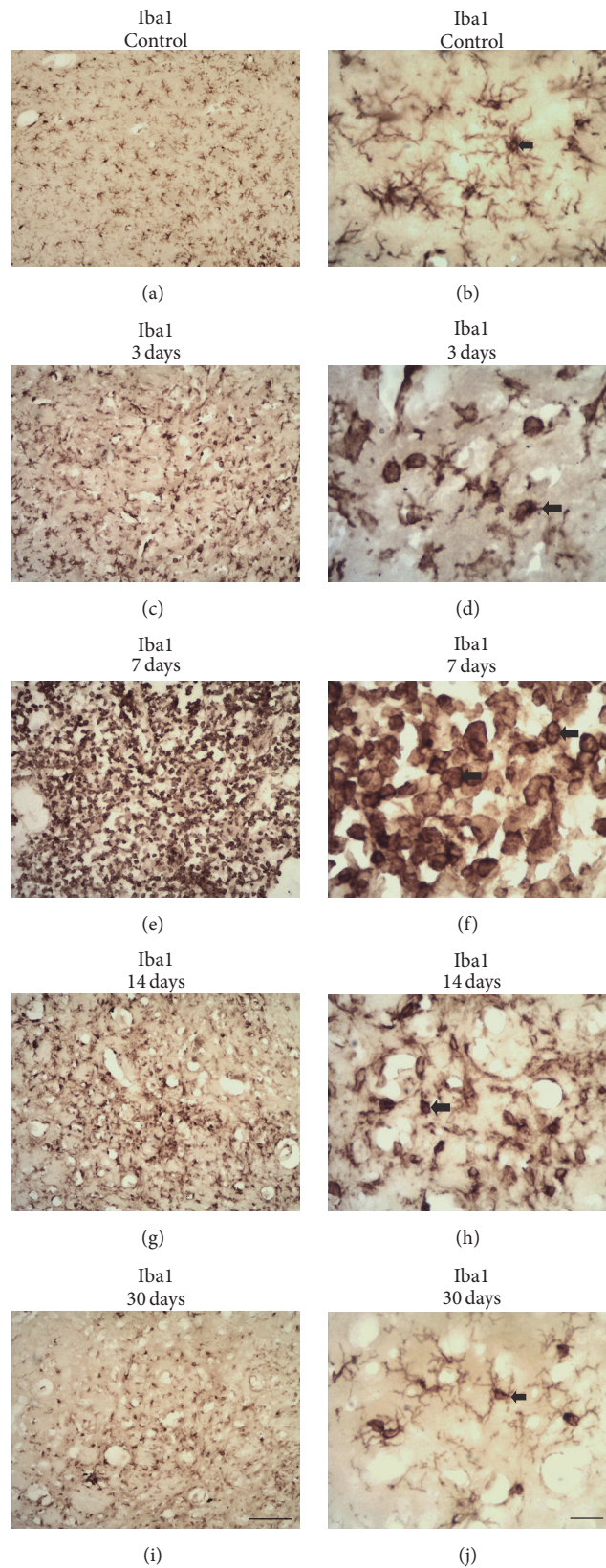
FIGURE 4: Progressive microglia activation after striatal focal ischemia revealed by Iba1 immunohistochemistry. Ramified microglia in a control animal injected with sterile saline (a-b). Morphological activation of microglia at 3 (c-d), 7 (e-f), 14 (g-h), and 30 (i-j) PLDs. Maximum activation occurred around 7 PLDs (e-f). Microglia activation decreased by 30 PLDs (i-j). Arrows point to Iba1+ ramified microglia (b, j) or round macrophages (d, f, h). Scale bars: (a), (c), (e), (g), and (i) (100 μm) and (b), (d), (f), (h), and (j) (20 μm).
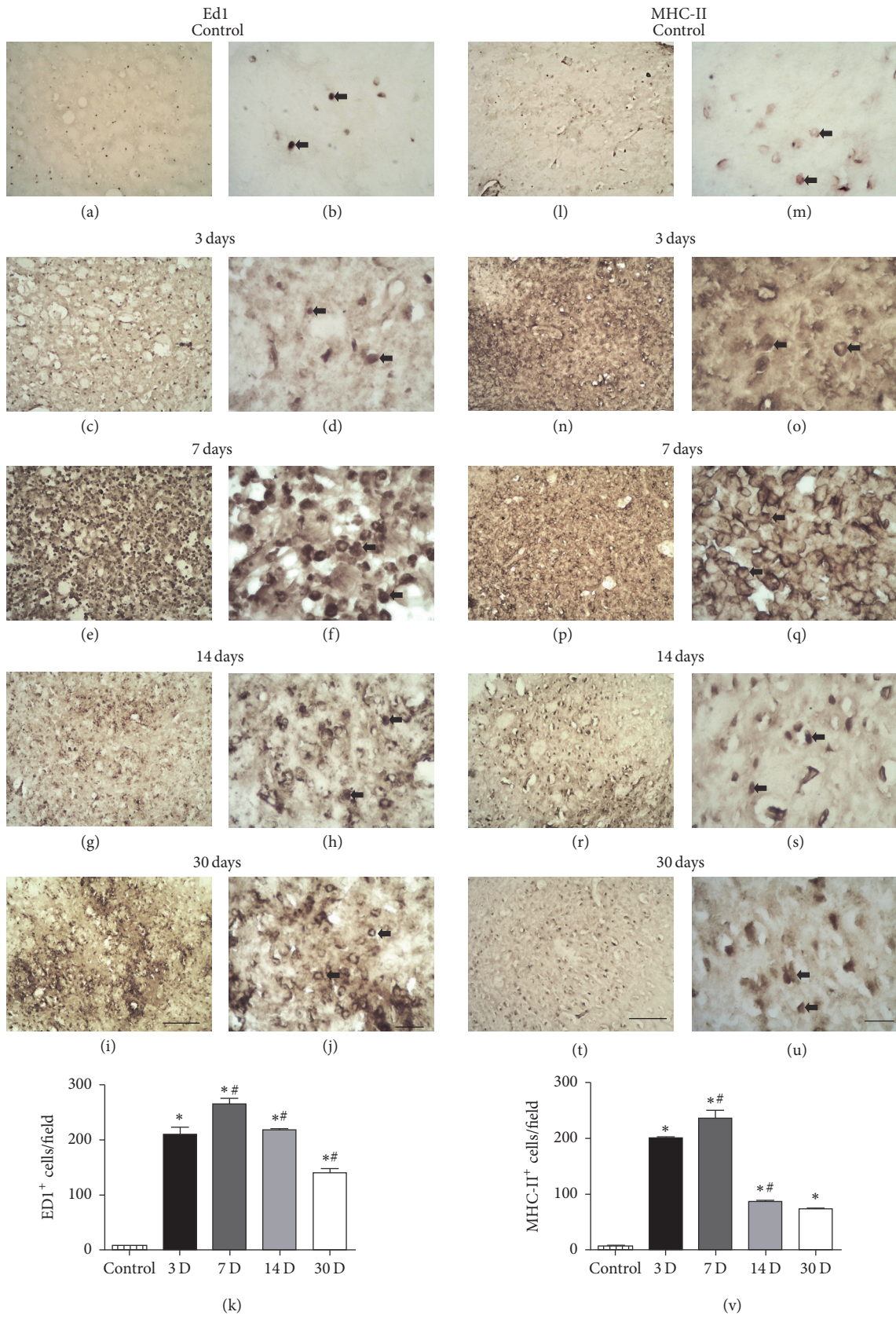
FIGURE 5: Microglia activation revealed by anti-CD68 and MHC-II immunohistochemistry. Control animals injected with sterile saline (a-b, l-m). Morphological activation of CD68+ or MHC-II+ microglia at 3 (c-d, n-o), 7 (e-f, p-q), 14 (g-h, r-s), and 30 (i-j, t-u) PLDs. Both techniques are labeled activated round macrophages (arrows). Quantitative analysis showed maximum number of cells at 7 PLDs with decrease at later survival times (k, v). $^{*}p < 0.05$ compared to control; $^{#}p < 0.05$ compared to previous survival time. Scale bars: (a), (c), (e), (g), (i), (l), (n), (p), (r), and (t) (100 μm) and (b), (d), (f), (h), (j), (m), (o), (q), (s), and (u) (20 μm).
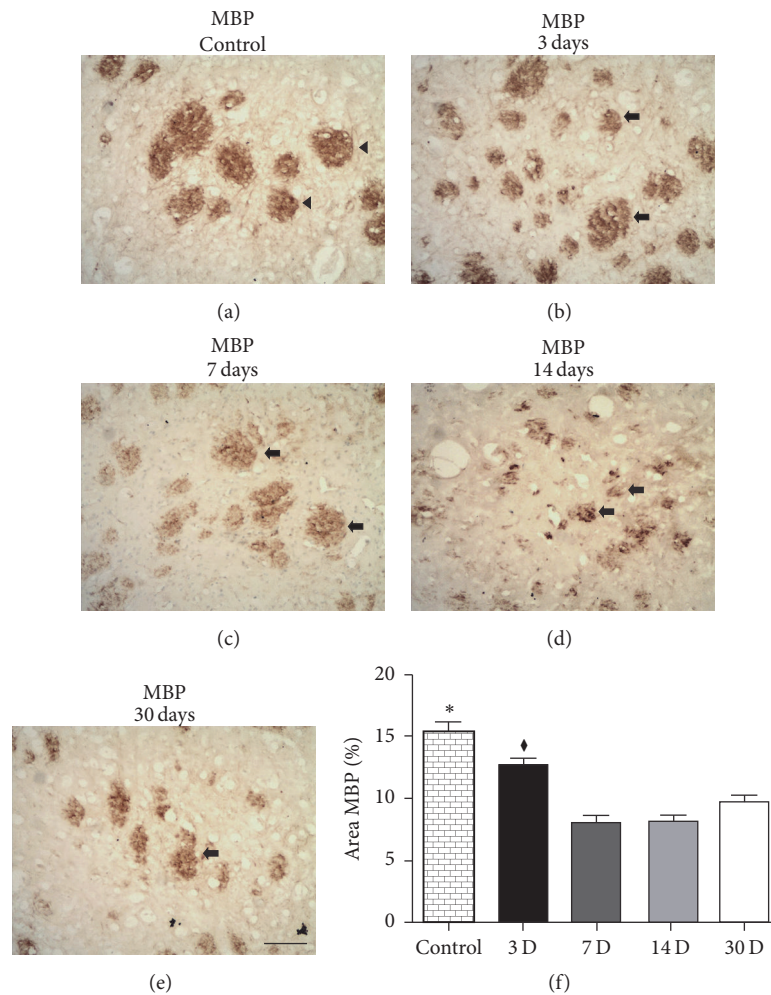
FIGURE 6: Myelin impairment revealed by anti-MBP immunohistochemistry. Control animal injected with sterile saline (a) or ischemic animals injected with ET-1 at 3 (b), 7 (c), 14 (d), and 30 (e) PLDs. There was a progressive impairment of MBP labeled WM tracts (arrows) compared to control (arrow in (a)). Quantitative analysis in (f). $^{*}p < 0.05$ compared to others groups; $^{\blacklozenge}p < 0.05$ compared to others survival time. Arrows point to WM tracts. Scale bars: 100 μm.

PLDs (Figures 7(l)–7(u)). The average number of Nogo-A+ cells in control animals was (97.11 ± 10.47). All ischemic groups statistically differed from the control animals, even at 30 PLDs (Figure 7(v)).

4. Discussion

We have investigated the patterns of glial activation and Tau-1 and Nogo-A immunoreactivity from 3 up to 30 days after microinjections of ET-1 into the striatum of adult rats. The ET-1 model of focal ischemia uses the vasoconstrictor actions of the peptide ET-1 [52, 53]. This peptide causes focal ischemic damage after microinjections into the CNS [54], which is suitable for reproducing the focal strokes frequently occurring in the human brain [55]. In addition, the ET-1 model is easily performed without the complicated surgical procedures of other stroke models like the MCAO intraluminal filament technique, which may induce hyperthermia and other surgical complications [56]. This stroke model has been used in several publications by our group [3, 4, 12, 13].

We thought it would be important to establish the temporal evolution of microglia activation, astrocytosis, oligodendrocyte damage, and Nogo-A immunoreactivity during the first month after ET-1-induced stroke, as a morphological basis for further functional studies seeking new neuroprotective drugs.

Striatal ET-1 microinjections induced progressive astrocyte activation, as revealed by GFAP immunohistochemistry. Maximum activation was present in the first two weeks with a decline at 30 PLDs. This is in agreement with a previous study using the MCAO stroke model [57]. Nevertheless, in this study, the description of GFAP immunoreactivity was incomplete. No illustrations were provided for all survival times. Here, we filled this gap providing a comprehensive description of astrocyte activation from 3 to 30 days after experimental stroke onset.

The mechanisms by which astrocytes are activated after stroke and other neural disorders are not established. The meaning of this glial cell activation has been a matter of
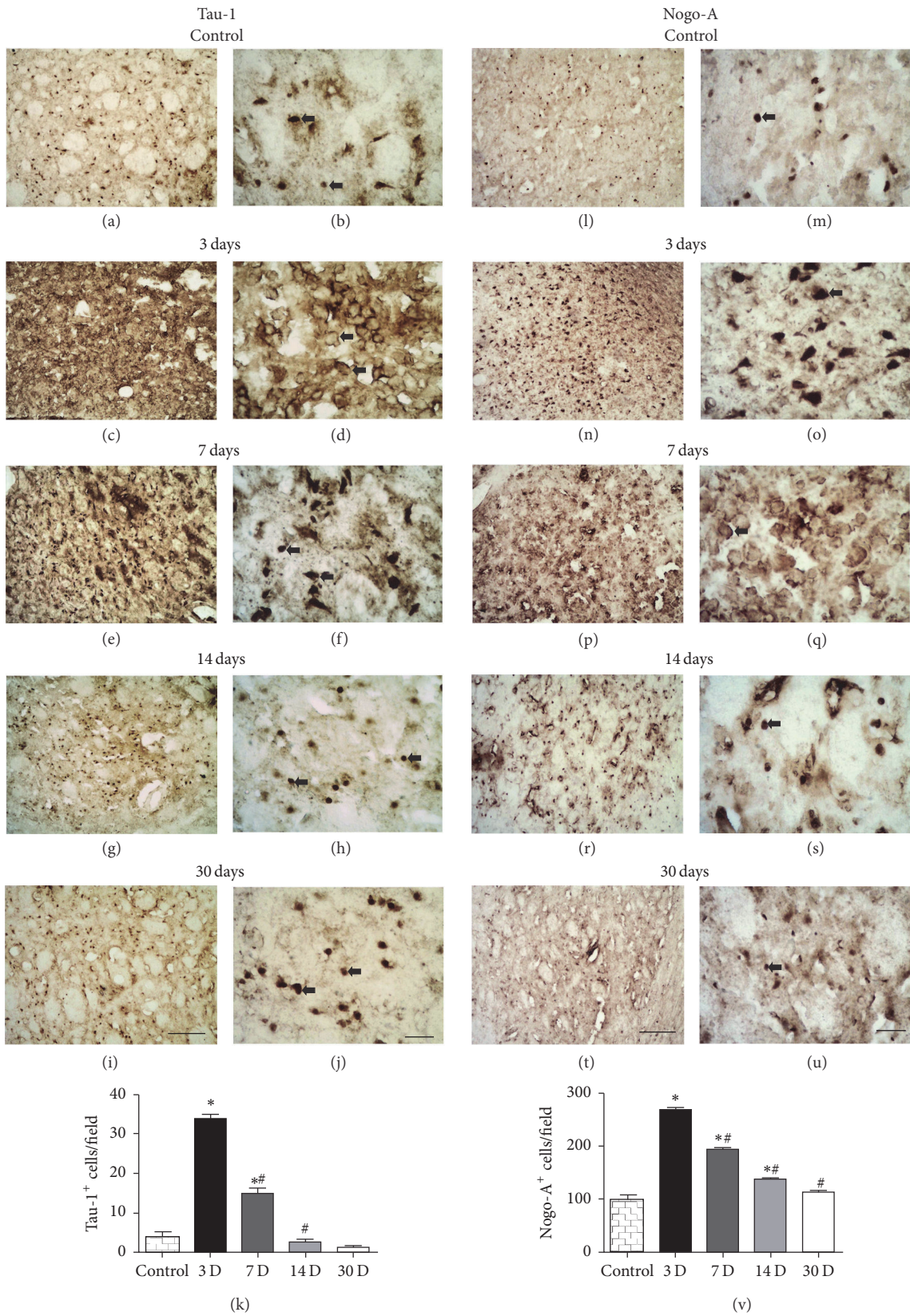
FIGURE 7: Oligodendrocyte damage (Tau-1+ cells) and increased Nogo-A immunoreactivity after focal striatal ischemia. Control animals injected with sterile saline (a-b, l-m). Tau-1 and Nogo-A+ cells at 3 (c-d, n-o), 7 (e-f, p-q), 14 (g-h, r-s), and 30 (i-j, t-u) PLDs. Quantitative analysis showed maximum numbers of Tau-1 and Nogo-A+ cells at 3 PLDs (k, v). There is a long-lasting increase in the number of Nogo-A+ cells up to 30 PLDs compared to control ($p < 0.05$, ANOVA-Tukey). [*] $p < 0.05$ compared to control; [#] $p < 0.05$ compared to previous survival time. Scale bars: (a), (c), (e), (g), (i), (l), (n), (p), (r), and (t) (100 μm) and (b), (d), (f), (h), (j), (m), (o), (q), (s), and (u) (20 μm).

continuous debate for many years [58]. These cells are an important component of the glial scar in chronic survival times after CNS stroke and trauma [59]. The expression of proteoglycans is a biochemical barrier for axonal regeneration concomitant with a mechanical impediment imposed by intense astrocyte reaction and some degree of proliferation [8, 59]. The proliferation of these glial cells is influenced by factors including survivin [60]. Astrocytes may release deleterious molecules including the proinflammatory cytokine tumor necrosis factor-α, metalloproteinases, and reactive oxygen derived species [58, 61].

Nevertheless, astrocyte activation has also beneficial functions after stroke and other neural disorders [58, 62]. Astrocytes seem to contribute to neuroblast migration to striatum after stroke by releasing stroma-derived factor-1α (SDF-1) [63, 64] and monocyte chemoattractant protein 1 (MCP-1) [63]. This is important considering that partial replacement of neuronal loss is afforded by adult neurogenesis after striatal damage [65]. In addition, these glial cells can uptake glutamate in both physiological and ischemic conditions, buffering neurotoxicity [66]. Astrocyte may also release growth factors, including brain-derived neurotrophic factors (BDNF), contributing to neuron survival after stroke in rats [67].

There was intense microglia activation following microinjections of ET-1 into the rat striatum between 3 and 30 days after ischemic onset. Maximum activation occurred around 7 PLDs, but microglia remained activated up to 30 PLDs. These results are in agreement with previous studies using ET-1 stroke model [3, 4, 54] or MCAO [7, 68].

Microglia activation is a general response to any kind of CNS damage [11]. In nonpathological conditions, these brain resident macrophages patrol the CNS using stochastic movements of their fine branches [69, 70]. In pathological conditions like ischemia and trauma, microglia change their morphology becoming amoeboid and highly phagocytic round cells (macrophages) [11, 71]. Concomitant with morphological alterations, microglia change their genetic machinery expressing several types of receptors on their membranes, increased levels of transcription factors, and cytoplasmic enzymes [11].

We have labeled microglia using three antibodies: Iba1, ED1, and MHC-II. Iba1 immunohistochemistry allowed labeling the general population of microglial cells [41]. ED1 and MHC-II labeled a population of activated microglia [7, 39]. ED1 and MHC-II+ cells comprise both macrophages derived from the resident microglia and blood-borne macrophages [72]. These markers do not differentiate the origin of activate macrophages present in the ischemic striatum. It has been shown, using chimeric animals, that resident microglia first respond to the damage followed by hematogenous macrophages [72, 73].

The reasons by which microglia are both detrimental and beneficial after stroke are unknown. Recently, we have hypothesized these glial cells might be beneficial and/or detrimental in different pathological niches following striatal ischemia, a phenomenon likely determined by different concentrations of specific ligands along the pathological environment, which might act on different receptors in the microglia membrane [11]. This is in agreement with a recent study showing that M1 and M2 microglia phenotypes are present in the ischemic striatum following MCAO [74].

Microinjections of ET-1 into the rat striatum induced damage of oligodendrocytes (maximum at 3 PLD) and progressive myelin impairment (maximum between 7 and 14 PLDs). It seems that myelin impairment follows damage to oligodendrocyte cell bodies. It has been shown that oligodendrocytes present structural changes in their cytoskeleton (dephosphorylation) following ischemia, excitotoxicity, and trauma, which is visualized as an increased immunoreactivity for Tau-1 [44, 50, 75]. Tau-1 immunoreactivity has been frequently used as a specific marker of damaged oligodendrocytes [51, 54, 76]. We [51] and other authors have shown that this pathological phenomenon occurs in the acute phase after stroke [54, 76], which is in agreement with the present results. In addition, damage to axonal cylinder may precede both oligodendrocyte damage and myelin impairment. It has been shown that damage to axonal cylinder occurs in an early time point (6 hours) after focal striatal damage induced by ET-1 [72].

The increased immunoreactivity for Tau-1 in oligodendrocytes may be an early event underlying oligodendrocyte pathology [77]. It has been shown that oligodendrocytes but not astrocytes are labeled by Tau-1 after ischemia [77]. The increased immunoreactivity for Tau-1 in oligodendrocytes may represent an attempt to preserve oligodendrocyte cytoskeleton likely from free radicals-mediated damage [51]. This is in agreement with a previous report showing that Tau protein is fundamental for microtubule assembly [78] and that this structure is especially vulnerable to ischemia induced oxidative stress [75, 79]. The decrease in the number of Tau-1+ cells in later survival times in this study may be due to the loss of oligodendrocytes by apoptosis. This hypothesis is supported by a previous report of our group showing that striatal oligodendrocytes become apoptotic in later survival times following excitotoxic damage and that minocycline treatment decreases the number of Tau-1+ cells and partially reverses the apoptotic damage [51]. Several other authors have shown that oligodendrocytes undergo apoptosis following acute neural disorders [80–82]. Further studies should be performed to investigate the mechanisms by which oligodendrocytes are damaged after stroke and to address the therapeutic potential of neuroprotective drugs in reducing the WM demise.

The results show an increased number of Nogo-A+ cells in the acute phase after ET-1 induced stroke. This number remained elevated up to 30 days compared to nonischemic animals. This is in agreement with previous report using the MCAO filament model [45, 83]. The expression of Nogo-A in both neurons and oligodendrocytes is correlated with reduced neuroplasticity after SCI [25, 34, 84] and stroke [31, 83, 85]. Both early and delayed treatments of animals with monoclonal antibodies against Nogo-A increase neuroplasticity in these acute neural disorders [25, 31, 32, 34, 83–85]. Nevertheless, Nogo-A may also be involved in the survival of neurons after ischemia [33]. It follows that the increased expression of Nogo-A in the ischemic striatum can be related to both detrimental and beneficial actions. Further studies

should consider this dual role of Nogo-A before the use of experimental approaches to neutralize the action of this protein.

5. Conclusion

Microinjections of ET-1 into the rat striatum induced conspicuous tissue loss, concomitant with progressive microglia and astrocyte activation, myelin impairment, oligodendrocyte damage, and Nogo-A up regulation. These pathological events were described from 3 to 30 days after ET-1-induced focal striatal ischemia. The establishment of the temporal evolution of these neuropathological events is an important step for future studies in which the manipulation of neuroinflammation and Nogo-A expression may be performed to enhance neuroprotection (in gray and white matter), adult neurogenesis, and functional recovery following striatal ischemic damage. We are addressing these issues in undergoing investigations.

Competing Interests

The authors declare that they have no competing interests.

Authors' Contributions

Rafael R. Lima and Luana N. S. Santana contributed equally to this work. Walace Gomes-Leal, Rafael R. Lima, and Luana N. S. Santana conceived the study, participated in the experimental design, and wrote the manuscript. Enio Mauricio N. dos Santos, Ijair Rogério dos Santos, and Adriano Gimarães-Santos performed stroke analyses. Ana Carolina A. Oliveira, Luanna M. P. Fernandes, and Patrycy Assis N. Tavares performed immunohistochemistry. Elder M. Nascimento contributed to quantitative analysis. All authors read and approved the final manuscript.

Acknowledgments

References

[1] M. A. Moskowitz, E. H. Lo, and C. Iadecola, "The science of stroke: mechanisms in search of treatments," *Neuron*, vol. 67, no. 2, pp. 181–198, 2010.

[2] E. H. Lo and M. Ning, "Mechanisms and challenges in translational stroke research," *Journal of Investigative Medicine*, vol. 64, no. 4, pp. 827–829, 2016.

[3] R. D. Souza-Rodrigues, A. M. R. Costa, R. R. Lima, C. D. Dos Santos, C. W. Picanço-Diniz, and W. Gomes-Leal, "Inflammatory response and white matter damage after microinjections of endothelin-1 into the rat striatum," *Brain Research*, vol. 1200, pp. 78–88, 2008.

[4] C. D. Dos Santos, C. W. Picanço-Diniz, and W. Gomes-Leal, "Differential patterns of inflammatory response, axonal damage and myelin impairment following excitotoxic or ischemic damage to the trigeminal spinal nucleus of adult rats," *Brain Research*, vol. 1172, no. 1, pp. 130–144, 2007.

[5] M. Tóth, P. Little, F. Arnberg et al., "Acute neuroinflammation in a clinically relevant focal cortical ischemic stroke model in rat: longitudinal positron emission tomography and immunofluorescent tracking," *Brain Structure and Function*, vol. 221, no. 3, pp. 1279–1290, 2016.

[6] Z. Zhang, Z. Zhang, H. Lu, Q. Yang, H. Wu, and J. Wang, "Microglial polarization and inflammatory mediators after intracerebral hemorrhage," *Molecular Neurobiology*, 2016.

[7] P. Thored, U. Heldmann, W. Gomes-Leal et al., "Long-term accumulation of microglia with proneurogenic phenotype concomitant with persistent neurogenesis in adult subventricular zone after stroke," *Glia*, vol. 57, no. 8, pp. 835–849, 2009.

[8] G. E. Barreto, X. Sun, L. Xu, and R. G. Giffard, "Astrocyte proliferation following stroke in the mouse depends on distance from the infarct," *PLoS ONE*, vol. 6, no. 11, Article ID e27881, 2011.

[9] P. Cordeau Jr., M. Lalancette-Hébert, Y. C. Weng, and J. Kriz, "Live imaging of neuroinflammation reveals sex and estrogen effects on astrocyte response to ischemic injury," *Stroke*, vol. 39, no. 3, pp. 935–942, 2008.

[10] Z. Chen and B. D. Trapp, "Microglia and neuroprotection," *Journal of Neurochemistry*, vol. 136, supplement 1, pp. 10–17, 2016.

[11] W. Gomes-Leal, "Microglial physiopathology: How to explain the dual role of microglia after acute neural disorders?" *Brain and Behavior*, vol. 2, no. 3, pp. 345–356, 2012.

[12] E. C. S. Franco, M. M. Cardoso, A. Gouvêia, A. Pereira, and W. Gomes-Leal, "Modulation of microglial activation enhances neuroprotection and functional recovery derived from bone marrow mononuclear cell transplantation after cortical ischemia," *Neuroscience Research*, vol. 73, no. 2, pp. 122–132, 2012.

[13] M. M. Cardoso, E. C. S. Franco, C. C. De Souza, M. C. Da Silva, A. Gouveia, and W. Gomes-Leal, "Minocycline treatment and bone marrow mononuclear cell transplantation after endothelin-1 induced striatal ischemia," *Inflammation*, vol. 36, no. 1, pp. 197–205, 2013.

[14] J. Yrjänheikki, T. Tikka, R. Keinänen, G. Goldsteins, P. H. Chan, and J. Koistinaho, "A tetracycline derivative, minocycline, reduces inflammation and protects against focal cerebral ischemia with a wide therapeutic window," *Proceedings of the National Academy of Sciences of the United States of America*, vol. 96, no. 23, pp. 13496–13500, 1999.

[15] M. Lalancette-Hébert, G. Gowing, A. Simard, C. W. Yuan, and J. Kriz, "Selective ablation of proliferating microglial cells exacerbates ischemic injury in the brain," *Journal of Neuroscience*, vol. 27, no. 10, pp. 2596–2605, 2007.

[16] J. Neumann, M. Gunzer, H. O. Gutzeit, O. Ullrich, K. G. Reymann, and K. Dinkel, "Microglia provide neuroprotection after ischemia," *The FASEB Journal*, vol. 20, no. 6, pp. 714–716, 2006.

[17] J. Neumann, S. Sauerzweig, R. Rönicke et al., "Microglia cells protect neurons by direct engulfment of invading neutrophil granulocytes: a new mechanism of CNS immune privilege," *The Journal of Neuroscience*, vol. 28, no. 23, pp. 5965–5975, 2008.

[18] W. Gomes-Leal, D. J. Corkill, M. A. Freire, C. W. Picanço-Diniz, and V. H. Perry, "Astrocytosis, microglia activation, oligodendrocyte degeneration, and pyknosis following acute spinal cord injury," *Experimental Neurology*, vol. 190, no. 2, pp. 456–467, 2004.

[19] Q.-P. Dong, J.-Q. He, and Z. Chai, "Astrocytic Ca^{2+} waves mediate activation of extrasynaptic NMDA receptors in hippocampal neurons to aggravate brain damage during ischemia," *Neurobiology of Disease*, vol. 58, pp. 68–75, 2013.

[20] A. Minagar, P. Shapshak, R. Fujimura, R. Ownby, M. Heyes, and C. Eisdorfer, "The role of macrophage/microglia and astrocytes in the pathogenesis of three neurologic disorders: HIV-associated dementia, Alzheimer disease, and multiple sclerosis," *Journal of the Neurological Sciences*, vol. 202, no. 1-2, pp. 13–23, 2002.

[21] G. R. Choudhury and S. Ding, "Reactive astrocytes and therapeutic potential in focal ischemic stroke," *Neurobiology of Disease*, vol. 85, pp. 234–244, 2016.

[22] W. Zheng, L. Talley Watts, D. M. Holstein, J. Wewer, and J. D. Lechleiter, "P2Y1R-initiated, IP3R-dependent stimulation of astrocyte mitochondrial metabolism reduces and partially reverses ischemic neuronal damage in mouse," *Journal of Cerebral Blood Flow and Metabolism*, vol. 33, no. 4, pp. 600–611, 2013.

[23] G. Yiu and Z. He, "Glial inhibition of CNS axon regeneration," *Nature Reviews Neuroscience*, vol. 7, no. 8, pp. 617–627, 2006.

[24] C. M. Galtrey and J. W. Fawcett, "The role of chondroitin sulfate proteoglycans in regeneration and plasticity in the central nervous system," *Brain Research Reviews*, vol. 54, no. 1, pp. 1–18, 2007.

[25] M. S. Chen, A. B. Huber, M. E. Van Der Haar et al., "Nogo-A is a myelin-associated neurite outgrowth inhibitor and an antigen for monoclonal antibody IN-1," *Nature*, vol. 403, no. 6768, pp. 434–439, 2000.

[26] T. Wang, J.-Q. Xiong, X.-B. Ren, and W. Sun, "The role of Nogo-A in neuroregeneration: a review," *Brain Research Bulletin*, vol. 87, no. 6, pp. 499–503, 2012.

[27] E. J. Bradbury, L. D. F. Moon, R. J. Popat et al., "Chondroitinase ABC promotes functional recovery after spinal cord injury," *Nature*, vol. 416, no. 6881, pp. 636–640, 2002.

[28] E. J. Bradbury and L. M. Carter, "Manipulating the glial scar: chondroitinase ABC as a therapy for spinal cord injury," *Brain Research Bulletin*, vol. 84, no. 4-5, pp. 306–316, 2011.

[29] J. J. Hill, K. Jin, X. O. Mao, L. Xie, and D. A. Greenberg, "Intracerebral chondroitinase ABC and heparan sulfate proteoglycan glypican improve outcome from chronic stroke in rats," *Proceedings of the National Academy of Sciences of the United States of America*, vol. 109, no. 23, pp. 9155–9160, 2012.

[30] S. Soleman, P. K. Yip, D. A. Duricki, and L. D. F. Moon, "Delayed treatment with chondroitinase ABC promotes sensorimotor recovery and plasticity after stroke in aged rats," *Brain*, vol. 135, no. 4, pp. 1210–1223, 2012.

[31] A. B. Seymour, E. M. Andrews, S.-Y. Tsai et al., "Delayed treatment with monoclonal antibody IN-1 1 week after stroke results in recovery of function and corticorubral plasticity in adult rats," *Journal of Cerebral Blood Flow and Metabolism*, vol. 25, no. 10, pp. 1366–1375, 2005.

[32] C. M. Papadopoulos, S.-Y. Tsai, J. L. Cheatwood et al., "Dendritic plasticity in the adult rat following middle cerebral artery occlusion and Nogo-a neutralization," *Cerebral Cortex*, vol. 16, no. 4, pp. 529–536, 2006.

[33] E. Kilic, A. Elali, U. Kilic et al., "Role of Nogo-A in neuronal survival in the reperfused ischemic brain," *Journal of Cerebral Blood Flow and Metabolism*, vol. 30, no. 5, pp. 969–984, 2010.

[34] L. Schnell and M. E. Schwab, "Axonal regeneration in the rat spinal cord produced by an antibody against myelin-associated neurite growth inhibitors," *Nature*, vol. 343, no. 6255, pp. 269–272, 1990.

[35] R. R. Lima, J. Guimaraes-Silva, J. L. Oliveira et al., "Diffuse axonal damage, myelin impairment, astrocytosis and inflammatory response following microinjections of NMDA into the rat striatum," *Inflammation*, vol. 31, no. 1, pp. 24–35, 2008.

[36] W. Gomes-Leal, D. J. Corkill, and C. W. Picanço-Diniz, "Systematic analysis of axonal damage and inflammatory response in different white matter tracts of acutely injured rat spinal cord," *Brain Research*, vol. 1066, no. 1-2, pp. 57–70, 2005.

[37] A. Thiel and W.-D. Heiss, "Imaging of microglia activation in stroke," *Stroke*, vol. 42, no. 2, pp. 507–512, 2011.

[38] G. B. Oliveira, E. D. A. Fontes Jr., S. De Carvalho et al., "Minocycline mitigates motor impairments and cortical neuronal loss induced by focal ischemia in rats chronically exposed to ethanol during adolescence," *Brain Research*, vol. 1561, pp. 23–34, 2014.

[39] C. D. Dijkstra, E. A. Döpp, P. Joling, and G. Kraal, "The heterogeneity of mononuclear phagocytes in lymphoid organs: distinct macrophage subpopulations in rat recognized by monoclonal antibodies ED1, ED2 and ED3," *Advances in Experimental Medicine and Biology*, vol. 186, pp. 409–419, 1985.

[40] R. S. Lopes, M. M. Cardoso, A. O. Sampaio et al., "Indomethacin treatment reduces microglia activation and increases numbers of neuroblasts in the subventricular zone and ischaemic striatum after focal ischaemia," *Journal of Biosciences*, vol. 41, no. 3, pp. 381–394, 2016.

[41] D. Ito, Y. Imai, K. Ohsawa, K. Nakajima, Y. Fukuuchi, and S. Kohsaka, "Microglia-specific localisation of a novel calcium binding protein, Iba1," *Molecular Brain Research*, vol. 57, no. 1, pp. 1–9, 1998.

[42] A. C. A. Oliveira, M. C. S. Pereira, L. N. D. S. Santana et al., "Chronic ethanol exposure during adolescence through early adulthood in female rats induces emotional and memory deficits associated with morphological and molecular alterations in hippocampus," *Journal of Psychopharmacology*, vol. 29, no. 6, pp. 712–724, 2015.

[43] F. B. Teixeira, L. N. D. S. Santana, F. R. Bezerra et al., "Chronic ethanol exposure during adolescence in rats induces motor impairments and cerebral cortex damage associated with oxidative stress," *PLoS ONE*, vol. 9, no. 6, Article ID e101074, 2014.

[44] E. A. Irving, J. Nicoll, D. I. Graham, and D. Dewar, "Increased tau immunoreactivity in oligodendrocytes following human stroke and head injury," *Neuroscience Letters*, vol. 213, no. 3, pp. 189–192, 1996.

[45] J. L. Cheatwood, A. J. Emerick, M. E. Schwab et al., "Nogo-a expression after focal ischemic stroke in the adult rat," *Stroke*, vol. 39, no. 7, pp. 2091–2098, 2008.

[46] E. A. Fontes-Júnior, C. S. Maia, L. M. Fernandes et al., "Chronic alcohol intoxication and cortical ischemia: study of their comorbidity and the protective effects of minocycline," *Oxidative Medicine and Cellular Longevity*, vol. 2016, Article ID 1341453, 10 pages, 2016.

[47] A. F. Silva Jr., M. S. S. Aguiar, O. S. Carvalho Jr. et al., "Hippocampal neuronal loss, decreased GFAP immunoreactivity and cognitive impairment following experimental intoxication of rats with aluminum citrate," *Brain Research*, vol. 1491, pp. 23–33, 2013.

[48] N. C. Fagundes, L. M. Fernandes, R. S. Paraense et al., "Binge drinking of ethanol during adolescence induces oxidative damage and morphological changes in salivary glands of female rats," *Oxidative Medicine and Cellular Longevity*, vol. 2016, Article ID 7323627, 11 pages, 2016.

[49] L. M. P. Fernandes, F. B. Teixeira, S. M. A. Junior, J. D. J. V. Pinheiro, C. D. S. F. Maia, and R. R. Lima, "Immunohistochemical changes and atrophy after chronic ethanol intoxication in rat salivary glands," *Histology and Histopathology*, vol. 30, no. 9, pp. 1069–1078, 2015.

[50] E. A. Irving, D. L. Bentley, and A. A. Parsons, "Assessment of white matter injury following prolonged focal cerebral ischaemia in the rat," *Acta Neuropathologica*, vol. 102, no. 6, pp. 627–635, 2001.

[51] J. S. Guimarães, M. A. M. Freire, R. R. Lima, C. W. Picanço-Diniz, A. Pereira, and W. Gomes-Leal, "Minocycline treatment reduces white matter damage after excitotoxic striatal injury," *Brain Research*, vol. 1329, pp. 182–193, 2010.

[52] K. Fuxe, A. Cintra, B. Andbjer, E. Anggard, M. Goldstein, and L. F. Agnati, "Centrally administered endothelin-1 produces lesions in the brain of the male rat," *Acta Physiologica Scandinavica*, vol. 137, no. 1, pp. 155–156, 1989.

[53] L. F. Agnati, M. Zoli, M. Kurosawa et al., "A new model of focal brain ischemia based on the intracerebral injection of endothelin-1," *Italian Journal of Neurological Sciences*, vol. 12, no. 3, supplement 11, pp. 49–53, 1991.

[54] P. M. Hughes, D. C. Anthony, M. Ruddin et al., "Focal lesions in the rat central nervous system induced by endothelin-1," *Journal of Neuropathology and Experimental Neurology*, vol. 62, no. 12, pp. 1276–1286, 2003.

[55] H. Delavaran, H. Sjunnesson, A. Arvidsson et al., "Proximity of brain infarcts to regions of endogenous neurogenesis and involvement of striatum in ischaemic stroke," *European Journal of Neurology*, vol. 20, no. 3, pp. 473–479, 2013.

[56] Q. Zhao, H. Memezawa, M.-L. Smith, and B. K. Siejö, "Hyperthermia complicates middle cerebral artery occlusion induced by an intraluminal filament," *Brain Research*, vol. 649, no. 1-2, pp. 253–259, 1994.

[57] R. K. Clark, E. V. Lee, C. J. Fish et al., "Development of tissue damage, inflammation and resolution following stroke: An Immunohistochemical and Quantitative Planimetric Study," *Brain Research Bulletin*, vol. 31, no. 5, pp. 565–572, 1993.

[58] A. Buffo, C. Rolando, and S. Ceruti, "Astrocytes in the damaged brain: molecular and cellular insights into their reactive response and healing potential," *Biochemical Pharmacology*, vol. 79, no. 2, pp. 77–89, 2010.

[59] G. Stoll, S. Jander, and M. Schroeter, "Inflammation and glial responses in ischemic brain lesions," *Progress in Neurobiology*, vol. 56, no. 2, pp. 149–171, 1998.

[60] S. Sukumari-Ramesh, C. H. Alleyne, and K. M. Dhandapani, "Astrocyte-specific expression of survivin after intracerebral hemorrhage in mice: a possible role in reactive gliosis?" *Journal of Neurotrauma*, vol. 29, no. 18, pp. 2798–2804, 2012.

[61] H. Neumann, R. Schweigreiter, T. Yamashita, K. Rosenkranz, H. Wekerle, and Y.-A. Barde, "Tumor necrosis factor inhibits neurite outgrowth and branching of hippocampal neurons by a Rho-dependent mechanism," *The Journal of Neuroscience*, vol. 22, no. 3, pp. 854–862, 2002.

[62] G. Barreto, R. E. White, Y. Ouyang, L. Xu, and R. G. Giffard, "Astrocytes: targets for neuroprotection in stroke," *Central Nervous System Agents in Medicinal Chemistry*, vol. 11, no. 2, pp. 164–173, 2011.

[63] Y.-P. Yan, K. A. Sailor, B. T. Lang, S.-W. Park, R. Vemuganti, and R. J. Dempsey, "Monocyte chemoattractant protein-1 plays a critical role in neuroblast migration after focal cerebral ischemia," *Journal of Cerebral Blood Flow & Metabolism*, vol. 27, no. 6, pp. 1213–1224, 2007.

[64] P. Thored, A. Arvidsson, E. Cacci et al., "Persistent production of neurons from adult brain stem cells during recovery after stroke," *Stem Cells*, vol. 24, no. 3, pp. 739–747, 2006.

[65] A. Arvidsson, T. Collin, D. Kirik, Z. Kokaia, and O. Lindvall, "Neuronal replacement from endogenous precursors in the adult brain after stroke," *Nature Medicine*, vol. 8, no. 9, pp. 963–970, 2002.

[66] O. P. Ottersen, J. H. Laake, W. Reichelt, F.-M. Haug, and R. Torp, "Ischemic disruption of glutamate homeostasis in brain: quantitative immunocytochemical analyses," *Journal of Chemical Neuroanatomy*, vol. 12, no. 1, pp. 1–14, 1996.

[67] Y. Béjot, A. Prigent-Tessier, C. Cachia et al., "Time-dependent contribution of non neuronal cells to BDNF production after ischemic stroke in rats," *Neurochemistry International*, vol. 58, no. 1, pp. 102–111, 2011.

[68] T. Morioka, A. N. Kalehua, and W. J. Streit, "Characterization of microglial reaction after middle cerebral artery occlusion in rat brain," *Journal of Comparative Neurology*, vol. 327, no. 1, pp. 123–132, 1993.

[69] A. Nimmerjahn, F. Kirchhoff, and F. Helmchen, "Neuroscience: resting microglial cells are highly dynamic surveillants of brain parenchyma in vivo," *Science*, vol. 308, no. 5726, pp. 1314–1318, 2005.

[70] D. Davalos, J. Grutzendler, G. Yang et al., "ATP mediates rapid microglial response to local brain injury in vivo," *Nature Neuroscience*, vol. 8, no. 6, pp. 752–758, 2005.

[71] W. J. Streit, "Microglia and the response to brain injury," *Ernst Schering Research Foundation Workshop*, no. 39, pp. 11–24, 2002.

[72] M. Schilling, M. Besselmann, M. Müller, J. K. Strecker, E. B. Ringelstein, and R. Kiefer, "Predominant phagocytic activity of resident microglia over hematogenous macrophages following transient focal cerebral ischemia: an investigation using green fluorescent protein transgenic bone marrow chimeric mice," *Experimental Neurology*, vol. 196, no. 2, pp. 290–297, 2005.

[73] M. Schroeter, S. Jander, I. Huitinga, O. W. Witte, and G. Stoll, "Phagocytic response in photochemically induced infarction of rat cerebral cortex: the role of resident microglia," *Stroke*, vol. 28, no. 2, pp. 382–386, 1997.

[74] X. Hu, P. Li, Y. Guo et al., "Microglia/macrophage polarization dynamics reveal novel mechanism of injury expansion after focal cerebral ischemia," *Stroke*, vol. 43, no. 11, pp. 3063–3070, 2012.

[75] E. A. Irving, K. Yatsushiro, J. McCulloch, and D. Dewar, "Rapid alteration of tau in oligodendrocytes after focal ischemic injury in the rat: involvement of free radicals," *Journal of Cerebral Blood Flow and Metabolism*, vol. 17, no. 6, pp. 612–622, 1997.

[76] M. M. Gresle, B. Jarrott, N. M. Jones, and J. K. Callaway, "Injury to axons and oligodendrocytes following endothelin-1-induced middle cerebral artery occlusion in conscious rats," *Brain Research*, vol. 1110, no. 1, pp. 13–22, 2006.

[77] V. Valeriani, D. Dewar, and J. McCulloch, "Quantitative assessment of ischemic pathology in axons, oligodendrocytes, and neurons: attenuation of damage after transient ischemia," *Journal of Cerebral Blood Flow & Metabolism*, vol. 20, no. 5, pp. 765–771, 2000.

[78] M. D. Weingarten, A. H. Lockwood, S. Y. Hwo, and M. W. Kirschner, "A protein factor essential for microtubule assembly," *Proceedings of the National Academy of Sciences of the United States of America*, vol. 72, no. 5, pp. 1858–1862, 1975.

[79] E. McCracken, V. Valeriani, C. Simpson, T. Jover, J. McCulloch, and D. Dewar, "The lipid peroxidation by-product 4-hydroxynonenal is toxic to axons and oligodendrocytes," *Journal of Cerebral Blood Flow and Metabolism*, vol. 20, no. 11, pp. 1529–1536, 2000.

[80] G. L. Li, M. Farooque, A. Holtz, and Y. Olsson, "Apoptosis of oligodendrocytes occurs for long distances away from the primary injury after compression trauma to rat spinal cord," *Acta Neuropathologica*, vol. 98, no. 5, pp. 473–480, 1999.

[81] J. C. Gensel, C. A. Tovar, J. C. Bresnahan, and M. S. Beattie, "Topiramate treatment is neuroprotective and reduces oligodendrocyte loss after cervical spinal cord injury," *PLoS ONE*, vol. 7, no. 3, Article ID e33519, 2012.

[82] R. P. Skoff, D. A. Bessert, J. D. E. Barks, D. Song, M. Cerghet, and F. S. Silverstein, "Hypoxic-ischemic injury results in acute disruption of myelin gene expression and death of oligodendroglial precursors in neonatal mice," *International Journal of Developmental Neuroscience*, vol. 19, no. 2, pp. 197–208, 2001.

[83] C. Wiessner, F. M. Bareyre, P. R. Allegrini et al., "Anti-Nogo-A antibody infusion 24 hours after experimental stroke improved behavioral outcome and corticospinal plasticity in normotensive and spontaneously hypertensive rats," *Journal of Cerebral Blood Flow and Metabolism*, vol. 23, no. 2, pp. 154–165, 2003.

[84] P. Freund, E. Schmidlin, T. Wannier et al., "Anti-Nogo-A antibody treatment promotes recovery of manual dexterity after unilateral cervical lesion in adult primates—re-examination and extension of behavioral data," *European Journal of Neuroscience*, vol. 29, no. 5, pp. 983–996, 2009.

[85] A. B. Seymour, E. M. Andrews, S.-Y. Tsai et al., "Delayed treatment with monoclonal antibody IN-1 1 week after stroke results in recovery of function and corticorubral plasticity in adult rats," *Journal of Cerebral Blood Flow & Metabolism*, vol. 25, no. 10, pp. 1366–1375, 2005.

Research Article

Virus Infections on Prion Diseased Mice Exacerbate Inflammatory Microglial Response

Nara Lins,[1] Luiz Mourão,[1] Nonata Trévia,[1] Aline Passos,[1] José Augusto Farias,[1] Jarila Assunção,[1] Amanda Quintairos,[1] João Bento-Torres,[1] Marcia Consentino Kronka Sosthenes,[1] José Antonio Picanço Diniz,[2] Pedro Fernando da Costa Vasconcelos,[2] and Cristovam Wanderley Picanço-Diniz[1]

[1]*Universidade Federal do Pará, Instituto de Ciências Biológicas, Laboratório de Investigações em Neurodegeneração e Infecção no Hospital Universitário João de Barros Barreto, Belém, Brazil*
[2]*Instituto Evandro Chagas, Laboratório de Microscopia Eletrônica and Departamento de Arbovirologia e Febres Hemorrágicas Virais, Belém, Brazil*

Correspondence should be addressed to Cristovam Wanderley Picanço-Diniz; cwpdiniz@gmail.com

We investigated possible interaction between an arbovirus infection and the ME7 induced mice prion disease. C57BL/6, females, 6-week-old, were submitted to a bilateral intrahippocampal injection of ME7 prion strain (ME7) or normal brain homogenate (NBH). After injections, animals were organized into two groups: NBH ($n = 26$) and ME7 ($n = 29$). At 15th week after injections (wpi), animals were challenged intranasally with a suspension of Piry arbovirus 0.001% or with NBH. Behavioral changes in ME7 animals appeared in burrowing activity at 14 wpi. Hyperactivity on open field test, errors on rod bridge, and time reduction in inverted screen were detected at 15th, 19th, and 20th wpi respectively. Burrowing was more sensitive to earlier hippocampus dysfunction. However, Piry-infection did not significantly affect the already ongoing burrowing decline in the ME7-treated mice. After behavioral tests, brains were processed for IBA1, protease-resistant form of PrP, and Piry virus antigens. Although virus infection in isolation did not change the number of microglia in CA1, virus infection in prion diseased mice (at 17th wpi) induced changes in number and morphology of microglia in a laminar-dependent way. We suggest that virus infection exacerbates microglial inflammatory response to a greater degree in prion-infected mice, and this is not necessarily correlated with hippocampal-dependent behavioral deficits.

1. Introduction

Infections and chronic neurodegenerative diseases acting together represent an increasing proportion in the health care budgets worldwide [1]. Infections often induce physiological, metabolic, and behavioral changes, characterized by fever, reduced activity (lethargy), decreased appetite (hypophagia), anhedonia, impaired cognitive function, anxiety, and depression [2]. These symptoms are known as "sickness behavior" which is part of the body's normal homeostatic response in response to infection. It is believed that these metabolic changes are triggered by proinflammatory mediators that are produced by activated immune cells and which communicate

with the brain by various routes [3]. The CNS effects generated by infection and systemic inflammatory responses are readily evident from both human disease and experimental animal models [4–9]. Emerging virus infections of the CNS are mainly associated with RNA viruses, many of which cause neurologic disease [10]. The Vesiculovirus Piry infection generates human disease characterized by rapid onset, high fever, headache, chills, photophobia, myalgia, dizziness, and weakness [11] and, in adult mice, a nonlethal CNS infection and injury to the limbic system including the hippocampus [12], a target region of the degenerative process induced by prion disease in mice [13]. This particularity to infect humans and damage the hippocampus of adult mice makes

Piry virus a particularly interesting arbovirus species to study the interaction between the hippocampus underlying prion disease neurodegeneration and viral infection.

Inflammatory preexistent conditions such as those associated with chronic neurodegenerative diseases in humans and mice seem to be aggravated by both peripheral and central infections [14–17]. Indeed, cognitive deficits of patients with Alzheimer's disease is further increased after a systemic infection and this is preceded by an increase in interleukin 1β [14] and mouse prion disease shows more intense neuropathological features and faster disease progression after systemic and central endotoxin challenges [15].

Thus, in the present report, we associated Piry virus, which generates symptoms of infectious disease in both human [16] and mice [11] to a mouse model of prion disease, to assess the influence of a nonlethal arbovirus encephalitis [12] on the progression of the ongoing hippocampal chronic neurodegeneration. We quantitated microgliosis using stereological unbiased method and assessed behavioral changes to measure directly the influence of a RNA virus infection on hippocampal microglial response and associated sickness behavior.

2. Methods

2.1. Housing Procedures. Animals were grouped in cages made with polyvinyl chloride (PVC). Cages with 4 to 6 mice were maintained in a room with controlled temperature (25°C) and light-dark cycle of 12 hours. Cages were lined with autoclaved rice straw, changed once a week. Food and water were offered ad libitum. The experiments were conducted in accordance with the recommendations in the Guide of the National Institutes of Health (NIH, USA), for the use of experimental animals and in accordance with the ethics committee of the Institute of Biological Sciences at the UFPA under the Protocol No. 1701/5. We used 40 mice for behavioral studies and 16 for neuropathological analysis.

2.2. Inoculation. To inoculate normal or prion infected brain homogenates, animals were anesthetized intraperitoneally (i.p.) with Avertin (2,2,2-tribromoethanol solution, 0.1 mL/5 g body weight) and carefully positioned in a stereotaxic apparatus (Insight Equipment Ltd.). Two openings were done in the skull to allow bilateral hippocampal infusion of 1 μL of the infected or normal homogenates (10% w/v in sterile phosphate buffered saline, pH 7.2–7.4) on each hemisphere. The injections were made with a 10 μL Hamilton syringe. The stereotaxic coordinates used for hippocampal injections adopted the bregma as a reference point and were −2.0 mm in the anteroposterior direction, ±1.7 mm lateral to the midline, and −1.6 mm from the cortical surface. After the infusion of the suspension, the needle was kept in place for 2 minutes to avoid backflow of the solution, after which it was removed slowly. The scalp was sutured, and mouse was removed and placed into a cage for recovery. The dorsal hippocampus was target used for the injection site. The subsequent hippocampal neurodegeneration gives rise to a defined sequence of behavioral alterations [17] that could be readily detected.

2.3. Experimental Groups and Piry Infections. After injections, animals were divided into two groups: NBH ($n = 26$) and ME7 ($n = 29$). At the end of 15th week postinjections animals were again anesthetized with 2,2,2 tribromoetanol 1% (0.1 mL/5 g body weight, i.p.) and inoculated intranasally either with an infected suspension of brain homogenate containing Piry virus or with an uninfected normal brain homogenate suspension. To prepare virus infected suspension, two infected brains from neonate mice were macerated and to this infected macerate 1.6 mL of antibiotic solution containing sterile penicillin and streptomycin (Penistrep) was added. This mixture was centrifuged at 4°C at 10.000 rpm. The supernatant was frozen and stored at −70°C, as a 20% stock solution. This solution was then diluted to a concentration of 0.001% with the same mixture of antibiotics. Each infected mouse received 5 μL of viral suspension in each nostril, while the control group was inoculated with the uninfected solution. Thus at the 16th week after intrahippocampal injection, ME7 and NBH groups were subdivided into NBH ($n = 16$) and NBH+Py ($n = 11$); and ME7 ($n = 18$) and ME7+Py ($n = 11$).

2.4. Behavioral Tests. Between the 8th and 21st weeks postinjection all subjects were daily submitted to the following behavioral tests: burrowing, open field, inverted screen, and rod bridge.

Burrowing. This test explores the typical behavior of certain rodents to remove and store food from a burrow. The burrow is simulated by a PVC tube, 15 cm long, 7.2 cm diameter, placed at an angle, with the open end 3 cm above the soil, filled with 150 g of standard rodent pellet food. To carry out this test from the 8th week postinjection onwards, each animal was daily placed into individual PVC cages (49 × 17 × 32.5 cm), for a period of two hours (between 14:00 and 16:00 h) to assess the amount of burrowed food. Subsequently, the mouse returns to its cage, and burrowing activity was measured by weighing the amount of food remaining in the tube.

Open Field. The open field test was conducted in a white PVC box (49 × 17 × 32.5 cm), with the floor divided into 9 squares of equal size (9 × 9 cm). Animals were placed in the apparatus facing the wall and remained in the arena for 3 minutes. The parameters analyzed were the number of crossed squares and the number of times the mouse reared. A crossed square was defined when the animal entered on it with its four paws; and the number of times the mouse reared was estimated according to the number of times the animals stand on its two hind paws. Record of rearing was also considered valid when mouse touched the walls.

Inverted Screen. To assess muscular strength, mice were placed in a stainless steel rectangular (58.3 cm × 43.5 cm) screen (1 × 1 cm squares), divided into 7.5 × 7.5 cm quadrants, and turned upside down. The screen was placed on the top of a plastic cage, in which the floor was covered with a soft

TABLE 1: Primary antibodies and dilutions.

Antibodyes	Suppliers	Dilution
Anti-Iba1	Wako Pure Chemical Industries, Ltd (Osaka, Japan)	1 : 500
Anti-PrP	Mouse monoclonal [8H4] to prion protein PrP	1 : 2500
Anti-Piry	Evandro Chagas Institute (Belem, PA, Brazil)	1 : 20

(*)Dilution in 0.1 M phosphate buffered saline pH 7.2–7.4.

material to avoid injures if the mice fell. Each animal was allowed to remain 60 seconds in the screen and the total number of squares crossed were recorded. If the animal falls in less than a minute, the time was also recorded.

Rod Bridge. Used to access the motor coordination, the apparatus was constituted by a bridge of wooden sticks (23 cm long) spaced 2 cm apart, placed into a plastic container (48 × 7.5 × 25 cm) containing water up to 2 cm below the sticks. The cage was placed at one end of the bridge and the animal was placed at the opposite end. The time taken to cover the distance and reach the cage extremity of the sticks bridge, and the number of errors during the walk were recorded. An error was considered every time when the animal missed one step.

2.5. Histology and Immunohistochemistry.

After reaching appropriate survival time, animals of each group were weighed and anesthetized with 2,2,2-tribromoethanol (0.04 mL/g of body weight, intraperitoneally) and perfused transcardially with heparinized saline followed by paraformaldehyde 4% in 0.1 M phosphate buffer (pH 7.2–7.4). Parasagittal sections of 70 μm thickness were cut on a vibratome (Leica VT1000, MK, UK) and selectively immunolabeled.

To assess the distribution of Piry viral antigens, and microglia in the mouse brain, immunohistochemistry was performed using polyclonal antibodies against Piry virus antigens and IBA1 respectively. Specific antibodies against Piry virus species were produced by the Department of Arbovirus and Hemorrhagic Fevers at the Instituto Evandro Chagas, as described elsewhere [18], and anti-IBA1 antibody by Wako Pure Chemical Industries, Ltd (Osaka, Japan). Detailed immunohistochemical procedures were described elsewhere [12, 19]. In brief, free-floating sections were rinsed in 0.1 M phosphate buffer and placed in a solution of 0.2 M boric acid (pH 9.0) at 70°C for 1 h for antigen retrieval, then rinsed in 0.1 M PBS with 5% Triton X-100, and incubated in a solution of methanol and 0.3% hydrogen peroxide for 10 min. After washing in PBS, the Mouse-on-Mouse (MOM) Blocking Kit (Vector Laboratories, Burlingame, CA, USA) was used as follows: MOM IgG blocking for 1 h followed by primary antibody for 72 h. All primary antibodies and dilutions are indicated in Table 1.

They were diluted in 0.1 M phosphate buffer saline, pH 7.2–7.4, and primary incubation was done for three days at 4°C, with gentle, continuous agitation. Sections were then incubated in MOM Biotinylated Anti-Mouse IgG Reagent

for 12 h, washed in PBS and transferred to avidin-biotin-peroxidase complex (ABC) solution (Vector Laboratories, Burlingame, CA, USA) for 1 h. They were washed again before incubation in 0.2 M acetate buffer (pH 6.0) for 5 min and revealed in GND solution (diaminobenzidine 0.6 mg/mL, ammonium nickel chloride 2.5 mg/mL, and glucose oxidase). All steps were carried out under gentle and constant agitation. As a negative control, normal horse serum was added to some slides in place of each of primary antibody used as a cell marker and slides were processed for immunohistochemistry as previously described. All sections were counterstained with cresyl violet to define layer limits and anatomical boundaries of the areas of interest.

Protease Resistant PrPc Immunolabeling. Sections immunolabeled to detect protease-resistant PrP were pretreated in formic acid 85%, 30 min, incubated in trypsin 0.1% at room temperature 10 minutes, and then transferred to a solution of 0.1 M citrate buffer, pH 6.0 at 90°C, 1 h. Sections were rinsed in 0.1 M phosphate-buffered saline (PBS) with Triton X-100 (5%). After washing in PBS, the protocol of Mouse-on-Mouse (MOM) Blocking Kit (Vector Laboratories, Burlingame, CA, USA) was conducted as follows: MOM IgG blocking for one hour, primary antibody for 72 hours (ABCAM, Mouse monoclonal [8H4] to Prion protein PrP 1 : 2500) diluted in 0.1 M PBS, washed in 0.1 M PBS three times 5 minutes followed by MOM Biotinylated Anti-Mouse IgG Reagent for 12 hours. Sections were treated with 0.3% hydrogen peroxide in 0.1 M PB, pH 7.2–7.4. Sections were then transferred to avidin-biotin-peroxidase complex (ABC) solution for 1 hour and washed again before incubation in acetate buffer 0.2 M pH 6.0 for 5 minutes and revealed in GND solution (diaminobenzidine 0.5 mg/mL, ammonium nickel chloride 0.6 mg/mL, and glucose oxidase). All steps were carried out under gently and constant agitation.

2.6. Stereology.

The estimate of the number of microglia was done in CA1 layers in both infected and controls and were performed using the optical fractionator method [20]. Table 2 shows stereological parameters used to count microglia.

The layers of interest were the strata pyramidale, radiatum, and lacunosum molecular of CA1, of the dorsal hippocampal formation. Their boundaries were defined using a 4x objective optical microscope (Nikon Eclipse 80i, Japan) equipped with a motorized stage to control the X, Y, and Z with help of a stage controller (MAC6000, Ludl Electronic Products, Hawthorne, NY, USA). This system is coupled to a computer containing the Stereoinvestigator program (MBF bioscience, Williston, VT, USA), which records the three-dimensional coordinates and stores the stereological data. We used PLANFLUOR 100x (NA 1.3; DF = 0.2 μM; Nikon, Japan) to count microglia.

The stratum oriens was not included in the counts to be the outermost layer of the CA1 hippocampus, where the reactions end up in shrunken anamorphic tissue (edge effect) with very intense background. In this layer the cells of interest, in many cases, were indistinguishable one from another and from the dark background, preventing stereological analysis.

TABLE 2: Stereological parameters.

Layer of interest	Counting box area (x, y) (μm^2)	Grid (μm^2)	Counting box height (z)	Guard zone
CA1-pyramidal layer	80×80	80×80	$12\,\mu m$	$2\,\mu m$
CA1-radiatum	60×60	90×90	$12\,\mu m$	$2\,\mu m$
CA1-lacunosum molecular	60×60	90×90	$12\,\mu m$	$2\,\mu m$

2.7. Photomicrography. For photomicrographs, we used a digital camera (AxioCam-ERc, Zeiss, Gottingen, Germany), coupled to a NIKON Eclipse 80i microscope. Digital photomicrographs were processed with Adobe Photoshop software; scaling and adjustments to the brightness and contrast were applied to the whole image.

2.8. Statistical Analysis. The results obtained by Stereoinvestigator and behavioral assays were statistically analyzed through BioEstat 5.3 software [21], applying parametric tests to detect differences or similarities among groups, accepting as significant ones in a confidence interval of 95% ($p < 0.05$). For comparisons between only two groups we used t-test for two related samples or t-tests for two independent samples. For analysis with 4 experimental groups we used two-way ANOVA, followed by Bonferroni post-hoc tests. Confidence levels were set at 95 or 99% ($p < 0.05$ or $p < 0.01$). The results are displayed in arithmetic mean and standard error values.

3. Results

3.1. Sickness Behavior. The animals infected by Piry arbovirus showed clinical signs of infection for a period of about 1-week postinfection. All animals that had their nostrils instilled with infected brain homogenate, showed transitory sickness behavioral signs, including ruffled fur, tremor, hunched posture, and less exploratory activity. All ME7 prion injected animals showed typical sickness behavioral changes as disease progressed. In contrast with virus infection transitory symptoms, chronic neurodegeneration of prion disease inflicts permanent symptoms that aggravate as disease progresses. Because immunohistochemistry for virus antigens and neuropathology of prion diseased animals confirmed that Piry virus and prion disease targeted the limbic system, including hippocampal formation, we choose to analyze hippocampal-dependent tasks.

3.2. Burrowing. To reduce possible bias generated by the variable interest of each animal in removal and store food, we normalized the scales of burrowing as follows: we estimate for each group the maximum value of burrowed food and expressed it as 100%. All other values were expressed as percentage values relative to this maximum (Figure 1).

At the 11th week, all groups started to burrow food with similar interest, and at 12th wpi, on average, no differences were detected between groups. Comparing the amount of burrowed food by ME7 and NBH groups on each time window, we found a significant decline in this activity from 14th to 15th wpi in ME7 infected groups (two-tail t-test, $t = 25.18$, at 14th wpi $p < 0.02$; two tail t-test, $t = 39.9$,

$p < 0.0004$, at 15th wpi). At 15th wpi, when $5\,\mu L$ of Piry infected brain homogenate or uninfected brain was instilled in the nostrils, all Piry infected animals had a decline in burrowing activity as compared with uninfected groups. The virus infection influence on burrowing activity is displayed in the pink area in Figure 1. At 16th wpi, NBH+Py and ME7+Py burrowed significantly less food than uninfected groups without interaction (two-way ANOVA Bonferroni post-hoc tests $p < 0.001$ without interaction). Note the decline in burrowing activity between the 15th and the 16th week in NBH+Py group and in the ME7+Py and the subsequent recovery only in the NBH+Py between the 17th and 18th wpi. Note that ME7 prion disease also generated a decline between the 17th and 18th wpi but this decline seems not to be related to viral infection.

Taken together, our findings show that prion disease significantly affected burrowing activity from 14th week onwards. Burrowing activity was also sensitive to Piry virus infection. Indeed, after nostril inoculation animals burrowed significantly less food during two weeks, after which only NBH+Py infected group recovered burrowing activity up to normal levels.

3.3. Open Field. In the open field test no viral infection effect was detected on the number of crossed squares, or in the number of mice raisings. Indeed, the differences between groups from the 15th wpi onwards were influenced only by prion disease (Figure 1).

3.4. Inverted Screen. In this test, the number of crossed squares was not affected significantly and did not distinguish between groups except at 18 wpi onwards where ME7 animals, both infected with Piry virus or virus uninfected, showed progressive reduction in the time remaining in the inverted screen (Figure 1). At the 21st wpi prion diseased animals cannot sustain their own body and fall-off.

3.5. Rods Bridge. This test assesses motor coordination. The curves in Figure 1 show that the time to go through the apparatus was similar among all groups until the 18th week, when the ME7 groups start to spend more time to complete the task (Figure 1). One week later the same effect is observed in ME7 and ME7+Py as compared to NBH and NBH+Py. Note that the number of errors increased significantly in groups with prion disease both in virus infected and virus uninfected subjects (Figure 1).

Supplementary Table S1 (in Supplementary Material available online at http://dx.doi.org/10.1155/2016/3974648) includes all means, standard deviations, and p values for all experimental groups' pertinent comparisons.
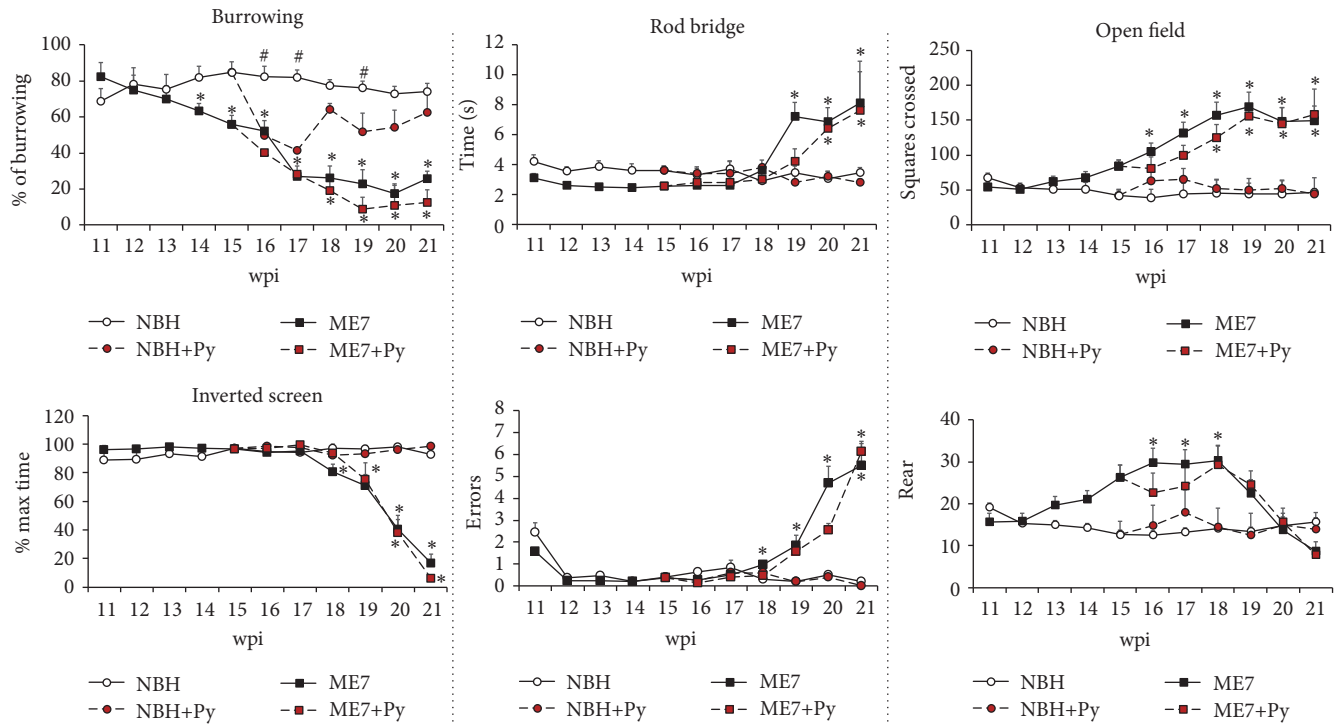
FIGURE 1: Influences of virus infection on prion disease progression. Burrowing activity was the most sensitive test to detect earlier associated behavioral changes occurring in both ME7 infected group (ME7) and virus infected prion diseased animals (ME7+Py). All other tests showed significant changes only at later stages of the disease. ∗ indicates significant differences between ME7 groups and respective controls (NBH versus ME7; NBH+Py versus ME7+Py; Bonferroni posttest $p < 0.01$). # indicates significant differences between NBH+Py and NBH groups (Bonferroni posttest $p < 0.05$).
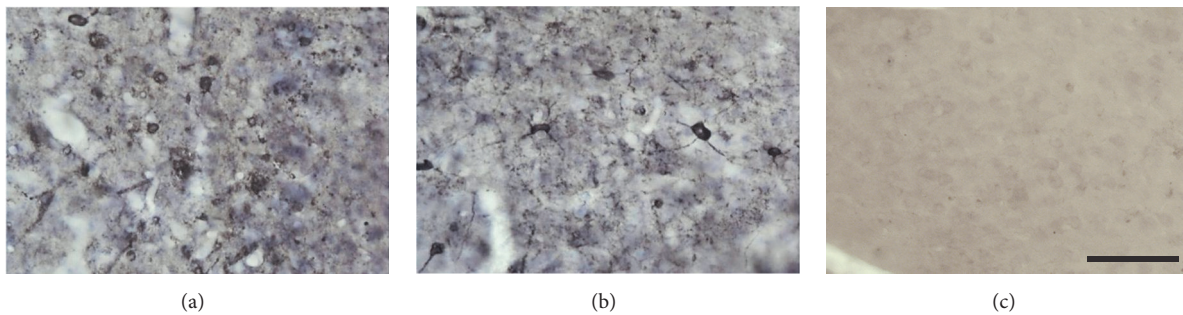
FIGURE 2: Photomicrographs from immunolabeled sections to detect Piry virus antigens in the brain of NBH and ME7 virus infected groups. Virus antigens were indirectly detected as immunostained cell somas and neuronal primary dendrites in the olfactory pathways in both NBH+Py (a) and ME7+Py (b) groups. Note the absence of virus antigens selective immunolabeling in NBH control group (c). We also did not observe any labeling after immunoreaction without anti-Piry polyclonal primary antibody (not illustrated). Scale bar = 25 μm.

3.6. Neuropathology

3.6.1. Piry Arbovirus Infection.
The immunohistochemical reaction to Piry arbovirus antigens, 8 days after the inoculation, showed virus tropism to specific regions of the central nervous system, including the olfactory areas and hippocampal formation. Virus antigens were detected in both NBH+Py (Figure 2(a)) and ME7+Py (Figure 2(b)) groups.

3.6.2. Protease Resistant PrPc.
Figure 3 shows immunostained sections for protease resistant PrPc taken from the hippocampus of control and ME7 prion diseased animals. Protease resistant PrPc deposits were frequently observed in ME7 injected subjects at 17th wpi.

3.6.3. Microglial Changes.
Qualitative analysis of the microglial cells one week after Piry arbovirus inoculation indicated that microglial cells from hippocampus seem to be more ramified (stage 1 of activation). Microgliosis was readily evident in prion diseased mice and it was aggravated by Piry virus infection. This microgliosis in the ME7 individuals was associated with remarkably microglial morphological

(a)

(b)

(c)

(d)
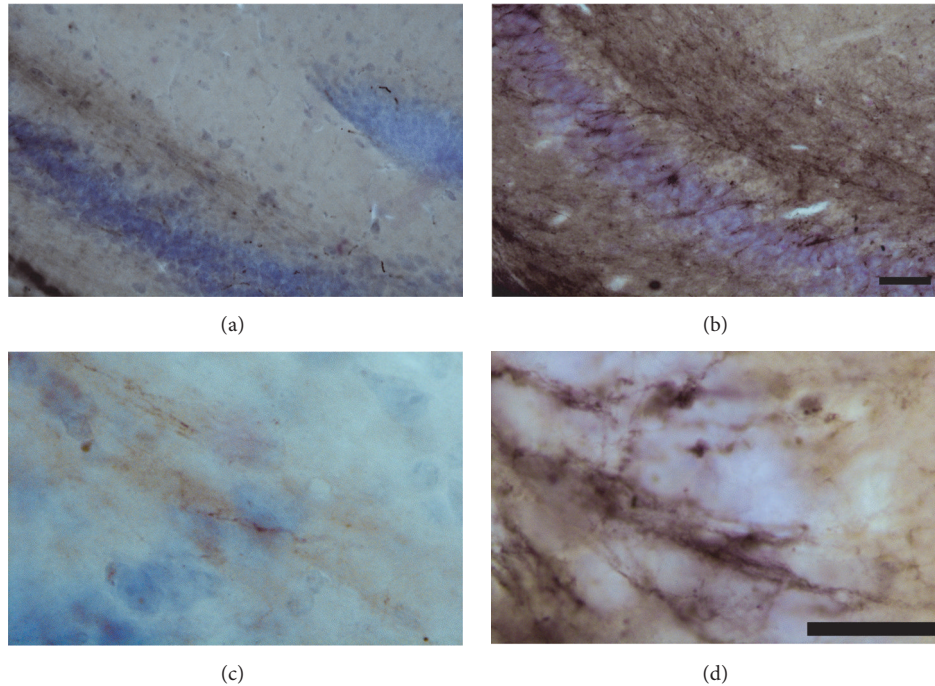
FIGURE 3: Photomicrographs to illustrate protease resistant PrPc immunolabeled hippocampal sections from control (a and c) and ME7 infected (b and d) subjects, counterstained with cresyl violet. Low power (a and b); scale bar = 50 μm; high power (c and d) = 25 μm.

changes that were accentuated in prion diseased mice infected by Piry virus (Figure 4).

As compared with controls, microglia from ME7 individuals shows larger cell bodies and shorter and more ramified branches whereas microglia from prion diseased animals infected with Piry virus (ME7+Py) was closer to the amoeboid morphology. Prion diseased animals showed microglial invasion of pyramidal cell layer. Viral infection and prion disease acting together cause a significant increase in the microgliogenesis (Tables 3–5). Indeed, the total number of microglia of each layer increased significantly in ME7 infected subjects after Piry virus infections.

Figure 5 shows mean and standard errors values of optical fractionator estimate of microglial numbers for each experimental group on each layer and the sum of the three layers expressed as CA1 total. Taken CA1 total as reference, it was found that the number of microglia increased 97% in the ME7 group as compared with NBH group (two-tail t-test for independent samples, $p = 0.025$). Although the isolated viral infection generates a 26% increase in microglia number compared to control, this increase was not statistically significant (two-tailed t-test $p > 0.05$). However, as compared to NBH, prion diseased animals with viral infection (ME7+Py) show on average an addictive effect (two-way ANOVA, $p = 0.01$), increasing 239% the total number of microglia (two tail t-test, $t = -4$ $p < 0.004$) (Figure 5).

Indeed, the number of microglia on each layer of CA1 increased significantly on the strata pyramidale, radiatum, and lacunosum molecular. At 17th wpi prion disease also induced significant microgliosis on pyramidal cell layer and stratum radiatum (two-tail t-tests for independent samples,

$p < 0.05$). Two-way ANOVA Bonferroni post hoc tests demonstrate significant interaction between virus infection and prion disease suggesting that virus infection also influenced microgliogenesis in prion diseased mice. The total number of CA1 microglia in prion diseased animals that were infected by Piry virus was significantly increased, suggesting that a concurrent virus infection exacerbates the inflammatory response, and this response seems to be laminar-dependent.

4. Discussion

We tested the hypothesis that an arbovirus infection would exacerbate the inflammatory response in a chronic neurodegeneration model of prion disease. To that end we investigated possible interaction between Piry virus infection and the ME7 induced mouse prion disease, assessing behavioral and neuropathological changes of prion disease with and without virus infection. The results of behavioral tests indicate that burrowing activity is sensitive to viral infection. Indeed, taking as a reference point the burrowing activity in the week previous to the inoculation, a reduction of approximately 40% of that activity was observed in both NBH+Py and ME7+Py groups. Because Piry virus was unable to induce changes in muscle strength, motor coordination, locomotor, and exploratory behaviors, using the inverted screen, Rod Bridge, and open field, respectively, we suggest that burrowing is by far the most sensitive test to detect early stages of the disease in both mice Piry virus infection and prion disease, in isolation or in combination. The neuropathological analysis of prion diseased subjects showed
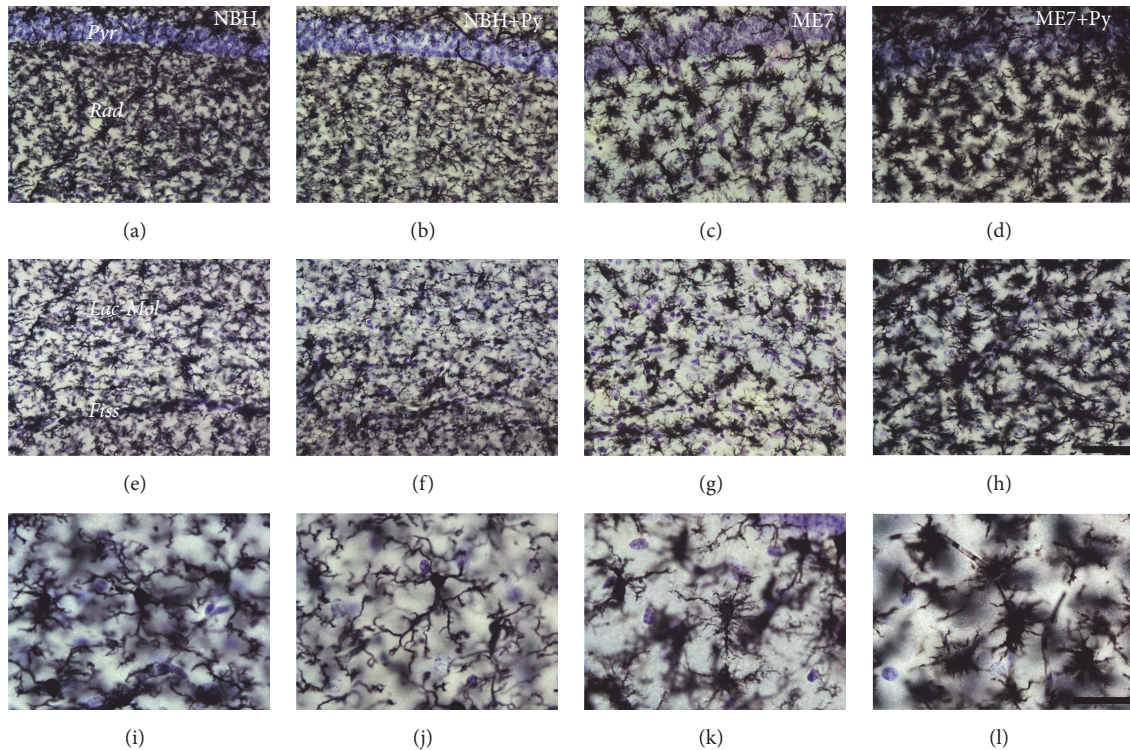
Figure 4: Photomicrographs of CA1 microglial cells taken from sections of NBH (a, e, and i); NBH+Py (b, f, and j); ME7 (c, g, and k); ME7+Py (d, h, and l). From left to right the 1st, 2nd, 3rd, and 4th columns correspond, respectively, to subjects intracerebrally (i.c.) injected with normal brain homogenate, NBH, with NBH and nasal instilled with Piry virus suspension, NBH+Py, i.c., injected with ME7 infected brain homogenate, ME7, i.c., injected with ME7 and nasal instilled with Piry virus suspension, ME7+Py. First row corresponds to pyramidal cell layer (Pyr) and stratum radiatum (Rad). Second row corresponds to lacunosum molecular layer (Lac-Mol), hippocampal fissure (Fiss), and small portion of the molecular layer of dentate gyrus below hippocampal fissure. The third row corresponds to high power pictures to illustrate different stages of microglial morphological activation. Note that microglia from ME7+Py group is closer to the amoeboid format (last stage of morphological change of activated microglia). Scale bars (a)–(h) = 50 μm; (i)–(l) = 25 μm.

that microglia changed significantly their morphology and number. Arbovirus infection alone changed microglial morphology but did not induce significant numerical changes in CA1 layers. However, the association between chronic neurodegenerative disease and arbovirus infection generated an exacerbated microglial response, with an increase over 200% in the total number of cells as compared to control. Neuropathological changes associated with virus infection in isolation coexisted with significant reduction in burrowing activity, but nonsignificant influences were detected on the other behavioral tests.

4.1. Behavioral Changes. The first sign of hippocampal-dependent sickness behavior was observed in burrowing activity tests at 14th wpi, while locomotor changes or exploratory activity on open field and muscle strength changed later in the disease (17th wpi) and these results are in line with previous reports [13, 17]. Our results show that the ME7 injection in the dorsal hippocampus reproduced the temporal course of the disease as previously described elsewhere [13]. ME7 infected brain homogenate injection showed clear hippocampal inflammatory response, protease resistant Preps deposits and correspondent change in burrowing

activity. This result is consistent with previous studies that demonstrated, regardless of the route of inoculation of the prion agent, the hippocampus is one of the main target of chronic neurodegeneration associated with the disease [22] and the burrowing test is sensitive and specific to hippocampal damage [23, 24]. The temporal identification of behavioral changes in the course of prion disease varies from one study to another, but it is known that changes in spontaneous behavior, such as decrease in burrowing activity and hyperactivity, occur before reduction in the performances on behavioral tests that require strength and motor coordination [17]. Our findings are in line with these descriptions.

The open field test, which evaluates the pattern of spontaneous exploratory activity, reproduced previous results [17]. However, in this study the hyperactivity, which appeared in other studies around the 12th wpi, only became apparent at 15th wpi.

As viral infection did not change motor function it is reasonable to suppose that the decrease in burrowing activity observed after viral inoculation may have been associated with hippocampal damage. A previous study with Piry virus infection in albino Swiss mice showed, as compared with

TABLE 3: CA1 microglial numbers from pyramidal cell layer from animals injected with normal brain homogenate (NBH) or NBH followed by Piry intranasal injection or with ME7 infected brain homogenate (ME7) or by ME7 followed by Piry virus intranasal injection.

Subjects	N	Thickness (μm)	CE (Scheaffer)
		Stratum pyramidale of CA1	
		NBH	
NBHVII-2	3681	28.5	0.05
NBHVII-3	2200	19.2	0.06
NBHVII-4	3357	19.2	0.05
Mean	3080	22.3	0.05
SD	779		
CV^2	0.064		
CE^2	0.003		
CE^2/CV^2	0.041		
CVB^2	0.061		
CVB^2 (% CV^2)	95.9		
		NBH+VIRUS	
NBHV-3	3412.64	18.7	0.04
NBHVI-1	2506.66	15.1	0.05
NBHVI-2	2094.18	18.2	0.05
NBHVI-4	3634.26	18.1	0.05
Mean	2912	17.5	0.05
SD	732		
CV^2	0.063		
CE^2	0.002		
CE^2/CV^2	0.035		
CVB^2	0.061		
CVB^2 (% CV^2)	96.5		
		ME7	
ME7IX-1	5631	22.5	0.04
ME7IX-4	4749	15.9	0.04
ME7X-2.	5625	20	0.04
ME7X-4	3507	24.1	0.05
Mean	4878	21	0.04
SD	1003		
CV^2	0.042		
CE^2	0.002		
CE^2/CV^2	0.045		
CVB^2	0.040		
CVB^2 (% CV^2)	95.5		
		ME7+VIRUS	
ME7VII-1	10834	22.1	0.04
ME7VII-4	7375	15.3	0.03
ME7VIII-1	10240	23.8	0.04
ME7VIII-4	6202	20.5	0.04
Mean	8663	20.4	0.04
SD	2230		
CV^2	0.066		
CE^2	0.001		
CE^2/CV^2	0.022		
CVB^2	0.065		
CVB^2 (% CV^2)	97.8		

$^{(*)}CVB^2 = CV^2 - CE^2$ (CV, coefficient of variation; CE, Scheaffer coefficient of error; CVB, biological variation coefficient).

TABLE 4: CA1 microglial numbers in the stratum radiatum of CA1 from animals injected with normal brain homogenate (NBH) or NBH followed by Piry intranasal injection or with ME7 infected brain homogenate (ME7) or by ME7 followed by Piry virus intranasal injection.

Subjects	N	Thickness (μm)	CE (Scheaffer)
		Stratum radiatum of CA1	
		NBH	
NBHVII-2	7877.17	29.2	0.05
NBHVII-3	5718.76	18.2	0.06
NBHVII-4	6755.67	19.0	0.05
Mean	6784	22.1	0.05
SD	1079		
CV^2	0.025		
CE^2	0.003		
CE^2/CV^2	0.113		
CVB^2	0.022		
CVB^2 (% CV^2)	89		
		NBH+VIRUS	
NBHV-3	8560.43	18.8	0.05
NBHVI-1	5478.32	15.0	0.05
NBHVI-2	6818.47	17.5	0.05
NBHVI-4	8078.08	18.1	0.04
Mean	7234	17.4	0.05
SD	1382		
CV^2	0.036		
CE^2	0.002		
CE^2/CV^2	0.064		
CVB^2	0.034		
CVB^2 (% CV^2)	93.6		
		ME7	
ME7IX-1	12363.62	22.5	0.05
ME7IX-4	11988.17	15.9	0.04
ME7X-2	15181.15	19.4	0.04
ME7X-4	8953.73	22.6	0.06
Mean	12122	20.1	0.05
SD	2548		
CV^2	0.044		
CE^2	0.002		
CE^2/CV^2	0.053		
CVB^2	0.042		
CVB^2 (% CV^2)	95		
		ME7+VIRUS	
ME7VII-1	28541.47	21.9	0.04
ME7VII-4	19120.84	15.2	0.04
ME7VIII-1	21131.22	21.4	0.04
ME7VIII-4	17769	20.8	0.05
Mean	21641	19.8	0.04
SD	4803		
CV^2	0.049		
CE^2	0.002		
CE^2/CV^2	0.034		
CVB^2	0.048		
CVB^2 (% CV^2)	97		

$^{(*)}CVB^2 = CV^2 - CE^2$ (CV, coefficient of variation; CE, Scheaffer coefficient of error; CVB, biological variation coefficient).

TABLE 5: CA1 microglial numbers from lacunosum molecular cell layer from animals injected with normal brain homogenate (NBH) or NBH followed by Piry intranasal injection or with ME7 infected brain homogenate (ME7) or by ME7 followed by Piry virus intranasal injection.

Subjects	N	Thickness (μm)	CE (Scheaffer)
Lacunosum molecular of CA1			
NBH			
NBHVII-2	8326.01	34.4	0.06
NBHVII-3	5533.11	18.5	0.06
NBHVII-4	8070.49	19.8	0.05
Mean	7310	24.2	0.06
SD	1544		
CV^2	0.045		
CE^2	0.003		
CE^2/CV^2	0.071		
CVB^2	0.041		
CVB^2 (% CV^2)	92.9		
NBH+VIRUS			
NBHV-3	8871	20.2	0.048
NBHVI-1	4969	15.6	0.059
NBHVI-2	4562	18.4	0.066
NBHVI-4	5784	19.3	0.058
Mean	6047	18.4	0.058
SD	1950		
CV^2	0.104		
CE^2	0.003		
CE^2/CV^2	0.032		
CVB^2	0.101		
CVB^2 (% CV^2)	96.8		
ME7			
ME7IX-1	10399	24.5	0.05
ME7IX-4	8764	16.7	0.05
ME7X-2.	8281	21.3	0.06
ME7X-4	6176	23.9	0.07
Mean	8405	21.6	0.06
SD	1741		
CV^2	0.043		
CE^2	0.003		
CE^2/CV^2	0.074		
CVB^2	0.040		
CVB^2 (% CV^2)	92.6		
ME7+VIRUS			
ME7VII-1	17412	22.9	0.04
ME7VII-4	10853	15.9	0.04
ME7VIII-1	15320	21.1	0.04
ME7VIII-4	9993	22.7	0.06
Mean	13395	20.7	0.05
SD	3553		
CV^2	0.070		
CE^2	0.002		
CE^2/CV^2	0.031		
CVB^2	0.068		
CVB^2 (% CV^2)	96.9		

(*)$CVB^2 = CV^2 - CE^2$ (CV, coefficient of variation; CE, Scheaffer coefficient of error; CVB, biological variation coefficient).
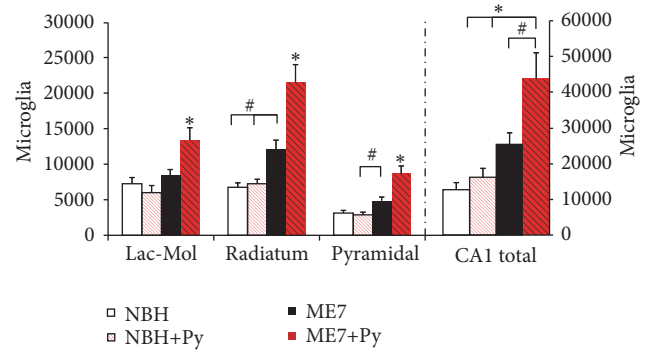
FIGURE 5: Stereological estimate of total microglia (CA1 total) and on CA1 lacunosum molecular (Lac-Mol) and radiatum and pyramidal layers. Note that as compared to all other groups, Piry (Py) virus infections in combination with intracerebral injection of ME7 infected brain homogenate (ME7+Py), significantly increased the number of microglia in all layers. Normal brain homogenate intracerebrally (i.c.) injection (NBH); NBH i.c. injection and virus suspension instilled intranasally (NBH+Py); ME7 infected brain homogenate (ME7). ∗ indicates significant differences between ME7+Py and all other groups and layers (one-way ANOVA, $p < 0.01$), and # indicates $p < 0.05$. Two-way ANOVA revealed that virus infection interacts with prion disease and exacerbates microglial response ($p = 0.01$).

uninfected mice, a reduction in locomotor activity, reflected as smaller traveled distance by infected mice in the open field test, on the 20th wpi [25]. This change after Piry virus infection was not observed in C57BL6 in the present report. Studies linking ME7 prion infection at 12th wpi and intraperitoneal injection of LPS show a decline in burrowing activity in NBH+LPS group and ME7+LPS. However, the NBH+LPS group recovers its activity 24 hours after LPS injection, while prion group returns to its basal activity after 48 hours [26]. In this same study, using the injection of LPS between the 14th and 15th weeks after injection of prion agent, animals with the underlying neurodegeneration revealed changes in the inverted screen test and the horizontal bar. These changes, however, were reversed after one week. In contrast, if the LPS inoculation is made at 12 weeks, no detectable influence on muscle strength or other motor disorders are observed, suggesting that the choice of the time window is decisive for the additive effects of infection on the course of chronic neurodegeneration. It is noteworthy that the injection of the LPS generates an inflammatory response from an innate immune response, and reactive inflammatory response to an infection by Vesiculovirus is described as an adaptive or acquired immune response [27].

4.2. Concurrent Virus Infection and Chronic Neurodegeneration. In prion diseased mice, the astrocytic and microglial activations start at early stages of the disease, but neuronal numbers remain unaltered [28].

As disease progresses, the number of nonneuronal cells increased, the proteoglycans of extracellular matrix are reduced and the behavioral changes appear in absence of neuronal death [28, 29]. Stereological analysis of microglia

and perineuronal nets in CA1 of albino Swiss mice revealed significant microgliosis between the 15th and 18th postinjection week, changing from 10,000 to 15,000 microglial cells, respectively, when the behavioral changes became apparent. At 13 wpi when behavioral changes became apparent an increase of microglial cells CD68 immunostained and in the levels of CD68 expression was found. The area with the highest expression of CD68 was the hippocampus, especially the stratum oriens and stratum radiatum. Our findings are consistent with these results. Although we did not estimate microglial numbers in the stratum oriens, we found an increase in the number of microglial cells in CA1, especially in the stratum radiatum and stratum pyramidale in prion diseased animals. In addition, when prion disease is aggravated by a concurrent arbovirus infection, an increase in the number of microglia is also observed in the lacunosummolecular layer.

Previous studies in albino Swiss mice assessed the microglial response to Piry virus infection at 8, 20, and 40 dpi and it became apparent that microgliosis was more intense at 8 dpi [25]. Link between the viral antigen immunolabeling, the number of microglial cells, and the reduction in perineuronal nets was not associated with neuronal death. However, when microglial activation was induced by Piry virus decays, type I perineuronal nets begin their recovery and this recovery coincides with the return to baseline of behavioral tests previously altered by virus infection [20]. Because of these results, it is suggested that these transient behavioral changes are related to the integrity of the extracellular matrix that is closely related to the long-term potentiation in the hippocampus [30]. In the present report, minor changes were detected in both morphology and number of microglia after an isolated Piry virus infection. These differences may be consequence of a number of factors, including different strains of mice, viral titer of the inoculum, or no linear correlation between virus infection and changes in microglial morphology and number. Indeed, it was previously described that microglia may be activated even in absence of morphological changes [31, 32]. Activated microglial cells in neurodegenerative disease or aging does not necessarily change their phenotypes after a systemic inflammatory insult if they were not previously activated to produce proinflammatory cytokines [33, 34].

The microglial activation in ME7 induced prion disease occurs between the 11th and 13th wpi, mainly in the CA1 and in the subiculum of ventral hippocampus.

These changes are associated with a decrease in perineuronal nets in CA1, subiculum, and entorhinal cortex [29]. Studies using the same model of neurodegeneration showed that there is an increase in the expression of receptors on microglial cells associated with the activation of phagocytes and associated signaling pathways, as well as an increase in IgG levels in the brain parenchyma of animals with prion disease. However, after a systemic inflammatory condition, it is suggested that a significant increase occurs in FcγR receptor levels, further reducing the phagocyte activation threshold, which could justify the increase in the number of microglial cells, and an increase in the damage to the parenchyma previously caused by chronic neurodegeneration [35]. As

viral inoculation was performed at 15th wpi and at this time, there were already changes in burrowing activity; it is possible that the magnitude of the response at that window does not represent the maximal response after virus infection. Alternatively, it may be possible that the decline of this activity is not linear throughout the progression of prion disease in coinfection regime, which makes it necessary to explore other time windows for viral inoculation to test this hypothesis.

It is known that viral pathogens invade the central nervous system more often than bacteria, but with the exception of Human Immunodeficiency Virus (HIV) that has been extensively studied [36]; little is known about the specific signaling pathways activated on microglia after arbovirus infections concurrent with prion disease. It has been shown that herpes family viruses such as cytomegalovirus and herpes simplex promote a microglial response with production of cytokines [37, 38]; however, little is known about the mechanisms of neural injury that result in the activation of microglial response. In the present report the immunostaining for Piry virus antigens after nostril inoculation of Piry virus infected brain homogenate showed tropism for neuronal cells and morphological phenotypes compatible with microglia and astrocytes. Neuronal and glial immunolabeled cells were found in the limbic system, including olfactory, septal, hippocampal formation, including CA3 and dentate gyrus, and in the trigeminal pathway. These findings are in line with previous description [12].

The Toll-like receptor system is responsible for the recognition of cell surface molecules of infectious agents, leading to the early innate immune response and the primary adaptive delayed response. Poly I:C, a synthetic double-stranded RNA, which acts as a ligand of TLR3 receptor (Toll-like receptor 3), has been used as a template to reproduce the acute phase of viral infection [39, 40]. Stimulation of these receptors induces the production of proinflammatory cytokines associated with a wide spectrum of behavioral changes, including fever [41] and hypoactivity [40]. The present report is the first to use a real arbovirus infection associated with prion disease. The arbovirus Piry infection showed longer changes in burrowing activity (up to 3 weeks) suggesting possible activation of both acute and adaptive immune responses [12].

4.3. Microglial Genesis.
Microglial survival is governed by two key molecules: granulocyte colony stimulating factor (G-CSF) and macrophage-colony stimulating factor-1 (MCSF-1). Osteopetrotic mice (op/op), which lack MCSF-1, have been shown to harbor 24% fewer microglia in the cerebral cortex than wild-type controls; however, the microglial morphology was relatively normal [42]. After an injury, microgliosis was significantly inhibited in MCSF-1 deficient mice compared to wild-type mice controls, and microglial morphology in both mutant and control mice changed to an activated profile [42].

Recently, another ligand for the MCSF-receptor was discovered, called IL-34. At the mRNA level, this ligand was highly expressed in the brain and, to a lesser extent, in other tissues [43]. In contrast, G-CSF controls bone marrow production of circulating blood cells. G-CSF has been also

implicated in the modulation of systemic immune responses by its inhibition of proinflammatory cytokines [44]. Interestingly, studies have shown that low plasma levels of G-CSF were associated with cognitive dysfunction in transgenic Alzheimer's mice [45]; moreover, low G-CSF levels in human plasma were predictive of the conversion from mild cognitive decline to an Alzheimer's type dementia [46].

It remains to be investigated which molecular mechanisms are subjacent to the inflammatory response, when combining acute viral infection and prion disease.

Taken together our findings revealed at the first time that an arbovirus infection in prion-infected mice exacerbates the microglial inflammatory response to a greater extent without correlation with hippocampal-dependent behavioral deficits.

Competing Interests

The authors declare that they have no competing interests.

References

[1] S. Banerjee, "The macroeconomics of dementia—will the world economy get Alzheimer's disease?" *Archives of Medical Research*, vol. 43, no. 8, pp. 705–709, 2012.

[2] B. L. Hart, "Biological basis of the behavior of sick animals," *Neuroscience and Biobehavioral Reviews*, vol. 12, no. 2, pp. 123–137, 1988.

[3] J. P. Konsman, P. Parnet, and R. Dantzer, "Cytokine-induced sickness behaviour: mechanisms and implications," *Trends in Neurosciences*, vol. 25, no. 3, pp. 154–159, 2002.

[4] A. Reichenberg, R. Yirmiya, A. Schuld et al., "Cytokine-associated emotional and cognitive disturbances in humans," *Archives of General Psychiatry*, vol. 58, no. 5, pp. 445–452, 2001.

[5] O. Cohen, A. Reichenberg, C. Perry et al., "Endotoxin-induced changes in human working and declarative memory associate with cleavage of plasma 'readthrough' acetylcholinesterase," *Journal of Molecular Neuroscience*, vol. 21, no. 3, pp. 199–212, 2003.

[6] K. S. Krabbe, A. Reichenberg, R. Yirmiya, A. Smed, B. K. Pedersen, and H. Bruunsgaard, "Low-dose endotoxemia and human neuropsychological functions," *Brain, Behavior, and Immunity*, vol. 19, no. 5, pp. 453–460, 2005.

[7] C. E. Wright, P. C. Strike, L. Brydon, and A. Steptoe, "Acute inflammation and negative mood: Mediation by cytokine activation," *Brain, Behavior, and Immunity*, vol. 19, no. 4, pp. 345–350, 2005.

[8] C. A. Thomson, A. McColl, J. Cavanagh, and G. J. Graham, "Peripheral inflammation is associated with remote global gene expression changes in the brain," *Journal of Neuroinflammation*, vol. 11, article 73, 2014.

[9] E. S. Wohleb, A. M. Fenn, A. M. Pacenta, N. D. Powell, J. F. Sheridan, and J. P. Godbout, "Peripheral innate immune challenge exaggerated microglia activation, increased the number of inflammatory CNS macrophages, and prolonged social withdrawal in socially defeated mice," *Psychoneuroendocrinology*, vol. 37, no. 9, pp. 1491–1505, 2012.

[10] K. J. Olival and P. Daszak, "The ecology of emerging neurotropic viruses," *Journal of NeuroVirology*, vol. 11, no. 5, pp. 441–446, 2005.

[11] R. Araújo, M. T. M. F. Araújo, and E. S. Travassos da Rosa, "Alterações ultraestrutu-rais na infecção experimental com arbovírus na Amazônia. Instituto Evandro Chagas: 50 anos de contribuição às Ciências Biológicas e à Medicina Tropical Belém," *Fundação Serviços de Saúde Pública*, vol. 4, pp. 451–465, 1986.

[12] A. A. de Sousa, R. R. dos Reis, C. M. de Lima et al., "Three-dimensional morphometric analysis of microglial changes in a mouse model of virus encephalitis: age and environmental influences," *European Journal of Neuroscience*, vol. 42, no. 4, pp. 2036–2050, 2015.

[13] S. Betmouni, R. M. J. Deacon, J. N. P. Rawlins, and V. H. Perry, "Behavioral consequences of prion disease targeted to the hippocampus in a mouse model of scrapie," *Psychobiology*, vol. 27, no. 1, pp. 63–71, 1999.

[14] C. Holmes, C. Cunningham, E. Zotova, D. Culliford, and V. H. Perry, "Proinflammatory cytokines, sickness behavior, and Alzheimer disease," *Neurology*, vol. 77, no. 3, pp. 212–218, 2011.

[15] M. I. Combrinck, V. H. Perry, and C. Cunningham, "Peripheral infection evokes exaggerated sickness behaviour in pre-clinical murine prion disease," *Neuroscience*, vol. 112, no. 1, pp. 7–11, 2002.

[16] F. P. Pinheiro, *Piry Fever. Viral Zoonosis*, CRC Press, Boca Raton, Fla, USA, 1981.

[17] C. Cunningham, "Mouse behavioural studies and what they can teach us about prion diseases," in *Neurodegeneration and Prion Disease*, D. Brown, Ed., pp. 111–137, Springer Science+Business Medi, New York, NY, USA, 2005.

[18] J. A. P. Diniz, M. R. T. Nunes, A. P. A. Travassos da Rosa et al., "Characterization of two new rhabdoviruses isolated from midges (*Culicoides* SPP) in the Brazilian Amazon: proposed members of a new genus, Bracorhabdovirus," *Archives of Virology*, vol. 151, no. 12, pp. 2519–2527, 2006.

[19] R. Borner, J. Bento-Torres, D. R. V. Souza et al., "Early behavioral changes and quantitative analysis of neuropathological features in murine prion disease: stereological analysis in the albino Swiss mice model," *Prion*, vol. 5, no. 3, pp. 215–227, 2011.

[20] A. A. de Sousa, R. Reis, J. Bento-Torres et al., "Influence of enriched environment on viral encephalitis outcomes: behavioral and neuropathological changes in albino Swiss mice," *PLoS ONE*, vol. 6, no. 1, Article ID e15597, 2011.

[21] M. Ayres, M. Ayres Jr., D. L. Ayres, and A. A. S. Santos, "BioEstat 5.0: Aplicações estatísticas nas áreas das ciências biológicas e médicas," Belém: Sociedade Civil Mamirauá, Brasília CNPq, 2007.

[22] R. H. Kimberlin, S. Cole, and C. A. Walker, "Pathogenesis of scrapie is faster when infection is intraspinal instead of intracerebral," *Microbial Pathogenesis*, vol. 2, no. 6, pp. 405–415, 1987.

[23] R. M. J. Deacon and J. N. P. Rawlins, "Hippocampal lesions, species-typical behaviours and anxiety in mice," *Behavioural Brain Research*, vol. 156, no. 2, pp. 241–249, 2005.

[24] R. M. J. Deacon, J. M. Raley, V. H. Perry, and J. N. P. Rawlins, "Burrowing into prion disease," *NeuroReport*, vol. 12, no. 9, pp. 2053–2057, 2001.

[25] A. A. de Sousa, R. Reis, J. Bento-Torres et al., "Influence of enriched environment on viral encephalitis outcomes: Behavioral and neuropathological changes in albino Swiss mice," *PLoS ONE*, vol. 6, no. 1, Article ID e15597, 2011.

[26] C. Cunningham, S. Campion, K. Lunnon et al., "Systemic inflammation induces acute behavioral and cognitive changes and accelerates neurodegenerative disease," *Biological Psychiatry*, vol. 65, no. 4, pp. 304–312, 2009.

[27] Z. Bi, M. Barna, T. Komatsu, and C. S. Reiss, "Vesicular stomatitis virus infection of the central nervous system activates both innate and acquired immunity," *Journal of Virology*, vol. 69, no. 10, pp. 6466–6472, 1995.

[28] C. Cunningham, R. Deacon, H. Wells et al., "Synaptic changes characterize early behavioural signs in the ME7 model of murine prion disease," *European Journal of Neuroscience*, vol. 17, no. 10, pp. 2147–2155, 2003.

[29] S. L. Franklin, S. Love, J. R. T. Greene, and S. Betmouni, "Loss of perineuronal net in ME7 prion disease," *Journal of Neuropathology and Experimental Neurology*, vol. 67, no. 3, pp. 189–199, 2008.

[30] O. Bukalo, M. Schachner, and A. Dityatev, "Modification of extracellular matrix by enzymatic removal of chondroitin sulfate and by lack of tenascin-R differentially affects several forms of synaptic plasticity in the hippocampus," *Neuroscience*, vol. 104, no. 2, pp. 359–369, 2001.

[31] A. Nimmerjahn, F. Kirchhoff, and F. Helmchen, "Neuroscience: resting microglial cells are highly dynamic surveillants of brain parenchyma in vivo," *Science*, vol. 308, no. 5726, pp. 1314–1318, 2005.

[32] G. Raivich, "Like cops on the beat: the active role of resting microglia," *Trends in Neurosciences*, vol. 28, no. 11, pp. 571–573, 2005.

[33] E. Martin, C. Boucher, B. Fontaine, and C. Delarasse, "Distinct inflammatory phenotypes of microglia and monocyte-derived macrophages in Alzheimer's disease models: effects of aging and amyloid pathology," *Aging Cell*, 2016.

[34] F. Cornejo and R. von Bernhardi, "Age-dependent changes in the activation and regulation of microglia," *Advances in Experimental Medicine and Biology*, pp. 205–226, 2016.

[35] K. Lunnon, J. L. Teeling, A. L. Tutt, M. S. Cragg, M. J. Glennie, and V. H. Perry, "Systemic inflammation modulates Fc receptor expression on microglia during chronic neurodegeneration," *The Journal of Immunology*, vol. 186, no. 12, pp. 7215–7224, 2011.

[36] J. W. Berman, M. J. Carson, L. Chang et al., "NeuroAIDS, drug abuse, and inflammation: building collaborative research activities," *Journal of Neuroimmune Pharmacology*, vol. 1, no. 4, pp. 351–399, 2006.

[37] M. M. Esiri, C. W. E. Drummond, and C. S. Morris, "Macrophages and microglia in HSV-1 infected mouse brain," *Journal of Neuroimmunology*, vol. 62, no. 2, pp. 201–205, 1995.

[38] M. C.-J. Cheeran, S. Hu, S. L. Yager, G. Gekker, P. K. Peterson, and J. R. Lokensgard, "Cytomegalovirus induces cytokine and chemokine production differentially in microglia and astrocytes: antiviral implications," *Journal of NeuroVirology*, vol. 7, no. 2, pp. 135–147, 2001.

[39] N. Guha-Thakurta and J. A. Majde, "Early induction of proinflammatory cytokine and type I interferon mRNAS following newcastle disease virus, poly [rI:rC], or low-dose LPS challenge of the mouse," *Journal of Interferon & Cytokine Research*, vol. 17, no. 4, pp. 197–204, 1997.

[40] T. R. Traynor, J. A. Majde, S. G. Bohnet, and J. M. Krueger, "Intratracheal double-stranded RNA plus interferon-γ: a model for analysis of the acute phase response to respiratory viral infections," *Life Sciences*, vol. 74, no. 20, pp. 2563–2576, 2004.

[41] M.-E. Fortier, S. Kent, H. Ashdown, S. Poole, P. Boksa, and G. N. Luheshi, "The viral mimic, polyinosinic:polycytidylic acid, induces fever in rats via an interleukin-1-dependent mechanism," *American Journal of Physiology—Regulatory Integrative and Comparative Physiology*, vol. 287, no. 4, pp. R759–R766, 2004.

[42] Y. Kondo and I. D. Duncan, "Selective reduction in microglia density and function in the white matter of colony-stimulating factor-1-deficient mice," *Journal of Neuroscience Research*, vol. 87, no. 12, pp. 2686–2695, 2009.

[43] C. J. Burns and A. F. Wilks, "C-FMS inhibitors: a patent review," *Expert Opinion on Therapeutic Patents*, vol. 21, no. 2, pp. 147–165, 2011.

[44] T. Hartung, S. von Aulock, and A. Wendel, "Role of granulocyte colony-stimulating factor in infection and inflammation," *Medical Microbiology and Immunology*, vol. 187, no. 2, pp. 61–69, 1998.

[45] J. Sanchez-Ramos, S. Song, V. Sava et al., "Granulocyte colony stimulating factor decreases brain amyloid burden and reverses cognitive impairment in Alzheimer's mice," *Neuroscience*, vol. 163, no. 1, pp. 55–72, 2009.

[46] S. Ray, M. Britschgi, C. Herbert et al., "Classification and prediction of clinical Alzheimer's diagnosis based on plasma signaling proteins," *Nature Medicine*, vol. 13, no. 11, pp. 1359–1362, 2007.

Research Article

NLRP3 Inflammasome Activation in the Brain after Global Cerebral Ischemia and Regulation by 17β-Estradiol

Roshni Thakkar,[1] Ruimin Wang,[1] Gangadhara Sareddy,[2] Jing Wang,[1] Dharma Thiruvaiyaru,[3] Ratna Vadlamudi,[2] Quanguang Zhang,[1] and Darrell Brann[1]

[1]*Department of Neuroscience and Regenerative Medicine, Medical College of Georgia, Augusta University, Augusta, GA, USA*
[2]*Department of Obstetrics and Gynecology, University of Texas Health Science Center, San Antonio, TX, USA*
[3]*Department of Mathematics, Augusta University, Augusta, GA, USA*

Correspondence should be addressed to Quanguang Zhang; qzhang@augusta.edu and Darrell Brann; dbrann@augusta.edu

17β-Estradiol (E2) is a well-known neuroprotective factor in the brain. Recently, our lab demonstrated that the neuroprotective and cognitive effects of E2 require mediation by the estrogen receptor (ER) coregulator protein and proline-, glutamic acid-, and leucine-rich protein 1 (PELP1). In the current study, we examined whether E2, acting via PELP1, can exert anti-inflammatory effects in the ovariectomized rat and mouse hippocampus to regulate NLRP3 inflammasome activation after global cerebral ischemia (GCI). Activation of the NLRP3 inflammasome pathway and expression of its downstream products, cleaved caspase-1 and IL-1β, were robustly increased in the hippocampus after GCI, with peak levels observed at 6-7 days. Expression of P2X7 receptor, an upstream regulator of NLRP3, was also increased after GCI. E2 markedly inhibited NLRP3 inflammasome pathway activation, caspase-1, and proinflammatory cytokine production, as well as P2X7 receptor expression after GCI (at both the mRNA and protein level). Intriguingly, the ability of E2 to exert these anti-inflammatory effects was lost in PELP1 forebrain-specific knockout mice, indicating a key role for PELP1 in E2 anti-inflammatory signaling. Collectively, our study demonstrates that NLRP3 inflammasome activation and proinflammatory cytokine production are markedly increased in the hippocampus after GCI, and that E2 signaling via PELP1 can profoundly inhibit these proinflammatory effects.

1. Introduction

The steroid hormone, 17β-estradiol (E2), is produced primarily by the ovaries in females and has multiple actions throughout the body and brain. In the brain, there is a significant body of work demonstrating that E2 is neuroprotective in both acute and chronic neurodegenerative disorders such as cerebral ischemia, traumatic brain injury, Alzheimer's disease, and Parkinson's disease [1–4]. For instance, in 1997, Simpkins et al. demonstrated for the first time that E2 was neuroprotective in an ovariectomized rat focal cerebral ischemia (FCI) model [5]. Since then, numerous studies have confirmed the neuroprotective effects of E2 in both focal and global cerebral ischemia (GCI) models and implicated both genomic and extranuclear signaling mechanisms in mediation of the E2 effects [4, 6–11]. In the brain, the neuroprotective actions of E2 have been implicated to be mediated

by the classical estrogen receptors, estrogen receptor-α (ER-α) and estrogen receptor-β (ER-β) [4, 9]. However, there is also evidence that a new putative ER called G-protein coupled receptor 1 (GPER1) may also contribute to neuroprotection [6, 12, 13].

Upon E2 binding to ER, several coregulatory proteins associate with the ER to regulate E2 transcriptional activity. The ER-coregulator protein association leads to formation of an "ER signalosome", which facilitates both ER genomic and extranuclear actions [14]. Recent work by our group led to the cloning and characterization of a novel ER coregulator, called proline-, glutamic acid-, and leucine-rich protein 1 (PELP1) [15, 16]. PELP1 is a multidomain scaffold protein that can interact with ERs using the nuclear receptor interaction motif, LXXLL, and with Src kinase and PI3K kinase using SH2 and PXXP motifs [16]. PELP1 is expressed in a variety of tissues, with highest expression in the brain, ovaries, testes,

and uterus [16–20]. In addition, PELP1 exhibits both nuclear and cytoplasmic localization [20], and phosphorylation of PELP1 can control its localization, interaction with other proteins, and stability in cells [16, 17]. To understand its importance in E2 actions in the brain, our group recently created a PELP1 forebrain-specific knockout (PELP1 FBKO) mouse model [16]. Using the PELP1 FBKO mouse model, we demonstrated a critical role for PELP1 in mediating E2 regulation of extranuclear and genomic signaling, as well as E2-induced neuroprotection and cognitive function in the hippocampus following ischemic injury [16].

While the role of E2 as a neuroprotective factor has been well established, its role in regulation of neuroinflammation has been less studied. Growing evidence suggests that neuroinflammation can contribute significantly to neuronal damage and cell death in neurodegenerative disorders, and that attenuation of neuroinflammation can be neuroprotective [21–23]. With respect to E2, several studies have shown that it can suppress microglial activation and proinflammatory cytokine production *in vivo* and *in vitro* [24–28], although the mechanisms underlying the effects remain unclear. A significant advance to the neuroinflammation field occurred in 2002, when Martinon and coworkers identified "inflammasomes" as key proteins that trigger the inflammatory response [29]. Inflammasomes are multiprotein complexes that mediate activation of caspase-1 and promote secretion of proinflammatory cytokines. Inflammasomes are activated in response to either pathogen associated molecular patterns (PAMPs), derived from invading pathogens, or damage-associated molecular patterns (DAMPs), released by dying cells [30]. Inflammasomes belong to the NOD-like receptor family (NLRs). NLRs are encoded by a family of 22 genes and are mainly divided as NLRP (NOD-like receptor with a pyrin domain) and NLRC (NOD-like receptors with CARD domain) family members [31].

The structure of NLRP includes a carboxy-terminal leucine rich repeat (LRR), a nucleotide binding domain called the NACHT domain, and an N-terminal pyrin domain (PYD). The PYD domain of inflammasome binds to a PYD domain of apoptosis associated speck like protein (ASC), which is an adaptor protein [31]. ASC also has a caspase activation and recruitment (CARD) domain, which binds to the CARD domain of the procaspase-1 enzyme. NLRP3 is the most abundantly found inflammasome and contributes to the majority of production of proinflammatory cytokines [23, 31, 32]. Inflammasomes are primed and activated by triggers like pathogens and metabolic and genotoxic stressors. For instance, the P2X7 receptor is activated by elevation of extracellular ATP, which then leads to activation of the NLRP3 inflammasome complex [33]. Once activated, inflammasomes enhance downstream activation of caspase-1 and release of proinflammatory cytokines, such as IL-1β and IL-18 [29, 34], which initiate a cascade of detrimental inflammatory events and apoptosis [35].

Of all of the inflammasome proteins, NLRP3 is by far the most studied inflammasome in cerebral ischemia studies. NLPR3 expression has been described in multiple brain cell types, including astrocytes, microglia, neurons, and endothelial cells [22, 36–39]. Numerous studies have

shown that NLRP3 is elevated in the brain of human stroke patients [40] and experimental stroke animals [40–44]. Furthermore, NLRP3 appears to have an important role in ischemic pathology as NLRP3 knockout animals have significantly reduced infarct size and neurovascular damage after focal cerebral ischemia [38]. Additionally, immunoglobulin treatment suppresses NLRP3 activity and strongly protects neurons in ischemic animals [40]. In addition, Aim2 and NLRC4 knockout animals have also been reported to have reduced inflammation and infarct size after focal cerebral ischemia, but the effects appear to be independent of IL-1β production [45].

With respect to E2 regulation of NLRP3 inflammasome activation, E2 has been reported in one study to suppress NLRP3 inflammasome gene expression in the cerebral cortex after focal cerebral ischemia (FCI) [46], while in a second study an ER-β agonist suppressed caspase-1, ASC, and IL-1β expression in the hippocampus after global cerebral ischemia (GCI) [47]. These studies suggest that E2 can regulate inflammasome activation; however, several important questions remain unanswered, including the following: (1) What is the temporal pattern of NLRP3 inflammasome expression in the hippocampus after GCI? (2) In which cell type in the hippocampus does NLRP3 inflammasome activation occur? (3) Does E2 only affect expression of the NLRP3 inflammasome or does it also regulate NLRP3 inflammasome complex formation? (4) What are the mechanisms underlying E2 regulation of the NLRP3 inflammasome? (5) Does the ER coregulator, PELP1, mediate E2 regulation of the NLRP3 inflammasome in the brain? The goal of the current study was to address these key questions. The results of the study reveal that both expression and complex formation of the NLRP3 inflammasome, as well as activated caspase-1 and IL-1β, are robustly increased in the hippocampus of both the rat and mouse after GCI, and this effect is strongly inhibited by E2 replacement. The results also demonstrate that NLRP3 inflammasome activation occurs in both microglia and astrocytes after GCI, and that E2 inhibits expression of both P2X7 and TXNIP, two well-known upstream inducers of NLRP3 inflammasome activation. Finally, the results reveal that the ER coregulator protein PELP1 is essential for mediation of E2 regulatory effects upon activation of the NLRP3 inflammasome.

2. Materials and Methods

2.1. Animals and Surgical Procedures

2.1.1. Ovariectomized Rat Studies. Augusta University Institutional Animal Care and Use Committee approved all animal procedures and the studies were conducted in accordance with National Institutes of Health guidelines for animal research. Three-month-old young adult Sprague Dawley rats were bilaterally ovariectomized under isoflurane anesthesia and separated into shams, ischemia-reperfusion injury, and injury with estrogen (E2) treatment groups. The E2 treatment group animals were immediately administered with 17β-estradiol dissolved in 20% β-cyclodextrin added to mini-pumps (0.5 μL/hr, 14-day release; Alzet, Cupertino, CA).

Pumps were placed in the upper mid-back region to allow subcutaneous administration of E2. The dose of E2 used led to production of physiological Diestrus I levels of circulating E2 (10–15 pg/mL). All rats, except for sham controls, were subjected to global cerebral ischemia (GCI) via 4-vessel occlusion method [48] after 7 days of ovariectomy. One day prior to occlusion, that is, 6 days after ovariectomy, all animals were anesthetized using ketamine/xylazine and their vertebral arteries were electrocauterized and the common carotid arteries were exposed. Twenty-four hours later, the common carotid arteries were transiently occluded with hemostatic clips for 12 minutes for all animals except the shams. Sham animals had their arteries exposed but not occluded. Ischemia-reperfusion was allowed to occur and animals were sacrificed using transcardial perfusion and decapitation at 1, 3, and 7 days after GCI.

2.1.2. PELP1 Forebrain-Specific Knockout Mouse Studies. Young adult female C27BL/6 PELP1 forebrain-specific knockout mice were generated as described by our group previously [16]. FLOX control as well as PELP1 knockout mice were bilaterally ovariectomized and implanted with either placebo or 17β-estradiol (E2) subcutaneous mini-pumps immediately following ovariectomy. After 7 days of ovariectomy, all animals except the shams were subjected to two-vessel occlusion for global cerebral ischemia (GCI). Animals were anesthetized briefly with ketamine/xylazine and the two common carotid arteries were exposed and occluded transiently with hemostatic clips for 40 minutes. Sham animals had their arteries exposed but not occluded. All animals were sacrificed using transcardial perfusion at 6 days after GCI.

2.2. Tissue Collection. All animals were transcardially perfused and decapitated at the desired time point after GCI. Brains were dissected in the midsagittal plane and fixed in 4% paraformaldehyde for 24 hours, cryoprotected in 30% sucrose, and sectioned on a cryostat to obtain 20-micron-thick hippocampal sections. These sections were then used for immunofluorescence staining and proximity ligation assay (Duolink). For RT-PCR and Western blot analysis, brains were collected and the hippocampal tissue was dissected out, frozen, and either processed for RNA isolation via one-step RT-PCR or homogenized for detection of proteins via Western blot analysis as described below.

2.3. RT-PCR. Hippocampal tissue samples were collected and RNA was isolated using the SV total RNA isolation system (Promega). The RNA was then used for the reverse transcriptase PCR reaction using the Superscript III one-step RT-PCR system with platinum Taq DNA Polymerase (Invitrogen) and the primers listed in Table 1 (Integrated DNA Technologies). The gene expression analyses were done using the comparative $\Delta\Delta Ct$ method. The mRNA level changes were expressed as fold change as compared to the sham animals. All Ct values for target genes were normalized to CypA gene [49].

2.4. Western Blot Analysis. Hippocampal tissue was collected 7 days after GCI as mentioned above. Individual hippocampal sample from each animal was homogenized in RIPA buffer using silica beads and a Mini-Beadbeater (Biospec Products, OK, USA). The homogenate was centrifuged at 13,000 rpm for 10 minutes at 4°C and the supernatant was used for protein estimation by Lowry's Assay (Lowry's Assay Kit, Sigma). Fifty micrograms of protein for each sample was separated on 15% sodium dodecyl sulfate-polyacrylamide gel electrophoresis, transferred on nitrocellulose membrane, and blocked with 5% bovine serum albumin for 1 hour at room temperature with gentle shaking. Blocking was followed by incubation with primary antibodies, NLRP3 (Santa-Cruz Biotechnology, sc-34408), ASC (Santa-Cruz Biotechnology, sc-22514-R), cl-caspase-1 (Santa-Cruz Biotechnology, sc-22165), and IL-1β (Abcam, ab9722), overnight at 4°C with gentle shaking. Glyceraldehyde 3-phosphate dehydrogenase (GAPDH, Santa-Cruz Biotechnology, sc-32233) was used as a loading control. The membrane was then washed with 1x TBST to remove unbound primary antibody and incubated with secondary Alexa Fluor 680 or 800 anti-rabbit/goat/mouse IgG for 1 hour at room temperature with gentle shaking. Blots were scanned using Odyssey Imaging System (LI-COR Bioscience, Lincoln, NB). The intensity of bands was quantified using ImageJ software. The immunoblot data was corrected for corresponding GAPDH values and presented as fold change in protein as compared to sham animals.

2.5. Immunofluorescence Staining and Confocal Microscopy Analysis. Twenty μm thick coronal sections were washed with PBS and 0.4% Triton-X PBS for 20 minutes. The sections were then blocked with 10% normal donkey serum for 1 hour at room temperature in PBS containing 0.1% Triton X-100, followed by incubation with primary antibody for 1–3 nights at 4°C in the same buffer. Primary antibodies used for this study included rabbit-NLRP3 (Santa-Cruz Biotechnology, sc-66846), rabbit-ASC (Santa-Cruz Biotechnology, sc-22514-R), goat-cleaved caspase-1 (Santa-Cruz Biotechnology, sc-22165), rabbit-IL-1β (Abcam, ab9722), goat-Iba1 (Abcam, ab5076), rabbit-P2X7 receptor (Sigma, P8232), and mouse-NeuN (Millipore, MAB377). After primary antibody incubation, sections were washed for 3×10 minutes at room temperature (RT), followed by incubation with the appropriate secondary antibody: Alexa-Fluor488/568/647 donkey anti-rabbit/anti-mouse/anti-goat (Invitrogen) RT/1 hour. Sections were then washed with PBS containing 0.1% Triton X-100 for 3×10 min, followed by 2×5 min with 1x PBS and briefly with water. The sections were then mounted with water-based mounting medium containing antifading agents and observed using confocal microscopy. All images were captured on a confocal laser microscope (Carl Zeiss, Germany) using the Zen software at 40x magnification and 50 μm scale bar.

2.6. Duolink Proximity Ligation Assay. Tissue sections were blocked in 5% (vol/vol) donkey serum for 1 hour at room temperature and incubated overnight with primary antibodies, goat-NLRP3 (Santa-Cruz Biotechnology, sc-34408), and rabbit-ASC (Santa-Cruz Biotechnology, sc-22514-R) at 4°C. These sections were then incubated with Duolink PLA probes, anti-Rabbit MINUS (Sigma-Aldrich, DUO92005)

Table 1

Gene	Forward primer	Reverse primer
NLRP3	5′ AGAAGCTGGGGGTTGGTGAATT 3′	5′ GTTGTCTAACTCCAGCATCTG 3′
ASC	5′ CCCATAGACCTCACTGATAAAC 3′	5′ AGAGCATCCAGCAAACCA 3′
Caspase-1	5′ AGGAGGGAATATGTGGG 3′	5′ AACCTTGGGCTTGTCTT 3′
IL-1β	5′ TGACCCATGTGAGCTGAAAG 3′	5′ AGGGATTTTGTCGTTGCTTG 3′
TXNIP	5′ CTGATGGAGGCACAGTGAGA 3′	5′ CTCGGGTGGAGTGCTTAG 3′
P2rX7	5′ CTACTCTTCGGTGGGGGCTT 3′	5′ AACCCTGGTCAGAATGGCAC 3′
CypA	5′ TATCTGCACTGCCAAGACTGAGTG 3′	5′ CTTCTTGCTGGTCTTGCCATTCC 3′

and anti-goat PLUS (Sigma-Aldrich, DUO92003) for 1 h at 37°C. Ligation and amplification were carried out at 37°C using the Duolink *in situ* detection reagent kit (Sigma-Aldrich, DUO92008) according to the manufacturer's protocol. All sections were then mounted on a slide and all images were captured on a confocal laser microscope (Carl Zeiss, Germany) using the Zen software at 40x magnification and 50 μm scale bar.

2.7. Antibody Specificity in Immunofluorescence Staining.
Specificity of inflammasome pathway factor antibodies used in immunofluorescence staining was tested by preabsorption with the antigen peptide or recombinant protein (IL-1β) available from the manufacturer. For preabsorption, fivefold concentration of each peptide, NLRP3, ASC, cleaved caspase-1, and IL-1β was incubated with primary antibody (at concentrations used for immunofluorescence staining) overnight at 4°C. The immunofluorescence staining (with DAPI) was then performed as described above, and images were captured on a confocal laser microscope (Carl Zeiss, Germany) using the Zen software at 40x magnification and 50 μm scale bar.

2.8. Quantification of Confocal Images.
The intensity of all confocal images captured at 40x magnification was quantified using MATLAB software (version R2013a by Mathworks, Natick, MA, USA) as described previously [50]. MATLAB is a programming environment with built-in image processing tools. The intensity threshold for injured animals was identified by applying a multilevel image threshold algorithm using Otsu's method in MATLAB [50]. This value was then used as an intensity threshold for sham and E2-treated animals. The algorithm digitized each image into a 1024 × 1024 matrix. The individual values contained in the matrix represented the intensity value of pixels of a particular color, that is, red, blue, or green. Using the threshold value obtained from the algorithm, the image was segmented into two regions: one above the threshold value and one below. Finally, dividing the segmented area with intensity above the threshold value by the total image area enabled image quantification. The data were obtained as relative area of fluorescence as compared to the entire area of the image. The data was expressed as percentage of area activated in the entire captured field. The quantification of immunofluorescence images was also confirmed by using ImageJ intensity analysis.

2.9. Statistical Analysis.
The independent two-sample t-test was conducted to investigate whether the mean fold change for mRNA of factors under study for each of the three time points (1, 3, and 7 days) was significantly different between the ischemic and the estrogen-treated rats. The one-way ANOVA test was conducted to investigate whether there is a significant difference among sham, ischemic, and E2-treated rats on day 7 after injury for all proteins under study. The two-way ANOVA test was conducted to investigate whether there is a significant difference among sham, ischemic, and E2-treated groups of FLOX control versus the PELP1 KO mice, as well as whether there is a significant interaction between group (sham, ischemic, and E2) and type (FLOX and KO) for all molecules under study. Whenever the difference for either of the ANOVA tests was found to be significant, *post hoc* tests such as Bonferroni's test or Tamhane's test was conducted to make pairwise comparisons of the groups of animals. All tests were conducted at a 5% level of significance using the IBM SPSS software (version 23).

3. Results

3.1. Temporal Expression of NLRP3 Inflammasome Pathway Factors in the Hippocampus after GCI and Regulation by Estradiol.
We first examined the temporal expression of NLRP3 inflammasome pathway factors and their regulation by E2 in the hippocampus after GCI. The first approach involved determining the temporal pattern of gene expression of inflammasome pathway molecules, NLRP3, ASC, caspase-1, and IL-1β. As shown in Figure 1, mRNA levels for these markers were detected using RT-PCR analysis from hippocampus tissue collected at days 1, 3, and 7 after GCI. The data are represented in terms of fold change as compared to the sham animals that did not undergo ischemia. The mRNA levels for NLRP3 (Figure 1(a)) were increased 2-fold and 1.5-fold at days 1 and 3, respectively, after injury. E2 treatment strongly suppressed NLRP3 gene expression at both days 1 and 3 after injury. Likewise, ASC mRNA levels were strongly elevated at days 1, 3, and 7 after GCI, and this effect was strongly inhibited by E2 treatment (Figure 1(b)). Caspase-1 mRNA levels were increased 2-fold at day 1 after injury and were significantly suppressed by E2 (Figure 1(c)). However, at days 3 and 7 after GCI, E2 paradoxically increased caspase-1 mRNA levels. It should be noted that the caspase-1 mRNA measured in this study represents expression of the procaspase-1, and
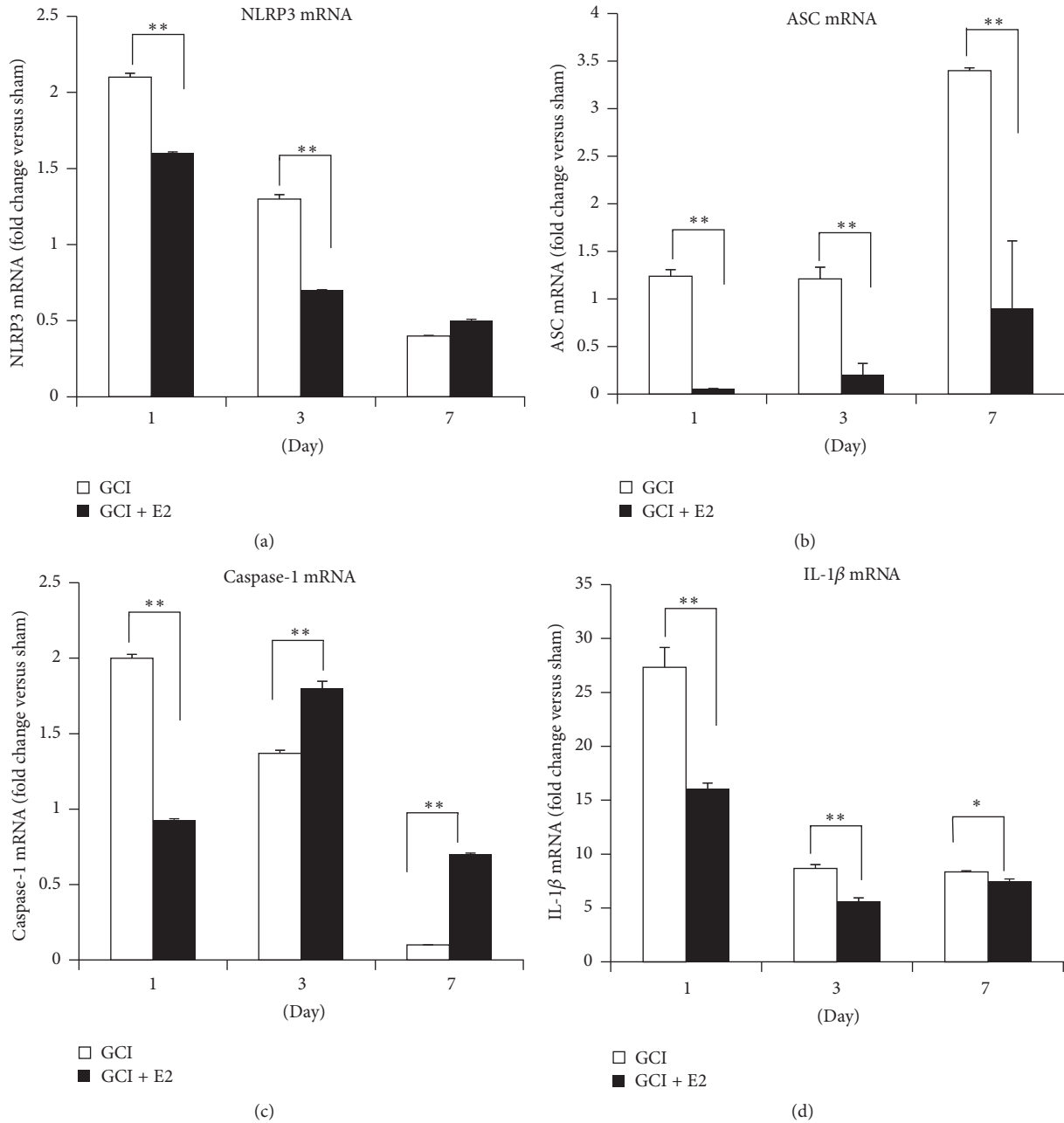
FIGURE 1: Temporal pattern of NLRP3, ASC, caspase-1, and IL-1β gene expression after GCI and their suppression by E2 treatment. mRNA samples were collected from the hippocampus of adult female ovariectomized rats, with and without E2, at various times after GCI. (a) NLRP3, (b) ASC, (c) caspase-1, and (d) IL-1β are all expressed temporally after GCI and their expression is robustly suppressed by E2 treatment at early time points after GCI (**$p \leq 0.0001$, *$p < 0.05$, GCI versus GCI + E2) (n = 5-6 animals per group).

that cleavage of the procaspase-1 protein is required for its activation. The effects of GCI and E2 upon the cleaved (active form of) caspase-1 are described below in a subsequent figure. Finally, IL-1β mRNA levels showed very high induction in the hippocampal CA1 region after GCI, with an 8–27-fold increase on days 1, 3, and 7 after GCI (Figure 1(d)). Similar to the results for the other NLRP3 inflammasome factors, E2 treatment robustly suppressed IL-1β mRNA levels

at all three days after GCI. We next examined GCI and E2 regulation of protein levels of the NLRP3 inflammasome pathway molecules in the hippocampus using Western blot analysis. Representative Western blot results are shown in Figures 2(a)–2(d), while quantification of the results from all samples is shown in Figures 2(e)–2(h). As shown in Figures 2(a)–2(h), the results demonstrate that protein levels of NLRP3, ASC, and "active" cleaved caspase-1 and cleaved

(a)

(b)

(c)

(d)

(e)

(f)

(g)

(h)
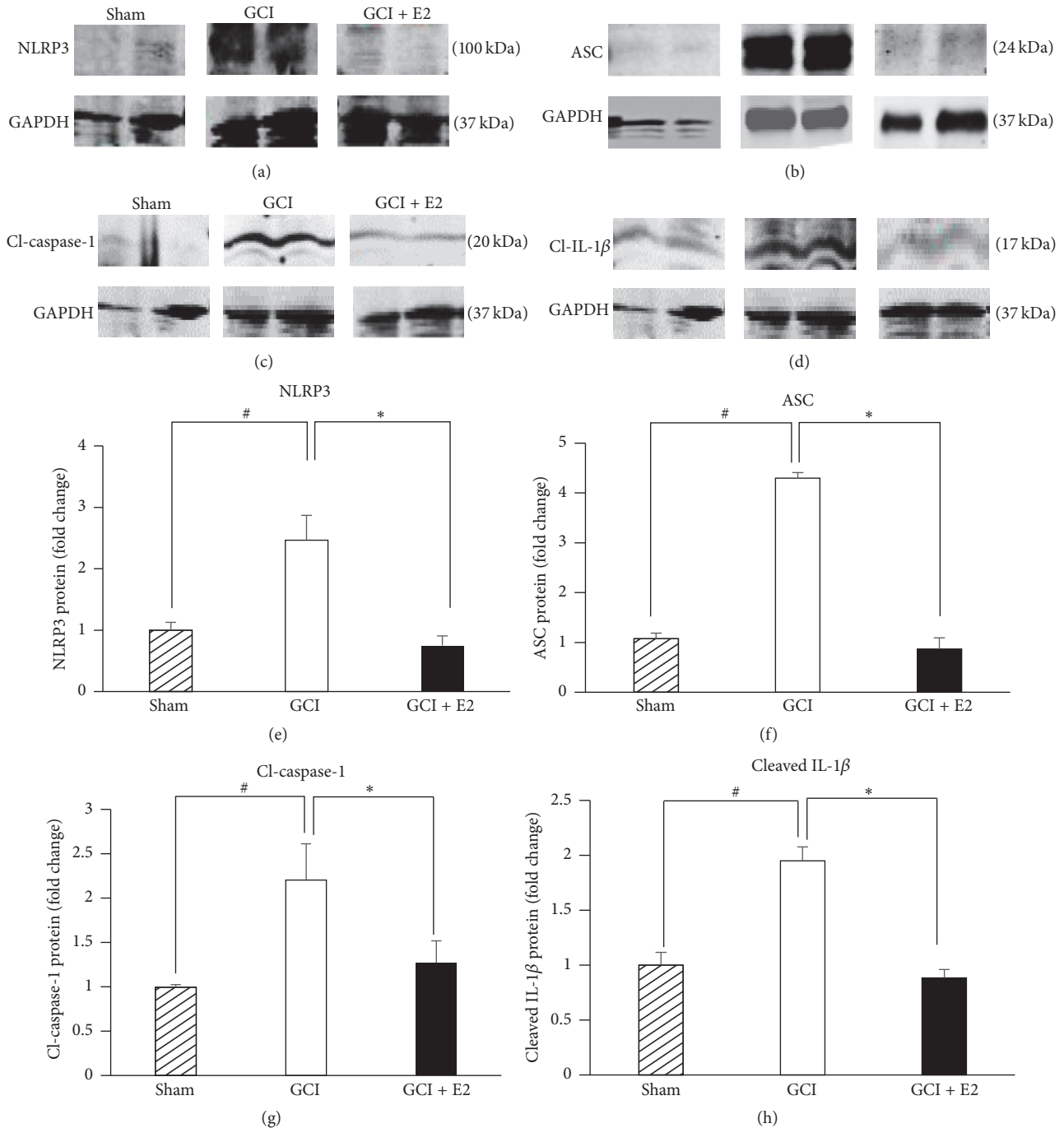
FIGURE 2: Increase in NLRP3, ASC, cleaved caspase-1, and cleaved IL-1β protein levels after GCI and its suppression by E2. Representative immunoblots from Western blot analysis of hippocampal samples collected 7 days after GCI show that (a) NLRP3, (b) ASC, (c) cleaved caspase-1, and (d) cleaved IL-1β are robustly increased after GCI as compared to shams and are significantly suppressed by E2 treatment. (e–h) Quantification of immunoblots using ImageJ software showed that NLRP3, cleaved caspase-1, and cleaved IL-1β levels are increased 2.5-fold after GCI and ASC is increased 6-fold. This increase in protein levels is significantly suppressed by E2 treatment ($^{\#}p < 0.05$ sham versus GCI; $^{*}p < 0.05$ GCI versus GCI + E2) (n = 4-5 animals per group).

IL-1β are significantly increased in the hippocampus at 7 days after GCI, and that E2 treatment significantly attenuates the elevation of the NLRP3 inflammasome proteins.

To further confirm the mRNA as well as Western blot results, we used immunofluorescence staining to detect the protein expression of NLRP3, ASC, "active" cleaved caspase-1 (cl-caspase-1), and IL-1β at 7 days after GCI. As shown in Figure 3(a), representative photomicrographs reveal that the expression of NLRP3, ASC, "active" cleaved caspase-1, and IL-1β was significantly increased in the hippocampal

(a)

(b)
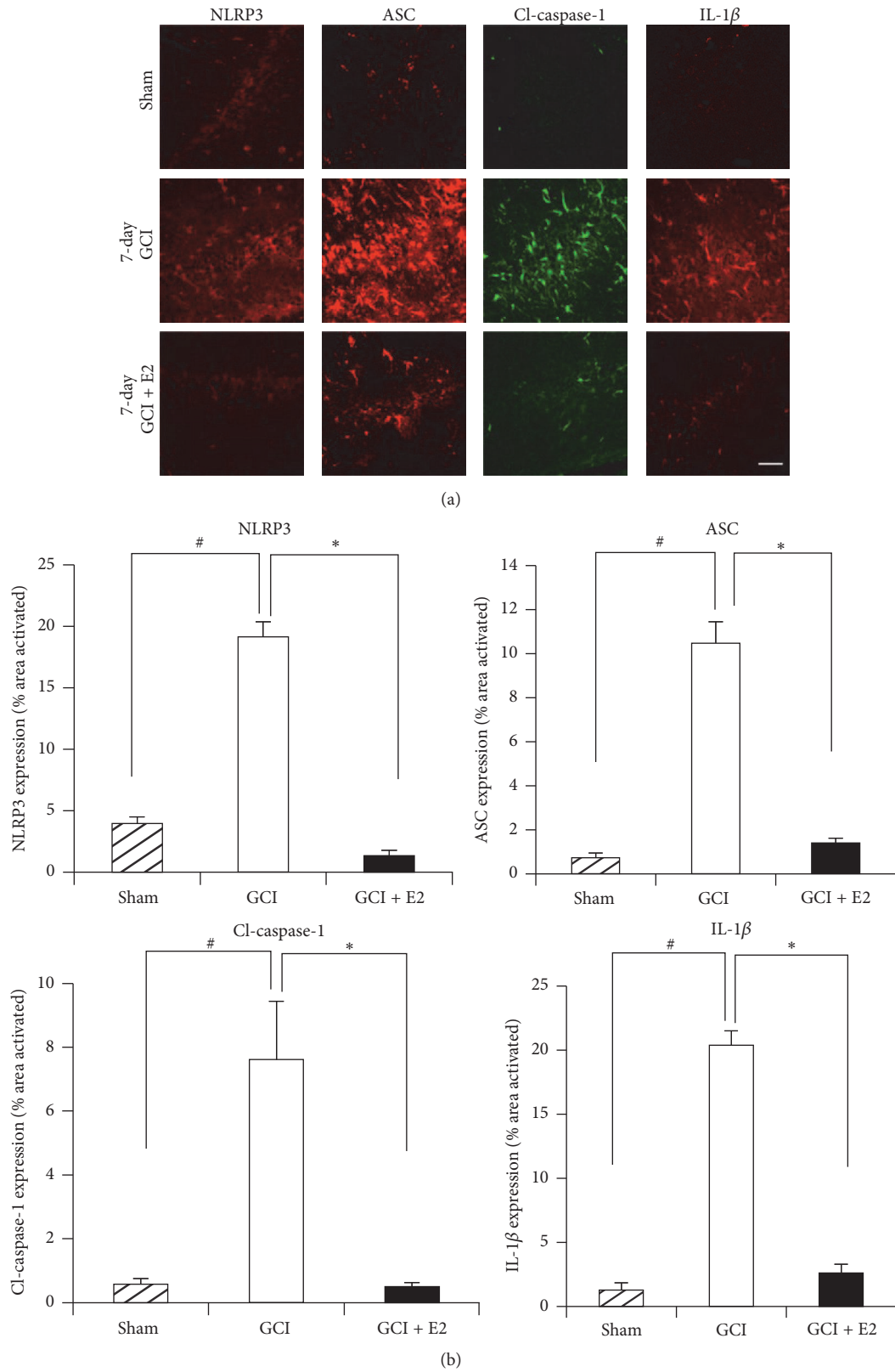
Figure 3: Expression of ASC, NLRP3, cleaved caspase-1, and IL-1β protein after GCI and suppression by E2. (a) Representative confocal images show that ASC, NLRP3, cleaved caspase-1, and IL-1β are activated in hippocampal CA1 region of the young adult female rat at day 7 after GCI. This expression is robustly suppressed by E2, as seen in the lower panel by reduced staining (magnification = 40x, scale bar = 50 μm). (b) Quantification of fluorescence intensity using MATLAB software shows a statistically significant suppression of all of these proteins at day 7 after GCI ([#] $p < 0.05$ sham versus GCI; [*] $p < 0.05$ GCI versus GCI + E2) (n = 5-6 animals per group).

(a)

(b)
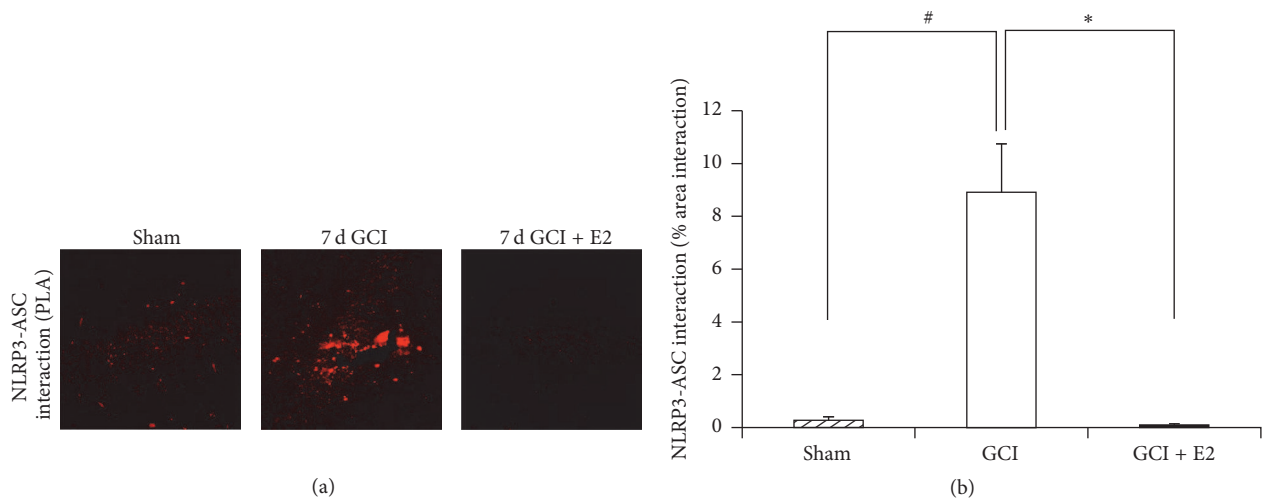
FIGURE 4: Proximity ligation assay demonstrating NLRP3-ASC complex formation after GCI and its suppression by E2. (a) Representative confocal images of proximity ligation assay (Duolink *in situ* co-IP) show that NLRP3-ASC complex is formed in hippocampal CA1 region of the young adult female rat at day 7 after GCI. This complex formation is robustly suppressed by E2 (magnification = 40x, scale bar = 50 μm). (b) Quantification of fluorescence intensity using MATLAB software shows a statistically significant suppression of complex formation at day 7 after GCI ($^\#p < 0.05$ sham versus GCI; $^*p < 0.05$ GCI versus GCI + E2) (n = 5-6 animals per group).

CA1 region of the rat hippocampus at 7 days after GCI, as compared to the sham controls. Furthermore, E2 treatment robustly suppressed the enhanced protein expression of NLRP3, ASC, "active" cleaved caspase-1, and IL-1β in the hippocampus after GCI. Figure 3(b) shows the results of quantification of the immunofluorescence staining intensity using MATLAB software. As shown in Figure 3(b), all of the NLRP3 inflammasome pathway molecules were highly expressed at day 7 after GCI and were significantly suppressed by E2. The specificity of the NLRP3 inflammasome pathway antibodies used in our studies was confirmed by preabsorption studies with antigen (or when not available, with the recombinant protein, e.g., for IL-1β). As shown in Supplementary Figure 1 (see Supplementary Material available online at http://dx.doi.org/10.1155/2016/8309031), antigen or recombinant protein preabsorption essentially completely abolished staining for the NLRP3 inflammasome molecules, demonstrating specificity of the antibodies. Therefore, coupled with the mRNA expression and Western blot data in Figures 1 and 2, the results in Figure 3 further confirm that expression of NLRP3 inflammasome pathway molecules is increased in the rat hippocampus after GCI and suppressed by E2 treatment.

Using triple immunofluorescent staining, we next determined the cell type of expression of NLRP3 inflammasome molecules in the hippocampal CA1 region at 7 days after GCI. As shown in Supplementary Figure 2, triple immunofluorescence staining of each of the NLRP3 inflammasome pathway molecules with either GFAP (astrocyte marker) or CD11b (microglial marker) and NeuN (neuronal marker) or DAPI revealed that NLRP3, ASC, "active" cleaved caspase-1, and IL-1β are colocalized with CD11b and GFAP in the hippocampal CA1 region at 7 days after GCI. This finding suggests that NLRP3 inflammasome pathway activation occurs primarily

in microglia and activated astrocytes in the hippocampus at 7 days after GCI.

3.2. Estradiol Suppresses NLRP3 Inflammasome Complex Formation in the Hippocampus after GCI. In the above studies, we examined E2 regulation of expression of NLRP3 inflammasome pathway factors after GCI. To further confirm activation of the NLRP3 inflammasome, we examined NLRP3 inflammasome *complex formation* after GCI, as assembly of the inflammasome complex is known to be essential for its activation. To examine NLRP3 inflammasome complex formation, we performed an *in situ* coimmunoprecipitation assay, also known as a proximity ligation assay (or Duolink assay), to measure the protein-protein interaction (complex formation) of NLRP3 and ASC in the rat hippocampal CA1 region at 7 days after GCI. ASC binding to NLRP3 is known to be critical for recruitment of caspase-1 and for NLRP3 inflammasome activation [31]. The protein-protein interaction in the proximity ligation assay was detected as red immunofluorescence signal under a confocal microscope. Representative photomicrographs of the proximity ligation assay results are shown in Figure 4(a), while quantification of the results from all images from all animals for intensity using MATLAB is shown in Figure 4(b). As shown in Figures 4(a) and 4(b), the results of the proximity ligation assay revealed a significant increase in NLRP3-ASC complex formation in the hippocampus after GCI, as compared to sham controls. Furthermore, E2 treatment strongly suppressed the GCI-induced NLRP3-ASC complex formation in the hippocampus.

3.3. Estradiol Regulates Expression of Upstream Activators of the NLRP3 Inflammasome. We hypothesized that E2 may control NLRP3 inflammasome activation by regulating the

(a)

(b)

(c)
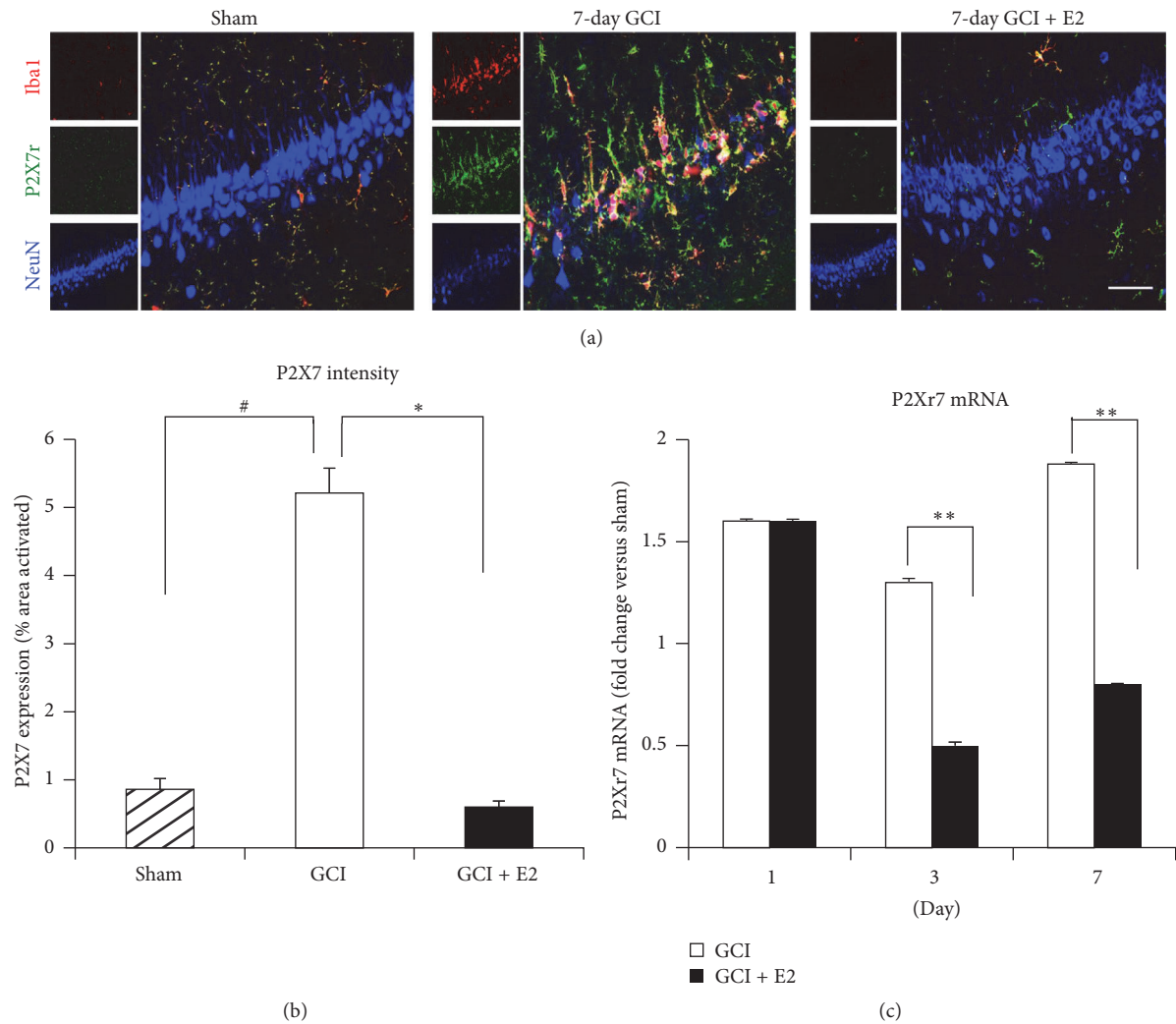
FIGURE 5: Increased expression of P2X7 receptor after GCI and its suppression by E2 treatment. (a) Representative confocal images stained for Iba1 (red), P2X7r (green), and NeuN (blue) show the activation of microglia and increased expression of P2X7r in the hippocampal CA1 region of young adult female rats 7 days after GCI. The P2X7 receptor colocalized very strongly with microglia (yellow color). This expression and microglial activation is suppressed by E2 treatment (magnification = 40x, scale bar = 50 μm). (b) Quantification of fluorescence intensity using MATLAB software shows a statistically significant suppression of P2X7 receptor by E2 at day 7 after GCI ($^{\#}p < 0.05$ sham versus GCI; $^{*}p < 0.05$ GCI versus GCI + E2) (n = 5-6 animals per group). (c) mRNA collected from rat hippocampus after GCI shows induction of P2rX7 gene and its significant suppression by E2 treatment at days 3 and 7 after GCI ($^{**}p < 0.0001$, GCI versus GCI + E2) (n = 5-6 animals/group).

expression of key upstream activators of the NLRP3 inflammasome. A well-known upstream activator of the NLRP3 inflammasome is the ionotropic purinergic P2X7 receptor. The P2X7 receptor becomes activated by extracellular ATP, which is a danger-associated molecular pattern (DAMP) released from damaged/dying neurons after injury [51]. We thus examined the ability of E2 to regulate protein and mRNA expression levels of the P2X7 receptor in the hippocampus using triple immunofluorescent staining and quantitative RT-PCR. Representative photomicrographs of the triple immunofluorescent staining results for P2X7 receptor, NeuN (neuronal marker), and Iba1 (microglial marker) are shown in Figure 5(a), while quantification of the results from all images from all animals for intensity using MATLAB is shown in Figure 5(b). As shown in Figures 5(a) and 5(b), triple

immunofluorescence colocalization results with specific antibodies to the P2X7 receptor, NeuN (neuronal marker), and Iba1 (microglial marker) revealed that immunoreactive protein levels of the P2X7 receptor in hippocampal CA1 region of rat are strongly upregulated at 7 days after GCI. Furthermore, the P2X7 receptor immunostaining signal was highly colocalized with the microglia marker Iba1, indicating its upregulation occurs in microglia. Intriguingly, P2X7 receptor immunoreactive protein levels in the hippocampal CA1 region were profoundly suppressed by E2 treatment. We next examined whether E2 could regulate gene expression of the P2X7 receptor in the hippocampus at various time points after GCI. As shown in Figure 5(c), P2X7 receptor mRNA levels were significantly increased (1.5–2-fold) in the hippocampus from days 1, 3, and 7 after GCI, as compared

to sham controls. E2 treatment had no effect upon the P2X7 receptor mRNA levels at day 1 after GCI but significantly attenuated its expression at days 3 and 7 after GCI. We also examined whether E2 could regulate another upstream regulator of NLRP3, thioredoxin interacting protein (TXNIP). Following increased production of reactive oxygen species (such as what occurs after ischemic injury), TXNIP is released from its complex with thioredoxin (TRX) and can bind to the LRR region of NLRP3 and activate it [52, 53]. As shown in Supplementary Figure 3A, immunofluorescence staining revealed that TXNIP expression was increased in rat hippocampal CA1 region at 7 days after GCI and that this expression is robustly suppressed by E2 treatment. Quantification of intensity of TXNIP for all images from all animals is shown in Supplementary Figure 3B. As shown in Supplementary Figure 3C, mRNA levels of TXNIP were also increased after GCI and significantly suppressed by E2 treatment at days 3 and 7 after GCI. These results suggest that E2 may potentially regulate the inflammasome complex activation via its ability to suppress expression of the NLRP3 inflammasome upstream regulators, P2X7 receptor and TXNIP.

3.4. The Estrogen Receptor Coregulator, PELP1, Is Essential for the Ability of Estradiol to Regulate the NLRP3 Inflammasome after GCI. To enhance understanding of the mechanisms involved in the E2 anti-inflammatory effects after GCI, we examined the role of the ER coregulator, PELP1. Prior work by our group using a PELP1 forebrain-specific KO (PELP1 FBKO) mouse model that we generated revealed that PELP1 is required for E2-induced rapid and genomic signaling, as well as the neuroprotective and cognitive-enhancing effects of E2 in the hippocampus after GCI [16]. Moreover, RNA-seq data comparing hippocampal gene expression in E2-treated FLOX control and PELP1 FBKO mice at 24 hours after GCI revealed that a number of inflammatory pathway genes were upregulated in the PELP1 FBKO mouse [16]. We therefore examined whether the ability of E2 to suppress expression of NLRP3 inflammasome pathway factors in the hippocampal CA1 region after GCI required PELP1 mediation. We utilized FLOX control and PELP1 FBKO mice and examined E2 regulation of NLRP3 inflammasome expression at 6 days after GCI, as this time point showed robust microglia activation and neuronal loss after GCI [16]. Representative photomicrographs of immunofluorescent staining results for NLRP3 and ASC are shown in Figures 6(a) and 6(c), respectively, while quantification of the results from all images from all animals for intensity using MATLAB is shown in Figures 6(b) and 6(d). As shown in Figures 6(a)–6(d), immunofluorescence staining of hippocampal CA1 region sections revealed that NLRP3 and ASC were markedly elevated at day 6 after GCI in FLOX control mice, and that E2 suppressed this effect. Intriguingly, the ability of E2 to suppress elevation of NLRP3 and ASC in the hippocampus was lost in PELP1 FBKO mice (Figures 6(a)–6(d)).

We next examined the downstream products of the NLRP3 inflammasome pathway, "active" cleaved caspase-1 and IL-1β, using immunofluorescence staining of hippocampal sections. Representative photomicrographs of

immunofluorescent staining results for "active" cleaved caspase-1 and IL-1β are shown in Figures 7(a) and 7(c), respectively, while quantification of the results from all images from all animals for intensity using MATLAB is shown in Figures 7(b) and 7(d). As shown in Figures 7(a)–7(d), immunoreactive protein levels of "active" cleaved caspase-1 and IL-1β were significantly enhanced in the hippocampal CA1 region at 6 days after GCI in FLOX control mice, and E2 strongly suppressed the elevation of both of these factors. Further, the ability of E2 to suppress elevation of "active" cleaved caspase-1 and IL-1β in the hippocampus was lost in PELP1 FBKO mice (Figures 7(a)–7(d)).

We next used the *in situ* proximity ligation assay to determine whether the ability of E2 to suppress NLRP3-ASC complex formation after GCI is compromised in PELP1 FBKO mice. Representative photomicrographs of the proximity ligation assay results are shown in Figure 8(a), while quantification of the results from all images from all animals for intensity of using MATLAB is shown in Figure 8(b). As shown in Figure 8, FLOX control mice demonstrated a significantly increased NLRP3-ASC complex formation in the hippocampal CA1 region at 6 days after GCI as detected by the proximity ligation assay, and E2 treatment completely attenuated the complex formation. However, the ability of E2 to inhibit the GCI-induced NLRP3-ASC complex formation was lost in PELP1 FBKO mice (Figures 8(a) and 8(b)).

Finally, we examined the effect of PELP1 deletion upon the ability of E2 to suppress expression of the P2X7 receptor in hippocampal CA1 region after GCI. Representative photomicrographs of triple immunofluorescent staining results for the P2X7 receptor, Iba1 (microglia marker), and NeuN (neuronal marker) are shown in Figure 9(a), while quantification of the results from all images from all animals for intensity using MATLAB is shown in Figure 9(b). As shown in Figures 9(a) and 9(b), triple immunofluorescence staining for the P2X7 receptor, Iba1 (microglia marker), and NeuN (neuronal marker) revealed that there was increased expression of the P2X7 receptor in the hippocampal CA1 region of FLOX control as well as PELP1 knockout mice after GCI. The P2X7 receptor immunoreactive signal colocalized with Iba1, indicating that the enhanced P2X7 expression occurred primarily in microglia. As was the case in the ovariectomized rat, P2X7 receptor expression was suppressed by E2 treatment in FLOX control mice that were subjected to GCI. The suppressive effect of E2 on P2X7 receptor expression required PELP1 mediation as evidenced by the loss of the suppressive effect of E2 in PELP1 FBKO mice (Figures 9(a) and 9(b)).

4. Discussion

The current study provides several important findings. First, it demonstrates that the NLRP3 inflammasome is robustly activated in microglia and astrocytes in the hippocampal CA1 region of both the rat and mouse after GCI. Secondly, it demonstrates that low dose E2 treatment profoundly suppresses NLRP3 inflammasome activation in the hippocampus after GCI. Thirdly, it provides novel insight into the mechanisms of E2 anti-inflammatory effects by demonstrating that E2 suppresses induction of the upstream activators of the

(a)

(b)

(c)

(d)

FIGURE 6: The ability of E2 to attenuate expression of NLRP3 and ASC after GCI is lost in PELP1 forebrain-specific knockout mice. (a and c) Representative confocal images show that NLRP3 and ASC are induced in hippocampal CA1 region at day 6 after GCI in FLOX control as well as PELP1 knockout mice. The expression of these markers is suppressed by E2 in the FLOX control mice but not in the PELP1 KO mice sections (KO = PELP1 knockout) (magnification = 40x, scale bar = 50 μm). (b and d) Quantification of fluorescence intensity using MATLAB software shows a statistically significant suppression of all of these proteins by E2 in FLOX but not in KO mice ([#] $p < 0.05$, sham versus GCI; [*] $p < 0.05$, GCI versus GCI + E2; [$] $p < 0.05$, FLOX GCI + E2 versus KO GCI + E2; NS, not significant, KO GCI versus KO GCI + E2) (n = 5-6 animals/group).

NLRP3 inflammasome (P2X7 and TXNIP) after GCI, and that the ER coregulator protein, PELP1, is essential for the anti-inflammatory actions of E2 in the hippocampus.

A unique strength of our study is that we used a novel genetic PELP1 forebrain-specific knockout model to elucidate the role of PELP1 in E2 anti-inflammatory actions. Based on the results of our study, we propose that E2 binds to ER and recruits the coregulator PELP1 to form an active transcriptional complex, which leads to attenuation of expression of the upstream inducers of the NLRP3 inflammasome, P2X7

(a)

(b)

(c)

(d)

FIGURE 7: The ability of E2 to attenuate expression of cleaved caspase-1 and IL-1β after GCI is lost in PELP1 forebrain-specific knockout mice. (a and c) Representative confocal images show that cleaved caspase-1 and IL-1β are induced in hippocampal CA1 region at day 6 after GCI in FLOX as well as PELP1 knockout mice. The expression of these markers is suppressed by E2 in the FLOX control mice but not in the PELP1 KO mice sections (KO = PELP1 knockout) (magnification = 40x, scale bar = 50 μm). (b and d) Quantification of fluorescence intensity using MATLAB software shows a statistically significant suppression of all of these proteins by E2 in FLOX but not in KO mice ($^{\#}p < 0.05$, sham versus GCI; $^{*}p < 0.05$, GCI versus GCI + E2; $^{\$}p < 0.05$, FLOX GCI + E2 versus KO GCI + E2; NS, not significant, KO GCI versus KO GCI + E2) (n = 5-6 animals/group).

and TXNIP in the hippocampus after GCI. Suppression of TXNIP and NLRP3 activation could also be due to E2 suppression of GCI-induced ROS generation, as we previously demonstrated that E2 profoundly suppresses NOX2 NADPH oxidase activity and superoxide induction after GCI [7].

Furthermore, in support of this possibility, NOX2 knockout mice have been shown to have a significantly reduced NLRP3 activation after FCI that correlated with reduced infarct size, reduced edema, and improved neurological outcome [38]. While we believe that E2 effects involve mediation by nuclear

(a)

(b)
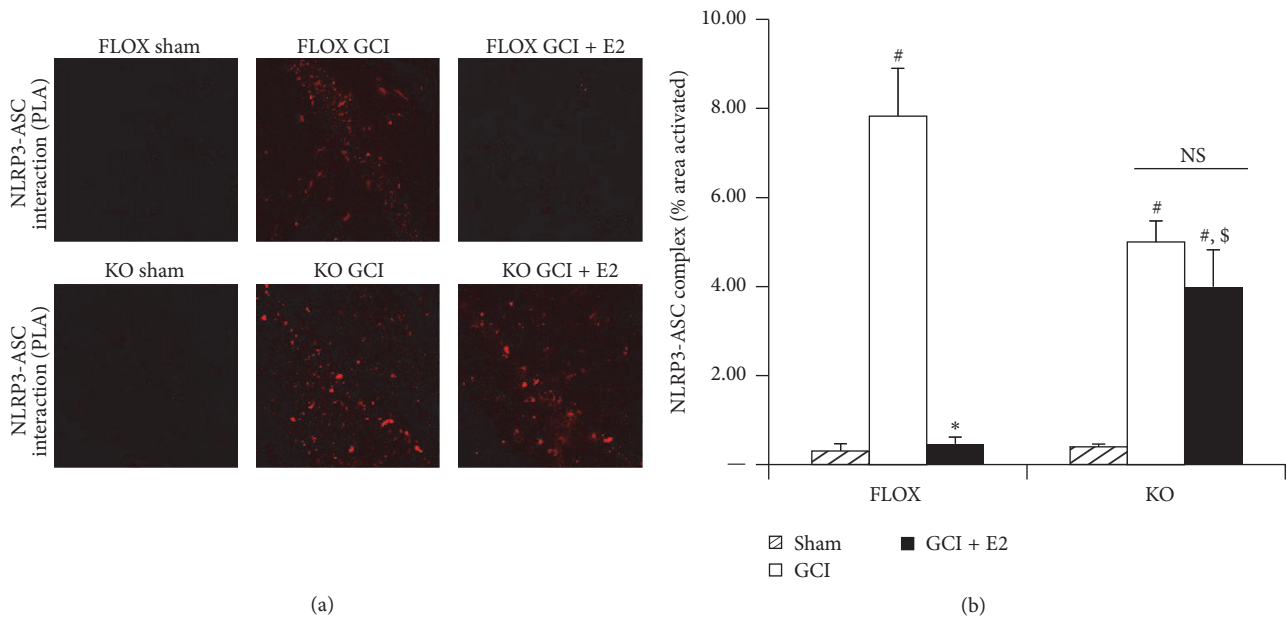
FIGURE 8: The ability of E2 to suppress NLRP3-ASC complex formation after GCI is lost in PELP1 forebrain-specific knockout mice. (a) Representative confocal images of Duolink *in situ* co-IP show that ASC-NLRP3 complex is formed in hippocampal CA1 region at day 6 after GCI. This complex formation is robustly suppressed by E2 in the FLOX but not in KO (KO = PELP1 knockout) (magnification = 40x, scale bar = 50 μm). (b) MATLAB analysis of the images shows a statistically significant suppression of complex formation by E2 in FLOX but not in KO mice ([#]$p < 0.05$, sham versus GCI; [*]$p < 0.05$, GCI versus GCI + E2; [$]$p < 0.05$, FLOX GCI + E2 versus KO GCI + E2; NS, not significant, KO GCI versus KO GCI + E2) (n = 5-6 animals/group).

ER, we cannot rule out the possibility that extranuclear ER signaling could be involved as well, as we previously demonstrated that PELP1 also mediates extranuclear ER-mediated rapid signaling effects in the hippocampus after GCI [16].

While our study did not address which ER mediates E2 effects upon the NLRP3 inflammasome after GCI, PELP1 can interact with and mediate the effects of both ER-α and ER-β in various cells throughout the body [54]. Intriguingly, both ER-α and ER-β have been implicated to mediate anti-inflammatory actions of E2 in the brain. Most relevant to our study, ER-β antisense oligonucleotide knockdown has been reported to attenuate E2 suppression of ASC, caspase-1, and IL-1β after GCI [47]. This study did not examine which inflammasome mediated the increase in IL-1β and was regulated by E2, but our work provides strong evidence that the NLRP3 inflammasome is activated in the hippocampus after GCI and strongly regulated by E2. ER-α has also been implicated in mediating some of the anti-inflammatory effects of E2 in the brain. For instance, Vegeto et al. [28] found that the ability of E2 to suppress lipopolysaccharide-induced microglial activation and monocyte recruitment in the brain is lost in ER-α knockout mice. However, this study did not assess the role for ER-α in inflammasome regulation. Finally, to our knowledge, no study has examined the role of GPER1 in the regulation of inflammasome activation in the brain. Studies are ongoing in our laboratory to further address this issue.

Of significant note, our study found that NLRP3 pathway factors were induced in both microglia and astrocytes after GCI. A similar multicell induction of NLRP3 pathway factors

has been reported previously in the cerebral cortex after focal cerebral ischemia [55] or traumatic brain injury [22], demonstrating that NLPR3 factors are expressed in neurons, astrocytes, and microglia after brain injury. Likewise, expression of P2X7 receptors has been reported in multiple brain cell types, including microglia, astrocytes, and neurons [56–59], and is increased after cerebral ischemia [60–62]. Thus, it appears that multiple cell types can express inflammasomes and be involved in neuroinflammation. While less is known about the role of NLRP3 inflammasome activation in astrocytes as compared to microglia, recent studies have found that astrocytes can express NLRP3 and ASC and display caspase-1 cleavage and release of IL-1β after induction with inflammatory agents, Aβ, or *in vitro* oxygen/glucose deprivation [36, 37, 63]. This suggests that inflammasome activation in astrocytes may also contribute to neuroinflammation after brain injury. In contrast, NLRP1 and Aim2 expression has been primarily reported in neurons in the ischemic or injured brain [64–66].

Finally, previous work by our laboratory and others has shown that E2 is profoundly neuroprotective and improves functional outcome after GCI and FCI [5, 9–11, 16, 67]. Based on our current results, we propose that E2 inhibition of NLRP3 inflammasome activation is an important contributing mechanism for E2 beneficial effects on neuronal survival and functional outcome after GCI. In support of this possibility, NLRP3 knockout mice have been shown to have significantly reduced infarct size after FCI, suggesting that NLRP3 inflammasome activation contributes to neuronal damage and cell death after cerebral ischemia [38].
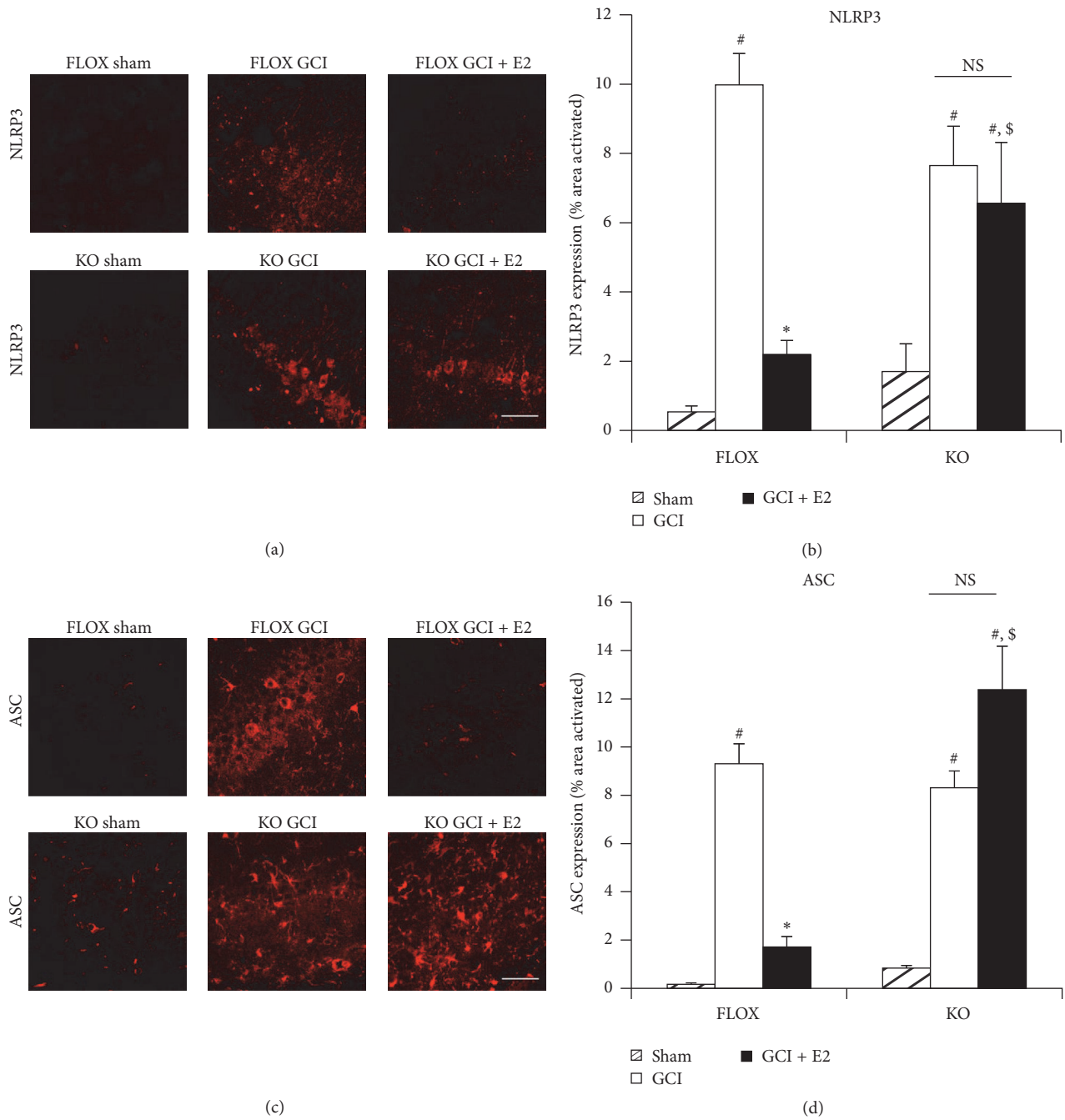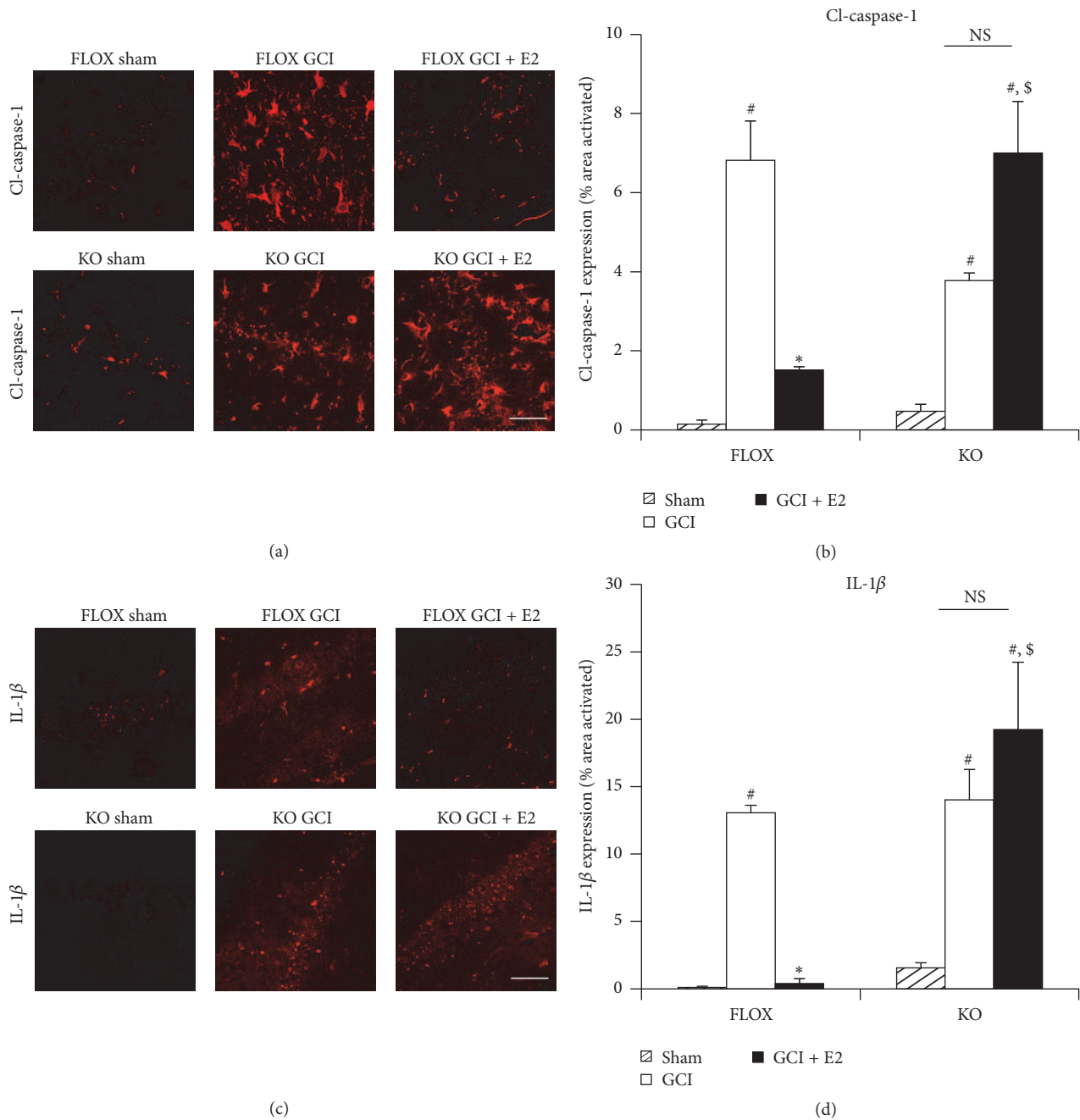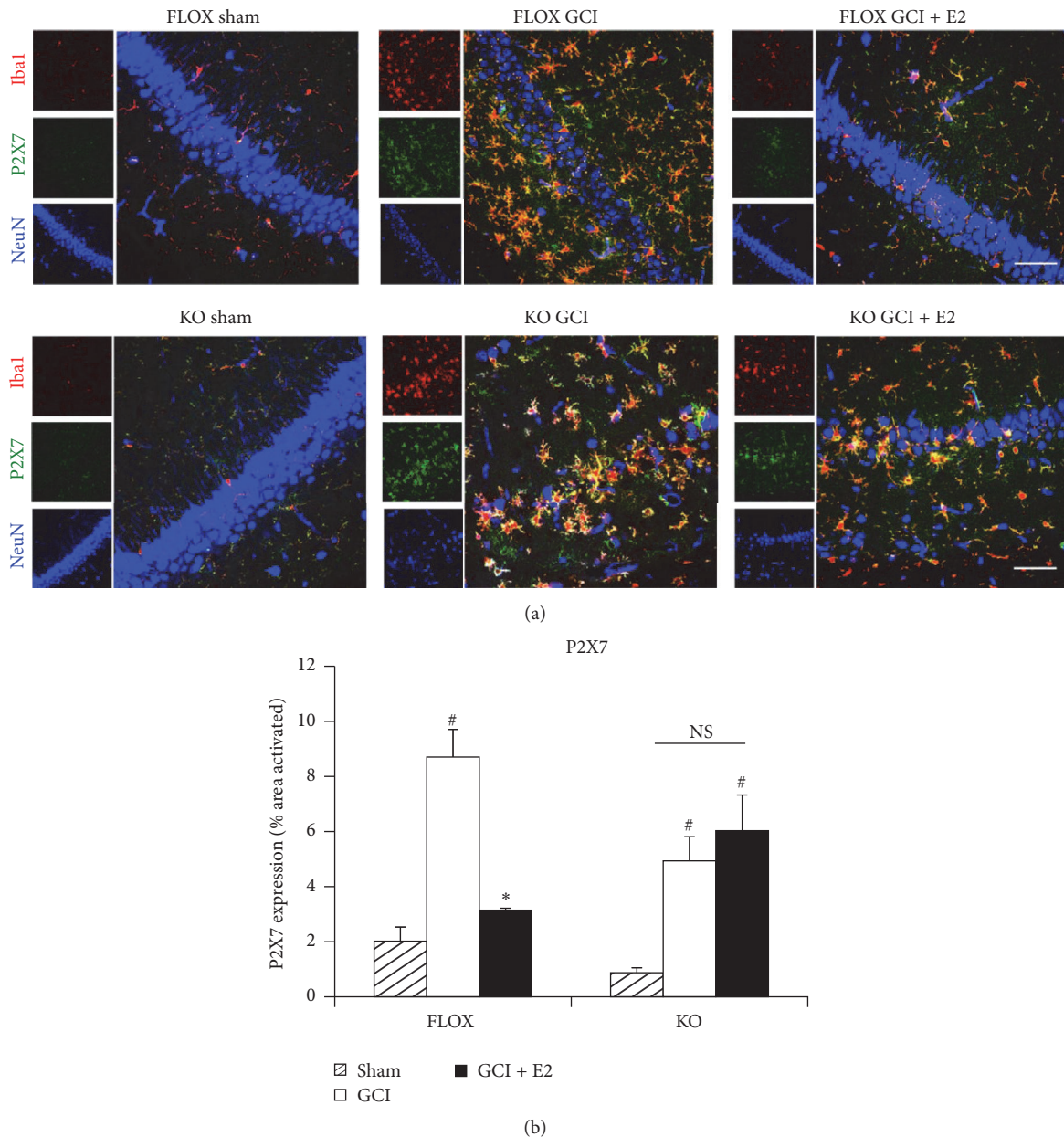
FIGURE 9: The ability of E2 to attenuate expression of P2X7 receptor after GCI is lost in PELP1 forebrain-specific knockout mice. (a) Representative confocal images stained for Iba1 (red), P2X7 receptor (green), and NeuN (blue) show the activation of microglia and increased expression of P2X7 receptor in the hippocampal CA1 region of young adult female FLOX control as well as PELP1 KO mice 6 days after GCI. The P2X7 receptor colocalized very strongly with microglia. This expression and microglial activation are suppressed by E2 treatment in FLOX control mice but not in PELP1 KO mice (KO = PELP1 knockout) (magnification = 40x, scale bar = 50 μm). (b) MATLAB analysis of the images shows a statistically significant suppression of all of these proteins by E2 in FLOX control but not in KO mice ($^{\#}p < 0.05$, sham versus GCI; $^{*}p < 0.05$, GCI versus GCI + E2; NS, not significant, KO GCI versus KO GCI + E2) (n = 5-6 animals/group).

Furthermore, intravenous immunoglobulin has been shown to suppress NLRP3 inflammasome-mediated neuronal cell death after ischemic stroke and to improve neurological outcome [40]. Finally, caspase-1 knockout mice, as well as caspase-1 inhibitor- or dominant negative-treated mice, have been all reported to have significantly decreased neuronal cell death and brain deficits following cerebral ischemia [68–71]. Collectively, these findings suggest that NLRP3 inflammasome activation and resultant neuroinflammation contribute significantly to the neuronal cell death and functional deficits that occur after cerebral ischemia, and that E2 inhibition of NLRP3 inflammasome activation may contribute significantly to its beneficial protective effects following cerebral ischemia.

In conclusion, the results of our study demonstrate that NLRP3 inflammasome activation is strongly increased in the hippocampus after GCI, and that E2 strongly suppresses both expression and activation of the NLRP3 inflammasome. The

effects of E2 require the ER-coregulator, PELP1, and involve attenuation of P2X7 and TXNIP, two well-known upstream inducers of NLRP3 inflammasome activation. These findings provide new insight into the anti-inflammatory effects of E2 in the brain and suggest that therapeutic targeting of the NLRP3 inflammasome for inhibition by E2 analogues or NLRP3 inflammasome selective inhibitors may have efficacy in the treatment of GCI, as well as other neurodegenerative disorders that involve NLRP3 inflammasome activation and neuroinflammation.

Abbreviations

ASC:	Apoptosis associated speck like protein
E2:	17β-Estradiol
ER-α:	Estrogen receptor alpha
ER-β:	Estrogen receptor-beta
FCI:	Focal cerebral ischemia
GCI:	Global cerebral ischemia
IL-1β:	Interleukin-1beta
NLRP3:	NOD-like receptor with a pyrin domain-3
PELP1:	Proline-, glutamic acid-, and leucine-rich protein 1
TXNIP:	Thioredoxin interacting protein.

Competing Interests

The authors declare that they have no competing interests.

Authors' Contributions

Roshni Thakkar and Ruimin Wang contributed equally to the studies and should be considered as co-first authors.

Acknowledgments

References

[1] D. Lebesgue, V. Chevaleyre, R. S. Zukin, and A. M. Etgen, "Estradiol rescues neurons from global ischemia-induced cell death: multiple cellular pathways of neuroprotection," *Steroids*, vol. 74, no. 7, pp. 555–561, 2009.

[2] J. W. Simpkins, E. Perez, Xiaofei Wang, Shaohua Yang, Yi Wen, and M. Singh, "The potential for estrogens in preventing Alzheimer's disease and vascular dementia," *Therapeutic Advances in Neurological Disorders*, vol. 2, no. 1, pp. 31–49, 2009.

[3] J. W. Simpkins, P. S. Green, K. E. Gridley, M. Singh, N. C. De Fiebre, and G. Rajakumar, "Role of estrogen replacement therapy in memory enhancement and the prevention of neuronal loss associated with Alzheimer's disease," *The American Journal of Medicine*, vol. 103, no. 3, pp. 19s–25s, 1997.

[4] E. B. Engler-Chiurazzi, C. Brown, J. Povroznik, and J. Simpkins, "Estrogens as neuroprotectants: estrogenic actions in the context of cognitive aging and brain injury," *Progress in Neurobiology*, 2016.

[5] J. W. Simpkins, G. Rajakumar, Y.-Q. Zhang et al., "Estrogens may reduce mortality and ischemic damage caused by middle cerebral artery occlusion in the female rat," *Journal of Neurosurgery*, vol. 87, no. 5, pp. 724–730, 1997.

[6] H. Tang, Q. Zhang, L. Yang et al., "GPR30 mediates estrogen rapid signaling and neuroprotection," *Molecular and Cellular Endocrinology*, vol. 387, no. 1-2, pp. 52–58, 2014.

[7] Q.-G. Zhang, L. Raz, R. Wang et al., "Estrogen attenuates ischemic oxidative damage via an estrogen receptor α-mediated inhibition of NADPH oxidase activation," *The Journal of Neuroscience*, vol. 29, no. 44, pp. 13823–13836, 2009.

[8] L.-C. Yang, Q.-G. Zhang, C.-F. Zhou et al., "Extranuclear estrogen receptors mediate the neuroprotective effects of estrogen in the rat hippocampus," *PLoS ONE*, vol. 5, no. 5, article e9851, 2010.

[9] D. W. Brann, K. Dhandapani, C. Wakade, V. B. Mahesh, and M. M. Khan, "Neurotrophic and neuroprotective actions of estrogen: basic mechanisms and clinical implications," *Steroids*, vol. 72, no. 5, pp. 381–405, 2007.

[10] D. B. Dubal, M. L. Kashon, L. C. Pettigrew et al., "Estradiol protects against ischemic injury," *Journal of Cerebral Blood Flow and Metabolism*, vol. 18, no. 11, pp. 1253–1258, 1998.

[11] T. Jover, H. Tanaka, A. Calderone et al., "Estrogen protects against global ischemia-induced neuronal death and prevents activation of apoptotic signaling cascades in the hippocampal CA1," *Journal of Neuroscience*, vol. 22, no. 6, pp. 2115–2124, 2002.

[12] M. Bourque, M. Morissette, and T. Di Paolo, "Neuroprotection in Parkinsonian-treated mice via estrogen receptor α activation requires G protein-coupled estrogen receptor 1," *Neuropharmacology*, vol. 95, pp. 343–352, 2015.

[13] E. R. Prossnitz and M. Barton, "Estrogen biology: new insights into GPER function and clinical opportunities," *Molecular and Cellular Endocrinology*, vol. 389, no. 1-2, pp. 71–83, 2014.

[14] M.-A. Arevalo, I. Azcoitia, and L. M. Garcia-Segura, "The neuroprotective actions of oestradiol and oestrogen receptors," *Nature Reviews Neuroscience*, vol. 16, no. 1, pp. 17–29, 2015.

[15] R. K. Vadlamudi, R.-A. Wang, A. Mazumdar et al., "Molecular cloning and characterization of PELP1, a novel human coregulator of estrogen receptor α," *The Journal of Biological Chemistry*, vol. 276, no. 41, pp. 38272–38279, 2001.

[16] G. R. Sareddy, Q. Zhang, R. Wang et al., "Proline-, glutamic acid-, and leucine-rich protein 1 mediates estrogen rapid signaling and neuroprotection in the brain," *Proceedings of the National Academy of Sciences of the United States of America*, vol. 112, no. 48, pp. E6673–E6682, 2015.

[17] G. R. Sareddy and R. K. Vadlamudi, "PELP1: structure, biological function and clinical significance," *Gene*, vol. 585, no. 1, pp. 128–134, 2016.

[18] M. M. Khan, M. Hadman, C. Wakade et al., "Cloning, expression, and localization of MNAR/PELP1 in rodent brain: colocalization in estrogen receptor-α- but not in gonadotropin-releasing hormone-positive neurons," *Endocrinology*, vol. 146, no. 12, pp. 5215–5227, 2005.

[19] M. M. Khan, M. Hadman, L. M. De Sevilla et al., "Cloning, distribution, and colocalization of MNAR/PELP1 with glucocorticoid receptors in primate and nonprimate brain," *Neuroendocrinology*, vol. 84, no. 5, pp. 317–329, 2007.

[20] R. K. Vadlamudi, R.-A. Wang, A. Mazumdar et al., "Molecular cloning and characterization of PELP1, a novel human coregulator of estrogen receptor α," *Journal of Biological Chemistry*, vol. 276, no. 41, pp. 38272–38279, 2001.

[21] M. T. Heneka, M. P. Kummer, A. Stutz et al., "NLRP3 is activated in Alzheimer's disease and contributes to pathology in APP/PS1 mice," *Nature*, vol. 493, no. 7434, pp. 674–678, 2013.

[22] H.-D. Liu, W. Li, Z.-R. Chen et al., "Expression of the NLRP3 inflammasome in cerebral cortex after traumatic brain injury in a rat model," *Neurochemical Research*, vol. 38, no. 10, pp. 2072–2083, 2013.

[23] G. Singhal, E. J. Jaehne, F. Corrigan, C. Toben, and B. T. Baune, "Inflammasomes in neuroinflammation and changes in brain function: a focused review," *Frontiers in Neuroscience*, vol. 8, article 315, 2014.

[24] E. Vegeto, V. Benedusi, and A. Maggi, "Estrogen anti-inflammatory activity in brain: a therapeutic opportunity for menopause and neurodegenerative diseases," *Frontiers in Neuroendocrinology*, vol. 29, no. 4, pp. 507–519, 2008.

[25] J. Dang, B. Mitkari, M. Kipp, and C. Beyer, "Gonadal steroids prevent cell damage and stimulate behavioral recovery after transient middle cerebral artery occlusion in male and female rats," *Brain, Behavior, and Immunity*, vol. 25, no. 4, pp. 715–726, 2011.

[26] C. M. Brown, T. A. Mulcahey, N. C. Filipek, and P. M. Wise, "Production of proinflammatory cytokines and chemokines during neuroinflammation: novel roles for estrogen receptors α and β," *Endocrinology*, vol. 151, no. 10, pp. 4916–4925, 2010.

[27] E. Vegeto, S. Belcredito, S. Ghisletti, C. Meda, S. Etteri, and A. Maggi, "The endogenous estrogen status regulates microglia reactivity in animal models of neuroinflammation," *Endocrinology*, vol. 147, no. 5, pp. 2263–2272, 2006.

[28] E. Vegeto, S. Belcredito, S. Etteri et al., "Estrogen receptor-alpha mediates the brain antiinflammatory activity of estradiol," *Proceedings of the National Academy of Sciences of the United States of America*, vol. 100, no. 16, pp. 9614–9619, 2003.

[29] F. Martinon, K. Burns, and J. Tschopp, "The inflammasome: a molecular platform triggering activation of inflammatory caspases and processing of proIL-β," *Molecular Cell*, vol. 10, no. 2, pp. 417–426, 2002.

[30] H. Guo, J. B. Callaway, and J. P.-Y. Ting, "Inflammasomes: mechanism of action, role in disease, and therapeutics," *Nature Medicine*, vol. 21, no. 7, pp. 677–687, 2015.

[31] J. G. Walsh, D. A. Muruve, and C. Power, "Inflammasomes in the CNS," *Nature Reviews Neuroscience*, vol. 15, no. 2, pp. 84–97, 2014.

[32] J. P. De Rivero Vaccari, W. D. Dietrich, and R. W. Keane, "Activation and regulation of cellular inflammasomes: gaps in our knowledge for central nervous system injury," *Journal of Cerebral Blood Flow and Metabolism*, vol. 34, no. 3, pp. 369–375, 2014.

[33] M. J. Leo Bours, P. C. Dagnelie, A. L. Giuliani, A. Wesselius, and F. Di Virgilio, "P2 receptors and extracellular ATP: a novel homeostatic pathway in inflammation," *Frontiers in Bioscience (Scholar Edition)*, vol. 3, no. 4, pp. 1443–1456, 2011.

[34] F. Martinon, A. Mayor, and J. Tschopp, "The inflammasomes: guardians of the body," *Annual Review of Immunology*, vol. 27, pp. 229–265, 2009.

[35] L. C. Freeman and J. P.-Y. Ting, "The pathogenic role of the inflammasome in neurodegenerative diseases," *Journal of Neurochemistry*, vol. 136, supplement 1, pp. 29–38, 2016.

[36] Z. Jian, S. Ding, H. Deng et al., "Probenecid protects against oxygen-glucose deprivation injury in primary astrocytes by regulating inflammasome activity," *Brain Research*, vol. 1643, pp. 123–129, 2016.

[37] S. Alfonso-Loeches, J. R. Ureña-Peralta, M. J. Morillo-Bargues, J. O.-D. La Cruz, and C. Guerri, "Role of mitochondria ROS generation in ethanol-induced NLRP3 inflammasome activation and cell death in astroglial cells," *Frontiers in Cellular Neuroscience*, vol. 8, article 216, 2014.

[38] F. Yang, Z. Wang, X. Wei et al., "NLRP3 deficiency ameliorates neurovascular damage in experimental ischemic stroke," *Journal of Cerebral Blood Flow and Metabolism*, vol. 34, no. 4, pp. 660–667, 2014.

[39] L. Lammerding, A. Slowik, S. Johann, C. Beyer, and A. Zendedel, "Poststroke inflammasome expression and regulation in the peri-infarct area by gonadal steroids after transient focal ischemia in the rat brain," *Neuroendocrinology*, vol. 103, no. 5, pp. 460–475, 2016.

[40] D. Yang-Wei Fann, S.-Y. Lee, S. Manzanero et al., "Intravenous immunoglobulin suppresses NLRP1 and NLRP3 inflammasome-mediated neuronal death in ischemic stroke," *Cell Death and Disease*, vol. 4, no. 9, article e790, 2013.

[41] D. Y.-W. Fann, T. Santro, S. Manzanero et al., "Intermittent fasting attenuates inflammasome activity in ischemic stroke," *Experimental Neurology*, vol. 257, pp. 114–119, 2014.

[42] Y. Tong, Z. H. Ding, F. X. Zhan et al., "The NLRP3 inflammasome and stroke," *International Journal of Clinical and Experimental Medicine*, vol. 8, no. 4, pp. 4787–4794, 2015.

[43] X. Wang, R. Li, X. Wang, Q. Fu, and S. Ma, "Umbelliferone ameliorates cerebral ischemia-reperfusion injury via upregulating the PPAR gamma expression and suppressing TXNIP/NLRP3 inflammasome," *Neuroscience Letters*, vol. 600, pp. 182–187, 2015.

[44] Y. Li, J. Li, S. Li et al., "Curcumin attenuates glutamate neurotoxicity in the hippocampus by suppression of ER stress-associated TXNIP/NLRP3 inflammasome activation in a manner dependent on AMPK," *Toxicology and Applied Pharmacology*, vol. 286, no. 1, pp. 53–63, 2015.

[45] A. Denes, G. Coutts, N. Lénárt et al., "AIM2 and NLRC4 inflammasomes contribute with ASC to acute brain injury independently of NLRP3," *Proceedings of the National Academy of Sciences*, vol. 112, no. 13, pp. 4050–4055, 2015.

[46] A. Slowik and C. Beyer, "Inflammasomes are neuroprotective targets for sex steroids," *Journal of Steroid Biochemistry and Molecular Biology*, vol. 153, pp. 135–143, 2015.

[47] J. P. De Rivero Vaccari, H. H. Patel, F. J. Brand, M. A. Perez-Pinzon, H. M. Bramlett, and A. P. Raval, "Estrogen receptor beta signaling alters cellular inflammasomes activity after global cerebral ischemia in reproductively senescence female rats," *Journal of Neurochemistry*, vol. 136, no. 3, pp. 492–496, 2016.

[48] W. A. Pulsinelli and J. B. Brierley, "A new model of bilateral hemispheric ischemia in the unanesthetized rat," *Stroke*, vol. 10, no. 3, pp. 267–272, 1979.

[49] K. Langnaese, R. John, H. Schweizer, U. Ebmeyer, and G. Keilhoff, "Selection of reference genes for quantitative real-time PCR in a rat asphyxial cardiac arrest model," *BMC Molecular Biology*, vol. 9, article 53, 2008.

[50] C. Kozlowski and R. M. Weimer, "An automated method to quantify microglia morphology and application to monitor activation state longitudinally in vivo," *PLoS ONE*, vol. 7, no. 2, Article ID e31814, 2012.

[51] A. Gombault, L. Baron, and I. Couillin, "ATP release and purinergic signaling in NLRP3 inflammasome activation," *Frontiers in Immunology*, vol. 3, article 414, 2012.

[52] R. Zhou, A. Tardivel, B. Thorens, I. Choi, and J. Tschopp, "Thioredoxin-interacting protein links oxidative stress to inflammasome activation," *Nature Immunology*, vol. 11, no. 2, pp. 136–140, 2010.

[53] L. Minutoli, D. Puzzolo, M. Rinaldi et al., "ROS-mediated NLRP3 inflammasome activation in brain, heart, kidney, and testis ischemia/reperfusion injury," *Oxidative Medicine and Cellular Longevity*, vol. 2016, Article ID 2183026, 10 pages, 2016.

[54] D. W. Brann, Q.-G. Zhang, R.-M. Wang, V. B. Mahesh, and R. K. Vadlamudi, "PELP1-A novel estrogen receptor-interacting protein," *Molecular and Cellular Endocrinology*, vol. 290, no. 1-2, pp. 2–7, 2008.

[55] L. Lammerding, A. Slowik, S. Johann, C. Beyer, and A. Zendedel, "Post-stroke inflammasome expression and regulation in the peri-infarct area by gonadal steroids after transient focal ischemia in the rat brain," *Neuroendocrinology*, vol. 103, no. 5, 2016.

[56] Y. Yu, S. Ugawa, T. Ueda et al., "Cellular localization of P2X7 receptor mRNA in the rat brain," *Brain Research*, vol. 1194, pp. 45–55, 2008.

[57] G. Collo, S. Neidhart, E. Kawashima, M. Kosco-Vilbois, R. A. North, and G. Buell, "Tissue distribution of the P2X7 receptor," *Neuropharmacology*, vol. 36, no. 9, pp. 1277–1283, 1997.

[58] K. Nagasawa, C. Escartin, and R. A. Swanson, "Astrocyte cultures exhibit P2X7 receptor channel opening in the absence of exogenous ligands," *Glia*, vol. 57, no. 6, pp. 622–633, 2009.

[59] A. Ohishi, Y. Keno, A. Marumiya et al., "Expression level of P2X7 receptor is a determinant of ATP-induced death of mouse cultured neurons," *Neuroscience*, vol. 319, pp. 35–45, 2016.

[60] X.-J. Li, R.-F. He, S. Li, X.-J. Li, and D.-L. Li, "Effects of progesterone on learning and memory and P2X7 receptor expression in the hippocampus after global cerebral ischemia/reperfusion injury in rats," *Zhongguo Ying Yong Sheng Li Xue Za Zhi*, vol. 28, no. 5, pp. 472–475, 2012.

[61] Y.-M. Lu, R.-R. Tao, J.-Y. Huang et al., "P2X 7 signaling promotes microsphere embolism-triggered microglia activation by maintaining elevation of Fas ligand," *Journal of Neuroinflammation*, vol. 9, article 172, 2012.

[62] A. Melani, S. Amadio, M. Gianfriddo et al., "P2X7 receptor modulation on microglial cells and reduction of brain infarct caused by middle cerebral artery occlusion in rat," *Journal of Cerebral Blood Flow and Metabolism*, vol. 26, no. 7, pp. 974–982, 2006.

[63] J. Couturier, I.-C. Stancu, O. Schakman et al., "Activation of phagocytic activity in astrocytes by reduced expression of the inflammasome component ASC and its implication in a mouse model of Alzheimer disease," *Journal of Neuroinflammation*, vol. 13, article 20, 2016.

[64] Y.-C. Wang, W.-Z. Li, Y. Wu et al., "Acid-sensing ion channel 1a contributes to the effect of extracellular acidosis on NLRP1 inflammasome activation in cortical neurons," *Journal of Neuroinflammation*, vol. 12, no. 1, article 246, 2015.

[65] S. E. Adamczak, J. P. De Rivero Vaccari, G. Dale et al., "Pyroptotic neuronal cell death mediated by the AIM2 inflammasome," *Journal of Cerebral Blood Flow and Metabolism*, vol. 34, no. 4, pp. 621–629, 2014.

[66] X. Wang, G. Chu, Z. Yang et al., "Ethanol directly induced HMGB1 release through NOX2/NLRP1 inflammasome in neuronal cells," *Toxicology*, vol. 334, pp. 104–110, 2015.

[67] Q.-G. Zhang, R. Wang, M. Khan, V. Mahesh, and D. W. Brann, "Role of Dickkopf-1, an antagonist of the Wnt/β-catenin signaling pathway, in estrogen-induced neuroprotection and attenuation of tau phosphorylation," *Journal of Neuroscience*, vol. 28, no. 34, pp. 8430–8441, 2008.

[68] R. M. Friedlander, V. Gagliardini, H. Hara et al., "Expression of a dominant negative mutant of interleukin-1β converting enzyme in transgenic mice prevents neuronal cell death induced by trophic factor withdrawal and ischemic brain injury," *Journal of Experimental Medicine*, vol. 185, no. 5, pp. 933–940, 1997.

[69] H. Hara, R. M. Friedlander, V. Gagliardini et al., "Inhibition of interleukin 1β converting enzyme family proteases reduces ischemic and excitotoxic neuronal damage," *Proceedings of the National Academy of Sciences of the United States of America*, vol. 94, no. 5, pp. 2007–2012, 1997.

[70] M. Rabuffetti, C. Sciorati, G. Tarozzo, E. Clementi, A. A. Manfredi, and M. Beltramo, "Inhibition of caspase-1-like activity by Ac-Tyr-Val-Ala-Asp-chloromethyl ketone induces longlasting neuroprotection in cerebral ischemia through apoptosis reduction and decrease of proinflammatory cytokines," *Journal of Neuroscience*, vol. 20, no. 12, pp. 4398–4404, 2000.

[71] G. P. Schielke, G.-Y. Yang, B. D. Shivers, and A. L. Betz, "Reduced ischemic brain injury in interleukin-1β converting enzyme- deficient mice," *Journal of Cerebral Blood Flow and Metabolism*, vol. 18, no. 2, pp. 180–185, 1998.

Research Article

Hydrogen Sulfide Regulates the $[Ca^{2+}]_i$ Level in the Primary Medullary Neurons

Xiaoni Liu,[1,2] Nana Zhang,[1] Yingjiong Ding,[1] Dongqing Cao,[3] Ying Huang,[1] Xiangjun Chen,[2] Rui Wang,[4] and Ning Lu[1]

[1]*Department of Physiology and Pathophysiology, Shanghai Medical College, Fudan University, Shanghai 200032, China*
[2]*Department of Neurology, Huashan Hospital, Fudan University, Shanghai 200040, China*
[3]*Department of Neurosurgery, Huashan Hospital, Fudan University, Shanghai 200040, China*
[4]*The Cardiovascular and Metabolic Research Unit, Laurentian University, Sudbury, ON, Canada P3E 2C6*

Correspondence should be addressed to Ning Lu; luning7@shmu.edu.cn

In the present study, we attempted to elucidate mechanisms for the regulation of intracellular calcium levels by H_2S in primary rat medullary neurons. Our results showed that NaHS significantly increased the level of $[Ca^{2+}]_i$ in rat medullary neurons in a concentration-dependent manner. L-Cysteine and SAM significantly raised the level of $[Ca^{2+}]_i$ in the medullary neurons while HA and/or AOAA produced a reversal effect. In addition, L-cysteine and SAM significantly increased but HA and/or AOAA decreased the production of H_2S in the cultured neurons. The $[Ca^{2+}]_i$ elevation induced by H_2S was significantly diminished by EGTA-Ca^{2+}-free solutions, and this elevation was also reduced by nifedipine or nimodipine and mibefradil, suggesting the role of L-type and/or T-type Ca^{2+} channels. Moreover, the effect of H_2S on $[Ca^{2+}]_i$ level in neurons was significantly attenuated by BAPTA-AM and thapsigargin, suggesting the source of Ca^{2+}. Therefore, we concluded that both exogenous and endogenous H_2S elevates $[Ca^{2+}]_i$ level in primarily cultured rat medullary neurons via both increasing calcium influx and mobilizing intracellular Ca^{2+} stores from ER.

1. Introduction

Hydrogen sulfide (H_2S) is an important gasotransmitter along with nitric oxide (NO), carbon monoxide (CO), and ammonium in addition to its conventional toxicological profile [1–3]. The endogenous production of H_2S in the human body is catalyzed by several enzymes, including two pyridoxal-5$'$-phosphate- (PLP-) dependent enzymes, namely, cystathionine-β-synthase (CBS) and cystathionine-γ-lyase (CSE), and 3-mercaptopyruvate sulfurtransferase (MST) [4]. L-Cysteine and homocysteine or their derivatives are the substrates of these H_2S-generating enzymes [4]. The expression of these H_2S-generating enzymes is tissue specific. CBS is highly expressed in the central nervous system (CNS). CSE is mainly expressed in the cardiovascular system [2] and MST is considered as another source of H_2S in the brain [5]. The physiological concentration of sulfide in brain tissue is

detected to be 50~160 μM [6], whereas the blood level of H_2S is estimated at low micromolar to high nanomolar range [7].

H_2S is a signaling molecule for neurotransmission and neuromodulation and is involved in learning, memory, and nociception [3]. H_2S has been reported to enhance the induction of long-term potentiation (LTP), a synaptic model in learning and memory, and increase the sensitivity of NMDA receptor mediated response, indicating a neuroprotective effect of H_2S on homocysteine-induced cerebrovascular pathology [8, 9]. NaHS attenuated the inflammation induced by LPS in microglia via inhibiting of p38-MAPK [10], suggesting the implication of H_2S in the neuroprotection or treatment of cerebral ischemia and neuroinflammatory diseases. It was also found that H_2S decreased blood pressure in various models of hypertension [11–14]. H_2S treatment reduced blood pressure and oxidative stress in angiotensin II induced hypertensive mice [15] and in spontaneously

hypertensive rats (SHRs) [14]. These findings indicate that H_2S, as an important neuromodulator, produces antineuroinflammatory, antioxidant, and antiapoptotic effects in neurons and glial cells. However, the underlying mechanisms are still unsettled.

Calcium is second messenger for neuronal functions, such as release of neurotransmitters [16], synaptic plasticity [17, 18], neuronal excitation, and gene transcription [16]. Changes of intracellular free Ca^{2+} concentration ($[Ca^{2+}]_i$) may directly alter neuronal excitability [19]. It was reported that H_2S increased $[Ca^{2+}]_i$ and induced Ca^{2+} waves in primary cultures of astrocytes [20] and regulated calcium homeostasis in microglial cells [21]. Another study showed that H_2S modulated calcium homeostasis in cultured rat cerebellar granule neurons (CGN) as it induced activation of Ca^{2+} entry through L-type Ca^{2+} channels and thereby of neuronal activity [22]. It has also been reported that H_2S increased $[Ca^{2+}]_i$ in SH-SY5Y neuronal cells by increasing Ca^{2+} influx via plasma membrane and the subsequent release of calcium from intracellular calcium store [19]. However, the regulation of H_2S on $[Ca^{2+}]_i$ in the medullary neurons has not been demonstrated.

We recently reported that H_2S exerts its cardiovascular effects by decreasing oxidative stress via inhibition of NADPH oxidase activity in the rostral ventrolateral medulla (RVLM) of SHRs [14]. RVLM, where sympathetic premotor neurons are located, is connected with other cardiovascular nuclei in the CNS, functioning to regulate the cardiovascular effects by regulating sympathetic nerve activity [23–25]. However, the molecular mechanisms for the neuromodulatory effect of H_2S on RVLM are not clear. In the present study, we used the primarily cultured medullary neurons to investigate the effects of H_2S on the level of $[Ca^{2+}]_i$. Our study provides the evidence that H_2S increases $[Ca^{2+}]_i$ in neurons through several different mechanisms.

2. Materials and Methods

2.1. Chemicals. DMEM/F-12, neurobasal medium, and B27 supplement were obtained from Gibco Invitrogen Corporation (Carlsbad, CA, USA). Fura-2 AM and BAPTA-AM were obtained from Dojindo Molecular Technologies, Inc. Sodium hydrosulfide hydrate (NaHS), EGTA, thapsigargin (TG), nifedipine, nimodipine, and mibefradil were obtained from Sigma-Aldrich. Fura-2 AM and TG were dissolved in dimethyl sulfoxide (DMSO). The final concentration of DMSO did not exceed 0.1%. Anti-MAP-2 antibody produced in mouse, anti-MAP-2 antibody produced in rabbit, anti-CBS antibody produced in mouse, and anti-MST antibody produced in rabbit were obtained from Abcam. Anti-glutamate antibody produced from rabbit was obtained from Sigma-Aldrich. FITC goat anti-rabbit IgG (H+L) and Cy3 goat anti-mouse IgG (H+L) were obtained from Beyotime Biotechnology. Alexa Fluor® 488 goat anti-rabbit IgG (H+L) and Alexa Fluor 594 goat anti-mouse IgG (H+L) were obtained from Invitrogen.

2.2. Cell Cultures. Primary cultures of medullary neurons were prepared from 14-day-old embryos of Sprague Dawley rats. The fetal rats were humanely taken out and killed by decapitation, and then brain slices containing the entire medullary were prepared. The dissected tissues were removed and transferred to D-hanks' solution containing (in g/L) 8.0 NaCl, 0.4 KCl, 0.134 $Na_2HPO_4 \cdot 12H_2O$, 0.06 KH_2PO_4, 0.35 $NaHCO_3$, and 1 glucose, pH 7.2~7.4, and finally chopped. The tissues were then treated with 0.125% trypsin in D-hanks' solution for 10~12 min at 37°C and gently triturated using flame-polished Pasteur pipettes. Cell suspension was centrifuged for 8 min at 1000 ×g. Then the cell pellets were resuspended in Dulbecco's modified Eagle's medium (DMEM) and F-12 supplement (1:1) with 10% fetal bovine serum (FBS) before plating onto glass-bottomed dishes coated with poly-L-lysine (20 μg/mL for 12~24 h) and kept at 37°C in 5% CO_2 incubator. After overnight incubation in DMEM, the medium was changed to neurobasal medium (Gibco) containing 15 mM glucose supplemented with 2% B27, 2 mM glutamine, 10 μg/mL penicillin, and 10 μg/mL streptomycin. The culture medium for medullary neurons was changed every 48 h. Microscopically, glial cells were not apparent in medullary neurons employing this protocol. The neurons were maintained for 7–10 days in primarily culture until used for calcium imaging.

2.3. Immunofluorescence Staining and Laser Confocal Microscopy. The primarily cultured medullary neurons were washed three times with D-hanks' solution and then cells were fixed with 1 mL 4% paraformaldehyde (PFA) in 0.1 M sodium phosphate buffer (0.1 M PB; pH 7.4) for 20 min. Afterward, cells were blocked with 1 mL 5% fetal bovine serum (FBS) for 30 min after being washed three times with D-hanks' solution. Then, cells were incubated with primary antibodies, namely, anti-MAP-2 (mouse, 1:200) and anti-glutamate (rabbit, 1:100), anti-MAP-2 antibody (rabbit, 1:200) and anti-CBS (mouse, 1:100), anti-MAP-2 antibody (mouse, 1:200) and anti-MST (rabbit, 1:50), and anti-MAP-2 antibody (rabbit, 1:200) and anti-CSE (mouse, 1:50), for 1 h at 37°C, plus an additional 12 h at 4°C. On the next day, the cell were washed three times with D-hanks' solution and incubated with fluorescent secondary antibodies, namely, FITC goat anti-rabbit IgG (H+L) (1:100) and Cy3 goat anti-mouse IgG (H+L) (1:100) or Alexa Fluor 488 goat anti-rabbit IgG (H+L) (1:500) and Alexa Fluor 594 goat anti-mouse IgG (H+L) (1:500), for 1 h at 37°C. Then cells were incubated with DAPI for 5 min at 37°C after being washed three times with D-hanks' solution. Finally, 500 μL D-hanks' solution was added to the cell dishes for confocal comicroscopy (Zeiss LSM510, Jena, Germany).

2.4. $[Ca^{2+}]_i$ Measurements. To determine the level of $[Ca^{2+}]_i$, neurons were loaded with Ca^{2+}-specific dye Fura-2 by incubating with 2.5 μM Fura-2/AM (Molecular Probes) in HBSS (140 mM NaCl, 5 mM KCl, 1 mM $MgCl_2$, 2 mM $CaCl_2$, 10 mM glucose, and 10 mM HEPES-NaHS [pH 7.3]) at 37°C for 30 minutes and subsequently washed three times with HBSS to remove the excess extracellular Fura-2/AM. $[Ca^{2+}]_i$ was

expressed as the ratio (R) of emitted fluorescence corresponding to excitation wavelengths of 340 nm and 380 nm. R/R_0 was applied to assess the change of $[Ca^{2+}]_i$ level, in which R_0 represents the fluorescent signal before drug treatment and R represents the signal after drug treatment.

To identify the source of Ca^{2+}, the increase in $[Ca^{2+}]_i$ induced by NaHS was determined in Ca^{2+}-free HBSS containing the extracellular Ca^{2+} chelator EGTA (2 mM). In addition, separate cultures were treated with two selective L-type Ca^{2+} channel blockers, nifedipine (10 μM) and nimodipine (10 μM), and with the selective T-type Ca^{2+} channel inhibitor mibefradil (2 μM). To determine the involvement of intracellular Ca^{2+} stores in neurons, the cultures were treated with the intracellular Ca^{2+}-chelating agent BAPTA-AM (50 μM) and thapsigargin (1 μM) with NaHS (200 μM) stimulation. Thapsigargin is known to release Ca^{2+} from the endoplasmic reticulum by inhibiting Ca^{2+} ATPase. All experiments were carried out at 37°C and were repeated 4~6 times using different batches of cells.

2.5. Cell Viability Assay.

Cell viability was analyzed by using Cell Counting Kit-8 (CCK-8, obtained from Dojindo). CCK-8 allows sensitive colorimetric assays for the determination of cell viability in cell proliferation and cytotoxicity assays. Dojindo's highly water-soluble tetrazolium salt, WST-8, is reduced by dehydrogenase activities in cells to give a yellow-color formazan dye, which is soluble in the tissue culture media. The amount of the formazan dye, generated by the activities of dehydrogenases in cells, is directly proportional to the number of living cells. The primary medullary neurons were cultured in 96-well plates at a cellular density of 0.5 $\times$ 10^4 cells/well. Cells were cultured for 6~7 days at 37°C in 5% CO_2 incubator. On the following day, the cultured neurons were treated for 30 min with different concentrations of NaHS. Afterward, each well of plates was added to 10 μL CCK-8 solution and then incubated at 37°C, 5% CO_2 for 2 h. Subsequently, the cell viability was assessed by measuring the absorbance at 450 nm.

2.6. Measurement of H$_2$S Production.

H_2S levels in primarily cultured neurons were measured according to previously described methods with some modifications [26]. Briefly, primarily cultured medullary neurons were homogenized in ice-cold Tris-HCl (100 mM, pH 8.5) followed by centrifugation at 12,000 ×g for 20 min at 4°C. Thirty μL supernatant was incubated with 80 μL monobromobimane (MBB) for 40 min on a shaker at room temperature. Reaction was terminated by adding 20% formic acid and the level of H_2S was tested by Gas Chromatograph-Mass Spectrometer (GC-MS). Proteins in the supernatant were quantified using BCA reagent (Shen Neng Bo Cai Corp.). H_2S concentrations were determined using a curve generated with sodium sulfide (0–40 μM) standards, and the H_2S concentrations in cultured cells were expressed as μM. H_2S concentrations in primarily cultured medullary neurons were divided by the protein concentrations and were expressed as μmol/g of protein.

2.7. Statistical Analysis.

Statistical significance was determined using independent t-test or one-way ANOVA followed by SPSS 19.0. Data are presented as mean ± SEM. Difference at the $P < 0.05$ level was considered statistically significant.

3. Results

3.1. CBS and MST Were Expressed in the Medullary Neurons.

The primarily cultured medullary neurons were stained with anti-MAP-2 (red, Figure 1(a)) and anti-Glutamate (green, Figure 1(b)), suggesting that more than 90% of cells cultured were medullary neurons and most of them were glutamate positive neurons (Figure 1(d)).

Double-immunofluorescence labeling was used to study the specific localization of CBS in the primary medullary neurons. Fluorescence micrograph of neurons showed that neurons were stained with anti-MAP-2 antibody (green, Figure 1(e)). Anti-CBS was also stained with neurons (red, Figure 1(f)), and the merge of double-immunofluorescence labeling showed that more than 80% of neurons cultured were expressed with CBS (Figure 1(h)).

As MST is considered as another source of H_2S in the brain [5], we also studied the expression of MST. Fluorescence micrograph of neurons showed that neurons were stained with anti-MAP-2 antibody (red, Figure 1(i)). Anti-MST was also stained with neurons (green, Figure 1(j)), and the merge of double-immunofluorescence labeling showed that MST was also expressed in the medullary neurons (Figure 1(l)).

As CSE is another mainly source of H_2S, we also studied the expression of CSE. Fluorescence micrograph of neurons showed that neurons were stained with anti-MAP-2 antibody (green, Figure 1(m)), while anti-CSE was negatively stained with neurons (red, Figure 1(n)), and the merge of double-immunofluorescence labeling showed that CSE was negatively expressed in the primarily cultured medullary neurons (Figure 1(p)).

3.2. Effect of Exogenous H$_2$S on $[Ca^{2+}]_i$ in the Primary Medullary Neurons.

NaHS, a H_2S donor, at 200 μM induced a significant $[Ca^{2+}]_i$ increase in neurons and the effect of NaHS occurred rapidly and reached a peak within 10 min after administration. The level of $[Ca^{2+}]_i$ started to decline after washout (Figure 2(a)). NaHS (50–300 μM) significantly increased the level of $[Ca^{2+}]_i$ in the medullary neurons in a concentration-dependent manner (Figures 2(b) and 2(c)). Moreover, the increase in $[Ca^{2+}]_i$ level induced by NaHS is persistent. We also examined cell viability after adding NaHS using CCK-8 assay. As shown in Figure 2(d), there was no significant difference in the cell viability between Control and the groups treated by NaHS at 50~300 μM for 30 min. These data suggested that exogenous H_2S could increase $[Ca^{2+}]_i$ level in medullary neurons, while the elevation of $[Ca^{2+}]_i$ induced by NaHS was not due to or caused by the cytotoxicity of NaHS.
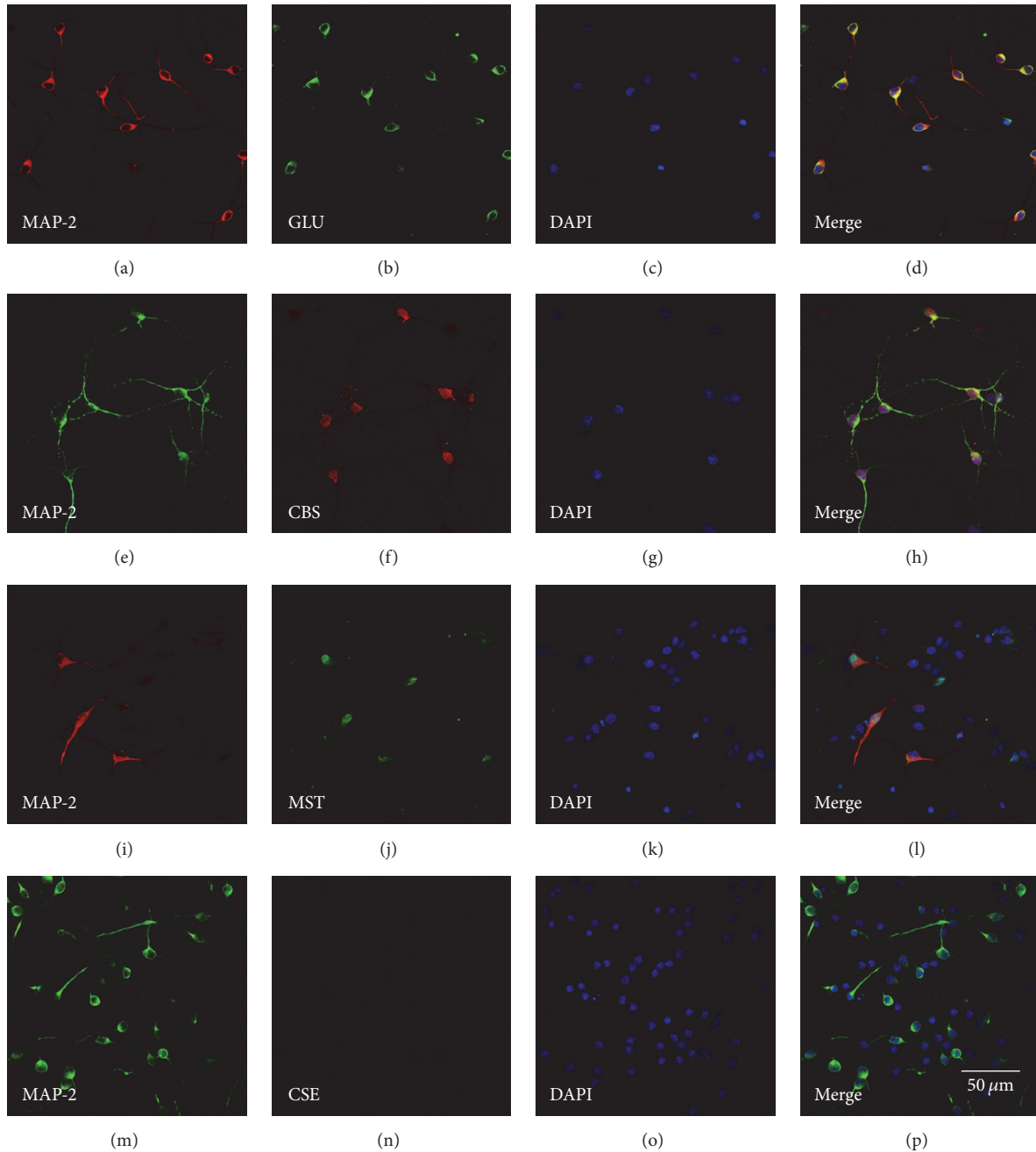
FIGURE 1: Identification of glutamate positive neurons ((a), (b), (c), and (d)) and the expression of CBS ((e), (f), (g), and (h)), MST ((i), (j), (k), and (l)), and CSE ((m), (n), (o), and (p)) in the rat primary medullary neurons. Confocal images showed that fluorescence micrograph of neurons stained with anti-MAP-2 antibody ((a), (e), (i), and (m), a neuronal maker), anti-glutamate antibody (b), anti-CBS antibody (f), anti-MST antibody (j), anti-CSE antibody (n), DAPI ((c), (g), (k), and (o)), or the merge of the other 3 photos ((d), (h), (l), and (p)). Scale bar = 50 μm.

3.3. Effect of Endogenous H_2S on $[Ca^{2+}]_i$ in the Primary Medullary Neurons. To investigate the endogenous H_2S n $[Ca^{2+}]_i$ in the primary medullary neurons, we applied L-cysteine (a substrate for H_2S), SAM (a CBS activator), and HA and AOAA (two CBS inhibitors), respectively. The results showed that L-cysteine and SAM significantly raised the level of $[Ca^{2+}]_i$ in the medullary neurons (Figures 3(a) and 3(b)) while HA and/or AOAA produced a reversal effect (Figures 3(c) and 3(d)). And HA or AOAA can no longer inhibit $[Ca^{2+}]_i$ level in the presence of SAM. However, the stimulatory effect of SAM on $[Ca^{2+}]_i$ was not affected by HA or AOAA (Figure 3(d)). In addition, L-cysteine and

(a)

(b)

(c)

(d)
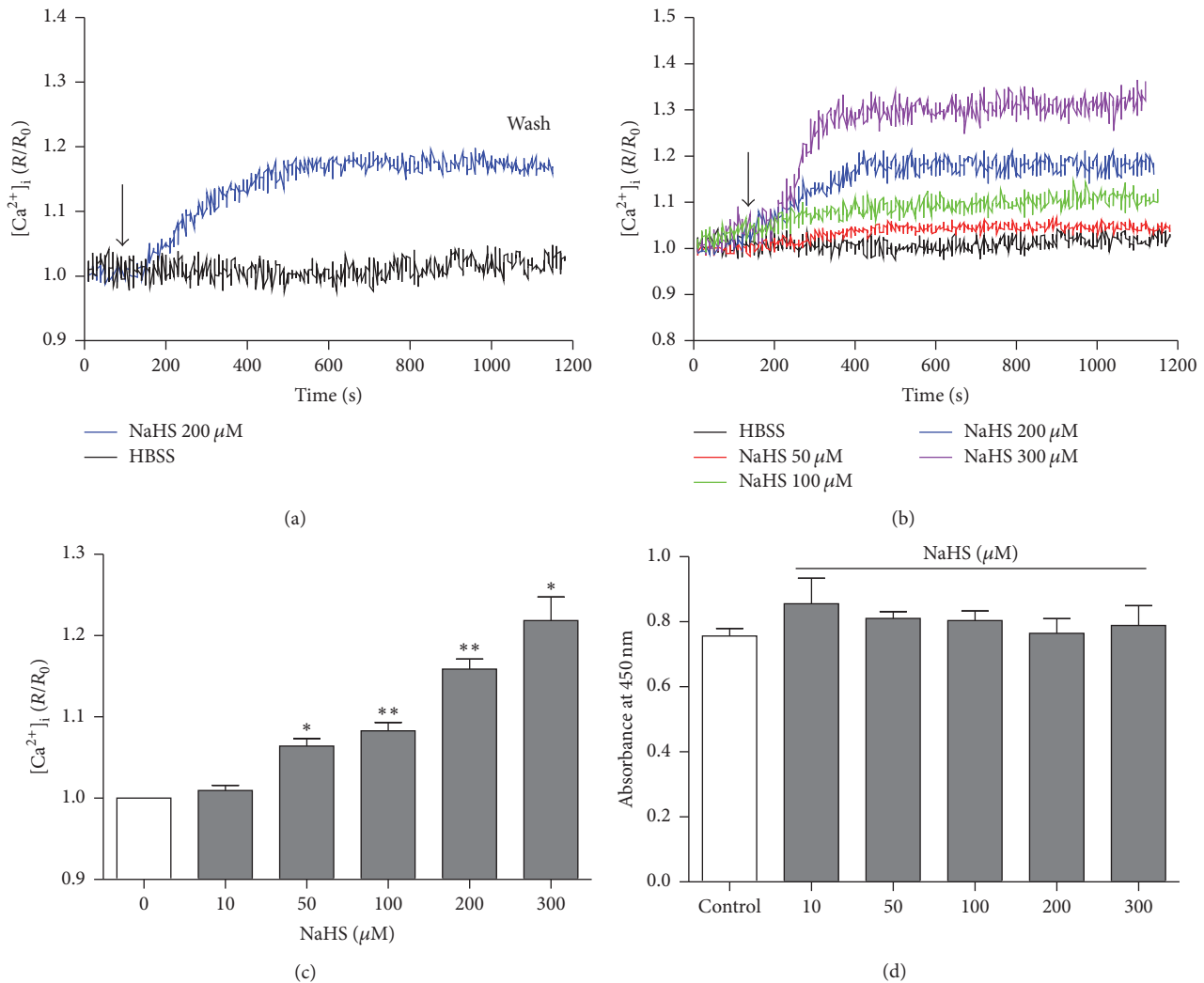
FIGURE 2: The effect of NaHS on $[Ca^{2+}]_i$ in the primarily cultured medullary neurons. (a) Typical elevation of $[Ca^{2+}]_i$ induced by NaHS at 200 μM and washout of NaHS led $[Ca^{2+}]_i$ to decline. (b) Typical effects of different concentrations of NaHS (50, 100, 200, and 300 μM) on $[Ca^{2+}]_i$. (c) Summary data of the peak increase in $[Ca^{2+}]_i$ in neurons stimulated with different concentrations of NaHS (50, 100, 200, and 300 μM). $^*P < 0.05$; $^{**}P < 0.01$. (d) The cell viability analyzed by CCK-8 has no significance among different concentrations of NaHS. $n = 6$ in each group.

SAM significantly increased but HA and/or AOAA (10 mM) decreased the production of H_2S in the cultured neurons (Figure 4).

3.4. The Evolvement of L-Type and T-Type Ca^{2+} Channels in the Effect of H_2S.

In order to determine the source of increased $[Ca^{2+}]_i$ in NaHS-stimulated medullary neurons, the cells were bathed either in Ca^{2+}-free HBSS (containing 2 mM EGTA) or in normal HBSS. Similar to the data shown in Figures 2(a) and 2(b), NaHS at 200 μM caused a robust increase in $[Ca^{2+}]_i$ within 10 min after incubation of normal Ca^{2+} containing HBSS (Figure 5(a)). This effect was partly abolished in cells bathed in Ca^{2+}-free HBSS (Figures 5(a) and 5(e)).

As shown in Figures 5(b) and 5(c), both nifedipine (10 μM) and nimodipine (10 μM), two L-type Ca^{2+} channel blockers, significantly suppressed the effect of NaHS at 200 μM (Figures 5(b), 5(c), and 5(e)). A selective T-type Ca^{2+} channel inhibitor, mibefradil (2 μM), also inhibited the elevation of $[Ca^{2+}]_i$ level induced by NaHS (Figures 5(d) and 5(e))

3.5. The Involvement of Intracellular Ca^{2+} Stores in the Effect of H_2S.

The neurons were treated with BAPTA-AM (an intracellular Ca^{2+} chelator) and thapsigargin (a sarco/endoplasmic reticulum Ca^{2+}-ATPase blocker) with or without NaHS. The effect of NaHS on $[Ca^{2+}]_i$ level in neurons was significantly attenuated by depletion of BAPTA-AM (50 μM, Figures 6(a) and 6(c)) and thapsigargin (TG, 1 μM, Figures 6(b) and 6(c)).

4. Discussion

In the present study, we attempted to elucidate mechanisms for the regulation of intracellular calcium levels by H_2S in
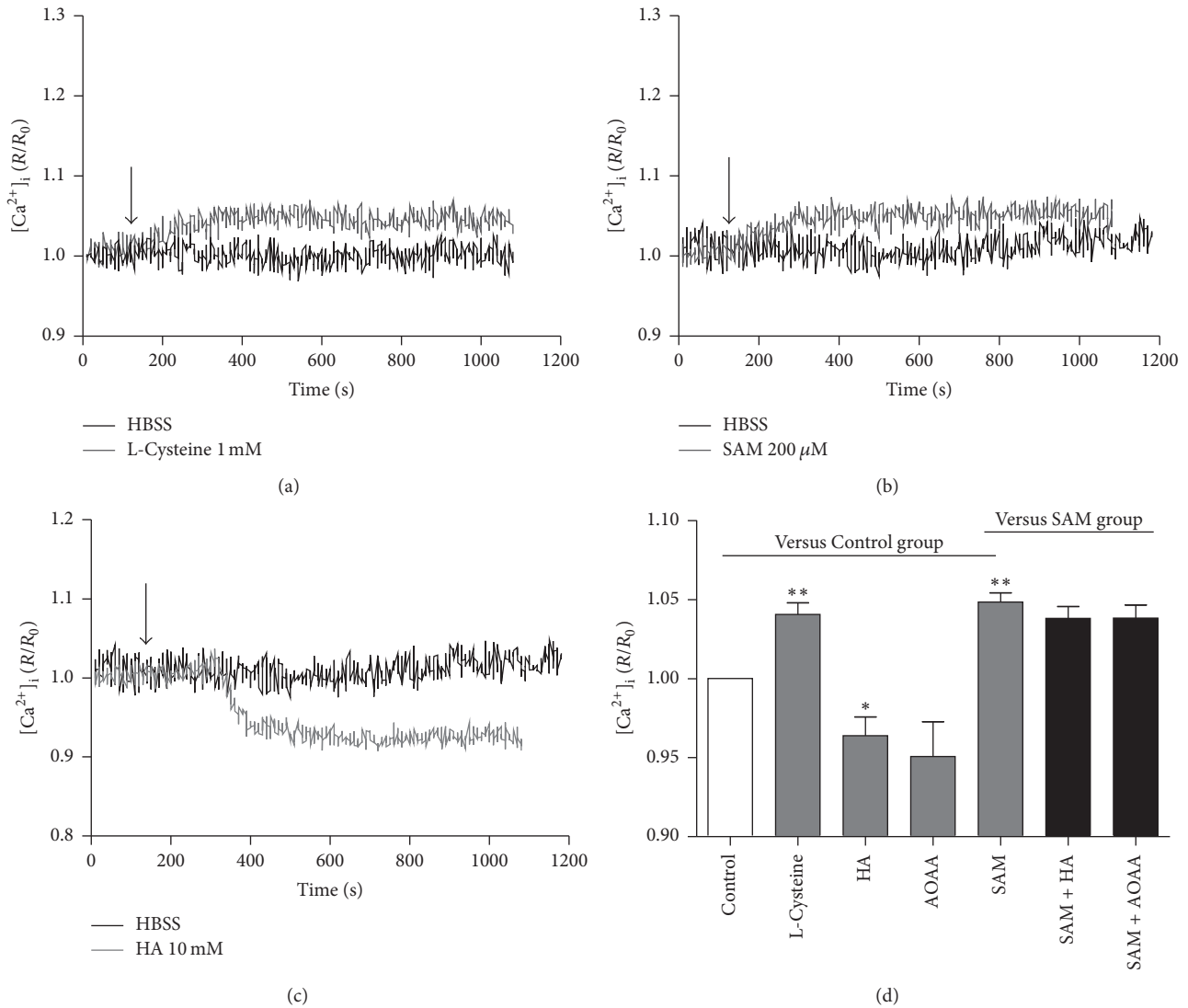
FIGURE 3: The effect of endogenous H_2S on the $[Ca^{2+}]_i$ level in the primarily cultured medullary neurons. (a) Typical elevation of $[Ca^{2+}]_i$ induced by L-cysteine (the H_2S precursor) at 1 mM. (b) Typical effects of SAM (an activator of CBS) at 200 μM on $[Ca^{2+}]_i$ level. (c) Typical effects of HA (an inhibitor of CBS) at 10 mM on $[Ca^{2+}]_i$ level. (d) Group data showed the effects of endogenous H_2S on the $[Ca^{2+}]_i$ level. AOAA (another inhibitor of CBS). $^{*}P < 0.05$, $^{**}P < 0.01$ versus Control group; $n = 6$ in each group.
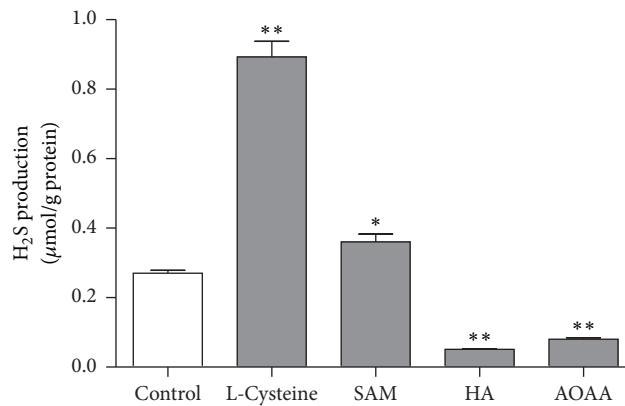
FIGURE 4: The production of H_2S in the primarily cultured medullary neurons treated by L-cysteine (1 mM), SAM (200 μM), HA (10 mM), and AOAA (10 mM), respectively. $^{*}P < 0.05$; $^{**}P < 0.01$. $n \geq 7$ in each group.
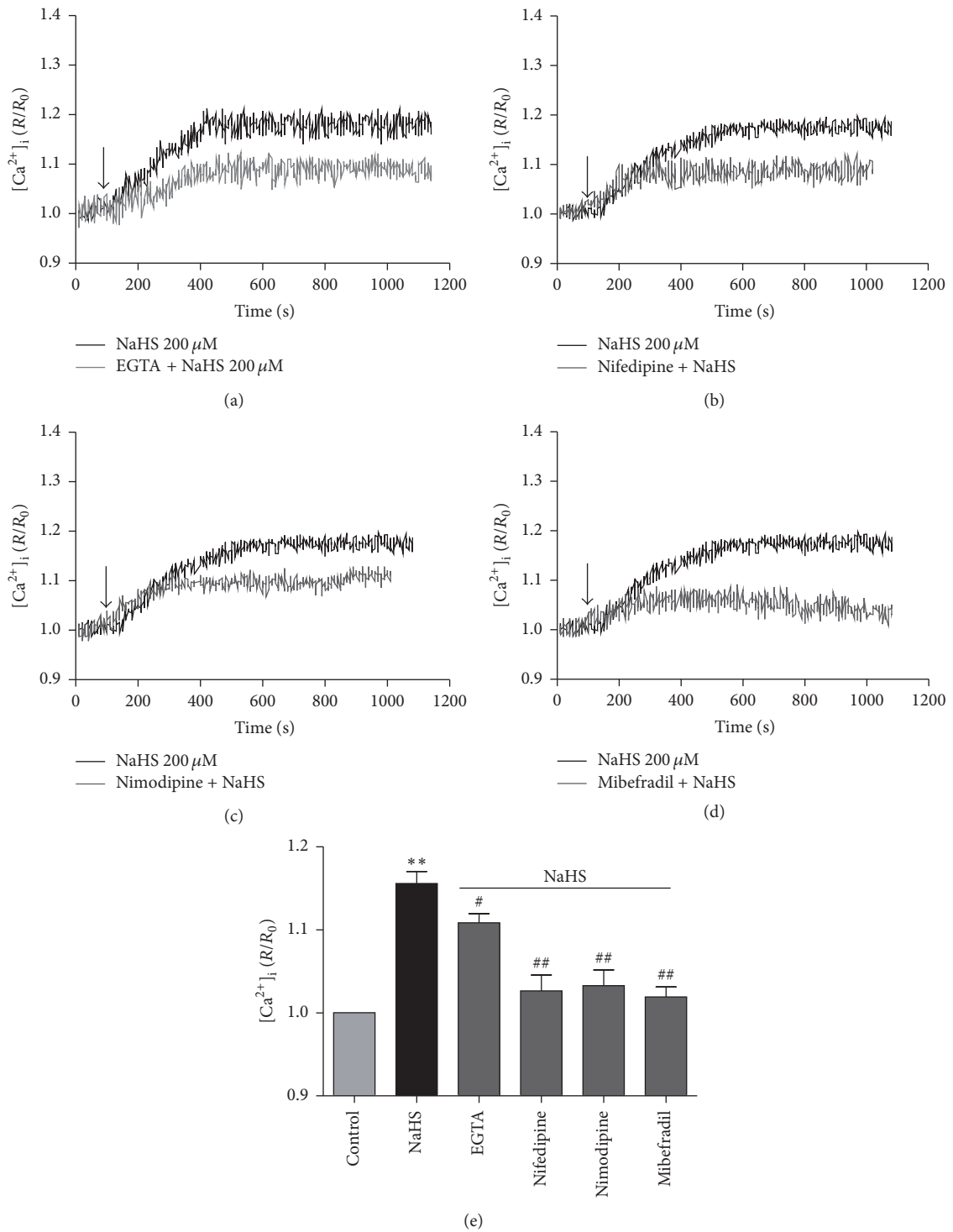
FIGURE 5: The effect of NaHS on $[Ca^{2+}]_i$ in the primarily cultured medullary neurons in Ca^{2+}-free solution or in the presence of L-type and/or T-type Ca^{2+} channels inhibitors. ((a)–(c)) Typical suppression of $[Ca^{2+}]_i$ level induced by NaHS in EGTA-treated Ca^{2+}-free solution (a) or in normal Ca^{2+} containing HBSS with or without nifedipine (10 μM, (b)), nimodipine (10 μM, (c)), and mibefradil (2 μM, (d)). (e) Group data showed that the effects of NaHS were attenuated by EGTA-Ca^{2+}-free solution and suppressed by nifedipine, nimodipine, or mibefradil. $^{**}P < 0.01$ versus Control; $^{#}P < 0.05$ versus NaHS group; $^{##}P < 0.01$ versus NaHS group. $n = 5$ in each group.

(a)

(b)

(c)
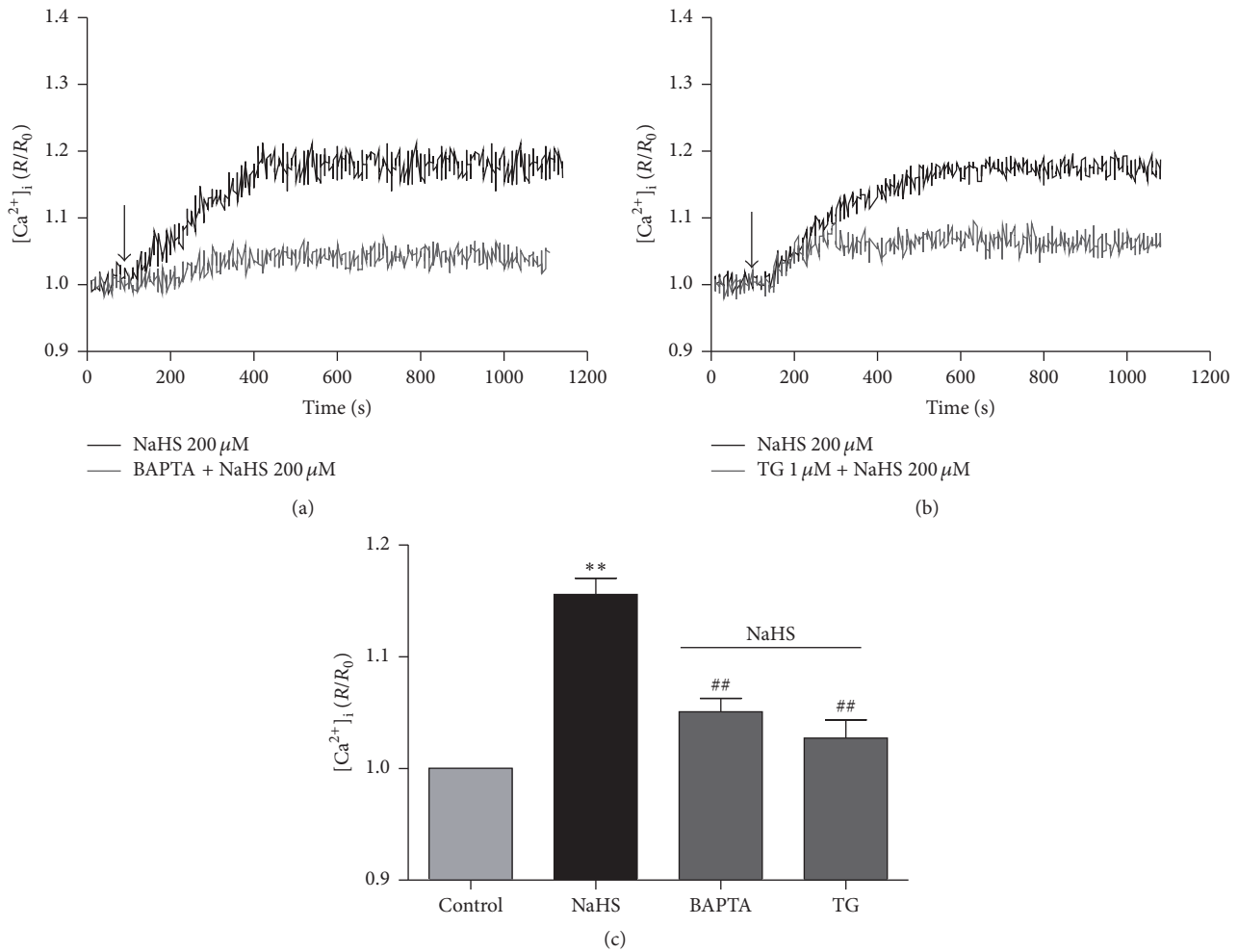
FIGURE 6: The effect of NaHS on $[Ca^{2+}]_i$ in the primarily cultured medullary neurons in the presence of intracellular Ca^{2+} chelator and sarco/endoplasmic reticulum Ca^{2+}-ATPase blocker. ((a), (b)) Typical suppression of $[Ca^{2+}]_i$ level induced by NaHS with or without BAPTA-AM (50 μM (a)) and thapsigargin (TG, 1 μM (b)). (c) Group data showed that the effects of NaHS were suppressed by BAPTA-AM and thapsigargin. $^{**}P < 0.01$ versus Control; $^{##}P < 0.01$ versus NaHS group. $n = 5$ in each group.

primary rat medullary neurons. The results provide the evidence for the first time on the primarily cultured medullary neurons that H_2S elevates $[Ca^{2+}]_i$ level via both increasing calcium influx and mobilizing intracellular Ca^{2+} stores from ER. Our conclusion is supported by the following findings: firstly, NaHS significantly increased the level of $[Ca^{2+}]_i$ in rat medullary neurons in a concentration-dependent manner. Secondly, L-cysteine and SAM significantly raised the level of $[Ca^{2+}]_i$ in the medullary neurons while HA and/or AOAA produced a reversal effect. In addition, L-cysteine and SAM significantly increased but HA and/or AOAA decreased the production of H_2S in the cultured neurons. Thirdly, the Ca^{2+} elevation induced by H_2S was significantly diminished by EGTA-Ca^{2+}-free solutions, and this elevation was also reduced by nifedipine or nimodipine (an antagonist of L-type Ca^{2+} channel) and mibefradil (an antagonist of T-type Ca^{2+} channel), suggesting the role of L-type and/or T-type Ca^{2+} channels. Lastly, the effect of H_2S on $[Ca^{2+}]_i$ level in neurons

was significantly attenuated by BAPTA-AM (an intracellular Ca^{2+} chelator, 50 μM) and thapsigargin (a sarco/endoplasmic reticulum Ca^{2+}-ATPase blocker, 1 μM), suggesting the source of Ca^{2+}.

Previous studies have demonstrated the crucial role of H_2S homeostasis in hypertension. Administration of H_2S donors and precursors decreases mean blood pressure in various hypertensive models (chronic inhibition of nitric oxide synthase, two-kidney-one-clip, and SHRs) [11–13, 27]. One of the molecular targets for the cellular effect of H_2S is K_{ATP} channels [28]. It has been reported that H_2S in the RVLM inhibits sympathetic vasomotor tone through opening K_{ATP} channels [29, 30]. We have shown that H_2S in RVLM suppressed the blood pressure in SHRs [14]. The signaling mechanisms in the CNS of the antihypertensive effect of H_2S have not been elucidated. On the other hand, the antihypertensive effects of H_2S in the caudal ventrolateral medulla (CVLM) involved K_{ATP} channels and glutamic acid receptor [31, 32]. Glutamate acid has been suggested to be

an important neurotransmitter in antihypertensive effects of H_2S. In order to provide more evidence for the regulation of H_2S on the cardiovascular effects, we mainly focused on the medullary neurons in vitro. To ensure the cultured medullary cells were the target neurons which were glutamate positive neurons, we demonstrated that glutamate was coexpressed in more than 90% of primarily cultured medullary neurons. H_2S is mainly produced endogenously by CBS and MST in the CNS [4, 5] and CBS is mainly expressed in the hippocampus and cerebellum, as well as the cerebral cortex and brain stem [8]. Our previous study has shown that CBS immunoreactivity was found in the rostral ventrolateral medulla (RVLM) neurons in vivo and the level of CBS proteins in the RVLM was lower in SHRs than in WKY rats [14]. In this study, our results showed that more than 80% of cultured medullary neurons were glutamate positive neurons, and CBS and MST were, respectively, expressed in these neurons in vitro, while the expression of CSE was negative in these primarily cultured medullary neurons. These results provided the basis of study of H_2S.

Calcium plays an important role in regulating a great variety of neuronal processes such as release of neurotransmitters, synaptic plasticity, neuronal excitation, and gene transcription. It was reported that H_2S increased $[Ca^{2+}]_i$ in SH-SY5Y neuronal cells by increasing Ca^{2+} influx via plasma membrane and in turn releasing calcium from intracellular calcium store [19]. Exerting its function as a gasotransmitter, H_2S regulates calcium homeostasis in neurons via both increasing calcium influx and mobilizing calcium from ER [19]. In CNS, H_2S activates L-type Ca^{2+} channels in rat cerebellar granule neurons to increase calcium signals which were inhibited by nifedipine and nimodipine [33] and in hippocampal slices and microglia to induce hippocampal LTP and Ca^{2+} waves in astrocytes [20]. H_2S also activates T-type Ca^{2+} channels in NG108-15 (neuroblastoma cell line) involved in neuronal differentiation [34] and activates TRPA1 channels in rat sensory neurons from dorsal root ganglion [35]. The regulation of $[Ca^{2+}]_i$ in the medullary neurons by H_2S has not been reported. Our results showed that NaHS (50–300 μM) significantly increased the level of $[Ca^{2+}]_i$ in rat medullary neurons in a concentration-dependent manner. On the other hand, L-cysteine and SAM significantly raised the level of $[Ca^{2+}]_i$ in the medullary neurons while HA and/or AOAA produced a reversal effect. Meanwhile, HA or AOAA can no longer inhibit $[Ca^{2+}]_i$ level in the presence of SAM. However, the stimulatory effect of SAM on $[Ca^{2+}]_i$ was not affected by HA or AOAA. The possible reasons may be considered as follows: on the one hand, the affinity of SAM to CBS is much greater than that of HA or AOAA so that the stimulatory effect of SAM is dominating; on the other hand, the possibility that the increasing effects of L-cysteine and SAM on Ca^{2+} may be a H_2S-independent manner is not ruled out and is needed to be addressed in the future. In addition, L-cysteine and SAM significantly increased the production of H_2S in the cultured neurons and HA and/or AOAA decreased the production of H_2S. These results suggested that both exogenous H_2S and endogenous H_2S increase the level of $[Ca^{2+}]_i$ in the medullary neurons.

$[Ca^{2+}]_i$ is controlled by Ca^{2+} channels in the membrane and intracellular Ca^{2+} stores [36]. The changes of $[Ca^{2+}]_i$ due to extracellular Ca^{2+} influx may be facilitated by voltage-gated channels, transmitter-gated Ca^{2+} permeant ion channels, transient receptor potential (TRP) ion channels, and Ca^{2+} pumps located in the plasma membrane [1, 36]. The function of status of intracellular Ca^{2+} stores is controlled by ryanodine receptor (RyR) channels, inositol triphosphate receptor (IP3R) channels, and sarcoendoplasmic reticular Ca^{2+} ATPases (SERCA) [1, 36]. In order to determine the source of $[Ca^{2+}]_i$ in NaHS-stimulated medullary neurons, we applied to the EGTA-Ca^{2+}-free solution and BAPTA-AM to chelate the extracellular Ca^{2+} and intracellular Ca^{2+}, respectively. The results showed that the Ca^{2+} elevation induced by H_2S was significantly diminished by EGTA-Ca^{2+}-free solutions and/or BAPTA-AM, suggesting that the elevation of $[Ca^{2+}]_i$ level in medullary neurons partly involved both an influx of extracellular Ca^{2+} and the intracellular Ca^{2+} stores. That thapsigargin (a sarco/endoplasmic reticulum Ca^{2+}-ATPase blocker) significantly attenuates the effect of H_2S on $[Ca^{2+}]_i$ level in neurons further suggests that NaHS releases calcium from intracellular Ca^{2+} stores.

In summary, the present study demonstrates that both exogenous H_2S and endogenous H_2S elevate $[Ca^{2+}]_i$ level in primarily cultured rat medullary neurons via both increasing calcium influx and mobilizing intracellular Ca^{2+} stores from ER.

Competing Interests

The authors declare that there is no conflict of interests regarding the publication of this paper.

Acknowledgments

References

[1] B. H. Tan, P. T.-H. Wong, and J.-S. Bian, "Hydrogen sulfide: a novel signaling molecule in the central nervous system," *Neurochemistry International*, vol. 56, no. 1, pp. 3–10, 2010.

[2] R. Wang, "Two's company, three's a crowd: can H_2S be the third endogenous gaseous transmitter?" *The FASEB Journal*, vol. 16, no. 13, pp. 1792–1798, 2002.

[3] R. Wang, "Gasotransmitters: growing pains and joys," *Trends in Biochemical Sciences*, vol. 39, no. 5, pp. 227–232, 2014.

[4] R. Wang, "Physiological implications of hydrogen sulfide: a whiff exploration that blossomed," *Physiological Reviews*, vol. 92, no. 2, pp. 791–896, 2012.

[5] N. Shibuya, M. Tanaka, M. Yoshida et al., "3-Mercaptopyruvate sulfurtransferase produces hydrogen sulfide and bound sulfane sulfur in the brain," *Antioxidants & Redox Signaling*, vol. 11, no. 4, pp. 703–714, 2009.

[6] J. C. Savage and D. H. Gould, "Determination of sulfide in brain tissue and rumen fluid by ion-interaction reversed-phase high-performance liquid chromatography," *Journal of Chromatography B: Biomedical Sciences and Applications*, vol. 526, pp. 540–545, 1990.

[7] R. Wang, C. Szabo, F. Ichinose, A. Ahmed, M. Whiteman, and A. Papapetropoulos, "The role of H_2S bioavailability in endothelial dysfunction," *Trends in Pharmacological Sciences*, vol. 36, no. 9, pp. 568–578, 2015.

[8] K. Abe and H. Kimura, "The possible role of hydrogen sulfide as an endogenous neuromodulator," *The Journal of Neuroscience*, vol. 16, no. 3, pp. 1066–1071, 1996.

[9] P. K. Kamat, P. Kyles, A. Kalani, and N. Tyagi, "Hydrogen sulfide ameliorates homocysteine-induced Alzheimer's disease-like pathology, blood–brain barrier disruption, and synaptic disorder," *Molecular Neurobiology*, vol. 53, no. 4, pp. 2451–2467, 2016.

[10] L.-F. Hu, P. T.-H. Wong, P. K. Moore, and J.-S. Bian, "Hydrogen sulfide attenuates lipopolysaccharide-induced inflammation by inhibition of p38 mitogen-activated protein kinase in microglia," *Journal of Neurochemistry*, vol. 100, no. 4, pp. 1121–1128, 2007.

[11] D. Stubbert, O. Prysyazhna, O. Rudyk, J. Scotcher, J. R. Burgoyne, and P. Eaton, "Protein kinase G Iα oxidation paradoxically underlies blood pressure lowering by the reductant hydrogen sulfide," *Hypertension*, vol. 64, no. 6, pp. 1344–1351, 2014.

[12] G. Yang, L. Wu, B. Jiang et al., "H_2S as a physiologic vasorelaxant: hypertension in mice with deletion of cystathionine γ-lyase," *Science*, vol. 322, no. 5901, pp. 587–590, 2008.

[13] H. Yan, J. Du, and C. Tang, "The possible role of hydrogen sulfide on the pathogenesis of spontaneous hypertension in rats," *Biochemical and Biophysical Research Communications*, vol. 313, no. 1, pp. 22–27, 2004.

[14] H. Yu, H. Xu, X. Liu et al., "Superoxide mediates depressive effects induced by hydrogen sulfide in rostral ventrolateral medulla of spontaneously hypertensive rats," *Oxidative Medicine and Cellular Longevity*, vol. 2015, Article ID 927686, 8 pages, 2015.

[15] M. R. Al-Magableh, B. K. Kemp-Harper, and J. L. Hart, "Hydrogen sulfide treatment reduces blood pressure and oxidative stress in angiotensin II-induced hypertensive mice," *Hypertension Research*, vol. 38, no. 1, pp. 13–20, 2015.

[16] M. J. Berridge, "Neuronal calcium signaling," *Neuron*, vol. 21, no. 1, pp. 13–26, 1998.

[17] M. A. Lynch, "Long-term potentiation and memory," *Physiological Reviews*, vol. 84, no. 1, pp. 87–136, 2004.

[18] R. Rizzuto, "Intracellular Ca^{2+} pools in neuronal signalling," *Current Opinion in Neurobiology*, vol. 11, no. 3, pp. 306–311, 2001.

[19] Q. C. Yong, C. H. Choo, B. H. Tan, C.-M. Low, and J.-S. Bian, "Effect of hydrogen sulfide on intracellular calcium homeostasis in neuronal cells," *Neurochemistry International*, vol. 56, no. 3, pp. 508–515, 2010.

[20] Y. Nagai, M. Tsugane, J.-I. Oka, and H. Kimura, "Hydrogen sulfide induces calcium waves in astrocytes," *The FASEB Journal*, vol. 18, no. 3, pp. 557–559, 2004.

[21] S. W. Lee, Y.-S. Hu, L.-F. Hu et al., "Hydrogen sulphide regulates calcium homeostasis in microglial cells," *GLIA*, vol. 54, no. 2, pp. 116–124, 2006.

[22] M. A. García-Bereguiaín, A. K. Samhan-Arias, F. J. Martín-Romero, and C. Gutiérrez-Merino, "Hydrogen sulfide raises cytosolic calcium in neurons through activation of L-type Ca^{2+} channels," *Antioxidants & Redox Signaling*, vol. 10, no. 1, pp. 31–42, 2008.

[23] M. Subramanian, C. Hahn-Townsend, K. A. Clark, S. M. J. MohanKumar, and P. S. MohanKumar, "Chronic estrogen exposure affects gene expression in the rostral ventrolateral medulla of young and aging rats: possible role in hypertension," *Brain Research*, vol. 1627, pp. 134–142, 2015.

[24] Y.-M. Chao, M.-D. Lai, and J. Y. H. Chan, "Redox-sensitive endoplasmic reticulum stress and autophagy at rostral ventrolateral medulla contribute to hypertension in spontaneously hypertensive rats," *Hypertension*, vol. 61, no. 6, pp. 1270–1280, 2013.

[25] P. G. Guyenet, "The sympathetic control of blood pressure," *Nature Reviews Neuroscience*, vol. 7, no. 5, pp. 335–346, 2006.

[26] S. Jin, S.-X. Pu, C.-L. Hou et al., "Cardiac H_2S generation is reduced in ageing diabetic mice," *Oxidative Medicine and Cellular Longevity*, vol. 2015, Article ID 758358, 14 pages, 2015.

[27] G. Zhong, F. Chen, Y. Cheng, C. Tang, and J. Du, "The role of hydrogen sulfide generation in the pathogenesis of hypertension in rats induced by inhibition of nitric oxide synthase," *Journal of Hypertension*, vol. 21, no. 10, pp. 1879–1885, 2003.

[28] W. Zhao, J. Zhang, Y. Lu, and R. Wang, "The vasorelaxant effect of H_2S as a novel endogenous gaseous K_{ATP} channel opener," *The EMBO Journal*, vol. 20, no. 21, pp. 6008–6016, 2001.

[29] Q. Guo, S. Jin, X.-L. Wang et al., "Hydrogen sulfide in the rostral ventrolateral medulla inhibits sympathetic vasomotor tone through ATP-Sensitive K+ Channels," *The Journal of Pharmacology and Experimental Therapeutics*, vol. 338, no. 2, pp. 458–465, 2011.

[30] G. S. Dawe, S. P. Han, J.-S. Bian, and P. K. Moore, "Hydrogen sulphide in the hypothalamus causes an ATP-sensitive K+ channel-dependent decrease in blood pressure in freely moving rats," *Neuroscience*, vol. 152, no. 1, pp. 169–177, 2008.

[31] Y. Lu, B. Li, H. Y. Cai, D. S. Cheng, D. H. Li, and H. Li, "The cardiovascular effects of hydrogen sulfide injected within the caudal ventrolateral medulla are associated with the opening of ATP-sensitive potassium channels and activation of glutamate receptors," *Chinese Jouanal of Hypertension*, pp. 463–467, 2014.

[32] W. Q. Liu, C. Chai, X. Y. Li, W. J. Yuan, W. Z. Wang, and Y. Lu, "The cardiovascular effects of central hydrogen sulfide are related to K(ATP) channels activation," *Physiological Research*, vol. 60, no. 5, pp. 729–738, 2011.

[33] G. Tang, L. Wu, and R. Wang, "Interaction of hydrogen sulfide with ion channels," *Clinical and Experimental Pharmacology and Physiology*, vol. 37, no. 7, pp. 753–763, 2010.

[34] K. Nagasawa, T. Tarui, S. Yoshida et al., "Hydrogen sulfide evokes neurite outgrowth and expression of high-voltage-activated Ca^{2+} currents in NG108-15 cells: involvement of T-type Ca^{2+} channels," *Journal of Neurochemistry*, vol. 108, no. 3, pp. 676–684, 2009.

[35] R. Miyamoto, K.-I. Otsuguro, and S. Ito, "Time- and concentration-dependent activation of TRPA1 by hydrogen sulfide in rat DRG neurons," *Neuroscience Letters*, vol. 499, no. 2, pp. 137–142, 2011.

[36] D. E. Clapham, "Calcium signaling," *Cell*, vol. 131, no. 6, pp. 1047–1058, 2007.

Review Article

Melatoninergic System in Parkinson's Disease: From Neuroprotection to the Management of Motor and Nonmotor Symptoms

Josiel Mileno Mack,[1] Marissa Giovanna Schamne,[1] Tuane Bazanella Sampaio,[1] Renata Aparecida Nedel Pértile,[2] Pedro Augusto Carlos Magno Fernandes,[3] Regina P. Markus,[3] and Rui Daniel Prediger[1]

[1]*Department of Pharmacology, Centre of Biological Sciences, Universidade Federal de Santa Catarina (UFSC), Campus Universitário, Florianópolis, SC, Brazil*
[2]*Queensland Brain Institute, University of Queensland (UQ), Brisbane, QLD, Australia*
[3]*Department of Physiology, Institute of Bioscience, University of São Paulo (USP), São Paulo, SP, Brazil*

Correspondence should be addressed to Rui Daniel Prediger; rui.prediger@ufsc.br

Melatonin is synthesized by several tissues besides the pineal gland, and beyond its regulatory effects in light-dark cycle, melatonin is a hormone with neuroprotective, anti-inflammatory, and antioxidant properties. Melatonin acts as a free-radical scavenger, reducing reactive species and improving mitochondrial homeostasis. Melatonin also regulates the expression of neurotrophins that are involved in the survival of dopaminergic neurons and reduces α-synuclein aggregation, thus protecting the dopaminergic system against damage. The unbalance of pineal melatonin synthesis can predispose the organism to inflammatory and neurodegenerative diseases such as Parkinson's disease (PD). The aim of this review is to summarize the knowledge about the potential role of the melatoninergic system in the pathogenesis and treatment of PD. The literature reviewed here indicates that PD is associated with impaired brain expression of melatonin and its receptors MT_1 and MT_2. Exogenous melatonin treatment presented an outstanding neuroprotective effect in animal models of PD induced by different toxins, such as 6-hydroxydopamine (6-OHDA), 1-methyl-4-phenyl-1,2,3,6-tetrahydropyridine (MPTP), rotenone, paraquat, and maneb. Despite the neuroprotective effects and the improvement of motor impairments, melatonin also presents the potential to improve nonmotor symptoms commonly experienced by PD patients such as sleep and anxiety disorders, depression, and memory dysfunction.

1. Introduction

Parkinson's disease (PD) is a chronic and progressive neurodegenerative disease, characterized by the degeneration of dopaminergic (DAergic) neurons in the *substantia nigra pars compacta* (SNc) and the subsequent decrease of dopamine (DA) levels in the striatum. PD is classically considered a complex motor disorder, related to the pronounced degeneration of the DAergic system, which manifests in bradykinesia, tremor, rigidity, and postural instability. Nowadays, PD is considered a progressive multisystem disease that affects a variety of neurotransmitters, being linked with nonmotor symptoms, such as impaired olfaction and gastrointestinal, genitourinary, cardiovascular, and respiratory dysfunctions, as well as visual, neuropsychiatric, and sleep-related disorder. Contrary to the well-defined motor symptoms, PD nonmotor signals and symptoms are still poorly understood and almost not considered in diagnostic and therapeutic protocols. Recent studies suggest that the nonmotor preclinical phase can span for more than 20 years.

New pharmacological tools for treating PD focus on the relief of symptoms that are observed when the disease is clinically developed. The development of neuroprotective drugs and therapies for impairing the progression or even

reducing the extension of the disease needs to rely on the understanding of neuroprotection. Neuroprotection definition is complex and involves the potential for preventing cell death, restoring function of damaged neurons, and increasing neuronal number. The development of drugs to slow or prevent the progression of PD might logically evolve from an improved understanding of the pathogenesis of such disease. In the past few years, certainly there were major advances in this area, improving the prospect for the introduction of neuroprotective therapies. However, despite extensive efforts and research, to date, there is no proven therapy to prevent cell death or to restore affected neurons to a normal state in PD. Preclinical studies in laboratory animals have provided several candidate neuroprotective drugs, but clinical endpoints are readily confounded by any symptomatic effect. Thus, these studies do not provide an unequivocal measure of disease progression that can be used to determine if a drug has a neuroprotective effect.

In this context emerges melatonin, an indolamine synthesized by several tissues such as the pineal gland and by extrapineal sources including macrophages, mast cells, and lymphocytes. Classically, melatonin has been considered the darkness hormone since its synthesis by the pineal gland follows the daily alternation between light and darkness. Melatonin synthesized by immune-competent cells acts in an autocrine or paracrine manner. Melatonin receptors (MT_1 and MT_2) are expressed in numerous areas of the central nervous system (CNS). Moreover, the physiological role of melatonin is by far wider than what was considered before including learning and memory, anxiety, depression, and neuroprotection. The present review attempts to provide a comprehensive picture of the role of the melatoninergic system in CNS and to highlight recent findings showing its potential as a new palliative and neuroprotective agent in PD.

2. Melatoninergic System

Melatonin was isolated in 1958 by the dermatologist Lerner from 50 grams of lyophilized bovine pineal glands powder [1]. Melatonin was named after its property of lightening the skin of frogs, toads, and fishes. In these early times, Wurtman and collaborators [2] examined the distribution of [^{3}H]-melatonin in endocrine and other organs of rats and cats. They showed that iris-choroid, ovary, and periphery organs innervated by the autonomic nervous system, including the heart, take up melatonin [2]. In 1965, a paper authored by Axelrod (Nobel Prize of Medicine, 1970) et al. showed the daily variation of melatonin pineal gland content and proposed that the neural pathway that links the retina to the pineal gland involves sympathetic postganglionic fibres originated in the superior cervical ganglia [3]. In the last years, there is increasing data supporting the concept that melatonin effects are not only due to nighttime pineal gland synthesis but also triggered by melatonin synthesized by extrapineal sources [4, 5].

In mammals, several tissues including the pineal gland, retina [6], macrophages [7, 8], mast cells, lymphocytes [4], human bone marrow cells [9], astrocytes [10–12], and enterochromaffin-like cells found in the gastric mucosa [13],

rat oocytes [14], placental trophoblasts [15, 16], and human colostrum phagocytes [17] synthesize melatonin. Melatonin (N-acetyl-5-methoxytryptamine) is synthesized by the acetylation of serotonin and the methylation of N-acetylserotonin [18]. The enzymes aryl-alkyl-N-acetyltransferase (AANAT) and acetylserotonin O-methyltransferase (ASMT), also known as hydroxyl-indole-O-methyltransferase (HIOMT), are highly conserved being detected in unicellular organisms, plants, and animals [19–21].

The pineal gland is an endocrine gland of epithelial origin, as the CNS, formed by pinealocytes (modified neurons), astrocytes, and microglia [18]. Nerve fibres originate from perikarya located in the sympathetic superior cervical ganglion and the parasympathetic sphenopalatine and optic ganglion innervate the gland [22]. Sympathetic activation by darkness is the key inducer of pineal melatonin synthesis. On the other hand, the role of parasympathetic innervation is still not clear. In rats, the muscarinic receptors are present only in the developmental phase [23]. In adult rats, the only cholinergic receptors detected are nicotinic, which leads to a great entrance of calcium ions and the release of glutamate. In turn, glutamate inhibits noradrenaline-induced pinealocytes melatonin synthesis [24]. More recently, the sources and cellular effect of gamma-aminobutyric acid (GABA) were described [25]. Although the cellular and molecular mechanisms involved in the response of these neurotransmitters and hormones are becoming clear, there are little cues regarding their functional role.

In addition, the pineal gland is a circumventricular organ capable of communicating blood signals to the brain through the cerebrospinal fluid [22]. In fact, it reacts to cytokines and to circulating hormones such as glucocorticoids [4, 26]. Pro- and anti-inflammatory mediators modulate pineal melatonin synthesis, adjusting the body to cope with inflammatory responses [26]. Therefore, the unbalance of pineal melatonin synthesis can predispose the organism to inflammatory and neurodegenerative diseases.

The conversion by AANAT of serotonin to N-acetylserotonin (the immediate precursor of melatonin) in pinealocytes is the key event for the daily rhythm of melatonin. Although melatonin is the nocturnal hormone in both diurnal and nocturnal animals, the regulation of its biosynthesis is specific for each one. In diurnal animals, only the activity of the enzyme AANAT is under daily control, while in nocturnal animals both transcription and translation are induced by darkness. AANAT has a very short life span; as soon as it is synthesized, the enzyme is ubiquitinated and targeted to the proteasome, being immediately degraded. This maintains the low level of melatonin during daytime, despite the constitutive synthesis of the enzyme. Darkness transmitted to the hypothalamic suprachiasmatic nuclei by the retinohypothalamic tract activates a polysynaptic pathway, which leads to the release of noradrenaline and adenosine triphosphate (ATP) by the sympathetic nerve terminals that reach the pineal gland [18]. The transcription factor cAMP responsive element-binding (CREB) and the protein kinase A (PKA), activated by cyclic-AMP dependent phosphorylation upon β-adrenergic stimuli, induce the transcription of the *Aanat* gene and the phosphorylation of the AANAT enzyme,

respectively [18]. The binding of phosphorylated-AANAT to the chaperone 14-3-3 impairs its entry in the proteasome and promotes the conversion of N-acetylserotonin in melatonin by ASMT enzyme [27]. Considering the onset of darkness, the raise in plasma melatonin starts much earlier in diurnal than nocturnal animals. Therefore, in humans, it is possible to detect melatonin as soon as 1 h after darkness, while in rodents at least 3 h is necessary to detect melatonin in the plasma [28, 29].

In the pineal gland, ASMT is regulated by the photoperiod. In Siberian hamsters, that are strict photoperiodic animals, ASMT activity was found to be about two times higher under short photoperiods than under long photoperiods, and the peak of melatonin follows the same profile [30]. In addition, this enzyme was shown to be the limiting step of the biosynthetic pathway [31]. Therefore, while AANAT is the key enzyme for determining the circadian rhythm of melatonin, ASMT is the photoperiodic enzyme; that is, it determines the higher melatonin amplitude in the winter when compared to summer nights.

The presence of melatonin in human appendix mucosa and rat digestive tract was described around 40 years ago. After the demonstration that the enzymes responsible for melatonin synthesis are present in the gastrointestinal tract and that the content of melatonin is maintained even after pinealectomy, it was proposed that melatonin should have a local role, independent of darkness control. Melatonin synthesized in the guts is drained to the liver via hepatic portal vein and may reach concentrations 15 times higher than the blood [32]. This information need to be taken into account due to expanding knowledge regarding the relevance of the gut-brain axis in triggering and management of inflammatory based CNS diseases.

The melatonin synthesized by immune-competent cells is highly relevant for surveillance of biotic and abiotic injuries and stress, as well as for the mounting and resolution of innate immune responses. Melatonin is synthesized by lymphocytes, thymus, spleen, and bone marrow [33–36] and was shown to modify the expression of cytokines and the reactive state of T- and B-lymphocytes [4]. In the last decades, the existence of an immune-pineal axis that considers both pineal and extrapineal productions and also the physiological/pathophysiological state of the organism was proposed [26].

In this context, the central transcription factor in defence responses, the nuclear factor kappa B (NF-κB), orchestrates the role of melatonin by inhibiting or activating its production by different sources [5]. The onset of an acute innate response induced by pathogen- or damage-associated molecular patterns (PAMPs and DAMPs, resp.) turns on/off the melatonin synthesis in a cell-dependent manner. Toll-like receptor 4 (TLR4) activation triggers NF-κB nuclear translocation, decreasing melatonin synthesis in pinealocytes and inducing its production by immune-competent cells [37–39]. The key event for this opposite effect lays on the NF-κB dimer that is preferentially activated in each cell. The NF-κB dimer translocated to the nuclei (p50/p50) in pinealocytes has no transactivating domain (TAD) and impairs *Aanat* transcription [40].

On the other hand, the translocation of a TAD positive NF-κB dimer (RelA/cRel) promotes the gene transcription in immunocompetent cells [41, 42]. The reduction of melatonin during the mounting of an innate immune response increases the expression of adhesion molecules that favour the migration of leukocytes from blood to tissues, playing a role in the inflammatory response mounting [43]. Recently, it was shown that the effect of darkness on endothelial cells primes the expression of microRNAs that negatively regulate cell adhesiveness, inflammatory response, and proliferation [44]. Melatonin synthesized by phagocytes acts in a paracrine manner favouring the phagocytosis of bacteria, fungi, parasites, and cellular debris [17, 41, 45, 46]. The synthesis of melatonin by the pineal gland is restored before the end of the acute inflammatory response, due to the inhibition of NF-κB by glucocorticoids released from the adrenal gland [29, 47, 48].

Melatonin effects are mediated by high affinity G protein coupled receptors (GPCRs) MT_1 and MT_2, by nuclear receptors, and by its ability to donate electrons, acting as an antioxidant molecule [49]. The history of melatonin receptors reveals the importance of understanding the kinetic of the radioligands. Experiments with [^{3}H]-melatonin did not indicate the presence of high affinity receptors, which were revealed after the use of [^{125}I]-2-iodo-melatonin, a molecule that did not cross the plasma membrane [50]. Besides its intrinsic free-radical scavenging characteristics, the antioxidant effect of melatonin may also occur by triggering the MT_1/MT_2-dependent induction of enzymes involved in the removal of reactive oxygen and nitrogen species (ROS and RNS), a pathway that requires much lower concentrations of the ligand [4]. Melatonin receptors may also form homo- and heterodimers, increasing the complexity of its pharmacology. Melatonin MT_2 receptors dimerize with serotonin $5HT_{2C}$ receptors in transfected human embryonic kidney cells (HEK 293) and human cortical cells [51]. Another interesting observation that could result in future basis for the understanding of melatoninergic drugs effects in health and disease is the dimerization of melatonin receptors with G protein-coupled receptor 50 (GPR50). GPR50 shares similarity with melatonin receptors but does not bind to melatonin [52]. MT_1 function is blocked by the formation of MT_1/GPR50 but this effect is not observed when MT_2 heterodimerizes with GPR50 [53]. Therefore, the results obtained with melatonin agonists and antagonists need to be followed by the understanding of the biology of melatonin receptors molecular complexity.

3. Melatoninergic System and Neuroprotection

Neuroprotective mechanisms preserve neuronal structure and function against acute or chronic insults of the CNS. Abrupt changes in brain irrigation by trauma or ischemia or the presence of neurotoxins demand immediate reactions of the nervous system cells. Deleterious effects triggered by endogenous molecules or by dysfunctional processes are the basis of neurodegenerative diseases and brain tumors. Inflammatory changes, ROS and RNS formation, mitochondrial dysfunction, excitotoxicity, apoptosis, and protein

aggregation are processes commonly found in these cases and related to neuron injuries [54].

Neuroprotective melatonin effects were shown at the molecular, cellular, and tissue level in animal models and in human trials conducted in patients with different CNS diseases. Reduction of inflammatory mediators, apoptosis, and unbalance of redox state are involved in the neuroprotection induced by melatonin [21, 55–57].

Several studies describe antioxidant effects of melatonin [58, 59]. Indeed, these protective effects are achieved by direct scavenger mechanisms or by melatonin receptors-mediated pathways. Melatonin and the metabolites N1-acetyl-5-methoxykynuramine (AMK) and N1-acetyl-N2-formyl-5-methoxykynuramine (AFMK) are electron donors and scavenge hydroxyl radicals, hydrogen peroxides, and singlet oxygen in a stoichiometric manner [60]. Activation of melatonin MT_1 and MT_2 receptors also exerts protective effects, in part dependent on the control of antioxidant enzymes expression such as glutathione peroxidase, glutathione reductase, and superoxide dismutase [61, 62].

The pivotal pathway for triggering inflammatory responses is the uncontrolled activation of the nuclear translocation of NF-κB dimers by PAMPs or DAMPs, promoting neuronal death [37]. Melatonin inhibits the nuclear translocation of NF-κB in several cellular models. Furthermore, melatonin exerts a protective effect by blocking NF-κB activation induced by lipopolysaccharide (LPS) in both rats and cells [63, 64]. NF-κB inhibitors block either the melatonin-induced neuroprotective or neurorestorative effects. Melatonin also inhibits other signalling pathways linked to innate immune responses, as nucleotide-binding oligomerization domain-like receptor family (NLR) pyrine domain-containing 3 (NLRP3) [65, 66]. This receptor located in the inflammasome upregulates apoptotic signalling pathways in the brain and peripheral inflammatory responses. Thus, melatonin impairs the activation of important signalling pathways that are responsible for triggering innate immune response. In the context of the immune-pineal axis, that activation of NF-κB initially inhibits the synthesis of melatonin by the pineal gland, favouring the mounting of the inflammatory response, and as the response progresses, it induces the synthesis of melatonin by microglia [5, 64].

Another interesting link between melatoninergic system and brain inflammatory responses is the regulation of the alpha-7-nicotinic acetylcholine receptors (α7nAchR) by melatonin [54, 67–69]. Cholinergic control of inflammation adjusts the intensity of appropriate immune responses and α7nAchR activation in immunocompetent cells shifts the immune responses towards a more anti-inflammatory profile. The expression and the functional response of α7nAchR located in the sympathetic neurons terminal present a daily variation dependent on the circadian rhythm of melatonin. Moreover, melatonin favours α7nAchR expression in the plasma membrane, reducing the desensitization due to internalization [68]. Therefore, melatonin improves α7nAchR-dependent cholinergic activities. Indeed, melatonin protects neurons from prion-mediated mitochondrial neurotoxicity by increasing the α7nAchR-mediated autophagic flux [54] and ischemic neurons survival by increasing the heme oxygenase-1 (HO-1) expression [69]. Furthermore, melatonin ameliorates cholinergic dysfunction and avoids neuronal apoptosis in the APP 695 transgenic mouse model of AD [67].

Interestingly, neurodegenerative disorders such as AD and PD are associated with impaired brain expression of both melatonin and α7nAchR [70–73] and disruption of nocturnal melatonin rhythm [74–76]. It is noteworthy that amyloid β (Aβ) peptides inhibit the synthesis of melatonin in rat pineal gland by activating NF-κB [77] and that melatonin treatment improves cognition and sleep in AD patients [78]. Long-term melatonin treatment induces receptor-dependent and receptors-independent neuroprotective effects in animal model of AD [62]. Receptor-independent effects of melatonin were observed on nonspatial cognitive performance, reduction of cortical and hippocampal amyloid plaques, and plasma Aβ_{1-42} levels. On the other hand, melatonin receptor-dependent effects were observed on spatial learning and memory and on the modulation of antioxidant enzymes [62]. Melatonin also attenuated Aβ-induced neurofilament hyperphosphorylation [55] and neuroinflammation [79]. Finally, melatonin restored mitochondrial function in a mouse model of AD via activation of melatonin receptors [56].

Disruption of melatoninergic system in diverse neurodegenerative diseases reinforces the potential neuroprotective effects of melatonin. Huntington's disease (HD) patients present a rhythm delay in nocturnal melatonin production [80]. The clinical relapses in multiple sclerosis are negatively correlated with melatonin levels [81] and no melatonin nocturnal peak is detected in AD [74] and stroke [82] patients. Interestingly, the reduction on nocturnal melatonin production occurs in early stages of AD [75]. Low night levels of melatonin are also commonly reported in schizophrenia patients [83].

The great exception is PD, which shows some controversies in the literature. Some reports refer no alteration [84, 85], small phase alterations [86], or decreased production of melatonin [87]. Nevertheless, Videnovic and colleagues [87] showed that, besides the reduction of circadian melatonin levels in PD, those patients with excessive daytime sleepiness present an even lower production of the hormone. Moreover, nocturnal working was shown to reduce the risk of PD while long daytime sleep was associated with increased occurrence of PD [88, 89].

Alongside the impaired production of melatonin, some neurodegenerative diseases also present altered expression of melatonin receptors. In PD patients, the expression of both MT_1 and MT_2 receptors is reduced in the amygdala and SNc [73]. Studies conducted in brains tissues of AD patients showed decreased expression of MT_1 and MT_2 in the cortex and in the pineal gland [71], MT_1 reduction in the suprachiasmatic nucleus [72], and a dual modulation in the hippocampus characterized by increased expression of MT_1 and decreased expression of MT_2 [70]. In addition, β-amyloid directly binds to MT_1 and MT_2 receptors, decreasing MT_1 binding sites and the activation of downstream pathways triggered by both melatonin receptors subtypes [77].

Finally, it is important to consider the role of extrapineal melatonin synthesized within the CNS as a resilience

mechanism against neurodegenerative processes. There are some important considerations regarding how melatonin reaches the CNS, the different capability of each brain area to synthesize melatonin under stressful conditions, and the relevance of melatonin metabolism inside the brain. Although i.p. administration of melatonin may reach the brain [90], daily circadian rhythm of melatonin in the cerebrospinal fluid is due to direct influx of melatonin from the pineal gland (i.e., independent of the plasma concentration) [91–93]. Acute injuries activate the immune-pineal axis blocking melatonin synthesis by the pineal gland and inducing it by immune-competent cells located in the injured area [5, 26]. Injection of LPS in the third ventricle increases AANAT expression in cortex, hippocampus, and cerebellum but induces melatonin synthesis only in the cerebellum [64]. This effect is mediated by the activation of NF-κB pathway and it was observed that cerebellar, but not cortical and hippocampal, neurons present reduced number of neuronal deaths after LPS injection. However, when LPS was given after the blockade of melatonin MT_1/MT_2 receptors with the nonselective competitive antagonist luzindole, there was a significant increase in cerebellar neuronal death.

Therefore, this review will assess the role of melatoninergic system in PD, focusing on the antioxidant, anti-inflammatory, motor, and nonmotor effects of melatonin. Besides the protective effects of melatonin described in the next sessions, a question that still has no answer is whether a putative local production of melatonin by some patients would explain the contradictory observations aforementioned regarding the nocturnal melatonin production in PD patients.

4. Parkinson's Disease

PD is characterized by a slow and progressive loss of DAergic neurons in the SNc, an important pathway for fine modulation of motor function [94]. The first report of PD is dated in 1817 in the James Parkinson's monograph "An Essay on the Shaking Palsy." Symptoms observed by Parkinson were described as "involuntary tremulous motion with lessened muscular power, in parts not in action even when supported, with a propensity to bend the trunk forward and to pass from walking to a running pace" [95]. Since then, PD is known as a movement disorder that mainly affects people of middle to old age [96].

PD is highly linked with the aging, being responsible for a significant increase in morbidity and mortality, affecting the social and economic life of individuals and society [57, 97]. According to the United Nations, it is believed that the number of elderly people in the world will reach 2 billion in 2050. Due to this, the World Health Organization (WHO) accounts that the number of cases of PD tends to increase and the importance of the disease as a public health problem will become even more significant. Additionally, PD is more common in males, with a ratio of men to women of 3 : 2 [98].

Although the symptoms and the neuropathology of PD have been well characterized, the mechanisms and causes of the disease remain unclear. Therefore, PD is described as a multifactorial disease that could be influenced by age and genetic and environmental factors [99–101]. PD is responsible for a significant increase in morbidity and mortality, affecting the social and economic life of individuals and society [57, 97].

The environmental hypothesis of PD aetiology is based on epidemiological studies showing the high frequency of the disease in individuals exposure to xenobiotics such as agricultural chemicals (pesticides, herbicides, etc.) and heavy metals (iron, manganese, aluminium, etc.) [102]. Other hypotheses of PD aetiology include genetic factors, natural aging process, increase of the formation of reactive species or inadequate functioning of its neutralizing mechanisms, and reduction of ATP stores that end up leading to neuronal death [103].

The majority of cases (90–95% of cases) are idiopathic, affecting 5% of population over 85 years old. However, in 5–10% of cases, PD can have a genetic component showing recessive and/or dominant modes of inheritance. Several genes mutations have been identified resulting in PD. Early onset PD or familial PD (occurring in people under 50 years of age) is less common, and recent data has identified some nuclear genes associated with familial PD, like *LRRK2*, *PARK2*, *SNCA*, *PARK7*, and *PINK1* [104].

Despite the knowledge derived from genetic research in PD, the accurate mechanism underlying the DAergic loss in PD is still not understood. However, mitochondrial dysfunction and oxidative stress in which there is an increase of the production of ROS, abnormal protein handling, neuroinflammation, excitotoxicity, and apoptotic processes have a central role in PD pathogenesis [101, 103].

The neuron's environment is a main contributor to neurodegeneration. Many evidences suggest that neurodegeneration can occur because of a cascade of events that affects the neuron's environment, called neuroinflammation [105]. Neuroinflammatory mechanisms involved in PD pathogenesis comprise microglial activation, astrogliosis, and lymphocytic infiltration and also involve alterations in the morphology of glial cells, including both astrocytes and microglia, indicating their interactions with the alterations in the homeostasis of the environment [101, 105]. Neurodegeneration in PD may be accompanied by an inflammatory reaction, characterized by activation of microglia, which leads to production of a number of inflammatory mediators (e.g., NF-κB, interleukin-1 (IL-1), IL-6, IL-1β, cyclooxygenase-2 (COX-2), tumoral necrosis factor-α (TNF-α), inducible nitric oxide synthase (iNOS), interferon-γ) and increased expression of different proinflammatory cytokines by glial cells. Besides, an increase in the level of these components in the substantia nigra and in the cerebrospinal fluid (CSF) and an elevation of γ/δ + T cells in the peripheral blood and CSF of patients with PD were also reported [101, 106, 107]. This increase in the proinflammatory cytokine levels could switch on different apoptotic pathways involved in the degeneration of DAergic neurons [94]. Taken together, oxidative stress, accumulation of endogenous cell metabolism products, excitotoxins like glutamate, toxic proteins, and a decrease of trophic factors can lead to apoptotic events of neurodegeneration [108, 109].

Oxidative stress also plays a pivotal role in DAergic neurodegeneration in PD. The DAergic neurons themselves seem

to contribute to ROS production through DA metabolism, which produces superoxide anion, hydroxyl radical, and hydrogen peroxide. Furthermore, the autoxidation of DA produces DA-quinone, a molecule that can damage the proteins structure [109].

Reactive species are involved in the protein aggregation. In PD, the presence of α-synuclein and ubiquitin aggregates in neurons in processes of degeneration is observed, especially in the DAergic neurons from SNc. These aggregates, known as Lewy bodies, are pathological markers for PD, being found in 85% of autopsies of PD patients [110, 111].

α-Synuclein plays an important role in synapse maturation and maintenance of neurons and its expression is developmentally regulated, redistributing from the cell bodies to synaptic terminals during periods of neuronal differentiation [112]. Also, this protein is upregulated during periods of synaptic plasticity [112]. Studies suggest that the α-synuclein can regulate the function of the two key proteins that control the amount of DA inside nerve terminals, regulating the uptake of extracellular DA by the DA transporter (DAT) and the packaging of cytosolic DA by the vesicular monoamine transporter 2 (VMAT2) [112]. Thus, the aggregation of α-synuclein triggers cellular mechanisms that lead to progressive death of DAergic neurons [113].

Many environmental toxicants, in particular pesticides, have been considered risk factors for PD. There are many studies evaluating the influence of exposure to heavy metals, solvents, and carbon monoxide in PD development [99, 114, 115]. Epidemiological studies have pointed a clear association between increased PD risk and specific environmental factors such as rural residence, drinking water from wells, and exposure to agricultural chemicals, including paraquat, rotenone, maneb, dieldrin, fungicides, and organochlorines [99, 102, 116, 117].

The degeneration of DAergic neurons in PD occurs mainly in the basal ganglia, a group of subcortical nuclei that control the voluntary movements (besides many other functions including procedural memory processing). The basal ganglia is composed of the striatum (putamen and caudate), globus pallidus externa and interna, subthalamic nucleus, SNc, and the substantia nigra pars reticulata (SNr). The basal ganglia forms neural loops extending from motor cortex to the motor thalamus and back to the cortex, and these loops seem to control the movements at a varying level of complexity [96]. The degeneration of DAergic neurons in PD occurs mainly in the nigrostriatal pathway and in minor extension in the ventral tegmental area [96].

Motor symptoms of PD begin to manifest when approximately 70% of DAergic neurons in the nigrostriatal pathway have been lost. In the beginning of the disease, the motor symptoms can be unnoticed or misinterpreted for a long time. Fatigue, lugubrious stiff face, impairment in the quality of speech, and extreme slowing down can be the first signals of PD and sometimes they can be confused with other diseases or with the aging itself [104]. The classical motor symptoms of PD include resting tremor, bradykinesia, muscular rigidity, and postural imbalance [118].

Additionally, a growing body of evidence demonstrates that PD patients commonly present sleep disturbances [87,

Table 1: Drugs used for symptomatic treatment of Parkinson's disease.

Drug	Mechanism of action
L-DOPA	DA precursor
L-DOPA + benserazide or carbidopa	DA precursor + peripheral dopa-decarboxylase inhibitor
Bromocriptine, pergolide, pramipexole, ropinirole	DA receptor agonists
Selegiline, rasagiline	Monoamine oxidase B inhibitors
Amantadine	Increase of DA release and glutamate NMDA receptor antagonist
Trihexyphenidyl, benztropine	Muscarinic receptor antagonists
Entacapone, tolcapone	Catechol-O-methyltransferase inhibitors

Adapted from [108].

119, 120], since DA is a neurotransmitter of major importance for the circadian cycle. Sleep disturbances are among the most common nonmotor symptoms of PD, affecting about 90% of PD patients. Impaired circadian function in PD is related not only to the disruption of sleep-wake cycle, but also to other functions such as autonomic imbalance, cognitive decline, and psychiatric disorders [121, 122].

Nowadays, it is well known that other neurotransmitter systems (e.g., cholinergic, noradrenergic, and serotonergic) also degenerate in PD, and the cell loss is extended to other brain regions besides the nigrostriatal pathway. This non-DAergic degeneration is a major cause of the nonmotor symptoms of PD such as cognitive decline, mood disorders, and autonomic dysfunctions. Nonmotor symptoms of PD are present across all the disease stages, but the frequency and severity increase with disease progression. Many studies have shown that these symptoms are highly incapacitating and have a major impact on the quality of life ahead of motor symptoms [123].

Besides the sleep disturbances, nonmotor symptoms of PD also include cognitive decline, depression, and anxiety [124, 125]. Most of studies demonstrated that the psychiatric symptoms are related to monoaminergic deficits within components of the limbic system implicated in emotional and affective functions [125]. As demonstrated by Braak et al. [126], the progressive death of DAergic neurons in PD occurs alongside the degeneration of noradrenergic and serotonergic systems.

The current available drugs for PD (see Table 1) mainly improve motor symptoms, without preventing the progression of the disease. Besides, the available treatments can cause several motor complications following chronic use [127] and eventually these treatments present low efficacy [128].

The most effective treatment for PD involves DA replacement therapy, made by the administration of its precursor 3,4-dihydroxy-L-phenylalanine (L-DOPA) associated with dopa-decarboxylase inhibitors (benserazide or carbidopa).
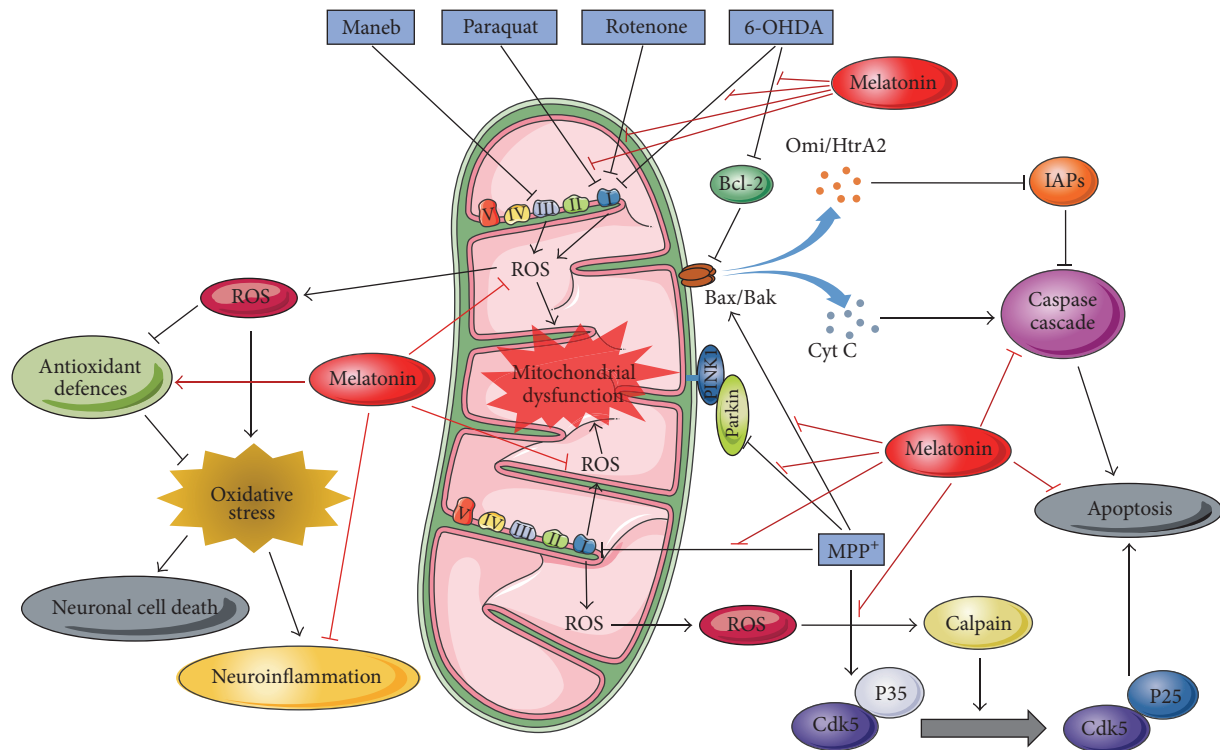
FIGURE 1: Summary of molecular mechanisms associated with neuroprotective effects of melatonin in *in vivo* and *in vitro* models of Parkinson's disease. The main molecular mechanism of neurotoxins is related to its ability to inhibit the complexes of the mitochondrial electron transport chain. The inhibition of these complexes leads to an increased production of reactive oxygen species (ROS) and, consequently, to mitochondrial dysfunction, oxidative stress, activation of apoptotic pathways, and neuroinflammation, culminating in neuronal cell death. Melatonin exerts neuroprotective effects through different mechanisms: protection of the complex I activity, neutralization of ROS, increased cell antioxidant defences, reducing neuroinflammation, inhibition of caspases cascade, and cellular apoptosis. Melatonin is also able to protect against induction of Bax and Cdk5/p35 expression and inhibition of Parkin/PINK1 and Bcl-2 expression induced by toxins in PD models. 6-OHDA: 6-hydroxydopamine; Bak: Bcl2 antagonist/killer; Bax: Bcl2 associated X; Bcl2: B cell leukemia/lymphoma 2; Cdk5: cyclin-dependent kinase 5; Cyt C: Cytochrome C; IAPs: inhibitors of apoptosis proteins; MPP$^+$: 1-methyl-4-phenylpyridinium; Omi/HtrA2: HtrA serine peptidase 2; ROS: reactive oxygen species.

Although such treatment improves motor symptoms of PD, the long-term treatment with L-DOPA is inefficient and causes numerous complications [129].

Aside from the treatment with L-DOPA, there are new treatment strategies focusing on the constant stimulation of the DAergic system, for example, the use of drugs with longer half-lives such as the DA receptor agonists ropinirole and pramipexole that allows the later use of L-DOPA or other drugs with short half-life [100, 130]. Table 1 summarizes the drugs available for symptomatic treatment of PD.

Despite all these options for PD treatment, none of these drugs prevent the disease progression. Therefore, there is a need to develop drugs or interventions that prevent or slow the progression of the degeneration of DAergic and non-DAergic neurons in PD.

5. Neuroprotective Potential of Melatoninergic System in Parkinson's Disease

Several studies have shown that PD patients exhibit changes in the melatonin production and in the expression of melatoninergic receptors MT_1 and MT_2 in the SNc [73, 84–87]. This reduction in endogenous melatonin production in PD patients, along with the discovery of the antioxidant activity of melatonin, has led to increasing interest in affording neuroprotection in PD. In this regard, it is known that the CNS is highly vulnerable to the effects of ROS, mainly due to high consumption of oxygen from this tissue, and that oxidative stress has a significant importance in the pathogenesis of PD [183].

Diverse neurotoxins have been used to mimic behavioural and neurochemical characteristics of PD in laboratory animals and thereby improve the knowledge about the pathogenesis and molecular mechanisms of the disease (Figure 1). These neurotoxins-based models are also useful for the screening of potential new treatments, including new agents aiming neuroprotection [184]. In this context, exogenous melatonin administration has demonstrated an outstanding neuroprotective effect in animal models of PD induced by different toxins such as 6-hydroxydopamine (6-OHDA), 1-methyl-4-phenyl,1-1,2,3,6-tetrahydropyridine (MPTP), rotenone, paraquat, and maneb (Table 2) [132, 144, 161, 164].

Table 2: Summary of studies presenting neuroprotective effects of melatonin in *in vivo* and *in vitro* models of PD.

Toxin	Subjects	Experimental approach	Main findings	Ref.
6-OHDA	Male Wistar rats	Unilateral injection of 6-OHDA (8 μg) into the right SNc. Treatment with melatonin (1 and 10 mg/kg, i.p.) before apomorphine administration.	Melatonin treatment inhibited apomorphine-induced rotational behaviour.	[131]
	PC12 cells	Preincubation (3 h) with melatonin (10^{-7} and 10^{-9} M). Incubation with 6-OHDA (25, 50, 100, and 250 μM).	Melatonin prevented the loss of cell viability and apoptosis induced by 6-OHDA. Melatonin also protected the reduction of mRNAs of antioxidant enzymes evoked by 6-OHDA.	[132]
	Male Sprague-Dawley rats	Unilateral injection of 6-OHDA (20 μg in 5 μL) into the right striatum. Melatonin (3 and 10 mg/kg, i.p.) was administrated 1 h before and immediately and 1 and 2 h after 6-OHDA injection. After that, the animals received a daily administration of melatonin in the next 3 days.	Melatonin treatment recovered the 6-OHDA-induced changes in striatal MDA and DA levels and TH activity.	[133]
	PC12 cells	Preincubation (3 h) with melatonin 10^{-7} M. Incubation with 25, 50, and 100 μM of 6-OHDA.	Melatonin protected cells from apoptosis and necrotic lesions induced by 6-OHDA.	[134]
	Male Sprague-Dawley rats	Unilateral injection of 6-OHDA (8 μg in 2 μL) into the right SNC. Melatonin treatment (50 ± 7.5 μg/h, s.c.) started immediately after 6-OHDA injection and it was maintained for 7 days.	Melatonin treatment prevented apomorphine-induced rotational behaviour and loss of complex I activity induced by 6-OHDA.	[135]
	Male Wistar rats	Unilateral injection of 6-OHDA into the right striatum (two injections of 12 μg in 1 μg of saline). Posttreatment (1 h) with melatonin (2, 5, 10, and 25 mg/kg, i.p.), daily for 7 days.	Melatonin prevented 6-OHDA-induced depletion of striatal DA and serotonin levels. Melatonin blocked the apomorphine-induced rotational behaviour.	[136]
	SK-N-SH cells	Preincubation (1 h) with melatonin (0.1, 0.5, 1.0, and 2.0 mM). Incubation with 6-OHDA (100 μM) for 24 h.	Melatonin protected against 6-OHDA-induced loss of cellular viability and increased activity of c-Jun-N terminal kinase signalling cascade.	[137]
	Male Sprague-Dawley rats	Unilateral injection of 6-OHDA (8.75 μg) into striatum. After lesion, animals received melatonin (0.4 or 4 μg/mL) in drinking water for 10 weeks.	Melatonin 4 μg/mL recovered motor deficits and normalized TH immunoreactivity and GDNF mRNA levels.	[138]
	Female Sprague-Dawley rats	Pretreatment with melatonin (0.5 mg/kg, i.p.) for 7 days. On day 8, animals received an unilateral injection of 6-OHDA (8 μg) into the lateral striatum.	Melatonin treatment prevented motor deficits (observed in the apomorphine-induced rotational behaviour, staircase test, disengage time, stepping test, initiation time, and postural balance test) induced by 6-OHDA administration.	[139]
	Male Wistar rats	Unilateral injection of 6-OHDA (8 μg) into the right medial forebrain bundle (MFB). Melatonin treatment (10 mg/kg, p.o.) began four days after 6-OHDA injection and continued for 30 days.	Melatonin treatment improved motor performance without evoking dyskinesia. Melatonin also protected TH-positive neurons and neuronal ultrastructure of striatum.	[140]

TABLE 2: Continued.

Toxin	Subjects	Experimental approach	Main findings	Ref.
	Male Wistar rats	Unilateral injection of 6-OHDA (12 µg) into the right MFB. Melatonin (10 mg/kg/day, i.p.) was administered 23 days before and 7 days after (pre- and posttreatment) or only 7 days after (posttreatment) the injection of 6-OHDA.	Melatonin decreased COX and caspase-3 activity and PGE2 levels and increased Bcl-2 levels that have been altered by 6-OHDA injection. Melatonin also prevented the loss of DAergic neurons in SNc.	[141]
	Male Sprague-Dawley rats	Unilateral injection of 6-OHDA (20 µg in 5 µL) into the right striatum. Melatonin (3 and 10 mg/kg, i.p.) was administered 1 h before and immediately and 1 and 2 h after 6-OHDA injection. After that, the animals received a daily administration of melatonin in the next 3 days.	Melatonin treatment reduced motor deficits and protected against 6-OHDA-induced loss of DAergic neurons in SNc and in dorsolateral striatum.	[142]
	Male Wistar rats	Unilateral injection of 6-OHDA (12 µg) into the right MFB. Melatonin (10 mg/kg/day) was administered 23 days before and 7 days after (pre- and posttreatment) or only 7 days after (posttreatment) the injection of 6-OHDA.	Melatonin treatment protected against the 7-OHDA-induced loss of DAergic neurons, increased antioxidant enzyme activities (SOD, catalase and GPx), and decreased lipid peroxidation. The pretreatment with melatonin was more effective in protecting against the 6-OHDA-induced deficits.	[143]
MPP^+	Female and male Sprague-Dawley rats	Pretreatment (30 min) with melatonin (10 mg/kg, i.p.). Unilateral injection of MPP^+ (7.4 µg) into the right SNc. Animals were subjected to an acute or chronic posttreatment with melatonin.	Melatonin treatment reduced lipid peroxidation and protected against DAergic neuronal loss induced by MPP^+.	[144]
	Hepatic mitochondria and striatal synaptosomes	Preincubation with melatonin (10^{-6} to 10^{-3} M). Incubation with MPP^+ (10^{-6} to 10^{-3} M).	Melatonin prevented the inhibition of complex I induced by MPP^+.	[145]
	Male Wistar rats	Unilateral injection of MPP^+ (0.1 µmol) into the right striatum. Melatonin (10 mg/kg, i.p.) was administered 1 h before and 1, 3, and 5 h after MPP^+ administration.	Melatonin reduced the MPP^+-induced DAergic toxicity and recovered the GSH levels.	[146]
	SH-SY5Y cells	Preincubation (4 h) with melatonin (200 µM). Incubation (72 h) with MPP^+ (1 mM).	Melatonin reduced MPP^+-induced mitochondrial DNA oxidative damage, accumulation of oxygen free radicals, generation of mitochondrial membrane potential collapse, and cell death.	[147]
	Cerebellar granule cells	Coincubation with MPP^+ (200 µM) and melatonin (1 mM) at the same time.	Melatonin protected cell viability and prevented apoptosis. Melatonin also reduced cdk5 expression and the cleavage of cdk5-35 to cdk5-25 induced by MPP^+. Melatonin prevented the MPP^+-induced	[148]
	SK-N-SH cells	Preincubation (1 h) with melatonin (1 mM). Incubation with MPP^+ (0.1 mM).	phosphorylation of c-Jun, activation of caspase-3, DNA fragmentation factor 45 (DFF45), and DNA fragmentation.	[149]
	Adult Wistar rats	Injection of 1 µL of 50 mM MPP^+ into the right striatum. Melatonin (10 mg/mL, i.p.) was administered 0, 1, 2, 3, 4, 24, 48, and 72 h after MPP^+ injection.	Melatonin protected DAergic neurons from apoptosis induced by MPP^+. Melatonin recovered mRNA and protein expression of fibroblast growth factor 9 that was reduced by MPP^+ injection.	[150]

TABLE 2: Continued.

Toxin	Subjects	Experimental approach	Main findings	Ref.
	C57BL/6 mice	Single injection of MPTP (20 mg/kg, s.c.). Melatonin (10 mg/kg i.p.) was administered 30 min prior to and every hour (for 3 h) after MPTP injection.	Melatonin treatment prevented MPTP-induced lipid peroxidation and TH-positive neurons loss in striatum.	[151]
	Male C57BL/6 mice	Single injection of MPTP (15 mg/kg, s.c.). Melatonin (5 or 10 mg/kg i.p.), deprenyl (0.37 mg/kg), or deprenyl plus melatonin (0.37 mg/kg and 5 or 10 mg/kg) was administered 30 min prior to MPTP.	Melatonin was able to protect the mitochondrial complex I activity and the oxidative damage in nigrostriatal neurons. Melatonin treatment also potentiates the protective effect of deprenyl on DA levels and TH activity.	[152]
	Male C57BL/6 mice	Four injections of MPTP (15 mg/kg, s.c.) with intervals of 2 h. After 24 h, the animals received three additional injections with the same dose and intervals. Melatonin (20 mg/kg s.c.) was administered 1 h before the first injection of MPTP.	Melatonin treatment prevented the MPTP-induced mitochondrial iNOS in striatum and SNc. Melatonin also protected complex I activity and inhibited lipid peroxidation.	[153]
	Rat astrocytoma cell	Preincubation with melatonin (50, 100, and 200 μM). Incubation with MPTP (400 μM).	Melatonin decreased the MPTP-induced oxidative and nitrosative stress, intracellular calcium, and activation of P-p38 MAPK. Melatonin also normalized the levels of inflammatory proteins, mRNA of proinflammatory cytokines, and NF-κB.	[154]
MPTP	Male C57BL/6 mice	Ten injections of MPTP (15 mg/kg, i.p.) during 5 weeks (2 injections a week). Melatonin (5 mg/kg, i.p.) was administered 1 week before, 5 weeks during, and 12 weeks after MPTP treatment.	Melatonin recovered mitochondrial respiration, ATP production, and antioxidant enzyme levels. Melatonin also protected against MPTP-induced DAergic neurons loss and locomotor activity deficits.	[155]
	Male Swiss mice	Four injections of MPTP (20 mg/kg, i.p.) with 2 h between them. Eight days after MPTP injections, animals received L-DOPA/carbidopa (100/10 mg/kg/twice/day, p.o.) and/or melatonin (5 or 10 mg/kg/day, p.o.) for 8 weeks.	Melatonin treatment recovered motor performance, striatal DA level, GSH, and antioxidant enzyme activities and reduced lipid peroxidation. Melatonin also improved the motor response to L-DOPA.	[156]
	Male BALB/c mice	MPTP (30 mg/kg, i.p.) was administrated in two injections (16 h apart). Melatonin treatment (10, 20, and 30 mg/kg, i.p.) 30 min before MPTP administration, followed by four doses of melatonin, at every 10 h.	Melatonin protected against the MPTP-induced TH-positive neurons loss in SNc and enhanced the effects of L-DOPA treatment.	[157]
	Embryos of zebrafish	Incubation with MPTP (600 μM). Incubation with melatonin (0.2 and 1.0 μM) at the same time or after the MPTP treatment.	Melatonin recovered motor behaviour of the embryos. Melatonin also restored gene expression and normal function of parkin/PINKI/DJ-1/MUL1 loop.	[158]

TABLE 2: Continued.

Toxin	Subjects	Experimental approach	Main findings	Ref.
	Drosophila melanogaster	Melatonin (5 mM) and/or rotenone (125 μM) were added to the feeding medium for 7 days.	Melatonin treatment prevented motor deficits and neuronal loss.	[159]
	Male Sprague-Dawley rats	Rotenone injection (6 μg in 1 μL) into the right SN. Melatonin (10, 20, and 30 mg/kg, i.p.) was administrated 30 min after rotenone injection and was given every 12 h for 4 days.	Melatonin reduced the levels of hydroxyl radicals in the isolated mitochondria and protected GSH levels and antioxidant enzymes activities in SN that were changed by rotenone injection.	[160]
Rotenone	Male Wistar rats	Rotenone injection (2.5 mg/kg, i.p.) for 10 days. Melatonin (10 mg/kg, i.p.) was administrated for 28 days after the rotenone injection.	Melatonin treatment protect TH-positive neurons in SNc and striatal levels of dopamine. Melatonin also inhibit the rotenone-induced depressant-like effect.	[161]
	Male Sprague-Dawley rats	Three injections of rotenone (4.0 μg in 2.0 μL/site) at three points along its rostrocaudal axis. Animals received melatonin (4.0 μg/mL) in drinking water, one week before and nine weeks after rotenone injections.	Melatonin treatment protected TH-positive neurons in striatum and SNc. Melatonin also inhibited the rotenone-induced loss in dopamine of SNc and apomorphine-induced rotations.	[162]
Maneb	PC12 cells	Incubation (2 h) with melatonin (1 nM) and/or maneb (1 μg/mL).	Melatonin prevented the maneb-induced disruption of the mitochondrial transmembrane potential, activation of caspase-3/7, loss in cell viability, and aggregation of α-synuclein.	[163]
Maneb plus paraquat	Male Swiss mice	Treatment with melatonin (30 mg/kg/day, i.p.) for 9 weeks. Treatment with maneb (30 mg/kg, i.p.) plus paraquat (10 mg/kg, i.p.) twice a week, for 9 weeks, 2 hours after melatonin injection.	Melatonin treatment protected the maneb/paraquat-induced lipid peroxidation, TH-positive neurons degeneration, increased nitrite content and mRNA levels of cytochrome P-450 2E1, GSTA4-4 activity, and increased levels of glutathione-S-transferase, P-p53, Bax, and caspase-9.	[164]
Lentiviral vector	Male Sprague-Dawley rats	Injection with lentiviral vectors encoding A30P mutant human α-synuclein (lenti-A30P) into the right SNc. Melatonin treatment (10 mg/kg/day, i.p.) 2 days before and 8 weeks after the injection of lenti-A30P.	Melatonin treatment prevented the loss of TH-positive neurons induced by injection of lenti-A30P.	[165]

6-OHDA: 6-hydroxydopamine; COX: cyclooxygenase; DA: dopamine; GDNF: glial cell-derived neurotrophic factor; GPx: glutathione peroxidase; GSH: reduced glutathione; GSTA4-4: glutathione S-transferase alpha 4; i.p: intraperitoneal; iNOS: inducible nitric oxide synthase; MAPK: mitogen-activated protein kinases; MDA: malondialdehyde; MPP$^+$: 1-methyl-4-phenylpyridinium; MFB: medial forebrain bundle; MPTP: 1-methyl-4-phenyl,1-1,2,3,6-tetrahydropyridine; NF-κB: nuclear factor-κB; PGE2: prostaglandins E2; s.c.: subcutaneous; SNc: substantia nigra pars compacta; SOD: superoxide dismutase; TH: tyrosine hydroxylase.

6-OHDA was the first toxin used to model the DAergic neurodegeneration similar to that seen in PD [185]. In DAergic neurons, 6-OHDA is internalized via DAT, reaching the interior of the cell where it will elicit its toxic effects [186]. The 6-OHDA exerts its toxicity mainly through two mechanisms: (1) autooxidation and (2) the inhibition of complexes I and IV of the mitochondrial electron transport chain. These mechanisms increase ROS production, which can induce neuroinflammation, microglial activation, and induction of apoptotic pathways culminating in cell death [186].

Unilateral nigrostriatal lesions induced by 6-OHDA followed by challenge with DA receptor agonists (e.g., apomorphine) lead to rotational behaviour in these animals; the rotational behaviour is mainly caused by the increased sensitivity to DA as a consequence of upregulation of DA receptors, in response to the reduced release of this neurotransmitter in the striatum [187]. Melatonin treatment confers DAergic neuroprotection through the normalization of oxidative unbalance generated by 6-OHDA administration, which was characterized by the measurement of expression and activity of antioxidant enzymes and levels of lipid peroxidation [132, 133, 143]. This effect may be due to the ability of melatonin to neutralize reactive species [188] or by the melatonin-induced increased activity [143] and expression of antioxidant enzymes [132]. Furthermore, Dabbeni-Sala et al. [135] demonstrated that melatonin is able to protect the 6-OHDA-induced inhibition of complex I activity of the mitochondrial electron transport chain in mice. In addition, melatonin also led to c-Jun phosphorylation inhibition, increased Bcl-2 levels, and decreased caspase-3 activity, blocking the apoptosis induced by 6-OHDA [132, 134, 137, 141] (Table 2).

The anti-inflammatory effect of melatonin was also observed in 6-OHDA model of PD. Melatonin inhibited COX enzyme activity and reduced the prostaglandin E2 levels (PGE2) [141]. Of high importance is the notion that the potential neuroprotective effects of melatonin in PD were demonstrated by independent research groups, where melatonin protected against the 6-OHDA-induced loss of tyrosine hydroxylase (TH) positive neurons in the SNc and striatal projections accompanied by significant improvement of motor impairments in rodents [131, 135, 136] (Table 2).

MPTP is another toxin widely used to mimic PD in animal models. This toxin was first described by Langston et al. [189] after causing a permanent Parkinsonism in drug users of northwestern California. The MPTP was accidentally produced during the synthesis of 1-methyl-4-phenyl-4-propion piperidine (MPPP). After administration, MPTP crosses the blood-brain barrier and is converted into the active toxin 1-methyl-4-phenylpyridinium (MPP$^+$) by the enzyme monoamine oxidase B (MAO-B) present on glial cells. MPP$^+$ has high selectivity for DAergic neurons since it is internalized by the DAT present in these cells. Inside the cell, MPP$^+$ inhibits the activity of complex I of the mitochondrial electron transport chain, causing an increase in the production of free radicals. This effect leads to activation of apoptotic pathways and consequent death of DAergic neurons [190]. MPTP studies often use systemic administration of this toxin or infusion of MPP$^+$ directly into the target structure, because MPP$^+$ does not cross the blood-brain barrier. Melatonin treatment prevented the loss of TH-positive neurons in the SNc at the same time which improved motor deficits induced by MPTP [144, 151]. Furthermore, melatonin, when coadministered with L-DOPA, was able to improve the motor benefits induced by L-DOPA [157] (Table 2).

The neuroprotective effect of melatonin seems to be mainly related to the its antioxidant activity, promoting reduced levels of lipid peroxidation, free radicals, oxidative damage in the mitochondrial DNA, and protection of the levels of GSH and antioxidant enzymes activity that are impaired by MPTP/MPP$^+$ administration [147, 151, 153, 155, 156] (Figure 1). Further, Khaldy et al. [191] showed that melatonin was able to prevent hydroxyl radical generation evoked by DA autoxidation evaluated *in vitro*. The mechanisms of melatonin neuroprotection (summarized in Figure 1) were investigated in *in vitro* and *in vivo* studies.

Some other mechanisms of melatonin neuroprotection have been demonstrated. Neurotrophic factors are important for the development, maintenance, and function of neurons and glial cells [192]. Glial cell line-derived neurotrophic factor (GDNF) is a neurotrophin known to promote the survival of DAergic neurons. GDNF expression was increased in rat C6 glioma cells exposed to melatonin [193]. The C17.2 neural stem cell line expresses MT$_1$ receptors and melatonin was also shown to increase GDNF expression in these cells [194]. Systemic MPTP administration in rats during 7 days decreased DA levels and increased GDNF mRNA expression in the striatum, while intrastriatal injections of melatonin further enhanced GDNF mRNA expression in this brain structure [195].

Another important neurotrophin that has potent effect in the survival and morphology of DAergic neurons is the brain-derived neurotrophic factor (BDNF) [196]. Howells and colleagues showed that BDNF expression is reduced in the SNc of PD patients [196]. However, nM concentrations of melatonin were shown to increase BDNF levels and exert neuroprotective effect in MT$_2$-knockout mice and in mouse cerebellar granule cells that underwent low-potassium toxic insults [197]. Rats tested under sleep deprivation and treated with melatonin also showed increased levels of BDNF in the cerebral cortex and hippocampus [198]. In addition, BDNF mRNA levels were increased in rat hippocampus and prefrontal cortex after acute administration of the MT$_1$/MT$_2$ agonist agomelatine [199]. Therefore, the regulation of the expression of neurotrophic factors by melatonin is likely part of the mechanism of neuroprotection exerted by melatonin.

Given the importance of α-synuclein alterations in PD, some studies have focused on the effect of melatonin in α-synuclein expression and aggregation. *In vitro* studies showed that melatonin protects dopaminergic cells such as SK-N-SH from the neurotoxicity induced by amphetamine (AMPH) and prevents the toxic overexpression of α-synuclein that occurs when these cells are exposed to AMPH [110, 200]. In this cell model, the AMPH increases α-synuclein expression while reducing TH phosphorylation, which is necessary for TH activation and DA synthesis [200]. An *in vivo* study by

Sae-Ung et al. [201] revealed that subcutaneous injections of AMPH in rats significantly increased α-synuclein levels in the SNc, nucleus accumbens, striatum, and prefrontal cortex. However, the concomitant administration of AMPH and melatonin drastically reduced α-synuclein accumulation [201]. In a model of kainic acid-induced neurotoxicity in C57BL/6 mice, the hippocampal α-synuclein aggregation was reduced by the oral administration of melatonin 1 h prior to kainic acid injection [202]. Taken together, these results demonstrate the potential of melatonin to modulate α-synuclein expression and protect DAergic cells against its undesirable toxic alterations (Table 2).

Melatonin also has a protective effect on the mitochondria, preventing the MPTP-induced inhibition of the complex I activity of the electron transport chain and the stimulation of iNOS activity, avoiding the potential collapse of mitochondrial membrane triggered by MPTP [145, 147, 153]. Neuroinflammation evoked by MPTP administration, characterized by increased levels of inflammatory proteins, mRNA proinflammatory cytokines, and NF-κB, was also attenuated by melatonin treatment [154] (Table 2).

The mechanism of MPTP toxicity appears to involve the stimulation of the phosphorylation of p38-MAPK, increasing the cdk5-35 expression and its cleavage to cdk5-25, which are involved in neurodegeneration [148, 154]. The administration of MPTP/MPP$^+$ also leads to a reduction in the mRNA and expression of fibroblast growth factor 9 (FGF9), which participates in the proliferation, differentiation, and survival of the cell. The expression and function of *parkin/PINK1/DJ-1/MUL1* loop, which plays an important role in maintaining mitochondrial homeostasis, are also altered by this toxin [150, 158]. All these changes were normalized by melatonin treatment [148, 150, 154, 158] (Table 2).

As described before, epidemiological studies have shown that exposure to certain pesticides increases the risk of developing PD and this has led to a growing interest in the development of animal models using environmental toxins such as rotenone, paraquat, and maneb [203]. Rotenone can exert its toxic effects by inhibiting the activity of complex I of the electron transport chain in mitochondria, leading to generation of ROS. Similar to MPTP, rotenone can be administered systemically or directly into the target brain structure of rodents and in cell cultures [186]. Melatonin has a protective effect against neurodegeneration caused by rotenone in different experimental protocols. Melatonin treatment reduced oxidative stress caused by rotenone, which was evidenced by reduced levels of hydroxyl radicals in the mitochondria, protection of GSH levels, and activity of antioxidant enzymes [160]. Melatonin also inhibited apoptosis induced by rotenone by reducing the Bax expression and release of Omi/HtrA2 [204]. This neuroprotective effect of melatonin culminated in the prevention of motor deficits evoked by rotenone administration in rodents and in a Parkinsonism model in *Drosophila melanogaster* [159, 161, 162] (Table 2).

Maneb and paraquat are pesticides used to mimic PD in cells and animals and they can be administered alone or in combination, which increases their toxicity. Paraquat and maneb can inhibit the biosynthesis of ATP and induce the formation of ROS by inhibiting the activity of complexes I and III of the mitochondrial electron transport chain, respectively [186]. Melatonin showed neuroprotective effect against toxicity induced by these pesticides through inhibition of oxidative stress and apoptotic pathways [163, 164]. In addition, melatonin was able to inhibit the aggregation of α-synuclein in P12 cells exposed to maneb [163] (Table 2).

In summary, melatonin demonstrated neuroprotective effects in different experimental models of PD. This neuroprotection seems to be mainly dependent on the modulation of the redox state of the cell by the melatonin [133, 143, 144, 147, 151, 153, 164]. However, the models currently used to mimic the PD have limitations and do not accurately correspond to the disease in humans. In addition, the adverse effects of chronic administration of melatonin are still poorly understood. Thus, further studies using genetic models of PD are necessary to confirm the neuroprotective potential of melatonin in the disease.

6. Melatoninergic System as a Putative Target for Treating Motor and Nonmotor Symptoms of Parkinson's Disease

6.1. Motor Symptoms. Many studies have assessed the possible role of melatonin in the modulation of motor symptoms of PD with discrepant findings [205]. The majority of studies showing the benefits of melatonin on evoked motor deficits in animal models of PD performed a pretreatment with melatonin. In such studies, melatonin exerts neuroprotective effects by preventing the death of DAergic neurons in the SNc and thus avoiding the development of motor dysfunction. However, Gutierrez-Valdez et al. [140] employed a different protocol where rats underwent a unilateral injection of 6-OHDA into the medial forebrain bundle and were treated with melatonin or L-DOPA, 4 days after the injury. Abnormal irregular movements (AIMs) evaluation, and the beam walking test were performed to assess dyskinesia and motor function. Melatonin was able to improve the rats walking ability without inducing the onset of AIMs, as in the case of L-DOPA treatment. Furthermore, melatonin treatment attenuated the loss of TH-positive neurons and protected the ultrastructural preservation of striatal neurons. These results suggest that although melatonin treatment started 4 days after the lesion, the beneficial effects on the motor symptoms were maintained. Other studies with PD models using 6-OHDA and MPTP also showed that treatment with melatonin, initiated shortly after administration of toxins, inhibited the onset of motor deficits. However, this effect seems to be related to the neuroprotective ability of melatonin instead of a direct action on the DAergic transmission [135, 136, 138, 156].

On the other hand, other studies failed to observe motor benefits of melatonin treatment in animal models of PD or PD patients. Medeiros et al. [206] showed that melatonin administration (3 mg, 1 h before bedtime) for 4 weeks in PD patients was able to improve the quality of sleep but did not affect motor symptoms in these patients. However, the evaluation of the melatonin effect was carried out during the day without analysis of the acute effect of melatonin. Yildirim and collaborators [141] evaluated the effects of pre-

and posttreatment with melatonin in animals that underwent a unilateral lesion with 6-OHDA in locomotor parameters, COX and caspase-3 activity, PGE2 and nitrite/nitrite levels, and apoptosis. Even though melatonin administration was able to prevent/recover parameters related to neuroinflammation and apoptosis, the pre- and the posttreatment were not able to restore the motor deficits induced by 6-OHDA injection. Moreover, Bassani et al. [161] reported that the melatonin posttreatment for 28 days preserved the TH-positive neurons and DA levels of rotenone-lesioned rats. In addition, they also observed that melatonin improved the depressive-like behaviour, but not locomotor deficits, of these animals.

Notably, the administration of melatonin *per se* has been linked to a reduction in locomotor activity in naïve animals. For instance, Chuang and Lin [207] demonstrated that the administration of high melatonin doses (60 mg/kg) led to a reduction in spontaneous locomotor activity of mice under normal conditions and also in response to thermal stress (cold, 4°C, and heat, 36°C). However, these changes were not observed with a lower dose of melatonin (30 mg/kg). Melatonin-treated animals showed a reduction in serotonin release in the hypothalamus, striatum, and nucleus accumbens, although DA levels were not altered. Furthermore, Willis and Armstrong [208] evaluated the effects of slow melatonin release via intracerebroventricular implants, pinealectomy, or exposure to constant light on the motor function of rats submitted to 6-OHDA or MPTP administration. Melatonin administration deteriorated motor performance, exacerbating the deficits evoked by these neurotoxins. Additionally, the experimental antagonism achieved by pinealectomy or melatonin synthesis inhibition by the exposure to light improved the induced motor deficits in PD models [208].

In this regard, previous studies have shown that light therapy may have a beneficial effect in motor and nonmotor symptoms of PD [209]. The improvement of motor symptoms by light was observed in animals with unilateral lesion with 6-OHDA, or with mechanical injury of the lateral hypothalamus [205]. Light therapy was also shown to be beneficial in PD patients. In a clinical study, 20 patients with PD received light therapy by exposure to fluorescent light for 1–1.5 hours at an intensity ranging between 1000 and 1500 lux, about 1 hour before bedtime. Several behavioural parameters were evaluated before the light therapy and after 2 and 5 weeks, at regular intervals.

Light therapy improved rigidity and bradykinesia, improved mood and sleep, reduced seborrhoea and impotence, and increased appetite [210]. In another study, 36 patients with PD received light therapy. The treatment consisted of exposure to 7500 lux illumination in the treated group and 950 lux in the placebo group, 30 min/day for 15 days. Patients were evaluated for motor symptoms, depression, and sleep disorders. The results revealed a significant improvement in tremors and depression presented by these patients [211]. Willis and colleagues [205] conducted a retrospective study where 129 PD patients were monitored for periods ranging from a few months to eight years. The treatment consisted of 1 h of exposure to a light intensity

ranging from 4000 lux to 6000 lux before bedtime. Motor and nonmotor symptoms were monitored. Patients were divided into 3 groups: patients who adhered, patients who adhered partially, and patients who did not adhere to the treatment. Patients who adhered to the treatment demonstrated an improvement of bradykinesia, rigidity, and balance. Symptoms of sleep disorders and depression also showed improvement. Additionally, increased medication was also lower in patients that fully or partially adhered in comparison to those who did not adhere.

Other studies also investigated the effects of melatonin receptors antagonism in animal models of PD. For instance, it was demonstrated that ML-23, an antagonist of melatonin receptors, enhanced the motor deficits induced by MPTP [212] and 6-OHDA [213]. This effect may be related to the interaction between the nigrostriatal and retinohypothalamic circuits, which converge towards the lateral hypothalamus. Additionally, the presence of visual impairments related to dopaminergic degeneration in patients with PD reinforces this concept [214].

The beneficial effects of melatonin antagonism on motor symptoms of PD can be explained by the melatonin action in the inhibition of DA release in various brain structures. This inhibition can occur at concentrations ranging from nM to μM and may be a consequence of the inhibition of calcium influx into neuronal terminals [215]. Studies have shown that DA metabolites exhibit a circadian variation with higher concentrations during the day and a reduction in the evening [216]. Khaldy et al. [217] demonstrated that the peak of melatonin release in C57BL/6 mice coincided with a reduction of DA levels in striatum. Moreover, this circadian cycle was disrupted by pinealectomy and restored by melatonin treatment [217]. The striatal DA release also modulates the activation of NMDA receptors. It has been proposed that the inhibition of striatal DA release by melatonin could also reduce striatal neurons response to glutamate released by cortical afferents [215].

In summary, although melatonin has shown a potential in improving motor deficits in animal models of PD, these effects appear to be related to its neuroprotective capacity. Nevertheless, in animal models and PD patients with established DAergic damage, melatonin may exacerbate motor deficits [205]. Moreover, the antagonism of melatonin receptors may lead to improvement in motor symptoms [208, 213]. Further studies are necessary to better understand the balance between DA and melatonin levels in the brain as well as its role in control of motor function.

6.2. Nonmotor Symptoms

6.2.1. Sleep Disturbances. Sleep disorders have been increasingly associated with PD and can arise as a prodromal symptom appearing years before the motor symptoms. These disorders may also reach the patient after the PD diagnosis worsening the life quality of patients and caregivers. The appearance of these disorders may be related to the degeneration of neural structures related to the sleep control. Among the sleep disorders that precede or appear in advanced stages of PD are excessive daytime sleepiness (EDS), rapid

eye movement (REM), sleep behaviour disorder (RBD), and insomnia [122, 218].

EDS is characterized as a chronic condition in which the individual is not able to remain awake during the day, inducing social problems and automobile accidents. Diagnosis can be performed with the use of a questionnaire such as Epworth Sleepiness Scale [218]. Studies have shown increased risk of PD in patients with EDS [87, 89]. Abbott and colleagues [219] showed an odds ratio of 3.3 for the development of PD in EDS patients monitored from 1994 to 2001. In this regard, the increase of daytime napping also has been associated with a major odds ratio of PD development in 3 different stages: established PD, recent PD, and prediagnosed PD [89]. Although there is some disagreement in the literature, the early onset of EDS has been established as a preclinical and premotor marker of PD.

The EDS may be present in PD as a persistent state of sleepiness or "sleep attacks" in which the patient begins to sleep suddenly. Although studies about the prevalence of EDS in PD show a large variation [218], its frequency appears to increase with disease progression. Tholfsen and colleagues [220] evaluated the frequency of EDS in drug-naive PD patients and after 1, 3, and 5 years of medication. EDS frequency increased from 11.8% at the baseline to 23.4% after 5 years in these patients. This elevation can be related to progressive loss of mesolimbic DAergic neurons and other non-DAergic neuronal circuits that modulate the sleep [218]. However, DAergic drugs used in PD treatment such as L-DOPA and DA receptor agonists may have sedative effects, contributing to the occurrence of EDS [221].

Changes in nocturnal sleep period may or may not be correlated with the appearance of EDS, which explains the variability in the response to the treatments that enhance night-time sleep. Some pharmacological treatments for EDS have been tested such as modafinil, caffeine, and amphetamine [221]. Modafinil is the most studied drug for this use; however, it shows modest effects on subjective parameters. Its mechanism of action is not completely understood but evidences suggest a link with the modulation of hypothalamic sleep-wake system. Modafinil promotes an increase in wakefulness by stimulating the tuberomammillary nucleus activity and reducing the promotion of sleep exerted by the ventrolateral preoptic area [221]. Caffeine did not provide benefits to sleepiness, but the patients displayed an improvement in motor symptoms of PD. Methylphenidate is an amphetamine that has shown some effect in reducing fatigue in PD patients; however, this drug has a high potential for the development of abuse [221].

The light treatment has been associated with improvement of the EDS symptoms. Mishima et al. [222] demonstrated that EDS was associated with the appearance of changes in melatonin levels and that the application of bright light therapy produced significant enhancements in symptoms. However, no study has evaluated the effect of light therapy in EDS presented in PD patients.

The relation between melatonin levels and EDS onset in patients with PD is still poorly explored. The cross-sectional study conducted by Videnovic and colleagues [87] with PD patients regularly receiving DAergic therapy revealed a diminished melatonin release. In addition, PD patients with EDS exhibited a lower release of melatonin than PD patients without EDS. Nevertheless, exogenous melatonin was not effective on EDS [223].

RBD is a parasomnia whose main features are the nocturnal dream enactment behaviour and loss of atonia of skeletal muscles. Abnormal motor behaviour (kicking) and vocals (screaming, laughing, and crying) also are commonly found in patients with this disorder. The motor symptoms provide fracture risk for the patient and their bed partner. The magnocellular nucleus in the medulla and subcoeruleus locus, which are related to the control of atony, appears to be altered in RBD. The appearance of RBD has been strongly linked to an increased risk of PD [121, 218, 224]. Schenck et al. [225] found that 38% of RBD patients evaluated in their study also have PD. In agreement, Iranzo and colleagues [226] observed that, of 44 patients diagnosed with idiopathic RBD (IRBD), 81% (36 patients) presented some degenerative syndrome, among them 16 have PD. The survival rate without any neurodegenerative syndrome from diagnosed IRBD patients was 65.2% at 5 years, 26.6% in 10 years, and 7.5% in 14 years. Thus, the diagnose of IRBD appears as a promising tool to assist in early diagnosis of PD.

Besides being present in the premotor phase of PD, RBD also follows the progression of motor symptoms of this disease. A study evaluating 57 patients newly diagnosed with PD and still without the use of DAergic therapy showed that 30% (17 patients) of the individuals had symptoms of RBD [227]. Other studies that investigated the presence of RBD in PD patients treated with DAergic drugs have found prevalence values ranging between 46% and 58% [228, 229]. Gjerstad and colleagues [230] evaluated the presence or absence of RBD in 231 patients with PD reexamining them after 4 and 8 years. Their data exhibited an elevation in the RBD frequency in these patients, from 14.6% to 27%, during the study period. This increase was associated with higher doses of L-DOPA and less Parkinsonism, firming the role of DAergic therapy in the onset of sleep-related disorders.

Although other studies have evaluated melatonin effect in improving sleep quality using subjective scales, only one study investigated the effect in patients diagnosed with RBD [206, 231]. Kunz and Bes studied six patients diagnosed with RBD who received treatment for 6 weeks with 3 mg of melatonin daily, 30 minutes before bedtime. As a result, a dramatic improvement in the symptoms of RBD in 5 patients within a week was observed and this improvement remained after discontinuation of treatment for weeks or months. Polysomnography performed 6 months later revealed that several parameters of REM sleep were normalized.

Insomnia is one of the most common sleep disorders in PD patients and its emergence may be related to uncontrolled motor symptoms, nocturia, depression, and circadian cycle disruption [218]. In a recent study, 689 patients with PD were submitted to a questionnaire in order to evaluate the quality of sleep. This study showed that the total number of patients who presented chronic inability to sleep was 36.9%; 18% had difficulty in initiating sleep, 81.54% interrupted sleep, 40.4% early morning awakenings, and 38.5% nonrestorative sleep [232].

Given the importance of the overnight motor symptoms in PD in the emergence of insomnia, treatments with DAergic drugs in order to reduce the night Parkinsonism have exhibited good efficacy. In this regard, studies assessing the benefits of slow release formulations of ropinirole, rotigotine, or L-DOPA showed an improvement in the sleep quality of patients with PD [233–235]. Several drugs are currently approved for the treatment of insomnia; however, only eszopiclone, an agonist of $GABA_A$ receptors, and doxepin, a tricyclic antidepressant, showed some efficacy in the treatment of insomnia in PD patients [221].

The role of melatonin in PD patients who suffer from insomnia is controversial. Although some studies have shown that treatment with different doses of melatonin leads to an improvement in the sleep quality, assessed subjectively by questionnaires or through polysomnography tests [206, 231], other studies show that the light therapy was beneficial for these patients [236]. PD patients exposed to a light intensity of 10000 lux (90 min/6 times a week) obtained an improvement in the insomnia, but there was a worsening in the questionnaires related to the symptoms of PD [237]. Other sleep disorders such as obstructive sleep apnoea, restless legs syndrome, and periodic leg movements during sleep are also often present in PD patients [218], but there is no specific study that associates these disorders with the modulation of the melatoninergic system.

As noted, even though progress has been made towards the characterization of sleep disorders during PD progression and the possible relationship with the melatoninergic system, more studies are needed for the development of effective therapeutic approaches that improve the quality of life of patients and caregivers.

6.2.2. Cognitive Deficits. Prevalence of cognitive deficits in PD patients has been poorly investigated [238]. A study carried out in the UK revealed that 36% of PD patients had cognitive impairment at least in one of three cognitive tasks performed: Minimental State Examination, a pattern recognition task, and the tower of London task [239]. Another report comparing untreated PD with controls found twofold increase in the proportion of cognitive dysfunction. Nevertheless, the lack of criteria for diagnosing cognitive impairment in PD patients makes these studies difficult to reproduce and compare [238].

Cognitive deficits detected in PD differ from individual cognitive impairment to minimal cognitive dysfunction to full-blown dementia like, being divided into mild cognitive impairment (MCI) or severe, leading to the dementia diagnosis (PD dementia (PDD)). This nonmotor symptom of PD may result from the natural course of the disease or could be associated with treatment interventions, such as adverse effects of drugs and deep brain stimulation (DBS). Executive function, memory, and visuospatial deficits are the three cognitive impairments more commonly detected in PD [238].

Executive function comprises essential abilities related to the decision-making process, such as retrieval from declarative memory, management of information in working memory, and cognitive flexibility and planning. Some studies have observed that executive dysfunction is higher during

early phase of PD and also that this impairment is a predisposing factor for greater severity of PD [240]. Also, memory deficits, working memory, short-term memory, visual short-term memory, declarative memory, and recognition memory are impaired in PD patients [238]. However, long-term and verbal short-term memory are not altered and explicit memory was shown to be partially lost [238].

Visuospatial dysfunction is well known in PD. Montse et al. [241] demonstrated that a decrease in spatial orientation functioning in PD may elicit the progression rating of the disease as reflected by three determinants variables found: age, duration of disease, and degree of dementia. Moreover, motor involvement has been suggested as major criterion for reduction of this memory, even in the early stages of the illness.

The pattern of cognitive deficits assessed in patients by cognitive tasks suggests the existence of subgroups, which may reflect regional differences in the underlying neuropathological processes [239]. In this way, grey matter loss in most of the brain regions has been correlated with a decrease of global cognitive score, but not with motor impairment. MCI subjects showed partial atrophy of grey matter in the temporal, parietal, and frontal cortex, bilateral caudal hippocampus, amygdala, and right putamen. Brain atrophy occurs as a consequence of the cell death, which is largely attributed to the formation of Lewy bodies in PDD [242].

There is increasing evidence about the role of melatonin in learning and memory processes (Table 3). Wang et al. [169] revealed a concentration-dependent inhibition of long-term potentiation (LTP) by melatonin in the CA1 dendritic layer of the Schaffer collateral of hippocampal slices in mice. LTP is a process in which the neuronal association is cooperatively and selectively strengthened by elevated synaptic activity through glutamate NMDA and α-amino-3-hydroxy-5-methyl-4-isoxazolepropionic acid (AMPA) receptors. Melatonin acts on LTP by modulating the postsynaptic nitric oxide (NO) signalling pathway [243]. Thus, this link between melatonin and LTP implies its role in the memory formation [169]. In addition, plasma melatonin levels decrease during aging, being related to the decline of neurogenesis and probably to cognitive alterations [244]. Despite this, the effect of melatonin on cognitive dysfunctions in PD has been poorly investigated, whereas more attention has been given to cognitive impairment in AD.

Datieva et al. [245] evaluated the effect of melatonin in 30 patients with early and late stages of PD and no significant difference was observed in cognitive autonomic disorders when compared to baseline. Using a MPTP rat model of PD, Capitelli et al. [246] investigated the effects of melatonin pretreatment (50 mg/kg, i.p.) in the animals' performance of two-way active avoidance task. The memory acquisition and retention process were impaired by MPTP, and melatonin was unable to restore this deficit.

The association between melatonin and cognitive dysfunction in PD was further addressed in animal models of PD using the novel object recognition (NOR) [247, 248], Morris water-maze (MWM), and passive avoidance tasks [249]. Agomelatine, an agonist of melatoninergic MT_1 and MT_2

TABLE 3: Summary of studies investigating the role of melatonin and its receptors in LTP and learning and memory processes.

Experimental approach	LTP	Main findings	MT receptor involved	Ref.
Melatonin 1 nM	Inhibits	Melatonin inhibits $GABA_A$ via MT_2.	MT_2	[166]
Melatonin 0.1 to 2.0 mM	Inhibits	Luzindole, an antagonist of MT receptors, blocks the inhibitory effect.	MT	[167]
Melatonin 100 μM	Inhibits	BMNEP, a specific ligand of the MT_2 receptors, mimics the inhibitory action.	MT_2	[168]
Melatonin 0.1 nM to 100 μM; $MT_1^{-/-}$ mice and $MT_2^{-/-}$ mice	Inhibits	Melatonin inhibitory action is prevented by luzindole and 2-propionamidotetraline, an MT_2 antagonist. $MT_2^{-/-}$ mice lost inhibitory effect on LTP, but not $MT_1^{-/-}$ mice.	MT_2	[169]
$MT_2^{-/-}$ mice	Inhibits	Slices from $MT_2^{-/-}$ mice exhibited smaller and decrement LTP compared to wild type mice. $MT_2^{-/-}$ mice showed impairment in the EPM on 2 consecutive days.	MT_2	[170]
$MT_1/MT_2^{-/-}$ mice	Enhances	$MT_1/MT_2^{-/-}$ mice demonstrated improvement in cognitive performance in the Barnes- and Y-maze tests.	MT_1/MT_2	[171]

receptors and an antagonist of serotonergic 5-HT_{2C} receptors, also elicits positive effects on memory [247]. Its chronobiotic activity on cognitive functions was investigated in the T maze left-right spatial discrimination test showing a more intense effect when administered in the evening and in the NOR exhibiting improvement in the memory independent of the administration period. Involvement of melatoninergic agonist and 5-HT_{2C} antagonist properties could be related to the memory facilitating effect of agomelatine [247]. Neu-P11, a melatoninergic (MT_1/MT_2) receptors agonist and serotonin 5-$HT_{1A/1D}$ agonist, was able to enhance the memory in the NOR and against deficit induced by $A\beta_{(1-42)}$ peptide [248].

Considering that sleep problems have been shown to contribute to neuropsychological deficits in otherwise healthy people, the nootropic effect of melatonin has been associated with its positive effect on sleep quality. As mentioned before, there is a high prevalence of sleep disturbances in PD patients, which are improved with melatonin treatment. Meta-analysis demonstrated a significant effect of sleep on global cognitive function, long-term verbal recall, long-term verbal recognition, shifting, updating, and fluid reasoning. Specifically in PD, an association between sleep disorders and memory and executive function deficits was found. However, this outcome should be analysed carefully due to the small number of studies and numerous methodological issues identified in them [250].

Furthermore, the differential role of MT receptors has also been investigated, mainly in the hippocampus, in order to elucidate nootropic effect of modulators in this system (Table 3). MT_1/MT_2 double knockout mice displayed ameliorated spatial and reference learning and memory performance in the Barnes maze and the Y-maze tests. These behavioural findings were consistent with the enhancement of LTP and brain p-CREB, p-ERK1/2, and key markers of synaptic activity expression levels [171]. However, other studies observed hippocampus LTP inhibition by melatonin

that was blocked by MT receptors antagonist [167] and by selective MT_2 receptor antagonist, suggesting a mediated effect by MT_2 receptor [168]. This hypothesis was confirmed using MT_1 knockout and MT_2 knockout mice, in which the inhibitory LTP action of melatonin was lost in $MT_2^{-/-}$ mice, but not in $MT_1^{-/-}$ mice [169].

This prevalent involvement of MT_2 receptor in the memory and cognitive functions has been demonstrated in the literature. Larson et al. [170] corroborate the data of Wang et al. [169], demonstrating smaller and decrement LTP in hippocampus slices from $MT_2^{-/-}$ mice. In addition, $MT_2^{-/-}$ mice showed learning deficits in the elevated plus-maze test (EPM) in two consecutive days, failing to shorten the transfer latencies to enter a closed arm on the second day. Comai and Gobbi [251] also report that $MT_2^{-/-}$ mice spent more time in the central platform of EPM, which could be linked to an impaired decision taking and cognitive flexibility.

Thus, these studies suggest an important role for melatoninergic system in memory and cognition function, probably linked to underlying process of LTP by MT_2 receptor. Nevertheless, due to contrasting results, more studies are required to clarify the role of melatoninergic modulators in LTP, as well as the importance of each MT receptor in this regard. After this, the potential use of melatoninergic modulators as cognitive enhancers, mainly for cognitive impairment linked to sleep disorders in PD and AD, should be considered in clinical and preclinical tests.

6.2.3. Depression. Depression represents one of the most common nonmotor symptoms in PD, occurring in 50–70% of patients [252, 253]. Many other diseases that affect elderly people also have depression as common symptom. However, patients with PD are more susceptible to developing depression than the general elderly population or patients with other chronic and disabling diseases [252]. In a recent

study conducted with more than 1400 individuals, depression was found to be more common in female than in male patients and had a bigger prevalence in individuals in the advanced stages of PD or in individuals that developed dementia [254].

Depression is an important feature to determine the quality of life in PD patients, and the caregivers of individuals with PD are also affected by the course of the disease [253]. Therefore, understanding depression in PD is a crescent need among all the professionals involved with this disease.

The aetiology of depression in PD is unclear, but alterations in neurotransmitters (monoaminergic) systems and limbic Lewy body pathology might contribute to this disorder. Besides, other previous pathologies like cerebrovascular disease and neurotrophic changes are also related to depression in PD. There is a hypothesis that claims that the monoaminergic deficits and lesions of frontal-subcortical circuits are the same in the brain of patients with PD and those with depression [118].

The main symptoms of depression are depressed mood, loss of pleasure (anhedonia), and feelings of worthlessness and guilty. The depressive syndrome also includes some somatic symptoms such as loss of appetite, sleep disturbances, psychomotor retardation, and altered facial expression [252]. However, these symptoms could also be present in PD patients without the depressive symptoms and the differentiation between these two situations is a great challenge for clinicians.

There are few studies investigating the course of depression among different stages of PD. One of the most important studies in the field evaluated patients with PD who were also diagnosed with major depression. One year later, the majority of these patients still showed major depression and the risk of dementia or a fast cognitive decline that was associated with major depression [255]. Nevertheless, more long-term studies that associate depression and PD are needed to clarify the predictors and prognostic of these patients.

There are contradictories views about depression as a nonmotor symptom of PD or a risk factor for PD development. Jacob et al. [256] and collaborators findings support the hypothesis that depression is a prodromal symptom of PD and not a risk factor for the disease. In a two-year study, it was observed that the development of PD was more common in individuals who had used antidepressants than among nonusers [257].

Depression and PD share some abnormalities in brain structure. In the SNc, there is a hyperechogenicity and in the brainstem raphe there is a reduced echogenicity. These alterations are common and severe in patients who have both PD and depression, and these changes are usually related to a history of depression before the development of PD [258]. Patients with PD and depression also presented a profound loss of striatal DAT availability and frontal hypoperfusion compared with nondepressed patients [252, 253]. These observations, besides confirming that depression can precede PD, are in agreement with Braak hypothesis of PD, in which the neurodegeneration in regions like the noradrenergic coeruleus-subcoeruleus complex and the serotonergic caudal raphe nucleus occurs before the motor symptoms [259].

Defining the mechanism behind depression in PD is very difficult. When people older than 65 years are affected by depression, there are numerous variables involved such as psychosocial issues, genetic factors, and age-related brain alterations that should be considered. In patients with PD that also develop depression, it is necessary to consider the involvement of factors like monoaminergic disturbances, cerebrovascular diseases, Lewy body pathology, functional changes in the limbic and subcortical circuits, hippocampal atrophy, alterations in neurogenesis and neurotrophic factors, and toxic stress, besides hypercortisolemia and inflammation [252].

The neurotransmitter systems affected in patients with depression and PD involve the noradrenergic, DAergic, and serotonergic pathways. These systems are also related to regulation of mood, and deregulations of these are associated with depression in the general population. Patients with PD and depression were shown to have increased serotonergic neuronal cell loss in the dorsal raphe nucleus and decreased levels of striatal serotonin and its transporter. The disruption of the nigrostriatal DA as well as other DAergic pathways in limbic and frontal circuits, and the loss of DAergic neurons in the ventral tegmental area, are also related to depression in PD. Indeed, the locus coeruleus is affected in early stages of PD and the increase of neurodegeneration in this area is correlated with depressed individuals with PD. Cognitive and mood impairments associated with PD could also be related to cholinergic deficits. Furthermore, new evidence suggests that stress hormones, immunomodulatory mediators, neurotrophic factors, and neuropeptides are also involved in the aetiology of depression in PD [252].

Although depression is highly prevalent among individuals with PD, a proper therapy for this disorder has not been well defined. The options of treatment for depression in PD found in literature are limited by a small sample size, short duration of action, design issues, or incompatible outcome measurements [253]. The classic options for the treatment of depression in PD include selective serotonin reuptake inhibitors (SSRI) (citalopram, sertraline, fluoxetine, and paroxetine); serotonin-noradrenalin reuptake inhibitors (SNRI) (desipramine, amitriptyline, nortriptyline, and doxepin); and some atypical agents as trazodone and nefazodone. These are also examples of the main medications used to treat depression in general population. Pramipexole, pergolide, atomoxetine, and memantine are also used, even though they are not so common. Finally, bupropion, a noradrenaline and DA reuptake inhibitor, is normally used to treat depression in PD patients and has effects under the depressive and motor symptoms [123, 124].

Depression in PD has a heterogeneous aetiology and responsiveness to treatments, and although there are a wide variety of treatment options, not all the patients with depression and PD respond to these drugs. Therefore, new strategies and new targets have been investigated to improve the current therapy and assure a good prospect of quality of life for these patients [124]. Melatonin is one of the substances that show beneficial effects for depression in PD patients.

The potential therapeutic effect of melatonin in mood disorders has been studied recently, because many patients

with depression presented disruption in melatonin circadian profile [161, 260]. Preclinical studies demonstrated that melatonin has antidepressant-like effects in several animal models of depression, such as in the forced swimming test [260], tail suspension test [261, 262], chronic mild stress paradigm [263], and nonmotor symptoms of a rodent model of PD [161].

In order to document the association between sleep and mood disorders, different studies in humans have been done demonstrating that the treatment with melatonin improves the total sleep time and decreases depressive symptoms. A new pharmaceutical tool for treating and preventing depression contains an association between a SSRI and melatonin; this association had a markedly positive impact on the sleep-wake rhythm of depressive patients [264]. Circadian disruption is linked to the changes in behaviour and sleep patterns that occur in depression, and this disease is associated with alterations in diurnal rhythm of melatonin output [265].

In the rotenone model of PD, the prolonged treatment with melatonin prevented the appearance of depressive-like behaviour, and this melatonin antidepressant effect was associated with its ability to restore the striatal DA levels [161]. Another study demonstrated that the antidepressant-like effect of melatonin in the tail suspension test could be associated with its direct interaction with DA D_1 and D_2 receptors [262]. Furthermore, the antidepressant effect of melatonin may also be attributed to the protection against the loss of DAergic neurons and the modulation of DAergic neurotransmission [161].

Since alterations in circadian rhythms are also implicated in the aetiology of depression and PD, dysfunction in the rhythmicity of circadian cycle is very common among PD patients with depression [161, 265]. Another important fact to be observed about melatonin and depression in PD is that the DAergic neurons in the nigrostriatal pathway are melanocytes, and the melatonin and DA coexist in a functional opposition regulating day/night activities. Thus, it is likely that the exogenous melatonin administration may alter the balance between DA and melatonin. In the study of Bolitho et al. [266], the DAergic treatment for PD profoundly increased the secretion of melatonin, regulating the circadian cycle and sleep timing.

Considering the relevance of circadian cycle in the pathogenesis of depression and PD, a new approach has been proposed for the treatment of this disorder using the melatonin analogous agomelatine. This drug is associated with the resynchronization of circadian rhythms and was shown to have antidepressant effect in humans.

Overall, from these limited results in this field, it appears that melatonin and melatonin analogous might be particularly useful to improve the depression in PD, but further studies are needed for the development of effective therapeutic approaches that improve the quality of life of patients and caregivers.

6.2.4. Anxiety. Despite the high prevalence of anxiety in PD patients, this issue has only recently attracted scientific attention. Anxiety disorder presents itself as the second mood disturbance most common in PD, with major impact on daily functioning and quality of life in patients [267].

Prevalence of anxiety in PD patients depends on the study sample features and methodology used to assess this nonmotor symptom [268]. Many studies suggest that approximately 20–50% of PD patients experience clinically relevant symptoms of anxiety [269, 270]. Generalized anxiety disorder (GAD), social phobias, panic attacks, and anxiety disorder Not Otherwise Specified (NOS) are the anxiety syndromes more often reported in PD when using the Diagnostic and Statistical Manual (DSM) of mental disorders criteria for the assessment [271]. Nevertheless, DSM has questionable validity to assess anxiety in PD, since symptoms in PD patients are atypical and therefore are classified as NOS [272]. Recently, Dissanayaka et al. [273] recommended the use of Parkinson's Anxiety Scale (PAS) and Geriatric Anxiety Inventory (GAI) in PD without dementia in order to present satisfactory psychometric features.

Anxiety is a nonmotor symptom of PD that can precede the onset of motor symptoms or develop after the diagnosis of the disease [268]. In order to understand the risk factors linked to anxiety in PD, Broen et al. [274] delineated a model using PD-specific and nonspecific factors. Previous history and the severity of depressive symptoms were considered nonspecific risk factors, which showed direct effect on anxiety. On the other hand, motor fluctuations and disease-related decline in daily activities were considered PD-specific factors and display less influence in the model.

Rutten et al. [275] concluded in their study that anxiety in PD involves affective and somatic symptom dimensions. In fact, several authors have associated anxiety disorders with severe gait problems [270], dyskinesias/fluctuations [270, 271], freezing [276], and depression [267, 270, 274, 276]. Furthermore, depression, urinary disorders, and sleep disruption were found as factors most likely to influence anxiety in PD [272].

Neurobiological alterations related to anxiety in PD are based on two theories [268, 269]. The reactive theory is associated with the diagnostic of PD and therefore with the DAergic lesion and motor impairment [271, 276]. DAergic involvement is supported by positive relationship between anxiety and motor fluctuations and withdrawal of DAergic medication or DBS [111]. Additionally, the mesolimbic DAergic pathway, in which neurodegeneration is observed in PD, sends projections to the amygdala, a key brain structure for the production and regulation of anxiety [277].

In contrast, psychological symptoms could result from early neurochemical changes; hence, epidemiologic observations demonstrate that PD patients have greater predisposition to anxiety disorders before the diagnosis [256]. Thus, anxiety may be a premotor symptom of PD linked with other neurotransmitters systems such as noradrenergic and serotonergic systems [269, 278]. Braak staging scheme for PD suggests early neurodegeneration of the raphe nucleus and the locus coeruleus, structures with abundance in serotonin and noradrenaline, respectively. Serotonin depletion results in an increased anxiety in PD [223], whereas noradrenaline reduction leads to a high frequency of anxiety in PD [279]. Additionally, other neurotransmitter systems

TABLE 4: Animal studies addressing the effects of melatonin on anxiety-like responses.

Test	Gender, species, stain	Melatonin treatment	Effects	Ref.
OFT	Male, rat, Wistar	1 mg/kg, i.p.	Anxiolytic	[172]
EPM	Male, rat, Wistar	1–20 mg/kg, i.p. at 12:00 h or 18:00 h	Anxiolytic during the dark phase	[173]
FET, LDT	Male, mouse	0.5–5 mg/kg, i.p.	Anxiolytic	[174]
Vogel test	Male, rat, Wistar	0.1–2.0 mg/kg, i.p.	Anxiolytic	[175]
FET, LDT	Male, mouse, C3H/He	5–25 mg/kg, p.o.	Anxiolytic	[176]
EPM, Vogel test, USV, social interaction test (SIT)	Male, rat, Wistar	2.5–80 mg/kg, i.p.	Anxiogenic at 80 mg/kg on the SIT No effect on the other tests	[177]
EPM, Vogel test, USV	Male, rat	10–75 mg/kg 2 h before 2 h after the dark phase	Anxiolytic on the EPM 2 h after the dark phase No effect on the Vogel test and USV	[178]
Vogel test	Male, rat, Wistar AF	20–80 mg/kg, i.p. at 17:00 to 20:00 h	Anxiolytic	[179]
EPM	Male, rat, Sprague-Dawley	50 mg/kg, i.p. in the morning and afternoon	Anxiolytic in the afternoon	[180]
EPM, OFT	Male and female, rat, Wistar	4 mg/kg, s.c. at 16:00 h for 8 weeks	Anxiolytic Gender-dependent	[181]
EPM, OFT, NSF	Male, rats, Sprague-Dawley	20 mg/kg, s.c.	Anxiolytic on the EPM and NSF No effect on the OFT	[182]

EPM: elevated plus-maze test; FET: free exploratory test; LDT: light/dark box test; NSF: novelty-suppressed feeding test; OFT: open field test; USV: ultrasonic vocalization.

such as gamma-aminobutyric acid (GABA) and glutamate neurotransmitters were shown to be altered in PD patients and may also influence anxiety [268, 269].

In spite of the data mentioned, the anxiety in PD is underdiagnosed and undertreated. The treatment of anxiety in patients with PD is the same as that in patients without PD, which is similar to depression treatments [269]. Even though depression and anxiety are frequently comorbid [270, 280], they are distinguished from each other, exhibiting distinct trajectories and different longitudinal relationships with demographic, motor, and nonmotor factors that were unique to each disorder [280].

The benzodiazepine (BDZ) midazolam was compared to melatonin on the perioperative effects in a double-blinded, placebo-controlled study [281]. Both treatments were able to decrease anxiety levels and elevate levels of sedation when compared to control subjects. Nevertheless, midazolam, tested at three different doses, induced impairment in the psychomotor skills and performance on the digit-symbol substitution test at all evaluated time points. Melatonin, at a dose of 0.05 mg/kg, was associated with preoperative anxiolysis and sedation without cognitive and psychomotor deficits. Preclinical trials also were carried out with melatonin and BDZ. Guardiola-Lemaître et al. [236] observed that melatonin enhanced anxiolytic-like action of diazepam in mice submitted to the four plates and tail suspension tests.

Anxiolytic effect of melatonin has also been evaluated on several behavioural tests of anxiety (Table 4). The first evidence of its influence on anxiety was obtained in rats by Golus and King [172] in the open field (OF) test. After this, anxiolytic-like activity of melatonin has been observed in several behavioural animal tests, such as light/dark box (LD),

elevated plus-maze (EPM), and Vogel tests [173–176, 178–182]. Papp et al. [178] reported the capacity of melatonin in increasing the open-arm exploration at the EPM only in the evening experiment and proving itself inactive in the Vogel and ultrasonic vocalization tests independent of timing [178]. Nonetheless, Millan et al. [177] data do not corroborate this conclusion. The variability found in the results may be related to dose and time of delivery, but there is a consensus that anxiolytic melatonin's effect is strongly time dependent [173, 179, 180] (Table 4).

In relation to clinic findings, Datieva et al. [245] described the effectiveness of melatonin in decreasing the anxiety state on Spielberger's scale without altering motor, cognitive autonomic, and depression levels in patients with early and late stages of PD. Melatonin treatment also presented itself as useful as an anxiolytic in perioperative treatment in nine of the ten studies. In addition, plasma melatonin is diminished at night in patients with panic disorder, which has an increased prevalence in PD patients [282].

Other modulators of melatoninergic system have been investigated on anxiety disorders. Agomelatine, Neu-P11, and UCM765 presented anxiolytic effects in behavioural animal tests independent of the timing of administration [177, 178, 180, 182], without inducing sedation [178]. Clinical data suggest that agomelatine has anxiolytic potential, which proved to be equal or higher than SSRIs and SNRIs for the treatment of GAD, a common anxiety disorder in PD [283]. Case reports suggest a potential of agomelatine as treatment for social anxiety [284] and panic disorders [285]. Kalyn et al. [286] assessed therapeutic efficacy, tolerability, and safety of agomelatine in elderly patients observing positive results in depression, anxiety, and anhedonia indicators. On the other

hand, anxiolytic action of UCM765 was shown to be mediated by MT_2 receptors [182] and anxiety levels did not alter in $MT_2{}^{-/-}$ mice in the EPM [251].

Different effects on anxiety found among melatonin and melatoninergic agonists mentioned here suggest the involvement of other neurotransmitter systems. The use of S22153, a melatonin receptor antagonist, was shown to block both melatonin and agomelatine anxiolytic effects in the EPM at night [178], reinforcing the participation of MT receptors in the nocturnal action. However, Millan et al. [177] did not report the same effect, suggesting that the anxiolytic action of agomelatine is more related to $5\text{-}HT_{2C}$ antagonism. Recently, the capacity of MT_2 and $5\text{-}HT_{2C}$ receptors to assemble into functional heteromers was identified, indicating a potential involvement of these heteromers in agomelatine effect [51]. The maintenance of anxiolytic action of agomelatine in daytime also corroborates the modulation of serotoninergic system. In addition, there are several evidences of the contribution of the GABAergic system to melatonin, agomelatine, and Neu-P11 effects [173, 174, 179, 180].

Melatonin can bind to GABA receptors like BDZ, barbiturates, and GABA, enhancing chloride influx [287]. Furthermore, enhancement or attenuation of $GABA_A$ receptor-mediated currents strongly depends on melatonin receptors activation [287]. Indeed, melatonin potentiated GABA-evoked current amplitude in suprachiasmatic nucleus, which express MT_1 receptors, and decreased in hippocampal CA1 neurons, which express MT_2 receptors [166]. Pharmacological interventions also elicit the involvement of GABAergic system in the effect of melatonin [173, 174, 236]; and in humans it has been used to reduce or eliminate BDZ administration in elderly patients [251].

Therefore, there are many studies supporting the anxiolytic potential of melatonin and other melatonin receptors agonists, demonstrating the cross talk between melatoninergic, GABAergic, and serotoninergic systems. Nonetheless, its use in PD, a disease with high prevalence of anxiety disturbances, has been underinvestigated in both preclinical and clinical studies.

Although research is at an early stage, the findings reviewed above highlight the sleep, memory, and anxiety- and mood-enhancing properties of melatonin in humans and rodents. Therefore, the performance of additional preclinical and clinical studies to verify the effects of melatonin and new drugs acting on melatoninergic system in the nonmotor symptoms of PD appears to be a promising field.

7. Conclusions

This article reviews the recent evidence that the melatonin plays an important role not only as a modulator of light-dark cycle, but fundamentally as an important factor for neuronal plasticity, protection, and survival in the CNS. Possible therapeutic opportunities for neurological disorders through the modulation of melatoninergic system are presented in the expectancy that this review may inspire clinical researchers and foster experimental approaches using melatonin receptors MT_1 and MT_2 as therapeutic targets.

Melatonin has anti-inflammatory and antioxidant properties acting as a free-radical scavenger, reducing hydroxyl free radicals, and improving mitochondrial homeostasis. It also regulates the expression of neurotrophins that are directly involved in the survival of dopaminergic neurons and reduces the aggregation of α-synuclein restoring deficits in the DAergic system. The unbalance of pineal melatonin synthesis can predispose the organism to inflammatory and neurodegenerative diseases such as PD. The literature reviewed here indicated that PD is associated with impaired brain expression of melatonin and its receptors MT_1 and MT_2. Moreover, melatonin administration has demonstrated an outstanding neuroprotective effect in animal models of PD induced by different toxins such as 6-OHDA, MPTP, rotenone, paraquat, and maneb. These studies have shown promising results with the improvement of motor deficits in animal models of PD and notably in nonmotor symptoms such as sleep disorders, anxiety, depression, memory, and cognition dysfunctions that are part of the symptoms commonly experienced by PD patients.

Future research aiming at the development of novel melatonin receptor selective ligands will help to elucidate the neurobiology and physiological role of melatonin as well as its potential as a novel palliative and neuroprotective agent in PD.

Competing Interests

The authors have no financial or personal conflict of interests related to this work.

Acknowledgments

References

[1] A. B. Lerner, J. D. Case, Y. Takahashi, T. H. Lee, and W. Mori, "Isolation of melatonin, the pineal gland factor that lightens melanocytes," *Journal of the American Chemical Society*, vol. 80, no. 10, p. 2587, 1958.

[2] R. J. Wurtman, J. Axelrod, and E. W. Chu, "Melatonin, a pineal substance: effect on the rat ovary," *Science*, vol. 141, no. 3577, pp. 277–278, 1963.

[3] J. Axelrod, R. J. Wurtman, and S. H. Snyder, "Control of hydroxyindole O-methyltransferase activity in the rat pineal," *The Journal of Biological Chemistry*, vol. 240, pp. 949–954, 1965.

[4] A. Carrillo-Vico, P. J. Lardone, N. Álvarez-Śnchez, A. Rodrĭguez-Rodrĭguez, and J. M. Guerrero, "Melatonin: buffering the immune system," *International Journal of Molecular Sciences*, vol. 14, no. 4, pp. 8638–8683, 2013.

[5] R. P. Markus, E. Cecon, and M. A. Pires-Lapa, "Immune-pineal axis: nuclear factor κB (NF-ΚB) mediates the shift in the melatonin source from pinealocytes to immune competent cells," *International Journal of Molecular Sciences*, vol. 14, no. 6, pp. 10979–10997, 2013.

[6] D. Acuña-Castroviejo, G. Escames, C. Venegas et al., "Extrapineal melatonin: sources, regulation, and potential functions," *Cellular and Molecular Life Sciences*, vol. 71, no. 16, pp. 2997–3025, 2014.

[7] E. Martins Jr., A. C. F. Ferreira, A. L. Skorupa, S. C. Afeche, J. Cipolla-Neto, and L. F. B. P. Costa Rosa, "Tryptophan consumption and indoleamines production by peritoneal cavity macrophages," *Journal of Leukocyte Biology*, vol. 75, no. 6, pp. 1116–1121, 2004.

[8] S. M. Muxel, M. A. Pires-Lapa, A. W. A. Monteiro et al., "NF-κB drives the synthesis of melatonin in RAW 264.7 macrophages by inducing the transcription of the arylalkylamine-N-acetyltransferase (AA-NAT) gene," *PLoS ONE*, vol. 7, no. 12, Article ID e52010, 2012.

[9] A. Conti, S. Conconi, E. Hertens, K. Skwarlo-Sonta, M. Markowska, and G. J. M. Maestroni, "Evidence for melatonin synthesis in mouse and human bone marrow cells," *Journal of Pineal Research*, vol. 28, no. 4, pp. 193–202, 2000.

[10] J. Stefulj, M. Hörtner, M. Ghosh et al., "Gene expression of the key enzymes of melatonin synthesis in extrapineal tissues of the rat," *Journal of Pineal Research*, vol. 30, no. 4, pp. 243–247, 2001.

[11] Y.-J. Liu, J. Zhuang, H.-Y. Zhu, Y.-X. Shen, Z.-L. Tan, and J.-N. Zhou, "Cultured rat cortical astrocytes synthesize melatonin: absence of a diurnal rhythm," *Journal of Pineal Research*, vol. 43, no. 3, pp. 232–238, 2007.

[12] G. S. Kinker, S. M. Oba-Shinjo, C. E. Carvalho-Sousa et al., "Melatonergic system-based two-gene index is prognostic in human gliomas," *Journal of Pineal Research*, vol. 60, no. 1, pp. 84–94, 2016.

[13] G. A. Bubenik, "Thirty four years since the discovery of gastrointestinal melatonin," *Journal of Physiology and Pharmacology*, vol. 59, supplement 2, pp. 33–51, 2008.

[14] K. Sakaguchi, M. T. Itoh, N. Takahashi, W. Tarumi, and B. Ishizuka, "The rat oocyte synthesises melatonin," *Reproduction, Fertility and Development*, vol. 25, no. 4, pp. 674–682, 2013.

[15] D. Lanoix, H. Beghdadi, J. Lafond, and C. Vaillancourt, "Human placental trophoblasts synthesize melatonin and express its receptors," *Journal of Pineal Research*, vol. 45, no. 1, pp. 50–60, 2008.

[16] A. Soliman, A.-A. Lacasse, D. Lanoix, L. Sagrillo-Fagundes, V. Boulard, and C. Vaillancourt, "Placental melatonin system is present throughout pregnancy and regulates villous trophoblast differentiation," *Journal of Pineal Research*, vol. 59, no. 1, pp. 38–46, 2015.

[17] G. N. Pontes, E. C. Cardoso, M. M. S. Carneiro-Sampaio, and R. P. Markus, "Pineal melatonin and the innate immune response: the TNF-α increase after cesarean section suppresses nocturnal melatonin production," *Journal of Pineal Research*, vol. 43, no. 4, pp. 365–371, 2007.

[18] V. Simonneaux and C. Ribelayga, "Generation of the melatonin endocrine message in mammals: a review of the complex regulation of melatonin synthesis by norepinephrine, peptides,

[19] D. Cazaméa-Catalan, L. Besseau, J. Falcón, and E. Magnanou, "The timing of Timezyme diversification in vertebrates," *PLoS ONE*, vol. 9, no. 12, Article ID e112380, 2014.

[20] K. J. Schippers and S. A. Nichols, "Deep, dark secrets of melatonin in animal evolution," *Cell*, vol. 159, no. 1, pp. 9–10, 2014.

[21] S. Park, Y. Byeon, H. Y. Lee, Y.-S. Kim, T. Ahn, and K. Back, "Cloning and characterization of a serotonin N-acetyltransferase from a gymnosperm, loblolly pine (*Pinus taeda*)," *Journal of Pineal Research*, vol. 57, no. 3, pp. 348–355, 2014.

[22] M. Møller and F. M. Baeres, "The anatomy and innervation of the mammalian pineal gland," *Cell and Tissue Research*, vol. 309, no. 1, pp. 139–150, 2002.

[23] C. Schomerus and H.-W. Korf, "Cholinergic signal transduction cascades in rat pinealocytes: functional and ontogenetic aspects," *Reproduction Nutrition Development*, vol. 39, no. 3, pp. 305–314, 1999.

[24] D. Villela, V. F. Atherino, L. D. S. Lima et al., "Modulation of pineal melatonin synthesis by glutamate involves paracrine interactions between pinealocytes and astrocytes through NF-κB activation," *BioMed Research International*, vol. 2013, Article ID 618432, 14 pages, 2013.

[25] H. Yu, S. G. Benitez, S. Jung et al., "GABAergic signaling in the rat pineal gland," *Journal of Pineal Research*, vol. 61, no. 1, pp. 69–81, 2016.

[26] R. P. Markus, Z. S. Ferreira, P. A. Fernandes, and E. Cecon, "The immune-pineal axis: a shuttle between endocrine and paracrine melatonin sources," *Neuroimmunomodulation*, vol. 14, no. 3-4, pp. 126–133, 2007.

[27] D. L. Terriff, C. L. Chik, D. M. Price, and A. K. Ho, "Proteasomal proteolysis in the adrenergic induction of arylalkylamine-N-acetyltransferase in rat pinealocytes," *Endocrinology*, vol. 146, no. 11, pp. 4795–4803, 2005.

[28] M. de Oliveira Tatsch-Dias, R. M. Levandovski, I. C. C. de Souza et al., "The concept of the immune-pineal axis tested in patients undergoing an abdominal hysterectomy," *NeuroImmunoModulation*, vol. 20, no. 4, pp. 205–212, 2013.

[29] P. A. C. M. Fernandes, B. Bothorel, D. Clesse et al., "Local corticosterone infusion enhances nocturnal pineal melatonin production in vivo," *Journal of Neuroendocrinology*, vol. 21, no. 2, pp. 90–97, 2009.

[30] C. Ribelayga, P. Pévet, and V. Simonneaux, "HIOMT drives the photoperiodic changes in the amplitude of the melatonin peak of the siberian hamster," *American Journal of Physiology—Regulatory Integrative and Comparative Physiology*, vol. 278, no. 5, pp. R1339–R1345, 2000.

[31] T. Liu and J. Borjigin, "N-acetyltransferase is not the rate-limiting enzyme of melatonin synthesis at night," *Journal of Pineal Research*, vol. 39, no. 1, pp. 91–96, 2005.

[32] G. A. Bubenik, G. M. Brown, and L. J. Grota, "Immunohistological localization of melatonin in the rat digestive system," *Experientia*, vol. 33, no. 5, pp. 662–663, 1977.

[33] P. J. Lardone, A. Rubio, I. Cerrillo et al., "Blocking of melatonin synthesis and MT1 receptor impairs the activation of Jurkat T cells," *Cellular and Molecular Life Sciences*, vol. 67, no. 18, pp. 3163–3172, 2010.

[34] P. J. Lardone, J. M. Guerrero, J. M. Fernández-Santos, A. Rubio, I. Martín-Lacave, and A. Carrillo-Vico, "Melatonin synthesized

by T lymphocytes as a ligand of the retinoic acid-related orphan receptor," *Journal of Pineal Research*, vol. 51, no. 4, pp. 454–462, 2011.

[35] M. C. Naranjo, J. M. Guerrero, A. Rubio et al., "Melatonin biosynthesis in the thymus of humans and rats," *Cellular and Molecular Life Sciences*, vol. 64, no. 6, pp. 781–790, 2007.

[36] A. Gómez-Corvera, I. Cerrillo, P. Molinero et al., "Evidence of immune system melatonin production by two pineal melatonin deficient mice, C57BL/6 and Swiss strains," *Journal of Pineal Research*, vol. 47, no. 1, pp. 15–22, 2009.

[37] S. da Silveira Cruz-Machado, C. E. Carvalho-Sousa, E. K. Tamura et al., "TLR4 and CD14 receptors expressed in rat pineal gland trigger NFKB pathway," *Journal of Pineal Research*, vol. 49, no. 2, pp. 183–192, 2010.

[38] S. da Silveira Cruz-Machado, L. Pinato, E. K. Tamura, C. E. Carvalho-Sousa, and R. P. Markus, "Glia-pinealocyte network: the paracrine modulation of melatonin synthesis by tumor necrosis factor (TNF)," *PLoS ONE*, vol. 7, no. 7, Article ID e40142, 2012.

[39] C. E. Carvalho-Sousa, S. da Silveira Cruz-Machado, K. E. Tamura et al., "Molecular basis for defining the pineal gland and pinealocytes as targets for tumor necrosis factor," *Frontiers in Endocrinology*, vol. 2, article 10, 2010.

[40] E. Cecon, P. A. Fernandes, L. Pinato, Z. S. Ferreira, and R. P. Markus, "Daily variation of constitutively activated nuclear factor kappa B (NFKB) in rat pineal gland," *Chronobiology International*, vol. 27, no. 1, pp. 52–67, 2010.

[41] M. A. Pires-Lapa, E. K. Tamura, E. M. A. Salustiano, and R. P. Markus, "Melatonin synthesis in human colostrum mononuclear cells enhances dectin-1-mediated phagocytosis by mononuclear cells," *Journal of Pineal Research*, vol. 55, no. 3, pp. 240–246, 2013.

[42] S. M. Muxel, M. F. Laranjeira-Silva, C. E. Carvalho-Sousa, L. M. Floeter-Winter, and R. P. Markus, "The RelA/cRel nuclear factor-kappaB (NF-κB) dimer, crucial for inflammation resolution, mediates the transcription of the key enzyme in melatonin synthesis in RAW 264.7 macrophages," *Journal of Pineal Research*, vol. 60, no. 4, pp. 394–404, 2016.

[43] E. K. Tamura, P. A. Fernandes, M. Marçola, S. D. S. Cruz-Machado, and R. P. Markus, "Long-lasting priming of endothelial cells by plasma melatonin levels," *PLoS ONE*, vol. 5, no. 11, Article ID e13958, 2010.

[44] M. Marçola, S. da Silveira Cruz-Machado, P. A. C. M. Fernandes, A. W. A. Monteiro, R. P. Markus, and E. K. Tamura, "Endothelial cell adhesiveness is a function of environmental lighting and melatonin level," *Journal of Pineal Research*, vol. 54, no. 2, pp. 162–169, 2013.

[45] B. de Luxán-Delgado, B. Caballero, Y. Potes et al., "Melatonin administration decreases adipogenesis in the liver of ob/ob mice through autophagy modulation," *Journal of Pineal Research*, vol. 56, no. 2, pp. 126–133, 2014.

[46] M. F. Laranjeira-Silva, R. A. Zampieri, S. M. Muxel, L. M. Floeter-Winter, and R. P. Markus, "Melatonin attenuates Leishmania (L.) amazonensis infection by modulating arginine metabolism," *Journal of Pineal Research*, vol. 59, no. 4, pp. 478–487, 2015.

[47] P. A. Fernandes, E. K. Tamura, L. D'Argenio-Garcia et al., "Dual effect of catecholamines and corticosterone crosstalk on pineal gland melatonin synthesis," *Neuroendocrinology*, 2016.

[48] Z. S. Ferreira, P. A. C. M. Fernandes, D. Duma, J. Assreuy, M. C. W. Avellar, and R. P. Markus, "Corticosterone modulates noradrenaline-induced melatonin synthesis through inhibition of nuclear factor kappa B," *Journal of Pineal Research*, vol. 38, no. 3, pp. 182–188, 2005.

[49] R. Jockers, P. Delagrange, M. L. Dubocovich et al., "Update on melatonin receptors: IUPHAR Review 20," *British Journal of Pharmacology*, vol. 173, no. 18, pp. 2702–2725, 2016.

[50] M. L. Dubocovich and M. Markowska, "Functional MT$_1$ and MT$_2$ melatonin receptors in mammals," *Endocrine*, vol. 27, no. 2, pp. 101–110, 2005.

[51] M. Kamal, F. Gbahou, J.-L. Guillaume et al., "Convergence of melatonin and serotonin (5-HT) signaling at MT2/5-HT$_2$C receptor heteromers," *The Journal of Biological Chemistry*, vol. 290, no. 18, pp. 11537–11546, 2015.

[52] L. Dufourny, A. Levasseur, M. Migaud et al., "GPR50 is the mammalian ortholog of Mel1c: evidence of rapid evolution in mammals," *BMC Evolutionary Biology*, vol. 8, article 105, 2008.

[53] A. Levoye, J. Dam, M. A. Ayoub et al., "The orphan GPR50 receptor specifically inhibits MT1 melatonin receptor function through heterodimerization," *The EMBO Journal*, vol. 25, no. 13, pp. 3012–3023, 2006.

[54] J.-K. Jeong and S.-Y. Park, "Melatonin regulates the autophagic flux via activation of alpha-7 nicotinic acetylcholine receptors," *Journal of Pineal Research*, vol. 59, no. 1, pp. 24–37, 2015.

[55] D. K. Lahiri, "Melatonin affects the metabolism of the β-amyloid precursor protein in different cell types," *Journal of Pineal Research*, vol. 26, no. 3, pp. 137–146, 1999.

[56] N. Dragicevic, N. Copes, G. O'Neal-Moffitt et al., "Melatonin treatment restores mitochondrial function in Alzheimer's mice: a mitochondrial protective role of melatonin membrane receptor signaling," *Journal of Pineal Research*, vol. 51, no. 1, pp. 75–86, 2011.

[57] A. H. V. Schapira and C. W. Olanow, "Neuroprotection in Parkinson Disease: mysteries, myths, and misconceptions," *Journal of the American Medical Association*, vol. 291, no. 3, pp. 358–364, 2004.

[58] L. C. Manchester, A. Coto-Montes, J. A. Boga et al., "Melatonin: an ancient molecule that makes oxygen metabolically tolerable," *Journal of Pineal Research*, vol. 59, no. 4, pp. 403–419, 2015.

[59] B. Poeggeler, S. Saarela, R. J. Reiter et al., "Melatonin—a highly potent endogenous radical scavenger and electron donor: New aspects of the oxidation chemistry of this indole accessed in vitro," *Annals of the New York Academy of Sciences*, vol. 738, pp. 419–420, 1994.

[60] R. Hardeland, D.-X. Tan, and R. J. Reiter, "Kynuramines, metabolites of melatonin and other indoles: the resurrection of an almost forgotten class of biogenic amines," *Journal of Pineal Research*, vol. 47, no. 2, pp. 109–126, 2009.

[61] S.-I. Choi, S. Dadakhujaev, H. Ryu, T. Im Kim, and E. K. Kim, "Melatonin protects against oxidative stress in granular corneal dystrophy type 2 corneal fibroblasts by mechanisms that involve membrane melatonin receptors," *Journal of Pineal Research*, vol. 51, no. 1, pp. 94–103, 2011.

[62] G. O'Neal-Moffitt, V. Delic, P. C. Bradshaw, and J. Olcese, "Prophylactic melatonin significantly reduces Alzheimer's neuropathology and associated cognitive deficits independent of antioxidant pathways in AβPP(swe)/PS1 mice," *Molecular Neurodegeneration*, vol. 10, no. 1, article 27, 2015.

[63] D. G. Franco and R. P. Markus, "The cellular state determines the effect of melatonin on the survival of mixed cerebellar cell culture," *PLoS ONE*, vol. 9, no. 9, Article ID e106332, 2014.

[64] L. Pinato, S. da Silveira Cruz-Machado, D. G. Franco et al., "Selective protection of the cerebellum against intracerebroventricular LPS is mediated by local melatonin synthesis," *Brain Structure & Function*, vol. 220, no. 2, pp. 827–840, 2015.

[65] Y. Dong, C. Fan, W. Hu et al., "Melatonin attenuated early brain injury induced by subarachnoid hemorrhage via regulating NLRP3 inflammasome and apoptosis signaling," *Journal of Pineal Research*, vol. 60, no. 3, pp. 253–262, 2016.

[66] F. Ortiz, D. Acuña-Castroviejo, C. Doerrier et al., "Melatonin blunts the mitochondrial/NLRP3 connection and protects against radiation-induced oral mucositis," *Journal of Pineal Research*, vol. 58, no. 1, pp. 34–49, 2015.

[67] Z. Feng, Y. Chang, Y. Cheng et al., "Melatonin alleviates behavioral deficits associated with apoptosis and cholinergic system dysfunction in the APP 695 transgenic mouse model of Alzheimer's disease," *Journal of Pineal Research*, vol. 37, no. 2, pp. 129–136, 2004.

[68] R. P. Markus, C. L. M. Silva, D. G. Franco, E. M. Barbosa Jr., and Z. S. Ferreira, "Is modulation of nicotinic acetylcholine receptors by melatonin relevant for therapy with cholinergic drugs?" *Pharmacology & Therapeutics*, vol. 126, no. 3, pp. 251–262, 2010.

[69] E. Parada, I. Buendia, R. León et al., "Neuroprotective effect of melatonin against ischemia is partially mediated by alpha-7 nicotinic receptor modulation and HO-1 overexpression," *Journal of Pineal Research*, vol. 56, no. 2, pp. 204–212, 2014.

[70] E. Savaskan, M. A. Ayoub, R. Ravid et al., "Reduced hippocampal MT2 melatonin receptor expression in Alzheimer's disease," *Journal of Pineal Research*, vol. 38, no. 1, pp. 10–16, 2005.

[71] P. Brunner, N. Sözer-Topcular, R. Jockers et al., "Pineal and cortical melatonin receptors MT1 and MT2 are decreased in Alzheimer's disease," *European Journal of Histochemistry*, vol. 50, no. 4, pp. 311–316, 2006.

[72] Y.-H. Wu, J.-N. Zhou, J. Van Heerikhuize, R. Jockers, and D. F. Swaab, "Decreased MT1 melatonin receptor expression in the suprachiasmatic nucleus in aging and Alzheimer's disease," *Neurobiology of Aging*, vol. 28, no. 8, pp. 1239–1247, 2007.

[73] N. Adi, D. C. Mash, Y. Ali, C. Singer, L. Shehadeh, and S. Papapetropoulos, "Melatonin MT1 and MT2 receptor expression in Parkinson's disease," *Medical Science Monitor*, vol. 16, no. 2, pp. BR61–BR67, 2010.

[74] K. Uchida, N. Okamoto, K. Ohara, and Y. Morita, "Daily rhythm of serum melatonin in patients with dementia of the degenerate type," *Brain Research*, vol. 717, no. 1-2, pp. 154–159, 1996.

[75] J.-N. Zhou, R.-Y. Liu, W. Kamphorst, M. A. Hofman, and D. F. Swaab, "Early neuropathological Alzheimer's changes in aged individuals are accompanied by decreased cerebrospinal fluid melatonin levels," *Journal of Pineal Research*, vol. 35, no. 2, pp. 125–130, 2003.

[76] A. Videnovic, D. P. Breen, R. A. Barker, and P. C. Zee, "The central clock in patients with Parkinson disease—reply," *JAMA Neurology*, vol. 71, no. 11, pp. 1456–1457, 2014.

[77] E. Cecon, M. Chen, M. Marçola, P. A. C. Fernandes, R. Jockers, and R. P. Markus, "Amyloid β peptide directly impairs pineal gland melatonin synthesis and melatonin receptor signaling through the ERK pathway," *FASEB Journal*, vol. 29, no. 6, pp. 2566–2582, 2015.

[78] A. G. Wade, M. Farmer, G. Harari et al., "Add-on prolonged-release melatonin for cognitive function and sleep in mild to moderate Alzheimer's disease: a 6-month, randomized, placebo-controlled, multicenter trial," *Clinical Interventions in Aging*, vol. 9, pp. 947–961, 2014.

[79] S. Rosales-Corral, D.-X. Tan, R. J. Reiter et al., "Orally administered melatonin reduces oxidative stress and proinflammatory cytokines induced by amyloid-β peptide in rat brain: a comparative, in vivo study versus vitamin C and E," *Journal of Pineal Research*, vol. 35, no. 2, pp. 80–84, 2003.

[80] N. A. Aziz, H. Pijl, M. Frölich et al., "Delayed onset of the diurnal melatonin rise in patients with Huntington's disease," *Journal of Neurology*, vol. 256, no. 12, pp. 1961–1965, 2009.

[81] M. F. Farez, I. D. Mascanfroni, S. P. Méndez-Huergo et al., "Melatonin contributes to the seasonality of multiple sclerosis relapses," *Cell*, vol. 162, no. 6, pp. 1338–1352, 2015.

[82] T. Ritzenthaler, N. Nighoghossian, J. Berthiller et al., "Nocturnal urine melatonin and 6-sulphatoxymelatonin excretion at the acute stage of ischaemic stroke," *Journal of Pineal Research*, vol. 46, no. 3, pp. 349–352, 2009.

[83] A. L. Morera-Fumero and P. Abreu-Gonzalez, "Role of melatonin in schizophrenia," *International Journal of Molecular Sciences*, vol. 14, no. 5, pp. 9037–9050, 2013.

[84] E. Fertl, E. Auff, A. Doppelbauer, and F. Waldhauser, "Circadian secretion pattern of melatonin in de novo Parkinsonian patients: evidence for phase-shifting properties of l-dopa," *Journal of Neural Transmission—Parkinson's Disease and Dementia Section*, vol. 5, no. 3, pp. 227–234, 1993.

[85] E. Fertl, E. Auff, A. Doppelbauer, and F. Waldhauser, "Circadian secretion pattern of melatonin in Parkinson's disease," *Journal of Neural Transmission—Parkinson's Disease and Dementia Section*, vol. 3, no. 1, pp. 41–47, 1991.

[86] R. Bordet, D. Devos, S. Brique et al., "Study of circadian melatonin secretion pattern at different stages of Parkinson's disease," *Clinical Neuropharmacology*, vol. 26, no. 2, pp. 65–72, 2003.

[87] A. Videnovic, C. Noble, K. J. Reid et al., "Circadian melatonin rhythm and excessive daytime sleepiness in Parkinson disease," *JAMA Neurology*, vol. 71, no. 4, pp. 463–469, 2014.

[88] H. Chen, E. Schernhammer, M. A. Schwarzschild, and A. Ascherio, "A prospective study of night shift work, sleep duration, and risk of Parkinson's disease," *American Journal of Epidemiology*, vol. 163, no. 8, pp. 726–730, 2006.

[89] J. Gao, X. Huang, Y. Park et al., "Daytime napping, nighttime sleeping, and parkinson disease," *American Journal of Epidemiology*, vol. 173, no. 9, pp. 1032–1038, 2011.

[90] C. Venegas, J. A. García, G. Escames et al., "Extrapineal melatonin: analysis of its subcellular distribution and daily fluctuations," *Journal of Pineal Research*, vol. 52, no. 2, pp. 217–227, 2012.

[91] M. A. Seifman, A. A. Adamides, P. N. Nguyen et al., "Endogenous melatonin increases in cerebrospinal fluid of patients after severe traumatic brain injury and correlates with oxidative stress and metabolic disarray," *Journal of Cerebral Blood Flow and Metabolism*, vol. 28, no. 4, pp. 684–696, 2008.

[92] J. Leston, C. Harthé, C. Mottolese, P. Mertens, M. Sindou, and B. Claustrat, "Is pineal melatonin released in the third ventricle in humans? A study in movement disorders," *Neurochirurgie*, vol. 61, no. 2-3, pp. 85–89, 2015.

[93] C. Legros, D. Chesneau, J. A. Boutin, C. Barc, and B. Malpaux, "Melatonin from cerebrospinal fluid but not from blood reaches sheep cerebral tissues under physiological conditions," *Journal of Neuroendocrinology*, vol. 26, no. 3, pp. 151–163, 2014.

[94] S. Singh and M. Dikshit, "Apoptotic neuronal death in Parkinson's disease: involvement of nitric oxide," *Brain Research Reviews*, vol. 54, no. 2, pp. 233–250, 2007.

[95] A. Samii, J. G. Nutt, and B. R. Ransom, "Parkinson's disease," *The Lancet*, vol. 363, no. 9423, pp. 1783–1793, 2004.

[96] D. Burch and F. Sheerin, "Parkinson's disease," *Thye Lancet*, vol. 365, no. 9459, pp. 622–627, 2005.

[97] Z. Mansouri, M. Sabetkasaei, F. Moradi, F. Masoudnia, and A. Ataie, "Curcumin has neuroprotection effect on homocysteine rat model of Parkinson," *Journal of Molecular Neuroscience*, vol. 47, no. 2, pp. 234–242, 2012.

[98] J. Massano, "Parkinson's disease: a clinical update," *Acta Medica Portuguesa*, vol. 24, no. 4, pp. 827–834, 2011.

[99] R. J. Dinis-Oliveira, F. Remião, H. Carmo et al., "Paraquat exposure as an etiological factor of Parkinson's disease," *NeuroToxicology*, vol. 27, no. 6, pp. 1110–1122, 2006.

[100] C. Rodríguez-Nogales, E. Garbayo, M. M. Carmona-Abellán, M. R. Luquin, and M. J. Blanco-Prieto, "Brain aging and Parkinson's disease: new therapeutic approaches using drug delivery systems," *Maturitas*, vol. 84, pp. 25–31, 2016.

[101] P. Michel, E. Hirsch, and S. Hunot, "Understanding dopaminergic cell death pathways in parkinson disease," *Neuron*, vol. 90, no. 4, pp. 675–691, 2016.

[102] A. L. McCormack, M. Thiruchelvam, A. B. Manning-Bog et al., "Environmental risk factors and Parkinson's disease: selective degeneration of nigral dopaminergic neurons caused by the herbicide paraquat," *Neurobiology of Disease*, vol. 10, no. 2, pp. 119–127, 2002.

[103] A. Wood-Kaczmar, S. Gandhi, and N. W. Wood, "Understanding the molecular causes of Parkinson's disease," *Trends in Molecular Medicine*, vol. 12, no. 11, pp. 521–528, 2006.

[104] D. Sulzer, "Multiple hit hypotheses for dopamine neuron loss in Parkinson's disease," *Trends in Neurosciences*, vol. 30, no. 5, pp. 244–250, 2007.

[105] R. M. Ransohoff, "How neuroinflammation contributes to neurodegeneration," *Science*, vol. 353, no. 6301, pp. 777–783, 2016.

[106] A. De Virgilio, A. Greco, G. Fabbrini et al., "Parkinson's disease: autoimmunity and neuroinflammation," *Autoimmunity Reviews*, vol. 15, no. 10, pp. 1005–1011, 2016.

[107] P. Jenner and C. W. Olanow, "The pathogenesis of cell death in Parkinson's disease," *Neurology*, vol. 66, no. 10, pp. S24–S30, 2006.

[108] N. Singh, V. Pillay, and Y. E. Choonara, "Advances in the treatment of Parkinson's disease," *Progress in Neurobiology*, vol. 81, no. 1, pp. 29–44, 2007.

[109] V. Dias, E. Junn, and M. M. Mouradian, "The role of oxidative stress in parkinson's disease," *Journal of Parkinson's Disease*, vol. 3, no. 4, pp. 461–491, 2013.

[110] S. Klongpanichapak, P. Phansuwan-Pujito, M. Ebadi, and P. Govitrapong, "Melatonin protects SK-N-SH neuroblastoma cells from amphetamine-induced neurotoxicity," *Journal of Pineal Research*, vol. 43, no. 1, pp. 65–73, 2007.

[111] A. F. G. Leentjens, K. Dujardin, L. Marsh, P. Martinez-Martin, I. H. Richard, and S. E. Starkstein, "Anxiety and motor fluctuations in Parkinson's disease: a cross-sectional observational study," *Parkinsonism and Related Disorders*, vol. 18, no. 10, pp. 1084–1088, 2012.

[112] A. Sidhu, C. Wersinger, and P. Vernier, "α-Synuclein regulation of the dopaminergic transporter: a possible role in the pathogenesis of Parkinson's disease," *FEBS Letters*, vol. 565, no. 1–3, pp. 1–5, 2004.

[113] B. Dehay and P. O. Fernagut, "Alpha-synuclein-based models of Parkinson's disease," *Revue Neurologique*, vol. 172, no. 6-7, pp. 371–378, 2016.

[114] E. Altschuler, "Aluminium-containing antacids as a cause of idiopathic Parkinson's disease," *Medical Hypotheses*, vol. 53, no. 1, pp. 22–23, 1999.

[115] L. E. Davis and J. C. Adair, "Parkinsonism from methanol poisoning: benefit from treatment with anti-Parkinson drugs," *Movement Disorders*, vol. 14, no. 3, pp. 520–522, 1999.

[116] S. H. Snyder and R. J. D'Amato, "MPTP: a neurotoxin relevant to the pathophysiology of Parkinson's disease: The 1985 George C. Cotzias Lecture," *Neurology*, vol. 36, no. 2, pp. 250–258, 1986.

[117] B. I. Giasson and V. M.-Y. Lee, "A new link between pesticides and Parkinson's disease," *Nature Neuroscience*, vol. 3, no. 12, pp. 1227–1228, 2000.

[118] A. J. Lees, J. Hardy, and T. Revesz, "Parkinson's disease," *The Lancet*, vol. 373, no. 9680, pp. 2055–2066, 2009.

[119] B. Bruguerolle and N. Simon, "Biologic rhythms and Parkinson's disease: a chronopharmacologic approach to considering fluctuations in function," *Clinical Neuropharmacology*, vol. 25, no. 4, pp. 194–201, 2002.

[120] G. L. Willis, "Parkinson's disease as a neuroendocrine disorder of circadian function: dopamine-melatonin imbalance and the visual system in the genesis and progression of the degenerative process," *Reviews in the Neurosciences*, vol. 19, no. 4-5, pp. 245–316, 2008.

[121] B. F. Boeve, M. H. Silber, T. J. Ferman et al., "Clinicopathologic correlations in 172 cases of rapid eye movement sleep behavior disorder with or without a coexisting neurologic disorder," *Sleep Medicine*, vol. 14, no. 8, pp. 754–762, 2013.

[122] D. P. Breen, R. Vuono, U. Nawarathna et al., "Sleep and circadian rhythm regulation in early Parkinson disease," *JAMA Neurology*, vol. 71, no. 5, pp. 589–595, 2014.

[123] K. R. Chaudhuri, D. G. Healy, and A. H. V. Schapira, "Non-motor symptoms of Parkinson's disease: diagnosis and management," *Lancet Neurology*, vol. 5, no. 3, pp. 235–245, 2006.

[124] K. R. Chaudhuri and A. H. Schapira, "Non-motor symptoms of Parkinson's disease: dopaminergic pathophysiology and treatment," *The Lancet Neurology*, vol. 8, no. 5, pp. 464–474, 2009.

[125] A. Bonito-Oliva, D. Masini, and G. Fisone, "A mouse model of non-motor symptoms in Parkinson's disease: focus on pharmacological interventions targeting affective dysfunctions," *Frontiers in Behavioral Neuroscience*, vol. 8, article 290, 2014.

[126] H. Braak, K. Del Tredici, U. Rüb, R. A. I. De Vos, E. N. H. Jansen Steur, and E. Braak, "Staging of brain pathology related to sporadic Parkinson's disease," *Neurobiology of Aging*, vol. 24, no. 2, pp. 197–211, 2003.

[127] A. Roy and K. Pahan, "Prospects of statins in Parkinson disease," *The Neuroscientist*, vol. 17, no. 3, pp. 244–255, 2011.

[128] P. K. Sonsalla, L.-Y. Wong, S. L. Harris et al., "Delayed caffeine treatment prevents nigral dopamine neuron loss in a progressive rat model of Parkinson's disease," *Experimental Neurology*, vol. 234, no. 2, pp. 482–487, 2012.

[129] S. Maranis, S. Tsouli, and S. Konitsiotis, "Treatment of motor symptoms in advanced Parkinson's disease: a practical approach," *Progress in Neuro-Psychopharmacology & Biological Psychiatry*, vol. 35, no. 8, pp. 1795–1807, 2011.

[130] J. Castro-Hernández, D. Afonso-Oramas, I. Cruz-Muros et al., "Prolonged treatment with pramipexole promotes physical interaction of striatal dopamine D3 autoreceptors with dopamine transporters to reduce dopamine uptake," *Neurobiology of Disease*, vol. 74, pp. 325–335, 2015.

[131] S. Burton, S. Daya, and B. Potgieter, "Melatonin modulates apomorphine-induced rotational behaviour," *Experientia*, vol. 47, no. 5, pp. 466–469, 1991.

[132] J. C. Mayo, R. M. Sainz, H. Uria, I. Antolin, M. M. Esteban, and C. Rodriguez, "Melatonin prevents apoptosis induced by 6-hydroxydopamine in neuronal cells: implications for Parkinson's disease," *Journal of Pineal Research*, vol. 24, no. 3, pp. 179–192, 1998.

[133] W. S. Joo, B. K. Jin, C. W. Park, S. H. Maeng, and Y. S. Kim, "Melatonin increases striatal dopaminergic function in 6-OHDA-lesioned rats," *NeuroReport*, vol. 9, no. 18, pp. 4123–4126, 1998.

[134] J. C. Mayo, R. M. Sainz, I. Antolín, and C. Rodriguez, "Ultrastructural confirmation of neuronal protection by melatonin against the neurotoxin 6-hydroxydopamine cell damage," *Brain Research*, vol. 818, no. 2, pp. 221–227, 1999.

[135] F. Dabbeni-Sala, S. Di Santo, D. Franceschini, S. D. Skaper, and P. Giusti, "Melatonin protects against 6-OHDA-induced neurotoxicity in rats: a role for mitochondrial complex I activity," *The FASEB Journal*, vol. 15, no. 1, pp. 164–170, 2001.

[136] L. M. V. Aguiar, S. M. M. Vasconcelos, F. C. F. Sousa, and G. S. B. Viana, "Melatonin reverses neurochemical alterations induced by 6-OHDA in rat striatum," *Life Sciences*, vol. 70, no. 9, pp. 1041–1051, 2002.

[137] B. Chetsawang, P. Govitrapong, and M. Ebadi, "The neuroprotective effect of melatonin against the induction of c-Jun phosphorylation by 6-hydroxydopamine on SK-N-SH cells," *Neuroscience Letters*, vol. 371, no. 2-3, pp. 205–208, 2004.

[138] R. Sharma, C. R. McMillan, C. C. Tenn, and L. P. Niles, "Physiological neuroprotection by melatonin in a 6-hydroxydopamine model of Parkinson's disease," *Brain Research*, vol. 1068, no. 1, pp. 230–236, 2006.

[139] S. Singh, R. Ahmed, R. K. Sagar, and B. Krishana, "Neuroprotection of the nigrostriatal dopaminergic neurons by melatonin in hemiparkinsonium rat," *Indian Journal of Medical Research*, vol. 124, no. 4, pp. 419–426, 2006.

[140] A. L. Gutierrez-Valdez, V. Anaya-Martínez, J. L. Ordoñez-Librado et al., "Effect of chronic L-dopa or melatonin treatments after dopamine deafferentation in rats: dyskinesia, motor performance, and cytological analysis," *ISRN Neurology*, vol. 2012, Article ID 360379, 16 pages, 2012.

[141] F. B. Yildirim, O. Ozsoy, G. Tanriover et al., "Mechanism of the beneficial effect of melatonin in experimental Parkinson's disease," *Neurochemistry International*, vol. 79, pp. 1–11, 2014.

[142] Y. S. Kim, W. S. Joo, B. K. Jin, Y. H. Cho, H. H. Baik, and C. W. Park, "Melatonin protects 6-OHDA-induced neuronal death of nigrostriatal dopaminergic system," *NeuroReport*, vol. 9, no. 10, pp. 2387–2390, 1998.

[143] O. Ozsoy, F. B. Yildirim, E. Ogut et al., "Melatonin is protective against 6-hydroxydopamine-induced oxidative stress in a hemiparkinsonian rat model," *Free Radical Research*, vol. 49, no. 8, pp. 1004–1014, 2015.

[144] B. K. Jin, D. Y. Shin, M. Y. Jeong et al., "Melatonin protects nigral dopaminergic neurons from 1-methyl-4-phenylpyridinium (MPP+) neurotoxicity in rats," *Neuroscience Letters*, vol. 245, no. 2, pp. 61–64, 1998.

[145] E. Absi, A. Ayala, A. Machado, and J. Parrado, "Protective effect of melatonin against the 1-methyl-4-phenylpyridinium-induced inhibition of complex I of the mitochondrial respiratory chain," *Journal of Pineal Research*, vol. 29, no. 1, pp. 40–47, 2000.

[146] T. C. Shur, I. C. Jih, H. H. Mei, and E. I-Chian Li, "Melatonin attenuates MPP$^+$-induced neurodegeneration and glutathione impairment in the nigrostriatal dopaminergic pathway," *Journal of Pineal Research*, vol. 32, no. 4, pp. 262–269, 2002.

[147] L.-J. Chen, Y.-Q. Gao, X.-J. Li, D.-H. Shen, and F.-Y. Sun, "Melatonin protects against MPTP/MPP$^+$-induced mitochondrial DNA oxidative damage in vivo and in vitro," *Journal of Pineal Research*, vol. 39, no. 1, pp. 34–42, 2005.

[148] D. Alvira, M. Tajes, E. Verdaguer et al., "Inhibition of the cdk5/p25 fragment formation may explain the antiapoptotic effects of melatonin in an experimental model of Parkinson's disease," *Journal of Pineal Research*, vol. 40, no. 3, pp. 251–258, 2006.

[149] J. Chetsawang, P. Govitrapong, and B. Chetsawang, "Melatonin inhibits MPP+-induced caspase-mediated death pathway and DNA fragmentation factor-45 cleavage in SK-N-SH cultured cells," *Journal of Pineal Research*, vol. 43, no. 2, pp. 115–120, 2007.

[150] J.-Y. Huang, Y.-T. Hong, and J.-I. Chuang, "Fibroblast growth factor 9 prevents MPP+-induced death of dopaminergic neurons and is involved in melatonin neuroprotection in vivo and in vitro," *Journal of Neurochemistry*, vol. 109, no. 5, pp. 1400–1412, 2009.

[151] D. Acuña-Castroviejo, A. Coto-Montes, M. G. Monti, G. G. Ortiz, and R. J. Reiter, "Melatonin is protective against MPTP-induced striatal and hippocampal lesions," *Life Sciences*, vol. 60, no. 2, pp. Pl23–Pl29, 1996.

[152] H. Khaldy, G. Escames, J. León, L. Bikjdaouene, and D. Acuña-Castroviejo, "Synergistic effects of melatonin and deprenyl against MPTP-induced mitochondrial damage and DA depletion," *Neurobiology of Aging*, vol. 24, no. 3, pp. 491–500, 2003.

[153] V. Tapias, G. Escames, L. C. López et al., "Melatonin and its brain metabolite N^1-acetyl-5-methoxykynuramine prevent mitochondrial nitric oxide synthase induction in Parkinsonian mice," *Journal of Neuroscience Research*, vol. 87, no. 13, pp. 3002–3010, 2009.

[154] R. Niranjan, C. Nath, and R. Shukla, "The mechanism of action of MPTP-induced neuroinflammation and its modulation by melatonin in rat astrocytoma cells, C6," *Free Radical Research*, vol. 44, no. 11, pp. 1304–1316, 2010.

[155] G. Patki and Y.-S. Lau, "Melatonin protects against neurobehavioral and mitochondrial deficits in a chronic mouse model of Parkinson's disease," *Pharmacology Biochemistry and Behavior*, vol. 99, no. 4, pp. 704–711, 2011.

[156] S. A. Zaitone, L. N. Hammad, and N. E. Farag, "Antioxidant potential of melatonin enhances the response to L-dopa in 1-methyl 4-phenyl 1,2,3,6-tetrahydropyridine-parkinsonian mice," *Pharmacological Reports*, vol. 65, no. 5, pp. 1213–1226, 2013.

[157] A. Naskar, V. Prabhakar, R. Singh, D. Dutta, and K. P. Mohanakumar, "Melatonin enhances L-DOPA therapeutic effects, helps to reduce its dose, and protects dopaminergic neurons in 1-methyl-4-phenyl-1,2,3,6-tetrahydropyridine-induced parkinsonism in mice," *Journal of Pineal Research*, vol. 58, no. 3, pp. 262–274, 2015.

[158] M. E. Díaz-Casado, E. Lima, J. A. García et al., "Melatonin rescues zebrafish embryos from the parkinsonian phenotype restoring the parkin/PINK1/DJ-1/MUL1 network," *Journal of Pineal Research*, vol. 61, no. 1, pp. 96–107, 2016.

[159] H. Coulom and S. Birman, "Chronic exposure to rotenone models sporadic Parkinson's disease in *Drosophila melanogaster*," *The Journal of Neuroscience*, vol. 24, no. 48, pp. 10993–10998, 2004.

[160] K. S. Saravanan, K. M. Sindhu, and K. P. Mohanakumar, "Melatonin protects against rotenone-induced oxidative stress in a hemiparkinsonian rat model," *Journal of Pineal Research*, vol. 42, no. 3, pp. 247–253, 2007.

[161] T. B. Bassani, R. W. Gradowski, T. Zaminelli et al., "Neuroprotective and antidepressant-like effects of melatonin in a rotenone-induced Parkinson's disease model in rats," *Brain Research*, vol. 1593, pp. 95–105, 2014.

[162] C. H. Carriere, N. H. Kang, and L. P. Niles, "Chronic low-dose melatonin treatment maintains nigrostriatal integrity in an intrastriatal rotenone model of Parkinson's disease," *Brain Research*, vol. 1633, pp. 115–125, 2016.

[163] M. Ishido, "Melatonin inhibits maneb-induced aggregation of α-synuclein in rat pheochromocytoma cells," *Journal of Pineal Research*, vol. 42, no. 2, pp. 125–130, 2007.

[164] N. K. Singhal, G. Srivastava, D. K. Patel, S. K. Jain, and M. P. Singh, "Melatonin or silymarin reduces maneb- and paraquat-induced Parkinson's disease phenotype in the mouse," *Journal of Pineal Research*, vol. 50, no. 2, pp. 97–109, 2011.

[165] J. M. Brito-Armas, V. Baekelandt, J. R. Castro-Hernández, T. González-Hernández, M. Rodríguez, and R. C. Fuentes, "Melatonin prevents dopaminergic cell loss induced by lentiviral vectors expressing A30P mutant alpha-synuclein," *Histology and Histopathology*, vol. 28, no. 8, pp. 999–1006, 2013.

[166] Q. Wan, H.-Y. Man, F. Liu et al., "Differential modulation of GABAA receptor function by Mel1a and Mel1b receptors," *Nature Neuroscience*, vol. 2, no. 5, pp. 401–403, 1999.

[167] M. V. Hogan, Y. El-Sherif, and A. Wieraszko, "The modulation of neuronal activity by melatonin: in vitro studies on mouse hippocampal slices," *Journal of Pineal Research*, vol. 30, no. 2, pp. 87–96, 2001.

[168] Y. El-Sherif, P. Witt-Enderby, P.-K. Li, J. Tesoriero, M. V. Hogan, and A. Wieraszko, "The actions of a charged melatonin receptor ligand, TMEPI, and an irreversible MT2 receptor agonist, BMNEP, on mouse hippocampal evoked potentials in vitro," *Life Sciences*, vol. 75, no. 26, pp. 3147–3156, 2004.

[169] L. M. Wang, N. A. Suthana, D. Chaudhury, D. R. Weaver, and C. S. Colwell, "Melatonin inhibits hippocampal long-term potentiation," *The European Journal of Neuroscience*, vol. 22, no. 9, pp. 2231–2237, 2005.

[170] J. Larson, R. E. Jessen, T. Uz et al., "Impaired hippocampal long-term potentiation in melatonin MT_2 receptor-deficient mice," *Neuroscience Letters*, vol. 393, no. 1, pp. 23–26, 2006.

[171] G. O'Neal-Moffitt, J. Pilli, S. S. Kumar, and J. Olcese, "Genetic deletion of MT1/MT2 melatonin receptors enhances murine cognitive and motor performance," *Neuroscience*, vol. 277, pp. 506–521, 2014.

[172] P. Golus and M. G. King, "The effects of melatonin on open field behavior," *Pharmacology, Biochemistry and Behavior*, vol. 15, no. 6, pp. 883–885, 1981.

[173] D. A. Golombek, M. Martini, and D. P. Cardinali, "Melatonin as an anxiolytic in rats: time dependence and interaction with the central GABAergic system," *European Journal of Pharmacology*, vol. 237, no. 2-3, pp. 231–236, 1993.

[174] G. Pierrefiche, R. Zerbib, and H. Laborit, "Anxiolytic activity of melatonin in mice: involvement of benzodiazepine receptors," *Research Communications in Chemical Pathology and Pharmacology*, vol. 82, no. 2, pp. 131–142, 1993.

[175] E. B. Naranjo-Rodriguez, A. O. Osornio, E. Hernandez-Avitia, V. Mendoza-Fernandez, and A. Escobar, "Anxiolytic-like actions of melatonin, 5-metoxytryptophol, 5-hydroxytryptophol and benzodiazepines on a conflict procedure," *Progress in Neuro-Psychopharmacology and Biological Psychiatry*, vol. 24, no. 1, pp. 117–129, 2000.

[176] C. Kopp, E. Vogel, M.-C. Rettori, P. Delagrange, and R. Misslin, "Anxiolytic-like properties of melatonin receptor agonists in mice: involvement of mt1 and/or MT2 receptors in the regulation of emotional responsiveness," *Neuropharmacology*, vol. 39, no. 10, pp. 1865–1871, 2000.

[177] M. J. Millan, M. Brocco, A. Gobert, and A. Dekeyne, "Anxiolytic properties of agomelatine, an antidepressant with melatoninergic and serotonergic properties: role of 5-HT2C receptor blockade," *Psychopharmacology*, vol. 177, no. 4, pp. 448–458, 2005.

[178] M. Papp, E. Litwa, P. Gruca, and E. Mocaër, "Anxiolytic-like activity of agomelatine and melatonin in three animal models of anxiety," *Behavioural Pharmacology*, vol. 17, no. 1, pp. 9–18, 2006.

[179] F. Loiseau, C. Le Bihan, M. Hamon, and M.-H. Thiébot, "Effects of melatonin and agomelatine in anxiety-related procedures in rats: Interaction with diazepam," *European Neuropsychopharmacology*, vol. 16, no. 6, pp. 417–428, 2006.

[180] S.-W. Tian, M. Laudon, L. Han et al., "Antidepressant- and anxiolytic effects of the novel melatonin agonist Neu-P11 in rodent models," *Acta Pharmacologica Sinica*, vol. 31, no. 7, pp. 775–783, 2010.

[181] F. Z. El Mrabet, S. Ouaaki, A. Mesfioui, A. El Hessni, and A. Ouichou, "Pinealectomy and exogenous melatonin regulate anxiety-like and depressive-like behaviors in male and female wistar rats," *Neuroscience & Medicine*, vol. 3, pp. 394–403, 2012.

[182] R. Ochoa-Sanchez, Q. Rainer, S. Comai et al., "Anxiolytic effects of the melatonin MT2 receptor partial agonist UCM765: comparison with melatonin and diazepam," *Progress in Neuro-Psychopharmacology and Biological Psychiatry*, vol. 39, no. 2, pp. 318–325, 2012.

[183] G. H. Kim, J. E. Kim, S. J. Rhie, and S. Yoon, "The role of oxidative stress in neurodegenerative diseases," *Experimental Neurobiology*, vol. 24, no. 4, pp. 325–340, 2015.

[184] V. Jackson-Lewis, J. Blesa, and S. Przedborski, "Animal models of Parkinson's disease," *Parkinsonism and Related Disorders*, vol. 18, no. 1, pp. S183–S185, 2012.

[185] U. Ungerstedt, "6-hydroxy-dopamine induced degeneration of central monoamine neurons," *European Journal of Pharmacology*, vol. 5, no. 1, pp. 107–110, 1968.

[186] J. Bové, D. Prou, C. Perier, and S. Przedborski, "Toxin-induced models of Parkinson's disease," *NeuroRx*, vol. 2, no. 3, pp. 484–494, 2005.

[187] J. S. Mendez and B. W. Finn, "Use of 6 hydroxydopamine to create lesions in catecholamine neurons in rats," *Journal of Neurosurgery*, vol. 42, no. 2, pp. 166–173, 1975.

[188] R. J. Reiter, D. X. Tan, and A. Galano, "Melatonin: exceeding expectations," *Physiology*, vol. 29, no. 5, pp. 325–333, 2014.

[189] J. W. Langston, P. Ballard, J. W. Tetrud, and I. Irwin, "Chronic parkinsonism in humans due to a product of meperidine-analog synthesis," *Science*, vol. 219, no. 4587, pp. 979–980, 1983.

[190] H. Mochizuki, N. Nakamura, K. Nishi, and Y. Mizuno, "Apoptosis is induced by 1-methyl-4-phenylpyridinium ion (MPP+) in ventral mesencephalic-striatal co-culture in rat," *Neuroscience Letters*, vol. 170, no. 1, pp. 191–194, 1994.

[191] H. Khaldy, G. Escames, J. León, F. Vives, J. D. Luna, and D. Acuña-Castroviejo, "Comparative effects of melatonin, L-deprenyl, trolox and ascorbate in the suppression of hydroxyl radical formation during dopamine autoxidation in vitro," *Journal of Pineal Research*, vol. 29, no. 2, pp. 100–107, 2000.

[192] C. F. Ibáñez and J.-O. Andressoo, "Biology of GDNF and its receptors—relevance for disorders of the central nervous system," *Neurobiology of Disease*, 2016.

[193] K. J. Armstrong and L. P. Niles, "Induction of GDNF mRNA expression by melatonin in rat C6 glioma cells," *NeuroReport*, vol. 13, no. 4, pp. 473–475, 2002.

[194] L. P. Niles, K. J. Armstrong, L. M. Rincón Castro et al., "Neural stem cells express melatonin receptors and neurotrophic factors: colocalization of the MT1 receptor with neuronal and glial markers," *BMC Neuroscience*, vol. 5, article 41, 2004.

[195] Y. P. Tang, Y. L. Ma, C. C. Chao, K. Y. Chen, and E. H. Y. Lee, "Enhanced glial cell line-derived neurotrophic factor mRNA expression upon (−)-deprenyl and melatonin treatments," *Journal of Neuroscience Research*, vol. 53, no. 5, pp. 593–604, 1998.

[196] D. W. Howells, M. J. Porritt, J. Y. F. Wong et al., "Reduced BDNF mRNA expression in the Parkinson's disease substantia nigra," *Experimental Neurology*, vol. 166, no. 1, pp. 127–135, 2000.

[197] M. Imbesi, T. Uz, and H. Manev, "Role of melatonin receptors in the effects of melatonin on BDNF and neuroprotection in mouse cerebellar neurons," *Journal of Neural Transmission*, vol. 115, no. 11, pp. 1495–1499, 2008.

[198] L. Zhang, H.-Q. Zhang, X.-Y. Liang, H.-F. Zhang, T. Zhang, and F.-E. Liu, "Melatonin ameliorates cognitive impairment induced by sleep deprivation in rats: role of oxidative stress, BDNF and CaMKII," *Behavioural Brain Research*, vol. 256, pp. 72–81, 2013.

[199] R. Molteni, F. Calabrese, S. Pisoni et al., "Synergistic mechanisms in the modulation of the neurotrophin BDNF in the rat prefrontal cortex following acute agomelatine administration," *The World Journal of Biological Psychiatry*, vol. 11, no. 2, pp. 148–153, 2010.

[200] S. Klongpanichapak, P. Phansuwan-Pujito, M. Ebadi, and P. Govitrapong, "Melatonin inhibits amphetamine-induced increase in α-synuclein and decrease in phosphorylated tyrosine hydroxylase in SK–N–SH cells," *Neuroscience Letters*, vol. 436, no. 3, pp. 309–313, 2008.

[201] K. Sae-Ung, K. Uéda, P. Govitrapong, and P. Phansuwan-Pujito, "Melatonin reduces the expression of alpha-synuclein in the dopamine containing neuronal regions of amphetamine-treated postnatal rats," *Journal of Pineal Research*, vol. 52, no. 1, pp. 128–137, 2012.

[202] C.-F. Chang, H.-J. Huang, H.-C. Lee, K.-C. Hung, R.-T. Wu, and A. M.-Y. Lin, "Melatonin attenuates kainic acid-induced neurotoxicity in mouse hippocampus via inhibition of autophagy and α-synuclein aggregation," *Journal of Pineal Research*, vol. 52, no. 3, pp. 312–321, 2012.

[203] C. Freire and S. Koifman, "Pesticide exposure and Parkinson's disease: epidemiological evidence of association," *NeuroToxicology*, vol. 33, no. 5, pp. 947–971, 2012.

[204] H. Zhou, J. Chen, X. Lu et al., "Melatonin protects against rotenone-induced cell injury via inhibition of Omi and Bax-mediated autophagy in Hela cells," *Journal of Pineal Research*, vol. 52, no. 1, pp. 120–127, 2012.

[205] G. L. Willis, C. Moore, and S. M. Armstrong, "A historical justification for and retrospective analysis of the systematic application of light therapy in Parkinson's disease," *Reviews in the Neurosciences*, vol. 23, no. 2, pp. 199–226, 2012.

[206] C. A. M. Medeiros, P. F. Carvalhedo de Bruin, L. A. Lopes, M. C. Magalhães, M. de Lourdes Seabra, and V. M. Sales de Bruin, "Effect of exogenous melatonin on sleep and motor dysfunction in Parkinson's disease. A randomized, double blind, placebo-controlled study," *Journal of Neurology*, vol. 254, no. 4, pp. 459–464, 2007.

[207] J. I. Chuang and M. T. Lin, "Pharmacological effects of melatonin treatment on both locomotor activity and brain serotonin release in rats," *Journal of Pineal Research*, vol. 17, no. 1, pp. 11–16, 1994.

[208] G. L. Willis and S. M. Armstrong, "A therapeutic role for melatonin antagonism in experimental models of Parkinson's disease," *Physiology & Behavior*, vol. 66, no. 5, pp. 785–795, 1999.

[209] S. Rutten, C. Vriend, O. A. van den Heuvel, J. H. Smit, H. W. Berendse, and Y. D. van der Werf, "Bright light therapy in Parkinson's disease: an overview of the background and evidence," *Parkinson's Disease*, vol. 2012, Article ID 767105, 9 pages, 2012.

[210] G. L. Willis and E. J. D. Turner, "Primary and secondary features of Parkinson's disease improve with strategic exposure to bright light: a case series study," *Chronobiology International*, vol. 24, no. 3, pp. 521–537, 2007.

[211] S. Paus, T. Schmitz-Hübsch, U. Wüllner, A. Vogel, T. Klockgether, and M. Abele, "Bright light therapy in Parkinson's disease: a pilot study," *Movement Disorders*, vol. 22, no. 10, pp. 1495–1498, 2007.

[212] G. L. Willis and A. D. Robertson, "Recovery from experimental Parkinson's disease in the 1-methyl-4-phenyl-1, 2,3,6-tetrahydropyridine hydrochloride treated marmoset with the melatonin analogue ML-23," *Pharmacology Biochemistry and Behavior*, vol. 80, no. 1, pp. 9–26, 2005.

[213] G. L. Willis, "Intraocular microinjections repair experimental Parkinson's disease," *Brain Research*, vol. 1217, pp. 119–131, 2008.

[214] I. Bodis-Wollner, "Visual deficits related to dopamine deficiency in experimental animals and Parkinson's disease patients," *Trends in Neurosciences*, vol. 13, no. 7, pp. 296–302, 1990.

[215] N. Zisapel, "Melatonin-dopamine interactions: from basic neurochemistry to a clinical setting," *Cellular and Molecular Neurobiology*, vol. 21, no. 6, pp. 605–616, 2001.

[216] K.-R. Shieh, Y.-S. Chu, and J.-T. Pan, "Circadian change of dopaminergic neuron activity: effects of constant light and melatonin," *NeuroReport*, vol. 8, no. 9-10, pp. 2283–2287, 1997.

[217] H. Khaldy, J. León, G. Escames, L. Bikjdaouene, J. J. García, and D. Acuña-Castroviejo, "Circadian rhythms of dopamine and dihydroxyphenyl acetic acid in the mouse striatum: effects of pinealectomy and of melatonin treatment," *Neuroendocrinology*, vol. 75, no. 3, pp. 201–208, 2002.

[218] A. Iranzo, "Sleep in neurodegenerative diseases," *Sleep Medicine Clinics*, vol. 11, no. 1, pp. 1–18, 2016.

[219] R. D. Abbott, G. W. Ross, L. R. White et al., "Excessive daytime sleepiness and subsequent development of Parkinson disease," *Neurology*, vol. 65, no. 9, pp. 1442–1446, 2005.

[220] L. K. Tholfsen, J. P. Larsen, J. Schulz, O.-B. Tysnes, and M. D. Gjerstad, "Development of excessive daytime sleepiness in early Parkinson disease," *Neurology*, vol. 85, no. 2, pp. 162–168, 2015.

[221] L. M. Trotti and D. L. Bliwise, "Treatment of the sleep disorders associated with Parkinson's disease," *Neurotherapeutics*, vol. 11, no. 1, pp. 68–77, 2014.

[222] K. Mishima, M. Okawa, Y. Hishikawa, S. Hozumi, H. Hori, and K. Takahashi, "Morning bright light therapy for sleep and behavior disorders in elderly patients with dementia," *Acta Psychiatrica Scandinavica*, vol. 89, no. 1, pp. 1–7, 1994.

[223] A. F. G. Leentjens, B. Scholtissen, F. W. Vreeling, and F. R. J. Verhey, "The serotonergic hypothesis for depression in Parkinson's disease: an experimental approach," *Neuropsychopharmacology*, vol. 31, no. 5, pp. 1009–1015, 2006.

[224] P. Jennum, J. A. Christensen, and M. Zoetmulder, "Neurophysiological basis of rapid eye movement sleep behavior disorder: informing future drug development," *Nature and Science of Sleep*, vol. 8, pp. 107–120, 2016.

[225] C. H. Schenck, B. F. Boeve, and M. W. Mahowald, "Delayed emergence of a parkinsonian disorder or dementia in 81% of older men initially diagnosed with idiopathic rapid eye movement sleep behavior disorder: a 16-year update on a previously reported series," *Sleep Medicine*, vol. 14, no. 8, pp. 744–748, 2013.

[226] A. Iranzo, E. Tolosa, E. Gelpi et al., "Neurodegenerative disease status and post-mortem pathology in idiopathic rapid-eye-movement sleep behaviour disorder: An Observational Cohort Study," *The Lancet Neurology*, vol. 12, no. 5, pp. 443–453, 2013.

[227] L. Plomhause, K. Dujardin, A. Duhamel et al., "Rapid eye movement sleep behavior disorder in treatment-naïve Parkinson disease patients," *Sleep Medicine*, vol. 14, no. 10, pp. 1035–1037, 2013.

[228] J.-F. Gagnon, M.-A. Bédard, M. L. Fantini et al., "REM sleep behavior disorder and REM sleep without atonia in Parkinson's disease," *Neurology*, vol. 59, no. 4, pp. 585–589, 2002.

[229] F. Sixel-Döring, E. Trautmann, B. Mollenhauer, and C. Trenkwalder, "Associated factors for REM sleep behavior disorder in Parkinson disease," *Neurology*, vol. 77, no. 11, pp. 1048–1054, 2011.

[230] M. D. Gjerstad, B. Boeve, T. Wentzel-Larsen, D. Aarsland, and J. P. Larsen, "Occurrence and clinical correlates of REM sleep behaviour disorder in patients with Parkinson's disease over time," *Journal of Neurology, Neurosurgery and Psychiatry*, vol. 79, no. 4, pp. 387–391, 2008.

[231] D. Kunz and F. Bes, "Melatonin as a therapy in REM sleep behavior disorder patients: an open-labeled pilot study on the possible influence of melatonin on REM-sleep regulation," *Movement Disorders*, vol. 14, no. 3, pp. 507–511, 1999.

[232] A. Ylikoski, K. Martikainen, M. Sieminski, and M. Partinen, "Parkinson's disease and insomnia," *Neurological Sciences*, vol. 36, no. 11, pp. 2003–2010, 2015.

[233] C. Trenkwalder, B. Kies, M. Rudzinska et al., "Rotigotine effects on early morning motor function and sleep in Parkinson's disease: a double-blind, randomized, placebo-controlled study (RECOVER)," *Movement Disorders*, vol. 26, no. 1, pp. 90–99, 2011.

[234] K. Ray Chaudhuri, P. Martinez-Martin, K. A. Rolfe et al., "Improvements in nocturnal symptoms with ropinirole prolonged release in patients with advanced Parkinson's disease," *European Journal of Neurology*, vol. 19, no. 1, pp. 105–113, 2012.

[235] M. Zibetti, M. Rizzone, A. Merola et al., "Sleep improvement with levodopa/carbidopa intestinal gel infusion in Parkinson disease," *Acta Neurologica Scandinavica*, vol. 127, no. 5, pp. e28–e32, 2013.

[236] B. Guardiola-Lemaître, A. Lenègre, and R. D. Porsolt, "Combined effects of diazepam and melatonin in two tests for anxiolytic activity in the mouse," *Pharmacology, Biochemistry and Behavior*, vol. 41, no. 2, pp. 405–408, 1992.

[237] S. Rios Romenets, L. Creti, C. Fichten et al., "Doxepin and cognitive behavioural therapy for insomnia in patients with Parkinson's disease—a randomized study," *Parkinsonism and Related Disorders*, vol. 19, no. 7, pp. 670–675, 2013.

[238] W. Ding, L.-J. Ding, F.-F. Li, Y. Han, and L. Mu, "Neurodegeneration and cognition in Parkinson's disease: a review," *European Review for Medical and Pharmacological Sciences*, vol. 19, no. 12, pp. 2275–2281, 2015.

[239] T. Foltynie, C. E. G. Brayne, T. W. Robbins, and R. A. Barker, "The cognitive ability of an incident cohort of Parkinson's patients in the UK. The CamPaIGN study," *Brain*, vol. 127, part 3, pp. 550–560, 2004.

[240] M. Richards, L. J. Cote, and Y. Stern, "Executive function in Parkinson's disease: set-shifting or set-maintenance?" *Journal of Clinical and Experimental Neuropsychology*, vol. 15, no. 2, pp. 266–279, 1993.

[241] A. Montse, V. Pere, J. Carme, V. Francesc, and T. Eduardo, "Visuospatial deficits in Parkinson's disease assessed by judgment of line orientation test: error analyses and practice effects," *Journal of Clinical and Experimental Neuropsychology*, vol. 23, no. 5, pp. 592–598, 2001.

[242] E. Mak, J. Zhou, L. C. S. Tan, W. L. Au, Y. Y. Sitoh, and N. Kandiah, "Cognitive deficits in mild Parkinson's disease are associated with distinct areas of grey matter atrophy," *Journal of Neurology, Neurosurgery and Psychiatry*, vol. 85, no. 5, pp. 576–580, 2014.

[243] Y. Takahashi and T. Okada, "Involvement of the nitric oxide cascade in melatonin-induced inhibition of long-term potentiation at hippocampal CA1 synapses," *Neuroscience Research*, vol. 69, no. 1, pp. 1–7, 2011.

[244] G. Ramírez-Rodríguez, N. M. Vega-Rivera, G. Benítez-King, M. Castro-García, and L. Ortíz-López, "Melatonin supplementation delays the decline of adult hippocampal neurogenesis during normal aging of mice," *Neuroscience Letters*, vol. 530, no. 1, pp. 53–58, 2012.

[245] V. K. Datieva, A. V. Rosinskaya, and O. S. Levin, "The use of melatonin in the treatment of chronic fatigue syndrome and circadian rhythm disorders in Parkinson's disease," *Zh Nevrol Psikhiatr*, vol. 113, no. 7, pp. 77–81, 2013.

[246] C. Capitelli, A. Sereniki, M. M. S. Lima, A. B. Reksidler, S. Tufik, and M. A. B. F. Vital, "Melatonin attenuates tyrosine hydroxylase loss and hypolocomotion in MPTP-lesioned rats," *European Journal of Pharmacology*, vol. 594, no. 1–3, pp. 101–108, 2008.

[247] V. Bertaina-Anglade, C. Drieu-La-Rochelle, E. Mocaër, and L. Seguin, "Memory facilitating effects of agomelatine in the novel object recognition memory paradigm in the rat," *Pharmacology Biochemistry and Behavior*, vol. 98, no. 4, pp. 511–517, 2011.

[248] P. He, X. Ouyang, S. Zhou et al., "A novel melatonin agonist Neu-P11 facilitates memory performance and improves cognitive impairment in a rat model of Alzheimer' disease," *Hormones and Behavior*, vol. 64, no. 1, pp. 1–7, 2013.

[249] G. Baydas, M. Özer, A. Yasar, M. Tuzcu, and S. T. Koz, "Melatonin improves learning and memory performances impaired by hyperhomocysteinemia in rats," *Brain Research*, vol. 1046, no. 1-2, pp. 187–194, 2005.

[250] M. E. Pushpanathan, A. M. Loftus, M. G. Thomas, N. Gasson, and R. S. Bucks, "The relationship between sleep and cognition in Parkinson's disease: a meta-analysis," *Sleep Medicine Reviews*, vol. 26, pp. 21–32, 2016.

[251] S. Comai and G. Gobbi, "Unveiling the role of melatonin MT2 receptors in sleep, anxiety and other neuropsychiatric diseases: a novel target in psychopharmacology," *Journal of Psychiatry and Neuroscience*, vol. 39, no. 1, pp. 6–21, 2014.

[252] D. Aarsland, S. Påhlhagen, C. G. Ballard, U. Ehrt, and P. Svenningsson, "Depression in Parkinson disease—epidemiology, mechanisms and management," *Nature Reviews Neurology*, vol. 8, no. 1, pp. 35–47, 2012.

[253] J. W. Cooney and M. Stacy, "Neuropsychiatric issues in Parkinson's disease," *Current Neurology and Neuroscience Reports*, vol. 16, no. 5, article 49, 2016.

[254] O. Riedel, J. Klotsche, A. Spottke et al., "Frequency of dementia, depression, and other neuropsychiatric symptoms in 1,449

outpatients with Parkinson's disease," *Journal of Neurology*, vol. 257, no. 7, pp. 1073–1082, 2010.

[255] S. E. Starkstein, J. P. Fedoroff, T. R. Price, R. Leiguarda, and R. G. Robinson, "Anosognosia in patients with cerebrovascular lesions. A study of causative factors," *Stroke*, vol. 23, no. 10, pp. 1446–1453, 1992.

[256] E. L. Jacob, N. M. Gatto, A. Thompson, Y. Bordelon, and B. Ritz, "Occurrence of depression and anxiety prior to Parkinson's disease," *Parkinsonism and Related Disorders*, vol. 16, no. 9, pp. 576–581, 2010.

[257] A. Alonso, L. A. García Rodríguez, G. Logroscino, and M. A. Hernán, "Use of antidepressants and the risk of Parkinson's disease: a prospective study," *Journal of Neurology, Neurosurgery and Psychiatry*, vol. 80, no. 6, pp. 671–674, 2009.

[258] U. Walter, D. Dressler, A. Wolters, M. Wittstock, and R. Benecke, "Transcranial brain sonography findings in clinical subgroups of idiopathic Parkinson's disease," *Movement Disorders*, vol. 22, no. 1, pp. 48–54, 2007.

[259] H. Braak and K. Del Tredici, "A new look at the corticostriatal-thalamocortical circuit in sporadic Parkinson's disease," *Der Nervenarzt*, vol. 79, no. 12, pp. 1440–1445, 2008.

[260] V. Micale, A. Arezzi, L. Rampello, and F. Drago, "Melatonin affects the immobility time of rats in the forced swim test: the role of serotonin neurotransmission," *European Neuropsychopharmacology*, vol. 16, no. 7, pp. 538–545, 2006.

[261] M. Mantovani, R. Pértile, J. B. Calixto, A. R. S. Santos, and A. L. S. Rodrigues, "Melatonin exerts an antidepressant-like effect in the tail suspension test in mice: evidence for involvement of N-methyl-D-aspartate receptors and the L-arginine-nitric oxide pathway," *Neuroscience Letters*, vol. 343, no. 1, pp. 1–4, 2003.

[262] R. W. Binfaré, M. Mantovani, J. Budni, A. R. S. Santos, and A. L. S. Rodrigues, "Involvement of dopamine receptors in the antidepressant-like effect of melatonin in the tail suspension test," *European Journal of Pharmacology*, vol. 638, no. 1–3, pp. 78–83, 2010.

[263] B. C. Detanico, Â. L. Piato, J. J. Freitas et al., "Antidepressant-like effects of melatonin in the mouse chronic mild stress model," *European Journal of Pharmacology*, vol. 607, no. 1–3, pp. 121–125, 2009.

[264] S. Rivara, D. Pala, A. Bedini, and G. Spadoni, "Therapeutic uses of melatonin and melatonin derivatives: a patent review (2012–2014)," *Expert Opinion on Therapeutic Patents*, vol. 25, no. 4, pp. 425–441, 2015.

[265] I. N. Karatsoreos and B. S. McEwen, "Timing is everything: a collection on how clocks affect resilience in biological systems," *F1000Research*, vol. 3, article 273, 2014.

[266] S. J. Bolitho, S. L. Naismith, S. M. W. Rajaratnam et al., "Disturbances in melatonin secretion and circadian sleep-wake regulation in Parkinson disease," *Sleep Medicine*, vol. 15, no. 3, pp. 342–347, 2014.

[267] T. Yamanishi, H. Tachibana, M. Oguru et al., "Anxiety and depression in patients with Parkinson's disease," *Internal Medicine*, vol. 52, no. 5, pp. 539–545, 2013.

[268] N. N. N. W. Dissanayaka, E. White, J. D. O'Sullivan, R. Marsh, N. A. Pachana, and G. J. Byrne, "The clinical spectrum of anxiety in Parkinson's disease," *Movement Disorders*, vol. 29, no. 8, pp. 967–975, 2014.

[269] R. D. S. Prediger, F. C. Matheus, M. L. Schwarzbold, M. M. S. Lima, and M. A. B. F. Vital, "Anxiety in Parkinson's disease: a critical review of experimental and clinical studies," *Neuropharmacology*, vol. 62, no. 1, pp. 115–124, 2012.

[270] N. N. W. Dissanayaka, A. Sellbach, S. Matheson et al., "Anxiety disorders in Parkinson's disease: prevalence and risk factors," *Movement Disorders*, vol. 25, no. 7, pp. 838–845, 2010.

[271] G. M. Pontone, J. R. Williams, K. E. Anderson et al., "Prevalence of anxiety disorders and anxiety subtypes in patients with Parkinson's disease," *Movement Disorders*, vol. 24, no. 9, pp. 1333–1338, 2009.

[272] S.-M. Jiang, Y.-S. Yuan, Q. Tong et al., "The association between clinically relevant anxiety and other non-motor symptoms in Parkinson's disease," *Neurological Sciences*, vol. 36, no. 11, pp. 2105–2109, 2015.

[273] N. N. W. Dissanayaka, E. Torbey, and N. A. Pachana, "Anxiety rating scales in Parkinson's disease: a critical review updating recent literature," *International Psychogeriatrics*, vol. 27, no. 11, pp. 1777–1784, 2015.

[274] M. P. Broen, S. Köhler, A. J. Moonen et al., "Modeling anxiety in Parkinson's disease," *Movement Disorders*, vol. 31, no. 3, pp. 310–316, 2016.

[275] S. Rutten, I. Ghielen, C. Vriend et al., "Anxiety in Parkinson's disease: symptom dimensions and overlap with depression and autonomic failure," *Parkinsonism and Related Disorders*, vol. 21, no. 3, pp. 189–193, 2015.

[276] E. C. Lauterbach, A. Freeman, and R. L. Vogel, "Correlates of generalized anxiety and panic attacks in dystonia and Parkinson disease," *Cognitive and Behavioral Neurology*, vol. 16, no. 4, pp. 225–233, 2003.

[277] A. Tessitore, A. R. Hariri, F. Fera et al., "Dopamine modulates the response of the human amygdala: a study in Parkinson's disease," *The Journal of Neuroscience*, vol. 22, no. 20, pp. 9099–9103, 2002.

[278] J. J. Chen and L. Marsh, "Anxiety in Parkinson's disease: identification and management," *Therapeutic Advances in Neurological Disorders*, vol. 7, no. 1, pp. 52–59, 2014.

[279] K. Del Tredici and H. Braak, "Dysfunction of the locus coeruleus-norepinephrine system and related circuitry in Parkinson's disease-related dementia," *Journal of Neurology, Neurosurgery and Psychiatry*, vol. 84, no. 7, pp. 774–783, 2013.

[280] N. Wee, N. Kandiah, S. Acharyya et al., "Depression and anxiety are co-morbid but dissociable in mild Parkinson's disease: A Prospective Longitudinal Study of patterns and predictors," *Parkinsonism and Related Disorders*, vol. 23, pp. 50–56, 2016.

[281] M. Naguib and A. H. Samarkandi, "The comparative dose-response effects of melatonin and midazolam for premedication of adult patients: a double-blinded, placebo-controlled study," *Anesthesia and Analgesia*, vol. 91, no. 2, pp. 473–479, 2000.

[282] F. Yousaf, E. Seet, L. Venkatraghavan, A. Abrishami, and F. Chung, "Efficacy and safety of melatonin as an anxiolytic and analgesic in the perioperative period: a qualitative systematic review of randomized trials," *Anesthesiology*, vol. 113, no. 4, pp. 968–976, 2010.

[283] G. Perna, A. Alciati, A. Riva, W. Micieli, and D. Caldirola, "Long-term pharmacological treatments of anxiety disorders: an updated systematic review," *Current Psychiatry Reports*, vol. 18, no. 3, article 23, 2016.

[284] J. A. S. Crippa, J. E. C. Hallak, A. W. Zuardi, M. H. N. Chagas, J. Quevedo, and A. E. Nardi, "Agomelatine in the treatment of social anxiety disorder," *Progress in Neuro-Psychopharmacology and Biological Psychiatry*, vol. 34, no. 7, pp. 1357–1358, 2010.

[285] K. M. Huijbregts, N. M. Batelaan, J. Schonenberg, G. Veen, and A. J. van Balkom, "Agomelatine as a novel treatment option in panic disorder, results from an 8-week open-label trial," *Journal of Clinical Psychopharmacology*, vol. 35, no. 3, pp. 336–338, 2015.

[286] Y. B. Kalyn, T. P. Safarova, O. B. Yakovleva et al., "Experience of the antidepressive therapy with valdoxan (agomelatine) in a psychogeriatric unit of the psychiatric hospital," *Zhurnal nevrologii i psikhiatrii im. S.S. Korsakova*, vol. 115, no. 11, pp. 55–62, 2015.

[287] L. Niles, "Melatonin interaction with the benzodiazepine-GABA receptor complex in the CNS," *Advances in Experimental Medicine and Biology*, vol. 294, pp. 267–277, 1991.

Research Article

Neurobehavioral and Antioxidant Effects of Ethanolic Extract of Yellow Propolis

Cinthia Cristina Sousa de Menezes da Silveira,[1] Luanna Melo Pereira Fernandes,[1,2] Mallone Lopes Silva,[1] Diandra Araújo Luz,[1] Antônio Rafael Quadros Gomes,[1] Marta Chagas Monteiro,[1,2] Christiane Schineider Machado,[3] Yohandra Reyes Torres,[3] Tatiana Onofre de Lira,[4] Antonio Gilberto Ferreira,[4] Enéas Andrade Fontes-Júnior,[1,2,5] and Cristiane Socorro Ferraz Maia[1,2,5]

[1]*Programa de Pós-Graduação em Ciências Farmacêuticas, Instituto de Ciências da Saúde, Universidade Federal do Pará, Belém, PA, Brazil*
[2]*Programa de Pós-Graduação em Neurociências e Biologia Celular, Belém, PA, Brazil*
[3]*Departamento de Química, Universidade Estadual do Centro-Oeste (UNICENTRO), 85010-990 Guarapuava, PR, Brazil*
[4]*Departamento de Química, Universidade Federal de São Carlos (UFSCar), 13565-905 São Carlos, SP, Brazil*
[5]*Laboratório de Farmacologia da Inflamação e do Comportamento, Faculdade de Farmácia, Instituto de Ciências da Saúde, Universidade Federal do Pará, 66075-900 Belém, PA, Brazil*

Correspondence should be addressed to Cristiane Socorro Ferraz Maia; crismaia@ufpa.br

Received 13 July 2016; Revised 8 September 2016; Accepted 19 September 2016

Academic Editor: Giuseppe Cirillo

Propolis is a resin produced by bees from raw material collected from plants, salivary secretions, and beeswax. New therapeutic properties for the Central Nervous System have emerged. We explored the neurobehavioral and antioxidant effects of an ethanolic extract of yellow propolis (EEYP) rich in triterpenoids, primarily lupeol and β-amyrin. Male Wistar rats, 3 months old, were intraperitoneally treated with Tween 5% (control), EEYP (1, 3, 10, and 30 mg/kg), or diazepam, fluoxetine, and caffeine (positive controls) 30 min before the assays. Animals were submitted to open field, elevated plus maze, forced swimming, and inhibitory avoidance tests. After behavioral tasks, blood samples were collected through intracardiac pathway, to evaluate the oxidative balance. The results obtained in the open field and in the elevated plus maze assay showed spontaneous locomotion preserved and anxiolytic-like activity. In the forced swimming test, EEYP demonstrated antidepressant-like activity. In the inhibitory avoidance test, EEYP showed mnemonic activity at 30 mg/kg. In the evaluation of oxidative biochemistry, the extract reduced the production of nitric oxide and malondialdehyde without changing level of total antioxidant, catalase, and superoxide dismutase, induced by behavioral stress. Our results highlight that EEYP emerges as a promising anxiolytic, antidepressant, mnemonic, and antioxidant natural product.

1. Introduction

Propolis is a bee resinous product elaborated from different parts of plants such as buds, bark, and tree exudates by bees. The chemical composition of propolis is highly variable and depends directly on the geographic origin and local flora. In addition, the season, climate, bee species or genus, and extraction method also influence the composition of the final extract of propolis [1–5].

Pharmacological effects have been described for propolis related to their different constituents. Regarding the Central Nervous System (CNS), new therapeutical tools have emerged. In fact, since 2003, bioactive components present in propolis have been investigated. For example, caffeic acid phenethyl ester (CAPE) studies have claimed this compound as a neuroprotector in a cerebral inflammatory model [6]. After that, CAPE demonstrated its effectiveness on models of neuroinflammation, such as the cerebral ischemia

model [7], and glutamate-induced excitotoxicity [8], through antioxidant or p38 phosphorylation and caspase-3 activation, respectively. In addition, the flavonoid pinocembrin, an important propolis constituent, has reduced brain lesion in an ischemia-reperfusion model, probably by its antioxidant and antiapoptotic activity [9].

In addition to flavonoids, other classes of compounds have been identified in several types of Brazilian propolis (green, red, and brown propolis) such as prenylated p-coumaric acids, acetophenone derivatives, lignans, other phenolic compounds, and di- and triterpenes [2]. Several samples of Brazilian yellow propolis were previously grouped according to their physicochemical and biological properties [10]; however, Brazilian yellow propolis has been scarcely studied [11]. Similar to yellow propolis from Cuba, sample of yellow propolis collected in the Central-Western Region of Brazil was mainly composed by triterpenoids belonging to oleanane, lupane, ursane, and lanostane skeletons [11–13].

Extracts of propolis have demonstrated several activities on the CNS. For example, the natural extract attenuated seizures induced by kainic acid, at least in part, via adenosine A1 receptor modulation [14]. In addition, a study [15] concluded that propolis elicited neuroprotected effect when given in combination with an anticonvulsant drug (e.g., valproate), against the neurophysiological disorders induced by pilocarpine epilepsy in rats, restoring the hippocampal neurotransmitter levels (e.g., dopamine and serotonin).

Nevertheless, solely in 2012, the effectiveness of propolis was investigated in psychiatric disorders. Firstly, a study demonstrated that the essential oil of Brazilian green propolis, rich in terpenoids, produces therapeutic effects on anxiety by hyperfunction of hypothalamic-pituitary-adrenal (HPA) axis reduction [16]. Researchers reported [17] that ethanol extract of Korean propolis exerted antidepressant activity by enhancing glucocorticoid receptor (GR) function. In this sense, our group hypothesized that the oil extract of brown propolis collected in south Brazil could potentiate the behavioral effects demonstrated previously by Lee experiment [17]. In fact, the oil extract of this brown propolis exerted stimulant, anxiolytic, and antidepressant effects at lower doses [18].

In the present paper, we explored the neurobehavioral effects of the ethanolic extract of yellow propolis sample collected in Mato Grosso do Sul, Brazil, which was demonstrated to be rich in triterpenoids [11]. Triterpenoid compounds have shown sedative, tranquillizer, and anticonvulsant activities [19–22].

2. Material and Methods

2.1. Propolis Origin, Extract Preparation, and Chromatography Fractionation

2.1.1. Propolis Sample. The yellow propolis sample produced by *Apis mellifera* bees was collected in January 2012 in Mato Grosso do Sul, Brazil. Yellow propolis was stored at −18°C until extraction [11].

2.1.2. Propolis Extraction. Yellow propolis sample was ground with a mortar and pestle and extracted by maceration in AP ethanol (Biotec, Brazil) (1 : 10 w/v) for 24 hours using an incubator (Tecnal, Brazil) at 160 rpm and room temperature. After the extraction time, the solution was vacuum-filtered to remove the insoluble parts. Then, the hydroalcoholic phase was placed in a freezer for 24 hours. After this time, the solution was again filtered through qualitative filter paper (Macherey-Nagel, Germany) to remove waxes. The extraction solution was dried by evaporating the solvent under reduced pressure rotary evaporator (Model 752, Fisatom, Brazil), equipped with vacuum pump (Prismatec, Brazil) and a water bath (Nova Química, Brazil) at 50°C. The dry ethanolic extract of the yellow propolis (EEYP) was weighed (yield 19.80% w/w) and a sample was solubilized with Tween 20 solution 5% using vortex apparatus for 30 minutes to a final concentration of 5 mg/mL.

2.1.3. Chromatography Fractionation. Three hundred milligrams of EEYP in hexane solution was applied on a silica gel chromatography column (particle size: 0.063–0.200 mm; pore size: 60 Å, MERCK G60; column size 3×80 cm). Elution was carried out with mixtures of increasing polarity organic solvents (hexane (100%), hexane/ethyl acetate (50 : 50, v/v), ethyl acetate (100%), and ethyl acetate/methanol (50 : 50, v/v)) to afford five major subfractions (F1 = 123.7 mg, F2 = 93.0 mg, F3 = 110.7 mg, F4 = 54.1 mg, and F5 = 84.1 mg).

2.2. Drugs and Solutions. The positive control treatments included diazepam (DZP: 7-chloro-1-methyl-5-phenyl-1,3-dihydro-2 H-1,4-benzodiazepin-2-one, Diazepamil®, Hipolabor Laboratory, Brazil), fluoxetine (FXT: N-methyl-3-phenyl-3-[4-(trifluoromethyl) phenoxy] propan-1-amine hydrochloride, Fluxene®, Eurofarma Laboratory, Brazil), and caffeine (CAF: Sigma-Aldrich®, USA). Tween 80 solution (5%) was used (Sigma-Aldrich, USA, distilled water and sodium chloride).

2.3. Animals. Three-month-old male Wistar rats (body weight = 122 ± 0.05 g; $n = 10$ per group) obtained from the Animal Facility, Biological Sciences Institute, Federal University of Pará (UFPA), were used in the experimental assays and kept in collective cages (5 animals per cage). Animals were maintained in a climate-controlled room on a 12 h reverse light/dark cycle (lights on 7:00 AM), with food and water *ad libitum*. All procedures were approved by the Ethics Committee on Experimental Animals of the Federal University of Pará under license number BIO-046-12 and followed the guidelines suggested by the NIH *Guide for the Care and Use of Laboratory Animals*. All behavioral assays were performed in the Laboratory of Pharmacology of Inflammation and Behavior at the Federal University of Pará.

Animals were divided into eight groups, defined as control group (vehicle) that received saline solution plus Tween 80 (5%) intraperitoneally (i.p.); EEYP at 1, 3, and 30 mg/kg i.p.; and positive control group diazepam 1 mg/kg i.p., for anxiety-like tests; fluoxetine 10 mg/kg i.p., for antidepressant-like test; and caffeine 10 mg/kg i.p., for memory test.

2.4. Behavioral Assays

2.4.1. Open Field (OF) Test.
EEYP, saline solution plus Tween 80 (5%), or diazepam was administered 30 min before the behavioral tests. Rats were placed individually in the center of a wooden arena ($100 \times 100 \times 40$ cm) divided into 25 quadrants to evaluate the number of sections visited by the animal over a period of 5 min. The test was videotaped and analyzed by Any Maze Stoelting software (USA). The parameters of total distance traveled (motor index), time spent, and distance traveled in the central area (emotional index) were measured.

2.4.2. Elevated Plus Maze (EPM) Test.
Following the open field (OF) test, the animals were subjected to the elevated plus maze (EPM) test, which consists of a plus-shaped wooden maze with two opposite open arms (50×10 cm) and two enclosed arms ($50 \times 10 \times 40$ cm) spreading out from a central platform (10×10 cm) elevated at a height of 50 cm from the floor. The animals were individually placed in the center of the EPM, facing one of the enclosed arms, and were allowed to explore the apparatus for 5 min following the previously described protocol [23]. The parameters measured were frequency of open arm entries (OAE); open arm time (OAT); and frequency of enclosed arm entries (EAE). The % OAE and % OAT were calculated according to the formula [(open/total) $\times$ 100]. An entry was counted whenever the animal placed four paws in an arm of the maze. An anxiogenic effect is defined as a decrease in the % OAE and/or % OAT.

2.4.3. Forced Swimming (FS) Test.
Following the EPM test, the animals were subjected to the forced swimming (FS) test. Rodents were individually dropped into cylindrical tank (50 cm in diameter; 70 cm high) containing water at 23 $\pm$ 1°C and were monitored for 5 min in inescapable conditions. Immobility time was recorded during the last 3 min. The first 2 min were considered habituation. The rats were judged as immobile whenever they stopped swimming and floated in an upright position for 2 s and when only small movements to keep their head above the water level were observed. The reduction in the immobility time was considered an antidepressant-like effect. The number of climbing events was measured to evaluate motor skills [24].

2.4.4. Step-Down Inhibitory Avoidance (IA) Test.
Animals were submitted to the inhibitory avoidance (IA) apparatus that was an acrylic box ($50 \times 25 \times 25$ cm^3) whose floor consisted of parallel stainless steel bars (1 mm in diameter) spaced 1 cm apart (Insight, Brazil). A platform (7 cm wide $\times$ 2.5 cm high) was placed on the floor against the left wall of the box. Using a previously reported protocol [25, 26], animals were placed on the platform and the time from latency to step-down on the grid with four paws was measured with an automatic device. Latency time was used as a measure of memory retention (maximum 180 s). A previous training session was carried out by giving the animals a 0.4 mA, 1.0 s scrambled foot shock immediately after they stepped down on the grid. Then, the animals were immediately removed from the apparatus until next session. In order to evaluate short-term memory, the test sessions were performed 1.5 h after training.

In addition to behavioral parameters already observed in the battery of tests, animals were also evaluated to detect the occurrence of adverse effects that may suggest toxicity. Signals of both stimulant (snout scratching, tremors, increased respiratory rate, paw licking, tail biting, arousal, nasal discharge, piloerection, stereotyped movements, and convulsions) and depressant (alienation of the environment, ataxia, catatonia, decreased respiratory rate, apathy, dyspnea, ptosis, sedation, and dorsal tone) activities were evaluated [27].

After the behavioral tests, blood samples were collected to determine oxidative stress.

2.5. Oxidative Biochemistry Assays.
Experiments to evaluate oxidative stress were designed in the *In Vitro* Activities Laboratory at the Federal University of Pará. After the behavioral assays, animal's blood samples were obtained by intracardiac puncturing. A basal group that was not submitted to the behavioral protocol was added to the biochemical oxidative assay. Nitric oxide (NO), malondialdehyde (MDA), trolox equivalent antioxidant capacity (TEAC), catalase (CAT), and superoxide dismutase (SOD) levels were measured.

2.5.1. Determination of Plasma Nitric Oxide (NO) Concentration.
The nitrate (NO_3^-) present in the serum samples was converted to nitrite with nitrate reductase, and the nitrite concentration was determined using the Griess method [28]. Briefly, 100 μL of the supernatant samples was incubated with an equal volume of Griess reagent for 10 min at room temperature. The absorbance was measured on a plate scanner (Spectra Max 250; Molecular Devices, Menlo Park, CA, USA) at 550 nm. The nitrite (NO_2^-) concentration was determined using a standard curve generated using sodium nitrite ($NaNO_2$). Nitrite production was expressed per μM.

2.5.2. Determination of Plasma Malondialdehyde (MDA) Concentration.
The MDA was used for the reaction of thiobarbituric acid reactive substances (TBARS) performed according to the adapted form [29] of a previously proposed method [30]. An aliquot of 1 mL of the reagent (TBA 10 nM) and 0.5 mL of the sample were added to each test tube. Then, the tubes were placed in a water bath at 94°C for 1 h. After this procedure, the samples were cooled in running water for about 15 minutes and then 4 mL of butyl alcohol was added to each sample. Subsequently, the samples were mixed on a vortex shaker, in order to obtain the maximum extraction of MDA into the organic phase. Finally, the tubes were centrifuged at 2,500 rpm for 10 minutes. A volume of 3 mL of supernatant was pipetted to carry out spectrophotometric reading at 535 mm. Results were expressed in nmol/mL.

2.5.3. Measurement of Trolox Equivalent Antioxidant Capacity (TEAC).
The trolox equivalent antioxidant capacity (TEAC) is a sensitive and reliable marker for detecting *in vivo* oxidative stress markers that may not be detectable through the measurement of a single, specific antioxidant [31]. TEAC

level of the blood serum sample was measured using a previously developed method [32]. In this assay, 7 mM of 2,2-azinobis, 3-ethylbenzothiazoline, 6-sulfonate (ABTS) was incubated with 2.45 mM of potassium persulfate and the ABTS-potassium persulfate (1 : 0.5, v/v) and the mixture was allowed to stand in the dark at room temperature for 12–16 h before use. For the study, the blue-green ABTS+ solution was diluted with ethanol 95% (v/v) until the absorbance reached 0.70 ± 0.02 at 734 nm. Then, 10 μL of the blood serum or trolox standard was mixed with 1 mL of ABTS+ solution, and decrease in absorbance at 734 nm was recorded after 4 min for all samples. The absorbance of the mixture was monitored at 734 nm after 6 min. For the blank, 10 μL of water instead of the sample was used and each sample was measured in triplicate. Total antioxidant potential of blood serum was expressed as μmol/mL of TEAC and was calculated through a calibration curve plotted with different amounts of trolox [33].

2.5.4. Measurement of Catalase (CAT) Activity.
CAT activity was determined according to a previously validated method [34]. Blood samples were haemolysed into ice water (1 : 3) and then diluted in a Tris based buffer (Tris 1 M/EDTA 5 mM, pH 8.0). To verify the decay of hydrogen peroxide (H_2O_2), aliquots of the diluted samples were added to 900 μL of the reaction solution (Tris base, H_2O_2 30% and ultrapure water, pH 8) [35]. The decrease of H_2O_2 concentration was established at $\lambda = 240$ nm at 25°C for 60 seconds. CAT activity was defined as the activity required to degrade 1 mol of H_2O_2 during 60 seconds (pH 8 and 25°C) and was expressed as U/mg protein. The molar extinction coefficient of H_2O_2 used for the calculation was 39.4 cm^2/mole. The enzymatic activity data obtained in CAT assays were normalized by the total protein concentrations, using the commercial kit (Doles, Brazil).

2.5.5. Measurement of Superoxide Dismutase (SOD) Activity.
Determination of SOD activity was performed following reported recommendations [36]. For this, blood samples were haemolysed into ice water (1 : 3) and then diluted in a Tris based buffer (Tris 1 M/EDTA 5 mM, pH 8.0). Total SOD activity of blood sample was determined by the inhibition of cytochrome c reduction [37]. This method evaluated the ability of SOD to catalyze the conversion of superoxide anion ($O_2{}^-$) to hydrogen peroxide (H_2O_2) and oxygen gas (O_2). The reduction of cytochrome c was mediated by superoxide anions generated by the xanthine/xanthine oxidase system and monitored at a wavelength of 550 nm. One unit of SOD was defined as the amount of enzyme required to inhibit the rate of cytochrome c reduction by 50%. SOD activity was measured using ultraviolet-visible (UV-VIS) spectrophotometer at a wavelength of 550 nm and was expressed in nmol/mL.

2.6. ^{1}H-NMR Analysis of EEYP and Fractions.
Proton nuclear magnetic resonance (^{1}H-NMR) analysis was recorded at 298 K in a Bruker UltraShielding™ Plus 600 MHz spectrometer operating at 14.6 T. EEYP and fractions were dissolved in a mixture of 100 μL D_2O (buffer phosphate, pH 7.04) and 600 μL CD_3OD. The solution was centrifuged at 13,000 rpm for 20 min at room temperature. The supernatant (600 μL) was transferred into an NMR tube of 5 mm. ^{1}H-NMR spectra were acquired using a NOESY pulse sequence for presaturation on water resonance and spoiled gradient during mixing time (noesygppr1d, Bruker terminology). The parameters settled in this sequence were 4.0 s for relaxation delay time, acquisition time of 3.99, data points of 140 k, mixing time of 10 ms, and 128 scans with a spectral window of 30 ppm. Spectra were processed by applying an exponential line broadening LB of 0.3 and manually phased trough Topspin 3.0 (Bruker Biospin).

2.7. Statistical Analysis.
Data were analyzed using one-way analysis of variance (ANOVA) followed by Tukey's test for multiple comparisons of behavior and oxidative stress test results. The Student t-test was used for multiple comparisons in determining NO. Data from each experimental group were expressed as the mean $\pm$ standard error of the mean (SEM) of 10 animals per group. P values less than 0.05 ($P < 0.05$) were considered to be indicative of significance. The graphical construction and statistical analysis were performed using GraphPad Prism 5.0 software (San Diego, California, USA).

3. Results

3.1. Yellow Propolis Did Not Cause Toxic or Adverse Effects During Tests.
EEYP did not elicit signals of toxicity reactions or adverse reactions. In fact, animals did not present toxic symptoms at the beginning (30 min after EEYP administration) nor at the end of the behavioral tests (195 min after EEYP administration).

3.2. Yellow Propolis Does Not Change the Animals Deambulation in the OF and It Exacerbates the Time of Exploration of Central Squares.
EEYP did not interfere in the animal ambulation, indicating no sedative effect of propolis (Figure 1(a)).

Figure 1(b) shows the results of locomotion in the central squares which is a parameter related to anxiety-like behavior. It was observed that animals treated with EEYP at dose ≥3 mg/kg had ambulation in the central area increased. Besides, administration of EEYP (30 mg/kg) also increased the exploration time spent in the central quadrants (Figure 1(c)), which suggests an anxiolytic-like effect.

3.3. Yellow Propolis Promotes Anxiolytic-Like Behavior in the EPM Test.
In the EPM test, EEYP increased the % OAE ($P < 0.05$, Figure 2(a)). In addition, animals treated with EEYP showed significant increase in the % OAT parameter (Figure 2(b); $P < 0.05$), confirming previous anxiolytic-like behavior, observed in the OF test. Indeed, animals treated with EEYP showed a similar behavior as those treated with the standard anxiolytic drug diazepam, showing the effectiveness and potential of yellow propolis in anxiolytic therapy.

The EAE parameter was not altered in the animals treated with EEYP or with diazepam (Figure 2(c)), which shows that
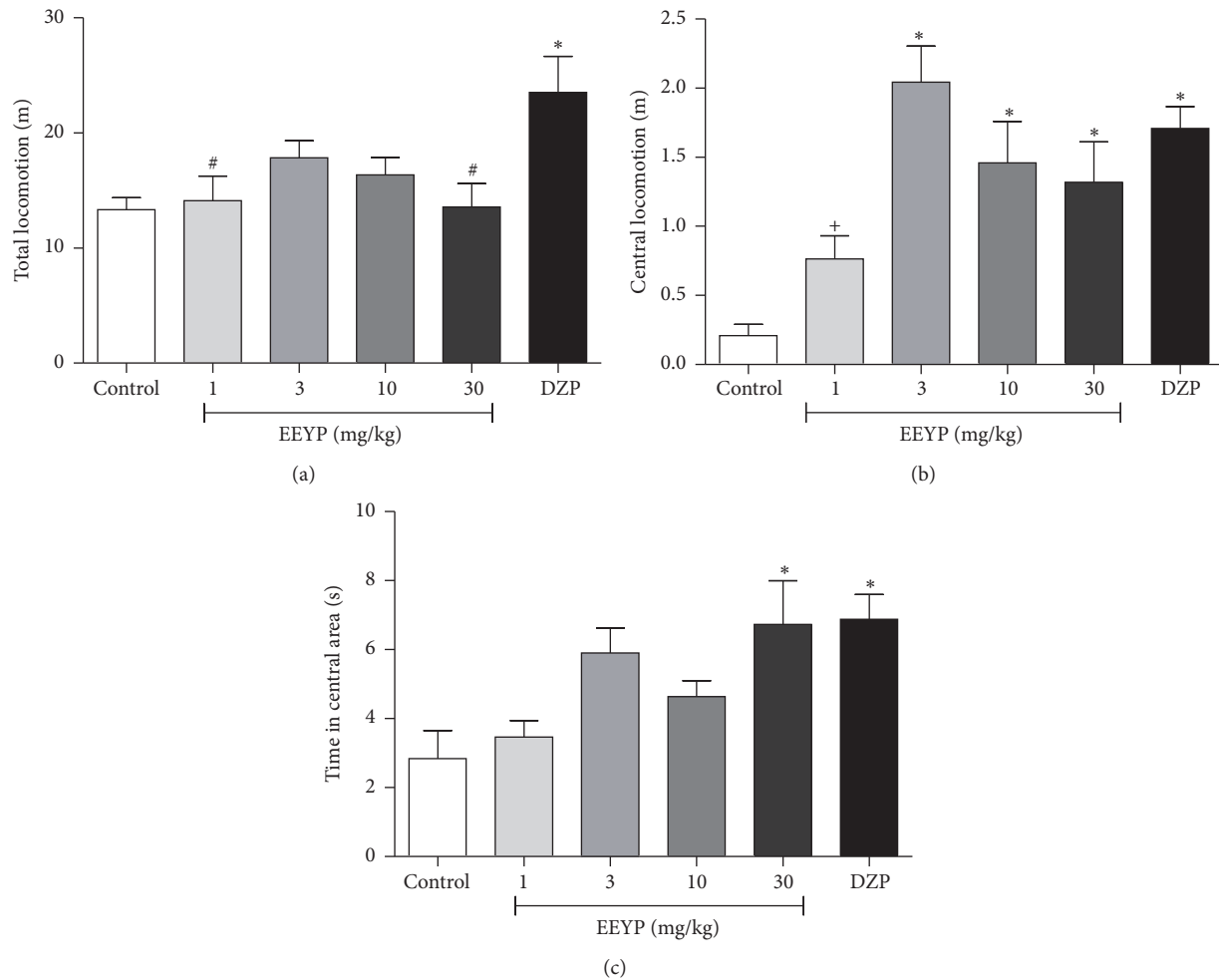
(a)

(b)

(c)

FIGURE 1: Effect of treatment with EEYP (1, 3, 10, and 30 mg/kg) on (a) total locomotion; (b) time in central area; and (c) central locomotion in the open field test. $^{*}P < 0.05$ *versus* control group; $^{#}P < 0.05$ *versus* diazepam (DZP) group; $^{+}P < 0.05$ *versus* EEYP 3 mg/kg group. Values are expressed as mean ± SEM from 10 animals per group (ANOVA and Tukey's test).

the animals did not present any level of sedation, which could impair motor behavior and consequently deambulation.

3.4. Yellow Propolis Promotes Antidepressant-Like Activities in FS Test. In the FS model, animals showed significant decrease in the immobility time ($P < 0.05$), indicating antidepressant-like behavior (Figure 3(a)). However, EEYP seems to be less effective than the standard drug fluoxetine (positive control).

The total swimming time (Figure 3(b)) of the animals treated with EEYP was not modified, which suggests that motor function was preserved. This result corroborates those observed in the OF and EPM tests, where the treated animals did not show motor behavior or spontaneous deambulation affected.

3.5. Yellow Propolis Promotes Cognitive Effects in the Step-Down IA Test. Animals treated with EEYP at 30 mg/kg showed an increase in the step-down latency, which indicates

positive mnemonic activity at this dose (Figure 4). Surprisingly, such effect was more prominent than caffeine group (positive control group).

3.6. Yellow Propolis Shows Antioxidant Activity in the Oxidative Stress Evaluation. The behavioral training stress (BTS) induced by behavioral tests *per se*, represented by the control group, showed increased NO levels. Treatment with EEYP reversed this effect at dose-dependent manner, returning to basal levels even at the lowest dose 1 mg/kg (Figure 5(a)). In addition, the control group also exhibited a significant increase in serum MDA levels, which highlights the existence of oxidative stress in these animals compared to basal group. All doses of EEYP were able to inhibit the lipidic peroxidation process, decreasing MDA levels compared to control group, which may indicate that EEYP exhibits antioxidant activity (Figure 5(b)).

Regarding the antioxidant activity, behavioral tests increased TEAC levels and the treatment with EEYP did
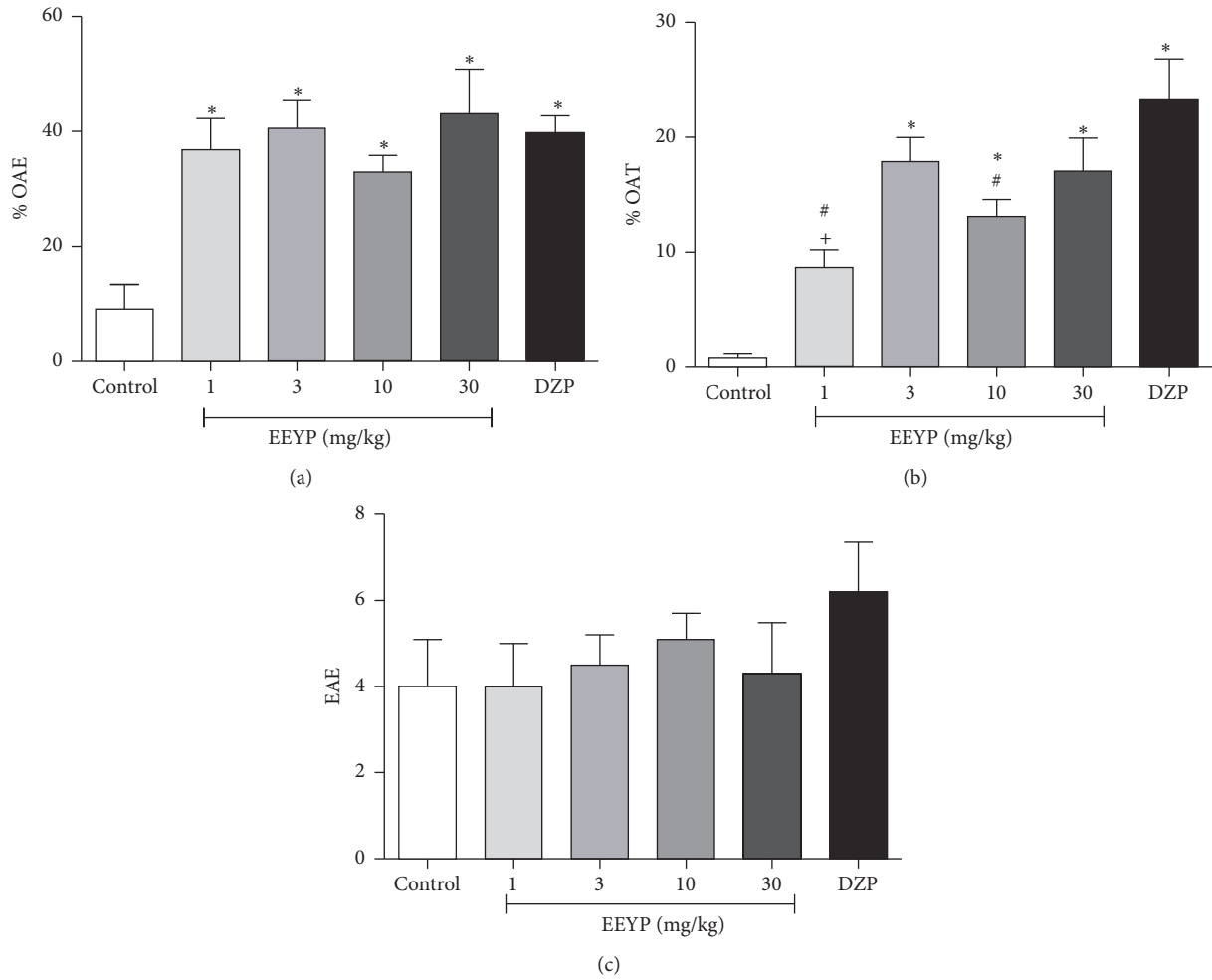
(a)

(b)

(c)

FIGURE 2: Effect of treatment with EEYP (1, 3, 10, and 30 mg/kg) on (a) entrances in the open arms (%); (b) time in the open arms (%); and (c) entrances in the enclosed arms in the elevated plus maze test. *$P < 0.05$ *versus* control group; #$P < 0.05$ *versus* diazepam (DZP) group; +$P < 0.05$ *versus* EEYP 3 mg/kg group. Values are expressed as mean ± SEM from 10 animals per group (ANOVA and Tukey's test).

(a)

(b)

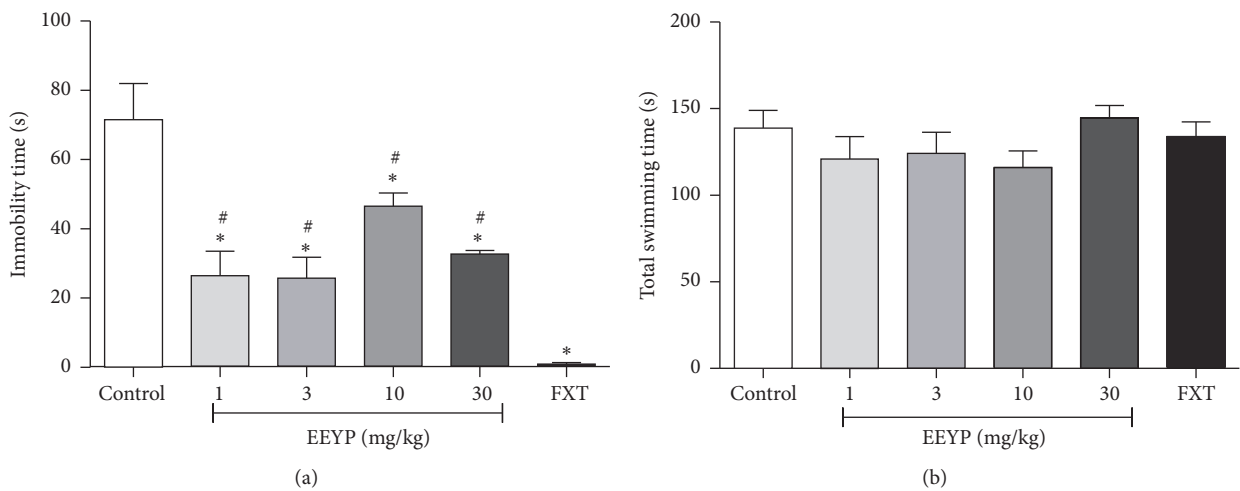FIGURE 3: Effect of treatment with EEYP (1, 3, 10, and 30 mg/kg) on (a) immobility time and (b) total swimming time in the forced swim test. *$P < 0.05$ *versus* control group; #$P < 0.05$ *versus* fluoxetine (FXT) group. Values are expressed as mean ± SEM from 10 animals per group (ANOVA and Tukey's test).
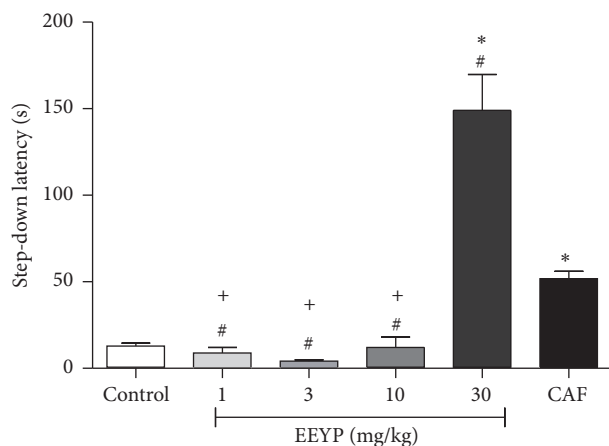
Figure 4: Effect of treatment with EEYP (1, 3, 10, and 30 mg/kg) on the step-down latency in the step-down inhibitory avoidance (IA) test. $*P < 0.05$ versus control group; $\#P < 0.05$ versus caffeine (CAF) group; $+P < 0.05$ versus EEYP 30 mg/kg group. Values are expressed as mean ± SEM from 10 animals per group (ANOVA and Tukey's test).

Table 1: Ratios between antioxidant (TEAC) factor and MDA levels of animals submitted to BTS and EEYP-treated BTS animals.

Groups	TEAC/MDA	P value
Control (BTS)	2.70 ± 1.23	
BTS+EEYP (1 mg/Kg)	$4.82 \pm 2.53^*$	0.0284
BTS+EEYP (3 mg/Kg)	$4.98 \pm 2.50^*$	0.0186
BTS+EEYP (10 mg/Kg)	4.23 ± 2.09	0.0614
BTS+EEYP (30 mg/Kg)	$5.46 \pm 2.19^*$	0.0027

$*P < 0.05$ versus control group.

signals at δ 4.69 (doublet) and δ 4.58 (multiplet), indicating geminal olefinic hydrogens. A doublet of doublets at δ 3.14 is typical for hydrogens bonded to carbinolic carbons in triterpenes and the constant coupling of 11.19 Hz indicated axial to axial coupling (Figure 7).

4. Discussion

The present study demonstrates, for the first time, that a sample of Brazilian yellow propolis, which is rich in triterpenes, mainly lupeol, shows anxiolytic- and antidepressant-like activities. Triterpenes may promote behavioral effects related to antioxidant mechanisms in rats. Acute administration of EEYP starting at 1 mg/Kg induced anxiolytic- and antidepressant-like activities, as well as cognitive and antioxidant effects as could be observed by carrying out different behavioral tests (OF, EPM, FS, and IA) followed by biochemical analysis.

Several studies have demonstrated the therapeutic potential of propolis, particularly its widely established antioxidant action, which has been related to the presence of flavonoids and phenolic acids in its composition. The activity of propolis on the CNS has also been reported [38]. However, little is known about the properties of the yellow Brazilian propolis, which has low content of phenolic compounds but is rich in terpene compounds [11]. Actually, the presence of triterpenes gives lipophilic characteristics to this sample of yellow propolis and it may facilitate drug passages across the blood-brain barrier.

Plants containing terpenoid compounds have been used as sedatives, tranquillizers, and anticonvulsants. Many volatile oils rich in terpenes have a variety of pharmacological activities such as anxiolytic, anticonvulsant, and antinociceptive [21, 39, 40]. Actually, the presence of triterpenes provides lipophilic characteristics to the yellow propolis, which may facilitate passage across the blood-brain barrier [41].

The results obtained in the OF test allow us to infer that the locomotor activity remained preserved after administration of EEYP. Indeed, we can ensure that sedative effect and motor impairment induced by EEYP were excluded from the data obtained in the behavioral experiments. In addition, the OF test indicates that EEYP presented anxiolytic activity. Similar results were also reported in a study where an oily extract of greenish brown propolis (dose ≥ 10 mg/kg) was found to have similar anxiolytic effects in the central ambulation of treated rats [18].

not change this parameter (Figure 6(a)). On the other hand, BTS inhibited antioxidant enzymes activities, such as CAT (Figure 6(b)) and SOD activities (Figure 6(c)). The treatment with EEYP also did not alter this enzymatic inhibition induced by behavioral stress, which indicates that others enzymatic or nonenzymatic pathways might be involved in antioxidant activity of EEYP. The ratio of TEAC to MDA was significantly higher in the EEYP-treated group if compared to control group (Table 1), mainly at dose of 30 mg/kg, confirming the antioxidant activity of EEYP.

3.7. Chemical Composition of Yellow Propolis. Previously, we reported the occurrence of a mixture of triterpenes belonging to ursane, lupane, oleanane, lanostane, and cycloartane skeletons in the Brazilian yellow propolis sample from Mato Grosso do Sul under evaluation [11]. The presence of such lipophilic compounds and the absence of aromatic compounds were confirmed by ^{1}H-NMR analysis of EEYP and fractions obtained by chromatography. By gas chromatography-mass spectrometry (GC-MS) analysis, lupeol and β-amyrin were identified as the main triterpenes in yellow propolis [11], representing 44.80% and 13.64%, respectively, of the total composition of the extract (see Table 1S in Supplementary Material available online at http://dx.doi.org/10.1155/2016/2906953). All fractions obtained by chromatographic fractionation of EEYP had similar chemical profiles by ^{1}H-NMR and showed the lack of aromatic compounds and predominance of high field resonances. By ^{1}H-NMR analysis of all fractions, lupeol was confirmed as one of the main constituents of yellow propolis (Figure 7) and its structure was assigned by comparing our data with ^{1}H-NMR from literature (Table 2S in Supplementary Material). Intense singlets in δ 0.76, 0.82, 0.86, 0.95, 0.97, and 1.06 are consistent with methyl groups bonded to quaternary sp^3 carbons. The olefinic unit was confirmed by
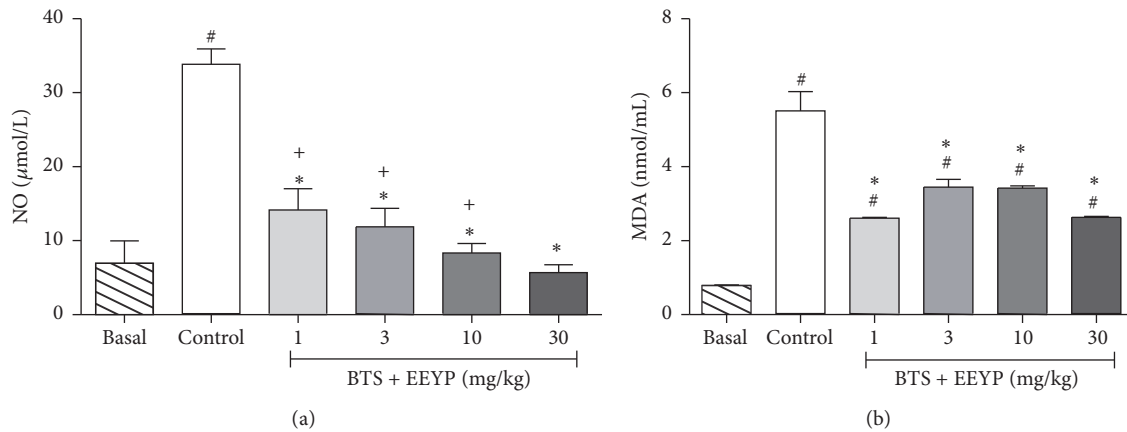
(a)

(b)

FIGURE 5: Effect of treatment with EEYP (1, 3, 10, and 30 mg/kg) on (a) nitric oxide (NO) and (b) malondialdehyde (MDA) levels of rats subjected to behavioral training stress (BTS). $^{*}P < 0.05$ *versus* control group; $^{\#}P < 0.05$ *versus* basal group; $^{+}P < 0.05$ *versus* EEYP 30 mg/kg group. Values are expressed as mean $\pm$ SEM from 10 animals per group (ANOVA and Tukey's test).

(a)

(b)

(c)

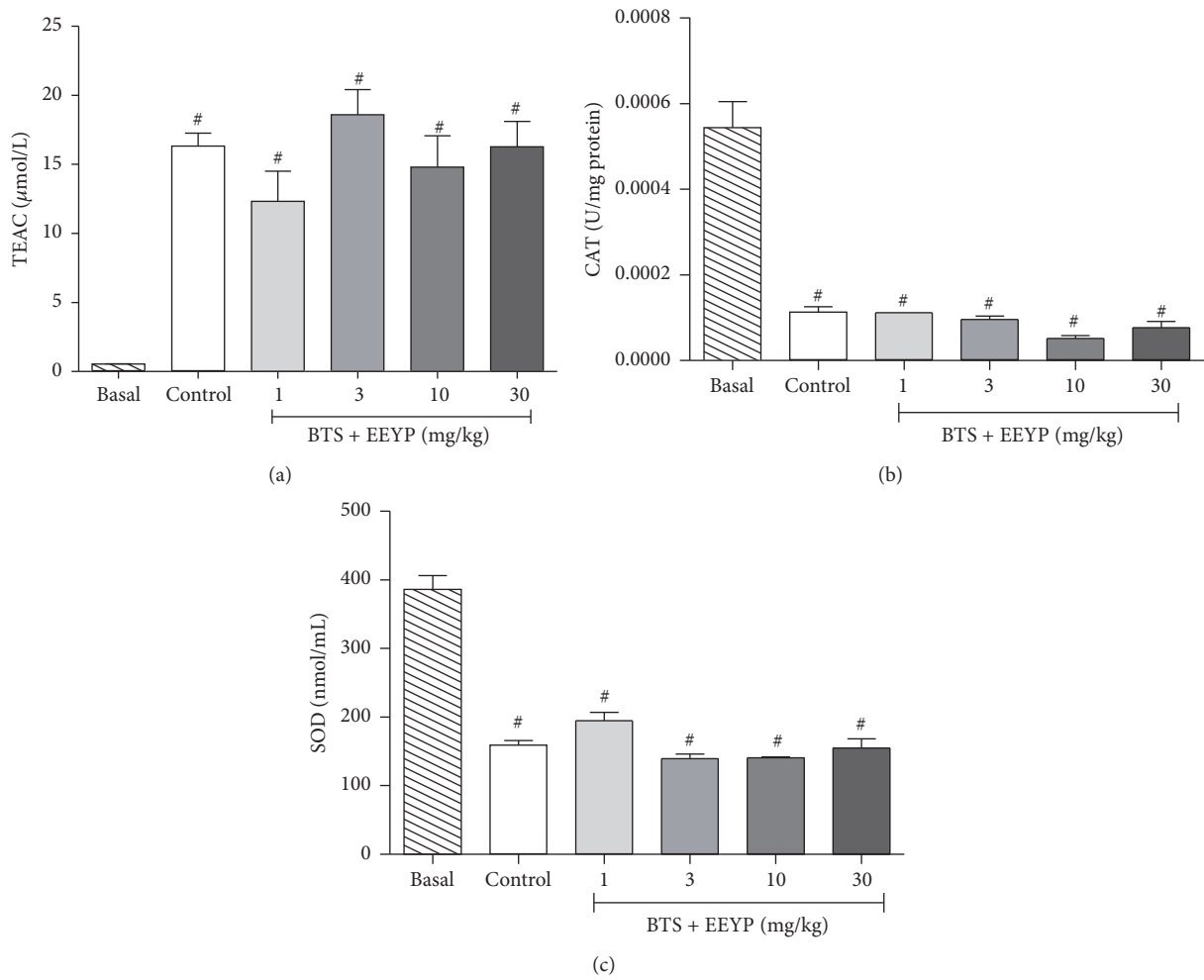FIGURE 6: Effect of treatment with EEYP (1, 3, 10, and 30 mg/kg) on (a) trolox equivalent antioxidant capacity, TEAC; (b) catalase, CAT; and (c) superoxide dismutase, SOD, activity of rats subjected to behavioral training stress (BTS). $^{*}P < 0.05$ *versus* control group; $^{\#}P < 0.05$ *versus* basal group. Values are expressed as mean $\pm$ SEM from 10 animals per group (ANOVA and Tukey's test).
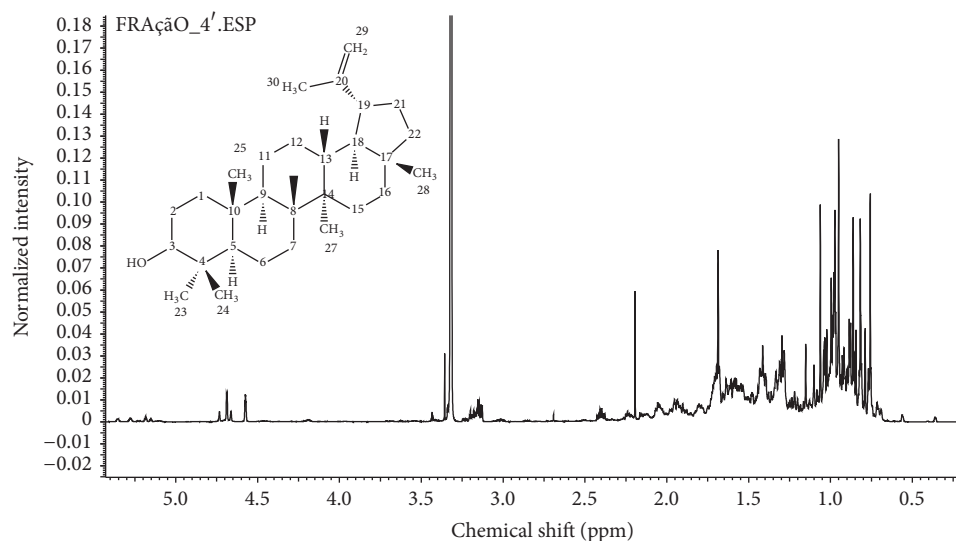
FIGURE 7: ^{1}H-NMR (600 MHz, $D_2O + CD_3OD$) of a chromatographic fraction (F4) containing lupeol as a main triterpene in yellow propolis.

The results obtained in the EPM test suggest that EEYP displays an anxiolytic-like effect starting at dose of 3 mg/kg that confirms the results obtained in the OF test. In addition, the walking ability of the animals was preserved in all treated groups, which indicates EEYP's ability to reduce anxiety while sedation was not induced. Similar results were obtained in animals treated with the oily extract of brown propolis at dose of 10 mg/kg [18]. As EEYP promoted such activity starting at 3 mg/Kg, we could infer that the hydroalcoholic extract was more potent than the oily extract [18], because it has elicited an anxiolytic-like effect in a dose at least 3-fold lower.

The behavioral results of animals treated with EEYP are consistent with studies of terpene compounds, such as carvacrol [42], (+)-epoxy limonene [43], linalool [44], 1,4-cineol [45], carvacryl acetate [46], and phytol [47], which also have shown anxiolytic action without changing locomotor activity.

In addition, our results are in agreement with a previous study [16], which found that the essential oil of a Brazilian green propolis sample, also rich in terpenes, reversed the anxiogenic behavior in mice and had no effect on locomotor activity. These effects were accompanied by a reduction in plasma levels of cortisol (CORT), adrenocorticotropic hormone (ACTH), and MDA with increase in SOD enzyme activity. These findings may suggest that the anxiolytic effects occur through the antagonism of hyperactivity of the HPA axis and the stimulation of antioxidant capacity in brain tissue [16].

Furthermore, several reports indicate that triterpenes exhibit anxiolytic-like activity. In this sense, a solution containing betulin, a triterpene structurally related to lupeol, has been patented as an anxiolytic remedy [48]. Posteriorly, it was demonstrated that betulin binds to gamma-aminobutyric acid A ($GABA_A$) which could explain the anxiolytic and anticonvulsant properties of this compound [49]. However, the authors also observed that lupane derivatives, such as lupeol, were not able to bind to $GABA_A$ receptors. In this sense, if lupeol produces anxiolytic effects, the probable mechanism does not include $GABA_A$ stimulation pathway. In fact, it has been shown that an isomeric mixture of triterpenes alpha- and beta-amyrin (2.5 and 5 mg/Kg, i.p.) from crude resin of *Protium heptaphyllum* induces enhancement of noradrenergic mechanisms [50]. Hence, we suggest that the anxiolytic effect observed can be induced by the monoaminergic system [51]. However, complementary studies are necessary to clarify the compounds responsible for anxiolytic activity and the precise mechanisms of action.

Beyond the anxiolytic-like effects, the EEYP showed antidepressant-like activity in the FS test. A previous study [18] also observed such activity. However, our data demonstrated that the EEYP revealed more prominent effects, at least 10-fold higher than the oily extract of propolis [18]. Similar results were also found when investigating the ethanolic extract of Korean propolis sample [17], which revealed a dose-dependent antidepressant activity, without changes to motor function. Lee and coauthors have found a reduction in GR function in the hippocampus, as well as HPA axis after the FS test, which was reversed by the propolis extract that is considered as one of the mechanisms of antidepressant therapy and may explain one probable mechanism of the propolis antidepressant activity.

Additionally, the isomeric mixture of triterpenes has also exhibited antidepressant response by noradrenergic mechanisms [50]. Similar effects, however, involving serotonergic transmission were observed with monoterpenes [52]. Thus, it is possible that the triterpenes found in EEYP have elicited the antidepressant effect through the monoaminergic pathway. Nevertheless, further investigations to elucidate the antidepressant mechanisms are required.

In the step-down IA test, animals treated with EEYP at 30 mg/kg showed increase in the step-down latency, indicating mnemonic activity at this dose. Cognitive effects were also

demonstrated by scopolamine-induced amnesia attenuation in rats after treatment with a water soluble fraction of propolis at dose of 100 mg/kg [53]. Furthermore, the fraction inhibited acetylcholinesterase activity in hippocampus of rats treated with scopolamine, enhancing the memory profile. In that study, the exact compound responsible for such effect was not identified; however, aromatic carboxylic acids and flavonoids were identified [53]. In this sense, our work highlights that the EEYP, which contains low levels of aromatic compounds and high contents of terpenes, triggered memory function at lower doses (30 mg/kg).

In stress conditions, excess generation of reactive oxygen species (ROS) and reactive nitrogen species (RNS) may lead to damage of various cell components, including induction of mitochondrial dysfunction, cytotoxic process of lipid cell membrane peroxidation, suppression of hippocampal synaptic plasticity [54], and triggering the activation of specific signaling pathways, such as proapoptotic pathways that result in apoptotic cell death [55]. Therefore, among other factors, such as genetic, neurochemical, neurobiological, and psychological, the oxidative stress plays an important role in the pathophysiology of anxiety and depression disorders [56]. In this regard, this oxidative/nitrosative stress can lead to the activation of intracellular signaling pathways and high levels of oxygen consumption in the brain, mainly in the hippocampus and prefrontal cortex, which consist of brain regions related to the pathophysiology of depression [56, 57]. Furthermore, oxidative stress also is associated with a dysregulation (hyper- or hypoactivity) of the hypothalamic-pituitary-adrenocortical (HPA) axis, which results in the increased levels of glucocorticoids (GCs) that alter antioxidant enzyme capacity, leading to the development of depressive disorders [58, 59]. During this oxidative process, increased lipid peroxidation and altered levels of antioxidant defenses, such as glutathione (GSH), CAT, and SOD enzymes, occur; therefore, strong antioxidants could be a promising approach to offering protection against anxiety and depression.

Regarding RNS, NO plays a vital role in CNS damage, since it reacts with the superoxide anion to produce peroxynitrite, which in turn triggers cell death by apoptosis process [60]. At least in part, the oxidative stress may elicit loss of the macromolecules function, as well as playing a key role in pathogenesis of several disorders, including neurodegenerative and others aging-associated diseases [61, 62]. Therefore, the TEAC activity increased altogether with higher NO and MDA levels in control group due to behavior stress, suggesting an enhanced ability to scavenge ROS in serum and tissue, as well as in the CNS. In this regard, our data also showed that EEYP treatment inhibited the NO levels elevation induced by BTS in a dose-dependent manner.

In the present study, lupeol was the main identified constituent of the yellow propolis. Lupeol acetate has been reported to significantly reduce NO production, inducible nitric oxide synthase (iNOS) protein levels, and lipopolysaccharide- (LPS-) induced cyclooxygenase- (COX-) 2 expression, showing antinociceptive and anti-inflammatory activities [63]. In another animal study, the lupeol also presented antinociceptive properties during inflammatory

pain, inhibiting interleukin- (IL-) 1β and tumor necrosis factor- (TNF-) α production induced by carrageenan [64]. Recently, it was reported that the chloroformic fraction of *Lafoensia pacari*, rich in β-sitosterol and lupeol, displays antidepressant-like activity by an action mechanism dependent on serotonergic and catecholaminergic systems, as well as increase of the hippocampal brain-derived neurotrophic factor (BDNF) protein concentration [65].

Other components presented in propolis also showed both neuroprotective and antioxidant effects. In fact, investigation of pinocembrin, a flavonoid present in high concentrations in some propolis, revealed an *in vivo* neuroprotective effect and also a reduction in NO production [9]. Furthermore, EEYP also reduced MDA levels induced by BTS at dose as low as 1 mg/kg, which confirms the antioxidant action of EEYP. This same effect was also observed when testing the essential oil of Brazilian green propolis but at a dose of 100 mg/kg [16]. Previous studies have shown that the essential oil of a sample of Brazilian propolis reduces plasma MDA levels, one biochemical marker of lipid peroxidation [66, 67].

On the other hand, cellular defense mechanisms against ROS-induced oxidative stress, involving enzymatic and/or nonenzymatic factors, play a key role in the ROS elimination and detoxification process of xenobiotic compounds [61, 68]. In this regard, our data showed that EEYP did not alter TEAC, as well as the inhibition of SOD and CAT activities induced by behavioral stress. However, the ratio between TEAC and MDA levels showed that the EEYP treatment displays antioxidants levels elevation relative to prooxidants, which supports the antioxidant effects of EEYP (Table 1). We suggest that the antioxidant activity of EEYP may be due to other enzymatic or nonenzymatic pathways, as glutathione (GSH). In this regard, there was a report that brown propolis extract from southeastern Brazil increases GSH levels in the skin of rats submitted to ultraviolet (UV) irradiation [69]. In agreement with these results, our group has revealed an antioxidant activity of an oily extract of brown propolis from the south of Brazil, related to NO levels reduction, with no effects on total antioxidant capacity changes in rats exposed to BTS [18]. Based on the literature, we suggest that the antioxidant activity of EEYP can be similar to a standard antioxidant (i.e., vitamin E), which has shown ability to inhibit the production of MDA and NO, as well as trigger the SOD activity in the same level of EEYP after administration in animal models [70–72].

The antioxidant action of Brazilian green propolis has been attributed to several components, such as flavonoids and terpenes [73]. In the same way, the antioxidant properties of EEYP are probably related to its terpenes constituents. Some studies have shown that terpene compounds are responsible for a strong antioxidant activity [74–78]. Monoterpenes, such as (−)-myrtenol, have shown an *in vitro* antioxidant activity, which prevents lipid peroxidation, as well as removing nitrite ion concentrations and hydroxyl radicals [79]. In addition, new (ent-)abietane-type diterpenoids and norditerpenoids were isolated from *Chloranthus sessilifolius* plants [80]. These authors showed that the former compound inhibited NO production in LPS-stimulated BV-2 microglial

cells, which evinces the antineuroinflammatory and antioxidant activities of these diterpenoids. Besides, (ent-)abietenes have been suggested as therapeutic alternatives for the treatment of neurodegenerative and other aging-associated diseases [80]. Moreover, the triterpenoid saponin (21-O-angeloyltheasapogenol E3; ATS-E3) isolated from *Camellia sinensis* plant seeds inhibited phagocytic uptake, ROS generation, and NO production by suppression of protein kinase B (PKB), also known as AKT; I kappa B kinase (IKK); and factor nuclear kappa B (NF-κB)-dependent inflammatory pathways in macrophage culture [78].

Several studies have shown that the supplementation with antioxidants, such as N-acetyl-cysteine (NAC), lipoic acid, tocopherol, resveratrol, and propolis, leads to a neuroprotective effect induced by glutamate excitotoxicity. In this context, elevated levels of extracellular glutamate may inhibit cystine uptake, which displays a marked decrease in intracellular GSH levels and stimulates the NO production even as it produces free radical, such as mitochondrial superoxide anion products, which promotes oxidative stress [60, 81–83]. In this respect, some constituents of propolis may exert neuroprotective effects via an antioxidant effects. Brazilian green propolis and its main constituents (chlorogenic acid, 3,4-di-O-caffeoylquinic acid, and 3,5-di-O-caffeoylquinic acid) were reported to inhibit lipid peroxidation in mouse forebrain homogenates and protect against the glutamate-induced cell damage by antioxidant activity [60]. In addition, Brazilian green propolis was shown to have neuroprotective effects in an *in vitro* model of neurotoxicity and to consist of a more potent inhibitor of H_2O_2-induced cell death, as well as to protect against the *in vivo* ischemic neuronal damage in a mice model of neuronal occlusion [84]. Recently, it was reported that the treatment with hydroalcoholic extract of red propolis (HERP) at dose of 10 mg/kg has anti-inflammatory action and exhibits neuroprotective properties, showing a significant improvement in the sciatic nerve injury (SNI) and increased number of myelinated fibres [85].

Although several drugs are available in the neurological disorders (i.e., anxiety, depression, and cognition) therapy, there is a lack of new drugs with better tolerability and efficacy. In this context, our results demonstrated that a sample of Brazilian yellow propolis appears as a potential drug for the treatment of CNS disorders.

5. Conclusions

In conclusion, our results indicate for the first time that Brazilian yellow propolis rich in triterpenes, mainly lupeol, elicits neurobehavioral effects such as anxiolytics and antidepressants at dose as low as 1 mg/kg. Indeed, EEYP also displays cognitive effects in Wistar rats at the highest dose of 30 mg/kg and it did not promote sedation. However, additional studies are needed to evaluate the signaling pathways that may be affected which can support the behavioral results reported in the present work.

List of Abbreviations

ABTS:	2, 2-Azinobis, 3-ethylbenzothiazoline, 6-sulfonate
ACTH:	Adrenocorticotropic hormone
ANOVA:	One-way analysis of variance
ATS-E3:	21-O-Angeloyltheasapogenol E3
BDNF:	Brain-derived neurotrophic factor
BTS:	Behavioral training stress
CAF:	Caffeine
CAPE:	Caffeic acid phenethyl ester
CAT:	Catalase
CNS:	Central Nervous System
CORT:	Cortisol
COX:	Cyclooxygenase
DZP:	Diazepam
EAE:	Frequency of enclosed arm entries
EEYP:	Ethanolic extract of yellow propolis
EPM:	Elevated plus maze test
FS:	Forced swimming test
FXT:	Fluoxetine
GABA$_A$:	Gamma-aminobutyric acid A
GR:	Glucocorticoid receptor
GSH:	Glutathione
HERP:	Hydroalcoholic extract of red propolis
HPA:	Hypothalamic-pituitary-adrenal
IA:	Step-down inhibitory avoidance
IKK:	I kappa B kinase
IL:	Interleukin
iNOS:	Inducible nitric oxide synthase
LPS:	Protein levels and lipopolysaccharide
MDA:	Malondialdehyde
NAC:	N-Acetyl-cysteine
NF-κB:	Nuclear factor kappa B
NO:	Nitric oxide
OAE:	Open arm entries
OAT:	Open arm time
OF:	Open field test
PKB:	Protein kinase B
RNS:	Reactive nitrogen species
ROS:	Reactive oxygen species
SEM:	Standard error of the mean
SNI:	Sciatic nerve injury
SOD:	Superoxide dismutase
TBARS:	Thiobarbituric acid reactive substances
TEAC:	Trolox equivalent antioxidant capacity
TNF:	Tumor necrosis factor
UV:	Ultraviolet.

Competing Interests

The authors have no financial or personal competing interests related to this work.

Authors' Contributions

All authors contributed to the design and execution of the project as well as partaking in the writing and editing the manuscript.

Acknowledgments

References

[1] M. Marcucci, "Propolis: chemical composition, biological properties and therapeutic activity," *Apidologie*, vol. 26, no. 2, pp. 83–99, 1995.

[2] V. S. Bankova, S. L. De Castro, and M. C. Marcucci, "Propolis: recent advances in chemistry and plant origin," *Apidologie*, vol. 31, no. 1, pp. 3–15, 2000.

[3] J. Adelmann, *Própolis: Variabilidade composicional, correlação com a flora e bioatividade antimicrobiana/antioxidante [Dissertação de Mestrado]*, Universidade Federal do Paraná, Curitiba, Brazil, 2005.

[4] V. Bankova, "Chemical diversity of propolis and the problem of standardization," *Journal of Ethnopharmacology*, vol. 100, no. 1-2, pp. 114–117, 2005.

[5] J. B. Daleprane and D. S. Abdalla, "Emerging roles of propolis: antioxidant, cardioprotective, and antiangiogenic actions," *Evidence-Based Complementary and Alternative Medicine*, vol. 2013, Article ID 175135, 8 pages, 2013.

[6] P. Montpied, F. de Bock, G. Rondouin et al., "Caffeic Acid Phenethyl Ester (CAPE) prevents inflammatory stress in organotypic hippocampal slice cultures," *Molecular Brain Research*, vol. 115, no. 2, pp. 111–120, 2003.

[7] M. E. Altuğ, Y. Serarslan, R. Bal et al., "Caffeic acid phenethyl ester protects rabbit brains against permanent focal ischemia by antioxidant action: a biochemical and planimetric study," *Brain Research*, vol. 1201, pp. 135–142, 2008.

[8] X. Wei, Z. Ma, C. V. Fontanilla et al., "Caffeic acid phenethyl ester prevents cerebellar granule neurons (CGNs) against glutamate-induced neurotoxicity," *Neuroscience*, vol. 155, no. 4, pp. 1098–1105, 2008.

[9] R. Liu, M. Gao, Z.-H. Yang, and G.-H. Du, "Pinocembrin protects rat brain against oxidation and apoptosis induced by ischemia-reperfusion both in vivo and in vitro," *Brain Research*, vol. 1216, pp. 104–115, 2008.

[10] Y. K. Park, S. M. Alencar, and C. L. Aguiar, "Botanical origin and chemical composition of Brazilian propolis," *Journal of Agricultural and Food Chemistry*, vol. 50, no. 9, pp. 2502–2506, 2002.

[11] C. S. Machado, J. B. Mokochinski, T. O. de Lira et al., "Comparative study of chemical composition and biological activity of yellow, green, brown, and red Brazilian propolis," *Evidence-Based Complementary and Alternative Medicine*, vol. 2016, Article ID 6057650, 11 pages, 2016.

[12] O. Cuesta-Rubio, A. L. Piccinelli, M. C. Fernandez, I. M. Hernández, A. Rosado, and L. Rastrelli, "Chemical characterization of Cuban propolis by HPLC-PDA, HPLC-MS, and NMR: the brown, red, and yellow Cuban varieties of propolis," *Journal of Agricultural and Food Chemistry*, vol. 55, no. 18, pp. 7502–7509, 2007.

[13] I. Márquez Hernández, O. Cuesta-Rubio, M. Campo Fernández et al., "Studies on the constituents of yellow cuban propolis: GC-MS determination of triterpenoids and flavonoids," *Journal of Agricultural and Food Chemistry*, vol. 58, no. 8, pp. 4725–4730, 2010.

[14] Y.-S. Kwon, D.-H. Park, E.-J. Shin et al., "Antioxidant propolis attenuates kainate-induced neurotoxicity via adenosine A1 receptor modulation in the rat," *Neuroscience Letters*, vol. 355, no. 3, pp. 231–235, 2004.

[15] F. Mannaa, K. A. El-Shamy, K. A. El-Shaikh, and M. El-Kassaby, "Efficacy of fish liver oil and propolis as neuroprotective agents in pilocarpine epileptic rats treated with valproate," *Pathophysiology*, vol. 18, no. 4, pp. 287–294, 2011.

[16] Y.-J. Li, H.-Z. Xuan, Q.-Y. Shou, Z.-G. Zhan, X. Lu, and F.-L. Hu, "Therapeutic effects of propolis essential oil on anxiety of restraint-stressed mice," *Human and Experimental Toxicology*, vol. 31, no. 2, pp. 157–165, 2012.

[17] M.-S. Lee, Y. H. Kim, W.-S. Park et al., "Novel antidepressant-like activity of propolis extract mediated by enhanced glucocorticoid receptor function in the hippocampus," *Evidence-Based Complementary and Alternative Medicine*, vol. 2013, Article ID 217853, 10 pages, 2013.

[18] J. S. S. Reis, G. B. Oliveira, M. C. Monteiro et al., "Antidepressant- and anxiolytic-like activities of an oil extract of propolis in rats," *Phytomedicine*, vol. 21, no. 11, pp. 1466–1472, 2014.

[19] D. P. De Sousa, F. F. De Farias Nóbrega, and R. N. De Almeida, "Influence of the chirality of (R)-(-)- and (S)-(+)-carvone in the central nervous system: a comparative study," *Chirality*, vol. 19, no. 4, pp. 264–268, 2007.

[20] D. P. De Sousa, F. F. F. Nóbrega, F. S. Claudino, R. N. De Almeida, J. R. Leite, and R. Mattei, "Pharmacological effects of the monoterpene α,β-epoxy-carvone in mice," *Brazilian Journal of Pharmacognosy*, vol. 17, no. 2, pp. 170–175, 2007.

[21] F. F. Perazzo, L. M. Lima, E. L. Maistro, J. E. Carvalho, V. L. G. Rehder, and J. C. T. Carvalho, "Effect of *Artemisia annua* L. leaves essential oil and ethanol extract on behavioral assays," *Revista Brasileira de Farmacognosia*, vol. 18, pp. 686–689, 2008.

[22] M. P. Leite, J. Fassin Jr., E. M. F. Baziloni, R. N. Almeida, R. Mattei, and J. R. Leite, "Behavioral effects of essential oil of *Citrus aurantium* L. inhalation in rats," *Revista Brasileira de Farmacognosia*, vol. 18, pp. 661–666, 2008.

[23] S. Pellow, P. Chopin, S. E. File, and M. Briley, "Validation of open: closed arm entries in an elevated plus-maze as a measure of anxiety in the rat," *Journal of Neuroscience Methods*, vol. 14, no. 3, pp. 149–167, 1985.

[24] R. D. Porsolt, G. Anton, N. Blavet, and M. Jalfre, "Behavioural despair in rats: a new model sensitive to antidepressant treatments," *European Journal of Pharmacology*, vol. 47, no. 4, pp. 379–391, 1978.

[25] C. D. S. F. Maia, G. M. R. D. S. Lucena, P. B. F. Corrêa et al., "Interference of ethanol and methylmercury in the developing central nervous system," *NeuroToxicology*, vol. 30, no. 1, pp. 23–30, 2009.

[26] G. M. Lucena, R. D. Prediger, M. V. Silva et al., "Ethanolic extract from bulbs of *Cipura paludosa* reduced long-lasting learning and memory deficits induced by prenatal methylmercury exposure in rats," *Developmental Cognitive Neuroscience*, vol. 3, no. 1, pp. 1–10, 2013.

[27] M. H. Malone, "Pharmacological approaches to natural products screening and evaluation," in *Natural Products and Plant*

Drugs with Pharmacological, Biological or Therapeutical Activity, H. Wagner and P. Wolf, Eds., pp. 23–53, Springer, Berlin, Germany, 1977.

[28] D. L. Granger, N. M. Anstey, W. C. Miller, and J. B. Weinberg, "Measuring nitric oxide production in human clinical studies," *Methods in Enzymology*, vol. 301, no. 1999, pp. 49–61, 1999.

[29] S. Percário, "Dosagem das LDLs modificadas através da peroxidação lipídica: correlação com o risco aterogênico," *Anais Médicos dos Hospitais e da Faculdade de Ciências Médicas da Santa Casa de São Paulo*, vol. 13, no. 49–52, pp. 7–9, 1994.

[30] H. I. Kohn and M. Liversedge, "On a new aerobic metabolite whose production by brain is inhibited by apomorphine, emetine, ergotamine, epinephrine, and menadione," *Journal of Pharmacology and Experimental Therapeutics*, vol. 82, no. 1994, pp. 292–300, 1994.

[31] A. A. Cohen, K. J. McGraw, and W. D. Robinson, "Serum antioxidant levels in wild birds vary in relation to diet, season, life history strategy, and species," *Oecologia*, vol. 161, no. 4, pp. 673–683, 2009.

[32] M. S. M. Rufino, R. E. Alves, E. S. Brito et al., "Determinação da atividade antioxidante total em frutas pela captura do radical livre DPPH," *Comunicado Técnico Embrapa*, vol. 127, no. 2007, pp. 1–4, 2007.

[33] R. Re, N. Pellegrini, A. Proteggente, A. Pannala, M. Yang, and C. Rice-Evans, "Antioxidant activity applying an improved ABTS radical cation decolorization assay," *Free Radical Biology & Medicine*, vol. 26, no. 9-10, pp. 1231–1237, 1999.

[34] H. Aebi, "Catalase in vitro," in *Methods in Enzymology*, L. Packer, Ed., vol. 105, pp. 121–126, Academic Press, Orlando, Fla, USA, 1984.

[35] B. Bukowska and S. Kowalska, "Phenol and catechol induce prehemolytic and hemolytic changes in human erythrocytes," *Toxicology Letters*, vol. 152, no. 1, pp. 73–84, 2004.

[36] J. M. McCord and I. Fridovich, "Superoxide dismutase. An enzymic function for erythrocuprein (hemocuprein)," *The Journal of Biological Chemistry*, vol. 244, no. 22, pp. 6049–6055, 1969.

[37] L. Flohé and F. Ötting, "Superoxide dismutase assays," *Methods in Enzymology*, vol. 105, pp. 93–104, 1984.

[38] T. Farooqui and A. A. Farooqui, "Beneficial effects of propolis on human health and neurological diseases," *Frontiers in Bioscience*, vol. 4, no. 2, pp. 779–793, 2012.

[39] S. K. Parmar, T. P. Sharma, V. B. Airao et al., "Neuropharmacological effects of triterpenoids," *Phytopharmacology*, vol. 4, no. 2, pp. 354–372, 2013.

[40] D. P. De Sousa, P. De Almeida Soares Hocayen, L. N. Andrade, and R. A. Andreatini, "A systematic review of the anxiolytic-like effects of essential oils in animal models," *Molecules*, vol. 20, no. 10, pp. 18620–18660, 2015.

[41] D. D. Shen, A. A. Artru, and K. K. Adkison, "Principles and applicability of CSF sampling for the assessment of CNS drug delivery and pharmacodynamics," *Advanced Drug Delivery Reviews*, vol. 56, no. 12, pp. 1825–1857, 2004.

[42] F. H. C. Melo, E. T. Venâncio, D. P. De Sousa et al., "Anxiolytic-like effect of Carvacrol (5-isopropyl-2-methylphenol) in mice: involvement with GABAergic transmission," *Fundamental and Clinical Pharmacology*, vol. 24, no. 4, pp. 437–443, 2010.

[43] A. A. C. de Almeida, J. P. Costa, R. B. F. de Carvalho, D. P. de Sousa, and R. M. de Freitas, "Evaluation of acute toxicity of a natural compound (+)-limonene epoxide and its anxiolytic-like action," *Brain Research*, vol. 1448, pp. 56–62, 2012.

[44] V. M. Linck, A. L. Da Silva, M. Figueiró, E. B. Caramão, P. R. H. Moreno, and E. Elisabetsky, "Effects of inhaled linalool in anxiety, social interaction and aggressive behavior in mice," *Phytomedicine*, vol. 17, no. 8-9, pp. 679–683, 2010.

[45] P. B. Gomes, M. L. Feitosa, M. I. G. Silva et al., "Anxiolytic-like effect of the monoterpene 1,4-cineole in mice," *Pharmacology Biochemistry and Behavior*, vol. 96, no. 3, pp. 287–293, 2010.

[46] L. F. Pires, L. M. Costa, O. A. Silva et al., "Anxiolytic-like effects of carvacryl acetate, a derivative of carvacrol, in mice," *Pharmacology Biochemistry and Behavior*, vol. 112, pp. 42–48, 2013.

[47] J. P. Costa, G. A. L. De Oliveira, A. A. C. De Almeida, M. T. Islam, D. P. De Sousa, and R. M. De Freitas, "Anxiolytic-like effects of phytol: possible involvement of GABAergic transmission," *Brain Research*, vol. 1547, pp. 34–42, 2014.

[48] T. Durst, Z. Merali, J. T. Arnason, E. P. Sanchez-Vindas, and A. L. Poveda, "Anxiolytic Marcgraviaceae compositions containing betulinic acid, betulinic acid derivates, and methods," Tech. Rep. WO/2002/091858, 2002.

[49] R. Muceniece, K. Saleniece, J. Rumaks et al., "Betulin binds to γ-aminobutyric acid receptors and exerts anticonvulsant action in mice," *Pharmacology Biochemistry and Behavior*, vol. 90, no. 4, pp. 712–716, 2008.

[50] G. F. Aragão, L. M. V. Carneiro, A. P. F. Junior et al., "A possible mechanism for anxiolytic and antidepressant effects of alpha- and beta-amyrin from *Protium heptaphyllum* (Aubl.) March," *Pharmacology Biochemistry and Behavior*, vol. 85, no. 4, pp. 827–834, 2006.

[51] G. Barrera, D. J. Echevarria, J.-F. Poulin, S. Laforest, G. Drolet, and D. A. Morilak, "One for all or one for one: Does co-transmission unify the concept of a brain galanin 'system' or clarify any consistent role in anxiety?" *Neuropeptides*, vol. 39, no. 3, pp. 289–292, 2005.

[52] S. L. Guzmán-Gutiérrez, H. Bonilla-Jaime, R. Gómez-Cansino, and R. Reyes-Chilpa, "Linalool and β-pinene exert their antidepressant-like activity through the monoaminergic pathway," *Life Sciences*, vol. 128, no. 205, pp. 24–29, 2015.

[53] J. Chen, Y. Long, M. Han, T. Wang, Q. Chen, and R. Wang, "Water-soluble derivative of propolis mitigates scopolamine-induced learning and memory impairment in mice," *Pharmacology Biochemistry and Behavior*, vol. 90, no. 3, pp. 441–446, 2008.

[54] M. Joëls, H. Karst, D. Alfarez et al., "Effects of chronic stress on structure and cell function in rat hippocampus and hypothalamus," *Stress*, vol. 7, no. 4, pp. 221–231, 2004.

[55] S. P. Cregan, A. Fortin, J. G. MacLaurin et al., "Apoptosis-inducing factor is involved in the regulation of caspase-independent neuronal cell death," *Journal of Cell Biology*, vol. 158, no. 3, pp. 507–517, 2002.

[56] M. Maes, P. Galecki, Y. S. Chang, and M. Berk, "A review on the oxidative and nitrosative stress (O&NS) pathways in major depression and their possible contribution to the (neuro)degenerative processes in that illness," *Progress in Neuro-Psychopharmacology & Biological Psychiatry*, vol. 35, no. 3, pp. 676–692, 2011.

[57] M. Joëls and T. Z. Baram, "The neuro-symphony of stress," *Nature Reviews Neuroscience*, vol. 10, no. 6, pp. 459–466, 2009.

[58] K. Mizoguchi, A. Ishige, M. Aburada, and T. Tabira, "Chronic stress attenuates glucocorticoid negative feedback: involvement of the prefrontal cortex and hippocampus," *Neuroscience*, vol. 119, no. 3, pp. 887–897, 2003.

[59] L. J. McIntosh, K. E. Hong, and R. M. Sapolsky, "Glucocorticoids may alter antioxidant enzyme capacity in the brain: baseline studies," *Brain Research*, vol. 791, no. 1-2, pp. 209–214, 1998.

[60] Y. Nakajima, M. Shimazawa, S. Mishima, and H. Hara, "Water extract of propolis and its main constituents, caffeoylquinic acid derivatives, exert neuroprotective effects via antioxidant actions," *Life Sciences*, vol. 80, no. 4, pp. 370–377, 2007.

[61] A. H. Bhat, K. B. Dar, S. Anees et al., "Oxidative stress, mitochondrial dysfunction and neurodegenerative diseases; a mechanistic insight," *Biomedicine & Pharmacotherapy*, vol. 74, pp. 101–110, 2015.

[62] E. Niedzielska, I. Smaga, M. Gawlik et al., "Oxidative stress in neurodegenerative diseases," *Molecular Neurobiology*, vol. 53, no. 6, pp. 4094–4125, 2015.

[63] Y.-F. Chen, C. Ching, T.-S. Wu, C.-R. Wu, W.-T. Hsieh, and H.-Y. Tsai, "*Balanophora spicata* and lupeol acetate possess antinociceptive and anti-inflammatory activities *in vivo* and *in vitro*," *Evidence-Based Complementary and Alternative Medicine*, vol. 2012, Article ID 371273, 10 pages, 2012.

[64] F. O. De Lima, V. Alves, J. M. Barbosa Filho et al., "Antinociceptive effect of lupeol: evidence for a role of cytokines inhibition," *Phytotherapy Research*, vol. 27, no. 10, pp. 1557–1563, 2013.

[65] P. M. Galdino, A. A. V. Carvalho, I. F. Florentino et al., "Involvement of monoaminergic systems in the antidepressant-like properties of *Lafoensia pacari* A. St. Hil.," *Journal of Ethnopharmacology*, vol. 170, pp. 218–225, 2015.

[66] G. Atungulu, M. Miura, E. Atungulu, Y. Satou, and K. Suzuki, "Activity of gaseous phase steam distilled propolis extracts on peroxidation and hydrolysis of rice lipids," *Journal of Food Engineering*, vol. 80, no. 3, pp. 850–858, 2007.

[67] G. Atungulu Griffiths, U. Toshitaka, T. Fumihiko, and H. Daisuke, "Effect of vapors from fractionated samples of propolis on microbial and oxidation damage of rice during storage," *Journal of Food Engineering*, vol. 88, no. 3, pp. 341–352, 2008.

[68] I. Solanki, P. Parihar, M. L. Mansuri, and M. S. Parihar, "Flavonoid-based therapies in the early management of neurodegenerative diseases," *Advances in Nutrition*, vol. 6, no. 1, pp. 64–72, 2015.

[69] Y. M. Fonseca, F. Marquele-Oliveira, F. T. M. C. Vicentini et al., "Evaluation of the potential of brazilian propolis against UV-induced oxidative stress," *Evidence-Based Complementary and Alternative Medicine*, vol. 2011, Article ID 863917, 8 pages, 2011.

[70] J. Li, D. Cai, X. Yao et al., "Protective effect of ginsenoside Rg1 on hematopoietic stem/progenitor cells through attenuating oxidative stress and the Wnt/β-catenin signaling pathway in a mouse model of d-galactose-induced aging," *International Journal of Molecular Science*, vol. 17, no. 6, pp. 1–17, 2016.

[71] X. Wang, R. Zhang, J. Du et al., "Vitamin E reduces hepatic fibrosis in mice with *Schistosoma japonicum* infection," *Molecular Medicine Reports*, vol. 5, no. 2, pp. 465–468, 2012.

[72] S. K. Das, S. Mukherjee, G. Gupta, D. N. Rao, and D. M. Vasudevan, "Protective effect of resveratrol and vitamin E against ethanol-induced oxidative damage in mice: biochemical and immunological basis," *Indian Journal of Biochemistry & Biophysics*, vol. 47, no. 1, pp. 32–37, 2010.

[73] Y. Nakajima, K. Tsuruma, M. Shimazawa, S. Mishima, and H. Hara, "Comparison of bee products based on assays of antioxidant capacities," *BMC Complementary and Alternative Medicine*, vol. 9, article 4, 2009.

[74] L. A. Tapondjou, L. B. T. Nyaa, P. Tane et al., "Cytotoxic and antioxidant triterpene saponins from *Butyrospermum parkii* (Sapotaceae)," *Carbohydrate Research*, vol. 346, no. 17, pp. 2699–2704, 2011.

[75] Y. A. Kim, C.-S. Kong, J. I. Lee et al., "Evaluation of novel antioxidant triterpenoid saponins from the halophyte *Salicornia herbacea*," *Bioorganic & Medicinal Chemistry Letters*, vol. 22, no. 13, pp. 4318–4322, 2012.

[76] S. Li, J. Zhao, Y. Liu et al., "New triterpenoid saponins from *Ilex cornuta* and their protective effects against H_2O_2-induced myocardial cell injury," *Journal of Agricultural and Food Chemistry*, vol. 62, no. 2, pp. 488–496, 2014.

[77] Z. Šarac, J. S. Matejić, Z. Z. Stojanović-Radić et al., "Biological activity of *Pinus nigra* terpenes—evaluation of FtsZ inhibition by selected compounds as contribution to their antimicrobial activity," *Computers in Biology and Medicine*, vol. 54, pp. 72–78, 2014.

[78] W. S. Yang, J. Ko, E. Kim et al., "21-O-angeloyltheasapogenol E3, a novel triterpenoid saponin from the seeds of tea plants, inhibits macrophage-mediated inflammatory responses in a NF-κB-dependent manner," *Mediators of Inflammation*, vol. 2014, Article ID 658351, 9 pages, 2014.

[79] M. R. C. Moreira, J. P. Costa, A. A. C. Almeida et al., "Anxiolytic and antioxidant potential of MYR11: support for the development of pharmaceutical formulations," in *Proceedings of the 4th Brazilian Congress of Biotechnology (CBBIOTEC '12)*, Guarujá, Brazil, 2012.

[80] L.-J. Wang, J. Xiong, S.-T. Liu, L.-L. Pan, G.-X. Yang, and J.-F. Hu, "ent-Abietane-type and related seco-/nor-diterpenoids from the rare chloranthaceae plant *Chloranthus sessilifolius* and their antineuroinflammatory activities," *Journal of Natural Products*, vol. 78, no. 7, pp. 1635–1646, 2015.

[81] D. T. Monaghan, R. J. Bridges, and C. W. Cotman, "The excitatory amino acid receptors: their classes, pharmacology, and distinct properties in the function of the central nervous system," *Annual Review of Pharmacology and Toxicology*, vol. 29, pp. 365–402, 1989.

[82] T. H. Murphy, M. Miyamoto, A. Sastre, R. L. Schnaar, and J. T. Coyle, "Glutamate toxicity in a neuronal cell line involves inhibition of cystine transport leading to oxidative stress," *Neuron*, vol. 2, no. 6, pp. 1547–1558, 1989.

[83] D. Han, C. K. Sen, S. Roy, M. S. Kobayashi, H. J. Tritschler, and L. Packer, "Protection against glutamate-induced cytotoxicity in C6 glial cells by thiol antioxidants," *American Journal of Physiology—Regulatory Integrative and Comparative Physiology*, vol. 273, no. 5, pp. R1771–R1778, 1997.

[84] M. Shimazawa, S. Chikamatsu, N. Morimoto, S. Mishima, H. Nagai, and H. Hara, "Neuroprotection by Brazilian green propolis against *in vitro* and *in vivo* ischemic neuronal damage," *Evidence-Based Complementary and Alternative Medicine*, vol. 2, no. 2, pp. 201–207, 2005.

[85] R. A. Barbosa, T. L. G. M. Nunes, T. L. G. M. Nunes et al., "Hydroalcoholic extract of red propolis promotes functional recovery and axon repair after sciatic nerve injury in rats," *Pharmaceutical Biology*, vol. 54, no. 6, pp. 993–1004, 2016.

Research Article

In Vitro Anti-AChE, Anti-BuChE, and Antioxidant Activity of 12 Extracts of *Eleutherococcus* Species

Daniel Załuski[1] and Rafał Kuźniewski[2]

[1]*Department of Pharmacognosy, Collegium Medicum, Jagiellonian University, 9 Medyczna Street, 30-688 Cracow, Poland*
[2]*Department of Pharmacognosy, Ludwik Rydygier Collegium Medicum, Nicolaus Copernicus University,*
 9 Marie Curie-Skłodowska Street, 85-094 Bydgoszcz, Poland

Correspondence should be addressed to Daniel Załuski; daniel_zaluski@onet.eu

Received 24 July 2016; Revised 7 September 2016; Accepted 15 September 2016

Academic Editor: Marta C. Monteiro

Neurodegenerative diseases are one of the most occurring diseases in developed and developing countries. The aim of this work focused on the screening of the natural inhibitors of AChE and BuChE and antioxidants in *Eleutherococcus* species. We found that the ethanol extracts of *E. setchuenensis* and *E. sessiliflorus* showed the strongest inhibition towards AChE (IC_{50}: 0.3 and 0.3 mg/mL, resp.). Among chloroform extracts, the most active appeared to be *E. gracilistylus* (IC_{50}: 0.37 mg/mL). In turn, the ethanol extract of *E. henryi* inhibited the strongest BuChE with IC_{50} value of 0.13 mg/mL. Among chloroform extracts, *E. gracilistylus*, *E. setchuenensis*, and *E. sessiliflorus* appeared to be the strongest with IC_{50} values of 0.12, 0.18, and 0.19 mg/mL. HPTLC screening confirmed the presence of inhibitors in extracts. All extracts exhibited anti-DPPH* activity and single antioxidants have been identified. To the best of our knowledge, no information was available on this activity of compounds in *Eleutherococcus*. These studies provide a biochemical basis for the regulation of AChE and BuChE and encourage us to continue isolation of active compounds.

1. Introduction

Acetylcholinesterase (AChE) and butyrylcholinesterase (BuChE) take part in the termination of nerve impulse transmission at the cholinergic synapses by rapid hydrolysis of acetylcholine (ACh). Excessive hydrolysis of acetylcholine (ACh) and butyrylcholine (BCh) is one of the causes of neurodegenerative diseases, such as Alzheimer's disease (AD), ataxia, or Parkinson's disease.

Alzheimer's disease (AD) is the most common cause of senile dementia in later life. This disease affects from 4% to 10% of the world's population over the age of 65 years. According to the statistics, in Poland, over 250 000 people suffer from AD, while in the United States the number of AD sufferers reached 4 million, and this number increases every single year. Inhibition of these enzymes serves as a strategy for the treatment of Alzheimer's disease (AD), senile dementia, ataxia, myasthenia gravis, and Parkinson's disease [1–4].

Many secondary plant metabolites and several synthetic substances exhibit anti-AChE and anti-BuChE activity; nevertheless, their use is still restricted. Currently used licensed drugs (tacrine, donepezil, and rivastigmine) show selectivity towards one of the two enzymes, which leads to a compensation mechanism and increased activity of the other one. It has been found that these compounds have adverse effects including gastrointestinal disturbances and problems associated with bioavailability. Besides, tacrine is hepatotoxic, and hepatoprotective drugs have to be used simultaneously. Rivastigmine (Exelon) was licensed for use in Europe in 2000. It is well known that synthetic inhibitors just slow the progress of the disease but do not cure it [5, 6].

One of the most intensively studied areas of research has been the investigation of plants with an anticholinesterase action. The increasing incidence of AD has given fresh impetus to the search for novel anti-AChE and anti-BuChE agents. New lead compounds are also needed in the field of pharmacotherapy, phytotherapy, and natural products.

A new source of AChE and BuChE inhibitors can be secondary metabolites present in *Eleutherococcus* species, which are native to Eastern Asia, the Himalayas, and Northeastern Russia. The main secondary metabolites are polyphenols that include eleutherosides B, B1, E, and E1 and are thought to be

the pharmacologically most active constituents [7–12]. These species have been used in old Chinese pharmacy for improving human's physical and mental efficiency. People used to believe that they improve cognitive functions, such as learning or memory; thus, scientists now take into account the use of *Eleutherococcus* in neurodegenerative ailments.

Only few papers describing a weak inhibitory effect of *E. senticosus* on the regeneration of neuritis damaged by amyloid β(25–35) have been found. The authors have suggested that *E. senticosus* may be a candidate useful for developing therapeutic drugs for Alzheimer's disease. But authors have not provided any explanation for the possible mechanism of the extract's action and the influence on AChE and BuChE activity. The studies of the other research group showed that *E. senticosus* improves mental process in rats and reduces hippocampal CA1 neuronal death [13, 14]. Nevertheless, no further information on the inhibitory activity of remaining species (*E. setchuenensis*, *E. divaricatus*, *E. henryi*, *E. sessiliflorus*, and *E. gracilistylus*) towards AChE and BuChE has been found.

On the basis of Załuski's previous studies, it is concluded that these plants are a very promising source of biologically active substances. They inhibit metalloproteinases (MMPs, belonging to the hydrolase enzyme family, like AChE and BuChE) and neutralize free radicals. It was established that MMPs and free radicals take part in the etiopathogenesis of Alzheimer's disease as well. Some authors have reported on the damaging effects of ROS on neurones and on PD, AD, and ALS development. The oxidative stress is involved in the propagation of cellular injury that leads to neuropathology [15, 16].

The discovery of new inhibitors of AChE and BuChE is a highly attractive target both scientifically and commercially; for these reasons, there is a need to examine anti-AChE and anti-BuChE activity of *Eleutherococcus* species. To our knowledge, there are no such phytochemical reports concerning these cultivars. As part of a program to search for bioactive constituents from *Eleutherococcus* species, this study was focused on the establishment of anti-AChE and anti-BuChE activities of six *Eleutherococcus* species and aimed to discuss the possible antienzymatic mechanism and the structure-activity relationship. The work aimed at searching for antioxidants as well.

2. Materials and Methods

2.1. Standards and Reagents. Physostigmine, Ellman's reagent (DTNB, 5,5′-dithiobis(2-nitrobenzoic acid)), ATCh (acetylthiocholine iodide), BTCh (S-butyrylthiocholine iodide), AChE (acetylcholinesterase, *Electrophorus electricus*), BuChE (human plasma butyrylcholinesterase), sodium phosphate buffer, pH 7.0, and DPPH (2,2-diphenyl-1-picrylhydrazyl) were obtained from Sigma-Aldrich. Ethanol was obtained from POCH (Lublin, Poland). All other reagents were of analytical grade.

2.2. Plant Material. The roots of *E. senticosus* (Rupr. et Maxim.) Maxim., *E. divaricatus* (Siebold et Zucc.) S. Y. Hu, *E. setchuenensis* (Harms) Nakai, *E. sessiliflorus* (Rupr. &

Maxim.) S. Y. Hu, *E. gracilistylus* (W. W. Smith) S. Y. Hu, and *E. henryi* Oliv. were collected at the arboretum in Rogów (Poland) in October 2015 (voucher specimen numbers: ES01, ED02, ESetch03, ESes04, EG05, and EH06). All plant samples were deposited at the Department of Pharmacognosy, Collegium Medicum, Jagiellonian University, Cracow, Poland.

2.3. Dried Material Extraction with 75% Ethanol. The air-dried roots (5 g each) were soaked in 50 mL 75% ethanol for 24 h. Next, the samples were subjected to triple UAE type extraction (ultrasonic bath, Polsonic, Warsaw, Poland) using 1×50 mL and 2×25 mL of 75% ethanol. The extraction was performed at room temperature for 15 min for each cycle. Finally, 100 mL of each extract was obtained. The solvents were dried with an evaporator under vacuum conditions at 45°C and subjected to lyophilisation.

2.4. Dried Material Extraction with Chloroform. The roots were extracted in the same way as extraction with 75% ethanol using chloroform.

2.5. Antienzymatic Studies: Antiacetylcholinesterase and Antibutyrylcholinesterase Activities. The inhibition of AChE and BuChE was determined by the spectrophotometric method of Ellman et al. [17], and absorbance was measured on a multidetection BioTek spectrophotometer. The enzyme activity was 5 U/mg protein, and concentration of ATCh and BTCh was 15 mmol, DTNB (0.15 mmol). The extracts concentrations were 0.1, 0.5, 1.0, and 1.5 mg/mL in 10% water ethanol solution. The final concentrations in the reaction's mixture were 2.2, 11, 22, and 33 μg/0.195 mL. Physostigmine was used as positive control at the following concentrations: 2, 3, 4, 15, 30, and 40 μg/0.195 mL. Every assay was done in triplicate.

2.6. HPTLC Screening for Inhibitors of AChE and BuChE: Direct Bioautography (DB) Technique. HPTLC was performed using the method described by Załuski et al. [12]. Si$_{60}$ HPTLC F$_{254}$ plates and the following mobile phases were used: chloroform : methanol : water 70 : 30 : 4 v/v/v for the ethanol extracts and chloroform : diethyl ether 1 : 1 v/v for the chloroform extracts. The plates were developed for a distance of 90 mm. After drying at room temperature, the plates were dipped into the solution of AChE or BuChE (5 s) and next into Ellman's reagent, redried, and incubated for 30 min at 37°C in humid atmosphere. Subsequently, the chromatoplates were immersed for 5 s in the dipping solution of substrates (acetylthiocholine). After 3 min, white spots for AChE and BuChE inhibiting compounds should be detected on a yellow (in Ellman's reaction) background. The enzyme activity was 5 U/mg protein, and the concentration of ACh and BuCh was 15 mmol, DTNB (0.15 mmol).

2.7. HPTLC Screening for Antioxidants: Direct Bioautography (DB) Technique. TLC was done according to the method of Załuski et al. [12]. Briefly, TLC was performed on 10 cm × 20 cm glass Si60 HPTLC$_{F254}$ plates using chloroform : methanol : water 70 : 30 : 4 v/v/v for the ethanol extracts and chloroform : diethyl ether 1 : 1 v/v for the chloroform extracts.

The plate was developed for a distance of 90 mm. The plate was dried at room temperature for 20 min. After this time, the plate was immersed into 0.5% DPPH solution for 5 sec. Active compounds appeared as yellow-white spots against a purple background. White spots were visualized under day light after 1 min, 30 min, 1 h, 2 h, 5 h, 10 h, and 24 h.

2.8. Statistical Analysis. Determinations were performed in triplicate. The obtained data were subjected to statistical analysis using Statistica 7.0. (StatSoft, Cracow). The evaluations were analyzed for one-factor variance analysis. Statistical differences between the treatment groups were estimated by Spearman's (R) and Pearson's (r) test. All statistical tests were carried out at a significance level of $\alpha = 0.05$.

3. Results and Discussion

3.1. Antienzymatic Activity. Various studies were performed concerning anticholinesterase activity of plant extracts or isolated compounds; however, up to now, most of the studies were focused on anti-AChE activity, not BuChE. Some of them are used to minimize the symptoms of neurodegenerative disorders, such as AD. Presently, several referenced natural acetylcholinesterase inhibitors are known, including physostigmine, galantamine, and huperzine A. The best known natural inhibitor of AChE is pyrroloindole alkaloid physostigmine isolated from *Physostigma venenosum*. Unfortunately, its use is limited due to poor intestinal absorption in humans. Another alkaloid, galantamine (Reminyl), isolated from *Galanthus nivalis* and *Leucojum vernum* is the additive to drugs used for the treatment of AD and was also licensed for use in early stages of AD in 2001. Their ingredients include plants extracts or pure isolates. A large number of alkaloids have been found to inhibit *in vitro* AChE. Studies on a variety of alkaloids have been performed focusing mainly on AChE activity, not BuChE. However, BuChE plays an important role as AChE, and the inhibition of just AChE can lead to a compensation mechanism and increased activity of the other one [6, 18]. Therefore, there is a need to search for inhibitors not only of AChE, but also of BuChE. Apart from enzymes activity, the second factor having an impact on neurodegenerative diseases is oxidative stress, which leads to neuronal damage.

In ancient times, people used to believe that *Eleutherococcus* species, especially *E. senticosus*, may have an impact on prevention of memory impairment or treatment of memory disorders. To give these observations a scientific basis, studies in this work aimed at the searching for both inhibitors AChE and BuChE and antioxidants in 12 extracts of six *Eleutherococcus* species (polar and nonpolar constituents).

The IC_{50} values for extracts measured by the microplate assay are shown in Table 1. In order to compare the antienzymatic activities of the extracts analyzed, physostigmine was used as the standard compound because of its well recognized activity. Physostigmine inhibited AChE in a dose-dependent way and 100% of inhibition was observed at concentration 30 μg/195 μL of the reaction mixture with IC_{50} value of 5 μg.

The ethanol extracts of *E. setchuenensis* and *E. sessiliflorus* showed the strongest inhibition towards AChE (IC_{50}: 0.3

TABLE 1: IC_{50} values for extracts (mg/mL). NA: not active.

Species	75% ethanol		Chloroform	
	AChE	BuChE	AChE	BuChE
E. senticosus	0.46 ± 0.04	0.73 ± 0.1	0.75 ± 0.08	0.71 ± 0.08
E. divaricatus	0.94 ± 0.09	0.54 ± 0.04	NA	1.68 ± 0.3
E. setchuenensis	0.3 ± 0.06	0.95 ± 0.2	1.08 ± 0.1	0.18 ± 0.01
E. sessiliflorus	0.3 ± 0.06	0.59 ± 0.04	NA	0.19 ± 0.01
E. henryi	1.75 ± 0.1	0.13 ± 0.02	NA	1.21 ± 0.2
E. gracilistylus	0.41 ± 0.02	1.22 ± 0.3	0.37 ± 0.05	0.12 ± 0.04

and 0.3 mg/mL, resp.); among chloroform extracts, the most active appeared to be *E. gracilistylus* (IC_{50}: 0.37 mg/mL). In turn, the ethanol extract of *E. henryi* was the strongest inhibitor towards BuChE with IC_{50} value of 0.13 mg/mL. Among chloroform extracts, *E. gracilistylus*, *E. setchuenensis*, and *E. sessiliflorus* appeared to be the strongest with IC_{50} values of 0.12, 0.18, and 0.19 mg/mL. According to Vinutha et al., plant extracts with an anti-AChE activity can be classified into 3 groups: potent group (>50% inhibition), moderate group (30–50% inhibition), and low activity group (<30% inhibition) [19].

Plant-based inhibitors of AChE and BuChE have been found in different plant families, such as Malvaceae, Rutaceae, Asteraceae, Fumariaceae, Papaveraceae, Lamiaceae, or Coniferaceae. According to scientific reports, some species used in traditional European medicine demonstrate inhibitory activity towards both AChE and BuChE. In screening studies, 12 species of plants have been used as remedies for the central nervous system. Of the 24 plant extracts (methanol and hexane), it was found that *Arnica chamissonis* Less. subsp. *foliosa* (Asteraceae) and *Ruta graveolens* L. (Rutaceae) had significant dose-dependent inhibition in the range between 29 and 88 μg/mL (IC_{50} dose). But this effect was less than of the references galantamine and physostigmine. Other species have not had any significant AChE and BuChE inhibitory activity. Comparing the results obtained in this work to those cited above, it may be concluded that the chloroform extract from the roots of *E. setchuenensis*, *E. sessiliflorus*, and *E. gracilistylus* exhibited similar activity, towards BuChE, to the hexane extract from the herb of *Ruta graveolens* and the flowers of *Arnica chamissonis*. The 50% of inhibition was observed for the extract concentrations of 61 and 88 μg/mL, respectively. In turn, the methanolic extracts from the herb of *Ruta graveolens* and the flowers of *Arnica chamissonis* showed stronger inhibition towards AChE than some *Eleutherococcus* species (IC_{50}: 34 and 29 μg/mL, resp.) [20]. The results of other studies have shown that from 180 medicinal plants only flavonoids isolated from *Agrimonia pilosa* Ledeb. inhibited AChE significantly [21]. Based on the results of already published studies, of 32 tested plants, the methanolic extracts from the roots of *Stephania suberosa* (L. L. Forman) and *Tabernaemontana divaricata* L. have shown high inhibitory activity, above 90%, at concentration of 0.1 mg/mL. In turn, the extracts from stems of *Piper interruptum* Opiz., seeds of *Piper nigrum* L., rootbarks of *Butea superba* Roxb., and roots of *Cassia fistula* L. showed 50–65% inhibitory activity

TABLE 2: Comparison of R_f values and a number of compounds for free radical scavenging HPTLC fingerprints for the ethanol extracts.

| Sample | R_f | | | | | | | | Number of compounds |
	0.18	0.54	0.61	0.66	0.70	0.76	0.79	0.82	
E. senticosus	+	+	+		+	+			5
E. divaricatus	+	+	+		+	+			5
E. setchuenensis	+	+	+		+	+	+	+	7
E. sessiliflorus	+	+	+		+	+			5
E. henryi	+	+	+	+	+	+	+	+	8
E. gracilistylus	+	+	+	+	+	+	+	+	8

on AChE at concentration of 0.1 mg/mL [22]. Biju et al. reported on anti-AChE activity of the ethanol extracts from *Baliospermum montanum*, *Humboldtia brunonis* Wall. var. *raktapushpa*, and *Pittosporum viridulum*. The IC$_{50}$ values obtained in this study were a little bit lower than those obtained in the presented work (137.5, 105.7, and 128.3 μg/mL for *Baliospermum montanum*, *Humboldtia brunonis*, and *Pittosporum viridulum*, resp.) [23]. The latest studies on the inhibition of AChE and BChE by the ethanol extracts from the leaves, stems, and flowers of *Euphorbia characias* subsp. *characias* revealed a weak effect with the IC$_{50}$ values in the range between 0.6 and 5.8 mg/mL for AChE and 0.3 and 1.2 for BuChE, respectively. The IC$_{50}$ values were, in some cases, ten orders of magnitude higher compared to the results obtained in this report [24]. According to Kaufmann et al., the methanolic extracts from *Berberis bealei* and *Phellodendron chinense* showed low IC$_{50}$ values towards AChE (34.1 and 8.03 mg/mL, resp.). Despite the fact that these plants contain the alkaloids berberine, coptisine, and palmatine as the predominant compounds, their activity was weaker in comparison to the obtained results [25]. The AChE and BuChE inhibitory activity of the roots, leaves, and stem of *Jatropha gossypifolia* has been described. It appeared that the leaves ethyl acetate extract and the roots dichloromethane extract inhibited AChE the strongest with IC$_{50}$ values 95.7 and 176.3 μg/mL. The roots dichloromethane extract inhibited BuChE with IC$_{50}$ value 77.6 μg/mL [26]. Taking into consideration anti-AChE and anti-BuChE activities of plants extracts, some authors state that such an activity is dependent on all compounds which act synergistically. Therefore, plant extracts are very often used alone or as a combination with synthetic drugs to reduce side effects or maximize therapeutic outcomes.

In the next step, the bioautography test was used to identify single potential inhibitors. The extracts were developed on HPTLC plates with the solvent system chloroform : methanol : water 70 : 30 : 4 v/v/v for the ethanol extracts and chloroform : diethyl ether 1 : 1 v/v for the chloroform extracts. The use of TLC screening for plant-based enzyme inhibitors is a rapid method and is free of disturbances due to the solvent. The AChE and BuChE inhibiting spots seen after spraying the substrate and enzyme are shown in Figures 1 and 2. All extracts have had AChE and BuChE inhibitors, which appeared as white spots on a pale yellow background. The same compounds have been identified as inhibitors of AChE and BuChE in the ethanol extracts at the R_f value as indicated

TABLE 3: Comparison of R_f values and a number of compounds for free radical scavenging HPTLC fingerprints for the chloroform extracts.

| Sample | R_f | | | | Number of compounds |
	0.33	0.52	0.62	0.70	
E. senticosus	+	+	+	+	4
E. divaricatus	+	+	+	+	4
E. setchuenensis		+	+	+	3
E. sessiliflorus		+	+	+	3
E. henryi		+	+	+	3
E. gracilistylus		+	+	+	3

in Figure 1. Each of the ethanol extracts had 4 inhibitors with R_f values 0.15, 0.19, 0.52, and 0.72 for AChE and 0.15, 0.17, 0.38, and 0.77 for BuChE. Considering chloroform extracts, 5 compounds in each extract have been identified to be potential inhibitors of AChE (R_f values 0.13, 0.27, 0.48, 0.66, and 0.78) and BuChE (R_f values 0.19, 0.39, 0.4, 0.53, and 0.70).

3.2. HPTLC-DB of Antioxidants. Since many of the constituents of herbal extracts possess an antioxidative capacity, it is believed that this property may be involved, at least in part, in the antineurodegenerative mechanism of the herbal extract. The second part of the experiment was focused on the chromatographic identification of DPPH* scavengers, based partially on the fingerprinting conditions and results obtained by Załuski et al. [12]. The results are presented in Figures 3 and 4, as well as in Tables 2 and 3. Compounds that exhibit antiradical potential show up as yellow spots against a purple background. We observed the plates after 1 min, 30 min, 1 h, 2 h, 5 h, 10 h, and 24 h from the time of immersion of the plate in 0.5% DPPH* solution. After 1 min, the ethanol extracts showed areas of activity on high R_f of 0.18 and 0.54. The compound at R_f 0.18 appeared as a strong-yellow spot, which correlates with its high anti-DPPH* activity. An additional yellow-coloured compound was observed to migrate at R_f of 0.61 and 0.7. Three other yellow spots at R_f values of 0.66, 0.79, and 0.82 appeared after 10 h. With all the investigated extracts, the richest in antioxidants are of *E. henryi* and *E. gracilistylus* (8 compounds). The results for all species remain in good agreement with the data referring to the spectrophotometric DPPH* assay method. Załuski et al. exhibited
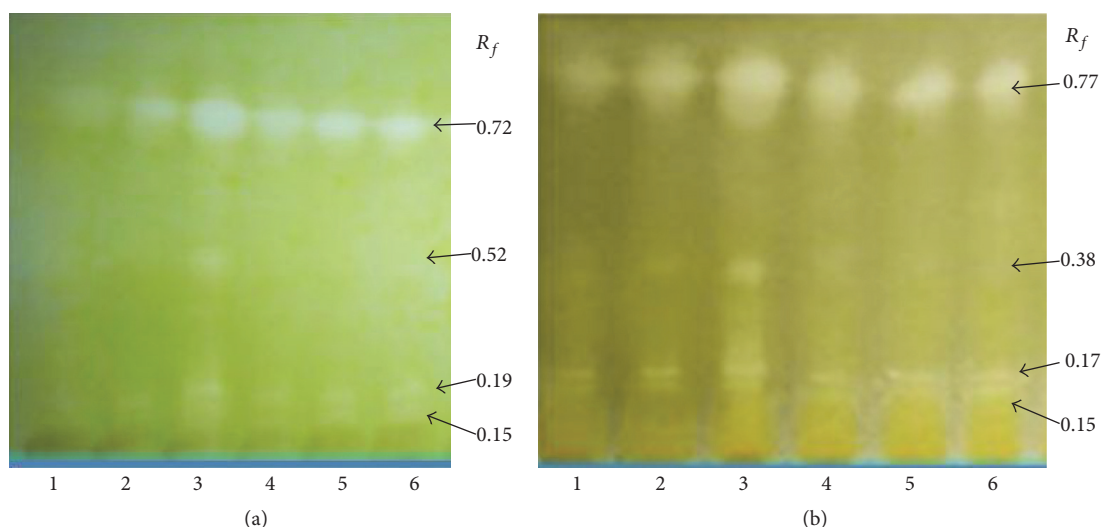
FIGURE 1: Screening of ethanol extracts of *Eleutherococcus* for AChE (a) and BuChE (b) inhibitors using the HPTLC assay method. White spots, corresponding to R_f values, on the yellow background represent the inhibition. (1) *E. senticosus*, (2) *E. divaricatus*, (3) *E. setchuenensis*, (4) *E. sessiliflorus*, (5) *E. henryi*, and (6) *E. gracilistylus*.
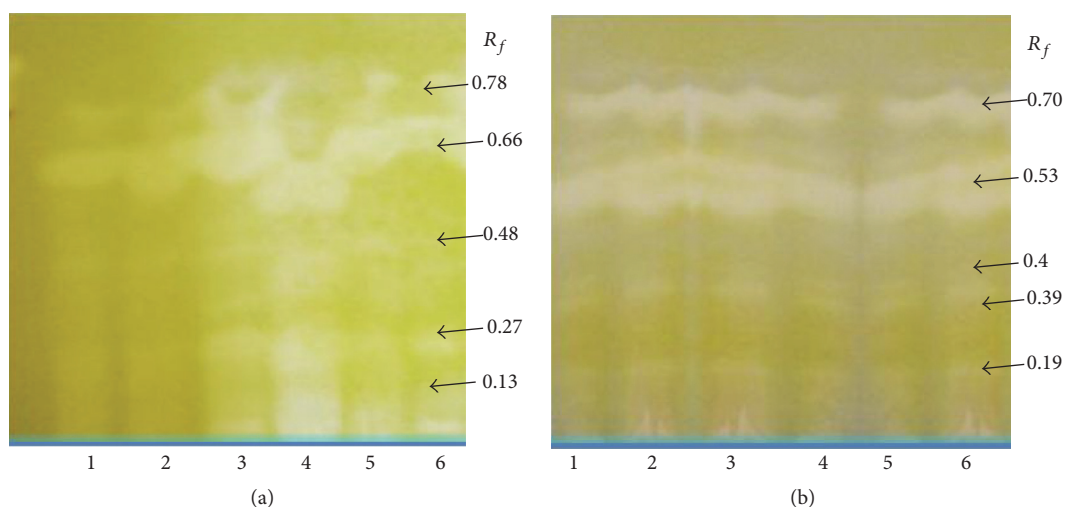

FIGURE 2: Screening of chloroform extracts of *Eleutherococcus* for AChE (a) and BuChE (b) inhibitors using the HPTLC assay method. White spots, corresponding to R_f values, on the yellow background represent the inhibition. (1) *E. senticosus*, (2) *E. divaricatus*, (3) *E. setchuenensis*, (4) *E. sessiliflorus*, (5) *E. henryi*, and (6) *E. gracilistylus*.

good radical scavenging activity of the ethanol extracts with EC_{50} values between 1.2 and 3.5 mg/mL [11].

Taking into account the speed of DPPH* decolourization by chloroform extracts, the differences have been noticed. Because of the presence of nonpolar compounds, the chloroform extracts exhibited a smaller number of inhibition zones. After 1 min, the extracts showed areas of activity on high R_f of 0.33, 0.52, 0.62, and 0.7. In all the analyzed species, compounds at R_f values of 0.52, 0.62, and 0.7 were detected. Among them, the compound at R_f value of 0.62 appeared as the most intensive yellow band.

3.3. Chemical Backgrounds of Anti-AChE, Anti-BuChE, and Antioxidant Activity of the Analyzed Extracts. This work has

been a continuation of the work on phytochemistry and bioactivity of *Eleutherococcus* species since 2008. The chemical profile of the species includes mainly polyphenols, of which the most abundant are eleutherosides B, E, and E1. This group of compounds is thought to be the most pharmacologically active. In Załuski's previous studies on *Eleutherococcus*, it was revealed that the analyzed species contain eleutherosides B, E, and E1, even in a larger amount than what the Polish or European Pharmacopoeia requires. According to the Polish Pharmacopoeia monograph, the root of *E. senticosus* should contain minimum 0.08% for the sum of eleutheroside B and eleutheroside E. On the basis of the HPTLC-densitometric assay, the amount of eleutheroside B ranged from 0.08 to 0.34%; that of eleutheroside E from 0.05 to
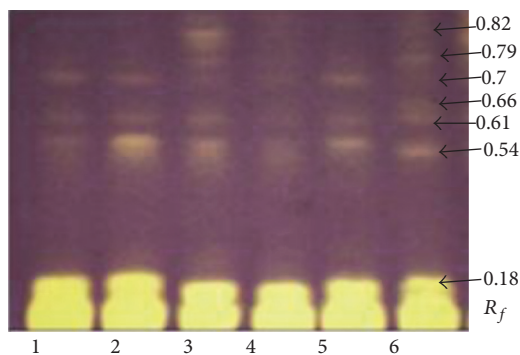
Figure 3: Screening of ethanol extracts of *Eleutherococcus* for anti-DPPH* scavengers using the HPTLC assay method. Yellow spots, corresponding to R_f values, on the purple background represent the inhibition. (1) *E. senticosus*, (2) *E. divaricatus*, (3) *E. setchuenensis*, (4) *E. sessiliflorus*, (5) *E. henryi*, and (6) *E. gracilistylus*.
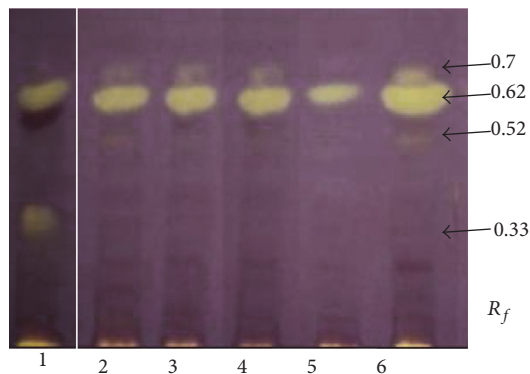

Figure 4: Screening of chloroform extracts of *Eleutherococcus* for anti-DPPH* scavengers using the HPTLC assay method. Yellow spots, corresponding to R_f values, on the purple background represent the inhibition. (1) *E. senticosus*, (2) *E. divaricatus*, (3) *E. setchuenensis*, (4) *E. sessiliflorus*, (5) *E. henryi*, and (6) *E. gracilistylus*.

0.13%; and that of eleutheroside E1 from 0.02 to 0.09%. Another compound is (+)-sesamin, which was isolated and identified by means of GC-MS, ^{1}H- and ^{13}C-NMR, and two-dimensional NMR experiments (HMQC, HMBC, COSY, and DEPT) [10, 27].

The second group of compounds present in the roots of *Eleutherococcus* species are essential oil and aroma components. (*E,E*)-Farnesol, an acyclic sesquiterpene alcohol, was the major constituent up to 43.6%, followed by α-pinene (18.8%) and pentadecanoic acids (12.3%), [28].

All above compounds contain in their structure the chemical groups that can interact with the active site of AChE and BuChE and can scavenge free radicals. They can act as chelators of metal ions playing as cofactors for an enzyme activity. The next possible mechanism is the interactions between active groups of inhibitors and amino acids of the active site of enzymes. However, further detailed studies on the mechanism of inhibition will provide reliable results.

In case of anti-DPPH* activity, Załuski at el.'s previous studies revealed that, in this activity, eleutheroside E1 can

be involved. This results from its molecular structure that demonstrates the one free OH group in the phenyl ring and four methoxy groups (two in each aromatic ring). This was called "Załuski's eleutheroside hypothesis" [9].

4. Conclusion

These basic studies on compounds present in *Eleutherococcus* species contribute to the development of general knowledge about plant-based drugs. The study confirms confirms the rightness of the traditional use of these species in prevention or treatment of memory impairment and gives useful information for further purifying steps to dereplicate active compounds. Further, more detailed studies will be done on spectral identification of isolates and in *in vivo* models.

Competing Interests

The authors declare no competing financial interests.

Acknowledgments

References

[1] A. Marston, J. Kissling, and K. Hostettmann, "A rapid TLC bio-autographic method for the detection of acetylcholinesterase and butyrylcholinesterase inhibitors in plants," *Phytochemical Analysis*, vol. 13, no. 1, pp. 51–54, 2002.

[2] S. Di Giovanni, A. Borloz, A. Urbain et al., "In vitro screening assays to identify natural or synthetic acetylcholinesterase inhibitors: thin layer chromatography versus microplate methods," *European Journal of Pharmaceutical Sciences*, vol. 33, no. 2, pp. 109–119, 2008.

[3] R. Statystyczny, *Główny Urząd Statystyczny (GUS)*, 2011 (Polish).

[4] A. Szczelik, *Choroby Wewnętrzne: Stan Wiedzy Na Rok 2010*, Medycyna Praktyczna, 2010 (Polish).

[5] L. S. Schneider, "New therapeutic approaches to Alzheimer's disease," *Psychiatry*, vol. 57, pp. 30–36, 1996.

[6] P. J. Houghton, Y. Ren, and M.-J. Howes, "Acetylcholinesterase inhibitors from plants and fungi," *Natural Product Reports*, vol. 23, no. 2, pp. 181–199, 2006.

[7] D. Załuski, Ł. Cieśla, and Z. Janeczko, "The structure-activity relationships of plant secondary metabolites with antimicrobial, free radical scavenging and inhibitory activity towards selected enzymes," in *Studies in Natural Product Chemistry (Bioactive Natural Products)*, A.-U. Rahman, Ed., vol. 45, pp. 217–249, Elsevier Science, Amsterdam, The Netherlands, 2015.

[8] D. Załuski and Z. Janeczko, "Variation in phytochemicals and bioactivity of the fruits of *Eleutherococcus* species cultivated in Poland," *Natural Product Research*, vol. 29, no. 23, pp. 2207–2211, 2015.

[9] D. Załuski, R. Kuźniewski, and Z. Janeczko, "HPTLC-profiling of eleutherosides, mechanism of antioxidative action of eleutheroside E1, the PAMPA test with LC/MS detection and

the structure-activity relationship," *Saudi Journal of Biological Sciences*, 2016.

[10] D. Załuski, E. Mendyk, and H. D. Smolarz, "Identification of MMP-1 and MMP-9 inhibitors from the roots of *Eleutherococcus divaricatus*, and the PAMPA test," *Natural Product Research*, vol. 30, no. 5, pp. 595–599, 2016.

[11] D. Załuski, H. D. Smolarz, and U. Gawlik-Dziki, "Bioactive compounds and antioxidative, antileukemic and anti-MMPs activity of *Eleutherococcus* species cultivated in Poland," *Natural Product Communications*, vol. 7, no. 11, pp. 1483–1486, 2012.

[12] D. Załuski, H. Smolarz, and A. Chomicki, "TLC screening for eleutherosides B, E, and E1, and isofraxidin in the roots of six *Eleutherococcus* species cultivated in Poland," *Acta Chromatographica*, vol. 22, no. 4, pp. 581–589, 2010.

[13] C. Tohda, M. Ichimura, Y. Bai, K. Tanaka, S. Zhu, and K. Komatsu, "Inhibitory effects of *Eleutherococcus senticosus* extracts on amyloid β(25-35)–induced neuritic atrophy and synaptic loss," *Journal of Pharmacological Sciences*, vol. 107, no. 3, pp. 329–339, 2008.

[14] D. Lee, J. Park, J. Yoon, M.-Y. Kim, H.-Y. Choi, and H. Kim, "Neuroprotective effects of *Eleutherococcus senticosus* bark on transient global cerebral ischemia in rats," *Journal of Ethnopharmacology*, vol. 139, no. 1, pp. 6–11, 2012.

[15] J. K. Andersen, "Oxidative stress in neurodegeneration: cause or consequence?" *Nature Reviews Neuroscience*, vol. 5, pp. S18–S25, 2004.

[16] V. K. Ramanan and A. J. Saykin, "Pathways to neurodegeneration: mechanistic insights from GWAS in Alzheimer's disease, Parkinson's disease, and related disorders," *American Journal of Neurodegenerative Disorders*, vol. 3, pp. 145–175, 2013.

[17] G. L. Ellman, K. D. Courtney, V. Andres Jr., and R. M. Featherstone, "A new and rapid colorimetric determination of acetylcholinesterase activity," *Biochemical Pharmacology*, vol. 7, no. 2, pp. 88–91, 1961.

[18] P. K. Mukherjee, V. Kumar, M. Mal, and P. J. Houghton, "Acetylcholinesterase inhibitors from plants," *Phytomedicine*, vol. 14, no. 4, pp. 289–300, 2007.

[19] B. Vinutha, D. Prashanth, K. Salma et al., "Screening of selected Indian medicinal plants for acetylcholinesterase inhibitory activity," *Journal of Ethnopharmacology*, vol. 109, no. 2, pp. 359–363, 2007.

[20] N. Wszelaki, A. Kuciun, and A. Kiss, "Screening of traditional European herbal medicines for acetylcholinesterase and butyrylcholinesterase inhibitory activity," *Acta Pharmaceutica*, vol. 60, no. 1, pp. 119–128, 2010.

[21] M. Jung and M. Park, "Acetylcholinesterase inhibition by flavonoids from *Agrimonia pilosa*," *Molecules*, vol. 12, no. 9, pp. 2130–2139, 2007.

[22] K. Ingkaninan, P. Temkitthawon, K. Chuenchom, T. Yuyaem, and W. Thongnoi, "Screening for acetylcholinesterase inhibitory activity in plants used in Thai traditional rejuvenating and neurotonic remedies," *Journal of Ethnopharmacology*, vol. 89, no. 2-3, pp. 261–264, 2003.

[23] J. Biju, C. T. Sulaiman, C. T. Sadashiva, G. Satheesh, and V. R. K. Reddy, "In vitro screening for acetylcholonesterase inhibition of *Baliospermum montanum*, *Humboldtia brunonis* Wall. var. *raktapushpa* and *Pittosporum viridulum*," *Journal of Applied Pharmaceutical Science*, vol. 3, pp. 63–65, 2013.

[24] M. B. Pisano, S. Cosentino, S. Viale et al., "Biological activities of aerial parts extracts of *Euphorbia characias*," *BioMed Research International*, vol. 2016, Article ID 1538703, 11 pages, 2016.

[25] D. Kaufmann, A. K. Dogra, A. Tahrani, F. Herrmann, and M. Wink, "Extracts from Traditional Chinese Medicinal plants inhibit acetylcholinesterase, a known Alzheimer's disease target," *Molecules*, vol. 21, no. 9, p. 1161, 2016.

[26] H. Saleem, I. Ahmad, M. N. Shahid et al., "In vitro acetylcholinesterase and butyrylcholinesterase inhibitory potentials of *Jatropha gossypifolia* plant extracts," *Acta Poloniae Pharmaceutica—Drug Research*, vol. 73, pp. 419–423, 2016.

[27] Ł. Cieśla, D. Załuski, H. D. Smolarz, M. Hajnos, and M. Waksmundzka-Hajnos, "HPTLC-densitometric method for determination of eleutherosides B, E, and E1 in different *Eleutherococcus* species," *Journal of Chromatographic Science*, vol. 49, no. 3, pp. 182–188, 2011.

[28] D. Załuski and H. D. Smolarz, "Influence of Polish climate conditions on content and the chemical variation of volatiles in the roots of six *Eleutherococcus* species and their potential use," *Records of Natural Products*, vol. 10, no. 2, pp. 240–244, 2016.

Research Article

HIV-1 Tat Regulates Occludin and Aβ Transfer Receptor Expression in Brain Endothelial Cells via Rho/ROCK Signaling Pathway

Yanlan Chen,[1] Wen Huang,[1] Wenlin Jiang,[1] Xianghong Wu,[2] Biao Ye,[1] and Xiaoting Zhou[1]

[1]*Department of Neurology, First Affiliated Hospital, Guangxi Medical University, Nanning 530021, China*
[2]*Department of Vasculocardiology, First Affiliated Hospital, Guangxi Medical University, Nanning 530021, China*

Correspondence should be addressed to Wen Huang; hwen1229@163.com

HIV-1 transactivator protein (Tat) has been shown to play an important role in HIV-associated neurocognitive disorders. The aim of the present study was to evaluate the relationship between occludin and amyloid-beta (Aβ) transfer receptors in human cerebral microvascular endothelial cells (hCMEC/D3) in the context of HIV-1-related pathology. The protein expressions of occludin, receptor for advanced glycation end products (RAGE), and low-density lipoprotein receptor-related protein 1 (LRP1) in hCMEC/D3 cells were examined using western blotting and immunofluorescent staining. The mRNA levels of occludin, RAGE, and LRP1 were measured using quantitative real-time polymerase chain reaction. HIV-1 Tat at 1 μg/mL and the Rho inhibitor hydroxyfasudil (HF) at 30 μmol/L, with 24 h exposure, had no significant effect on hCMEC/D3 cell viability. Treatment with HIV-1 Tat protein decreased mRNA and protein levels of occludin and LRP1 and upregulated the expression of RAGE; however, these effects were attenuated by HF. These data suggest that the Rho/ROCK signaling pathway is involved in HIV-1 Tat-mediated changes in occludin, RAGE, and LRP1 in hCMEC/D3 cells. HF may have a beneficial influence by protecting the integrity of the blood-brain barrier and the expression of Aβ transfer receptors.

1. Introduction

Tight junction (TJ) proteins are essential components of blood-brain barrier (BBB) integrity [1, 2]. Signaling between pericytes and endothelial cells is critical for BBB maintenance [3, 4]. Occludin was the first integral membrane protein to be identified within TJs. Occludin has four transmembrane domains and a long COOH-terminal cytoplasmic domain (domain E). Occludin itself can localize at TJs and directly associates with ZO-1 [5]. Occludin plays a pivotal role in maintaining the homeostasis of the central nervous system [2], and its destruction increases the diffusion of viruses and other microorganisms across the BBB [6].

BBB dysfunction appears to be a particularly important component of HIV-associated neurocognitive disorders (HAND) [7]. HIV-1 transactivator protein (Tat) can be actively released from HIV-1-infected cells and easily cross cell membranes and the BBB, causing HAND [8, 9]. High levels of extracellular HIV-Tat have been recently reported in cerebrospinal fluid of HIV-infected patients [10]. HIV-1 Tat has been shown to disrupt TJs associated with astrocytes along the BBB, increasing the permeability of the barrier [11]. HIV-1 exposure also increases intracellular levels of amyloid-beta (Aβ) in human cerebral microvascular endothelial cells (hCMEC/D3) [12]. The BBB plays a critical role in both HIV-1 and Aβ pathology [13]. BBB disruption mediates some of the tissue damage that accompanies HIV-1 infection of the brain and so facilitates entry of the virus into the central nervous system [14]. The BBB endothelial cells respond to inflammatory stimuli, such as cytokines and Aβ, ultimately causing BBB disruption. Furthermore, the BBB plays a multifaceted role both upstream and downstream of the amyloid cascade to cause inflammation and oxidative stress, which can promote the accumulation of Aβ in the brain [15]. Several HIV-1 proteins have been shown to be amyloidogenic. HIV-1 Tat protein has been reported to inhibit Aβ-degrading enzyme

neprilysin, leading to increased levels of soluble $A\beta$ in cell culture [16].

Ras homolog gene family, member A (RhoA), is a small guanosine triphosphate-binding protein. Rho-associated kinase (ROCK) was the first downstream effector of Rho to be identified [17], and ROCK has been reported to mediate BBB disruption [18]. Rho-ROCK signaling was involved in mural cell recruitment to the vessel wall in brain, which was involved in maintaining BBB integrity [19]. Hydroxyfasudil (HF), a specific inhibitor of ROCK with strong effectiveness and selectivity [20, 21], promotes neuronal regeneration and is clinically used in patients with disorders such as spinal-cord injuries and stroke [22, 23]. Therefore, ROCK can be considered a promising molecular target for the treatment of neurological diseases [24, 25].

However, whether the Rho/ROCK signaling pathway is involved in HIV-induced BBB disruption and the expression of $A\beta$ transfer receptors is not completely understood. Therefore, the aim of the present study was to evaluate the relationship between occludin, $A\beta$ transfer receptors, and the Rho/ROCK signaling pathway in hCMEC/D3 cells.

2. Materials and Methods

2.1. HIV-1 Tat. Recombinant HIV-1 Tat clade B protein (Prospec, Rehovot, Israel), produced in *Escherichia coli*, is formed of a single, nonglycosylated, polypeptide chain containing 86 amino acids encoded by exons, with a molecular mass of 14 kDa. The amino acid sequence is as follows: MEPVDPRLEP WKHPGSQPKT ACTNCYCKKC CFHCQVCFIT KALGISYGRK KRRQRRRPPQ GSQTHQVSLS KQPTSQSRGD PTGPKE. It is recommended that lyophilized HIV-1 Tat is stored desiccated below −18°C and reconstituted in sterile 18 MΩ-cm H_2O.

2.2. Cell Cultures. hCMEC/D3 cells were provided as a gift from Dr. P.-O. Couraud (Institut Cochin, Paris, France). Endothelial basal medium (EBM)-2 (Lonza, Walkersville, MD, USA) was supplemented with 5% fetal bovine serum (Lonza, Switzerland), 1 ng/mL basic fibroblast growth factor (Sigma-Aldrich, USA), 5 μg/mL ascorbic acid (Sigma-Aldrich), 1/100 chemically defined lipid concentrate (Gibco, NY, USA), 10 mmol/L HEPES (Beyotime, Jiangsu, China), 1.4 μmol/L hydrocortisone (Sigma-Aldrich, USA), and 1% penicillin-streptomycin (Beyotime), as recommended by the manufacturer (Lonza, Walkersville, MD, USA). This solution is called complete EBM-2 medium. hCMEC/D3 cells were seeded into flasks coated with 1 mg/mL collagen type I (R&D Systems) and cultured in complete EBM-2 medium, maintained at 37°C in a humidified atmosphere of 5% CO_2.

2.3. Cell Viability. hCMEC/D3 cells at the exponential growth phase were seeded onto 96-well plates at a density of 1×10^4 cells/well in 200 μL serum-free medium and treated with HIV-1 Tat at various concentrations (0, 0.25, 0.5, 1, or 1.250 μg/mL), heat-inactivated Tat, or the Rho inhibitor HF (0, 10, 30, 50, 80, or 100 μmol/L; Tianjin Chase Sun Pharmaceutical Co, Tianjin, China) for different periods of time (0, 6, 12, 24, or 30 h). The cells were incubated with 15 μL 3-(4,5-dimethylthiazol-2-yl)-2, 5-diphenyltetrazolium bromide solution (MTT, 5 mg/mL; Sigma-Aldrich, USA) for additional 4 h at 37°C and 5% CO_2. The optical density in each well was measured at 570 nm using a 96-well plate reader (Thermo Scientific, USA). HIV-1 Tat at 1 μg/mL and HF at 30 μmol/L for 24 h had no effect on the viability of hCMEC/D3 cells, so these concentrations were used in subsequent experiments.

hCMEC/D3 cells were pretreated with 30 μmol/L HF for 2 h prior to exposure to 1 μg/mL HIV-1 Tat, and cells were then incubated for 24 h without serum. The HIV-1 Tat concentrations used in the present study are consistent with data from the literature, which indicate that concentrations of Tat in HIV-infected patients can reach the range of μg/mL of serum [26]. Heat-inactivated Tat (as another control) was obtained by heating the protein at 90°C for 1 h, which inactivates the biological potentials of Tat.

2.4. Western Blot Analysis. Treated endothelial cultures were washed three times and lysed in a RIPA cell lysis buffer (Beyotime) containing protease inhibitor cocktail tablets (Beyotime). The lysates were centrifuged at 12,000 ×g for 15 min, the supernatants were collected, and protein concentrations were measured using the BCA Protein Assay Kit (Beyotime). Total proteins were mixed with 5x SEMS-PAGE protein sample buffer solution (Beyotime), then boiled for 5 min at 100°C, and stored at −20°C until use. Equal masses of proteins (20 μg) were separated on SDS-polyacrylamide gel and electrophoresed. Proteins were blotted onto polyvinylidene fluoride membranes (0.22/0.45 μm; Millipore, Billerica, MA, USA). The membranes were blocked with 5% fat-free milk at room temperature for 1 h and then incubated at 4°C overnight with different primary antibodies diluted in primary antibody dilution buffer (Beyotime). The primary antibodies were as follows: occludin (1 : 1000, mouse monoclonal antibody; Invitrogen, Carlsbad, CA, USA), RAGE (1 : 1000, rabbit monoclonal antibody; Abcam), LRP1 (1 : 10,000, rabbit monoclonal antibody; Abcam), and GAPDH (1 : 10,000; Proteintech Group, Chicago, IL, USA). The membranes were then incubated for 1 h with IRDye 680RD goat anti-rabbit immunoglobulin (Ig) G and IRDye 680RD goat anti-mouse IgG secondary antibodies (both 1 : 10,000; LI-COR Biosciences, Lincoln, NE, USA) diluted in secondary antibody dilution buffer (Beyotime). Proteins were visualized by scanning the membrane on an Odyssey Infrared Imaging System (LI-COR Biosciences) with the 700 and 800 nm channels. The density of bands was calculated using Image–J software (National Institutes of Health, Bethesda, MD, USA). Protein levels were represented by the ratios of optical densities in their bands, normalized against GAPDH.

2.5. Reverse Transcription- (RT-) PCR and Quantitative Real-Time PCR. Total RNA was extracted from hCMEC/D3 cells using TRIzol reagent (Invitrogen) and reverse transcribed into cDNA using the Prime-Script RT reagent kit (Takara Bio, Dalian, Japan) according to the manufacturer's instructions. The resulting cDNA was used as a template for RT-PCR.

The primer sequences were as follows: occludin (Invitrogen): 5′-TCAGGGAATATCCACCTATCACTTCAG-3′ and 5′-CATCAGCAGCAGCCATGTACTCTTCAC-3′; RAGE (Takara): 5′-CAACGGCTCCCTCTTCCTT-3′ and 5′-TTG-GTCTCCTTTCCATTCCTGT-3′; LRP1 (Takara): 5′-CGC-CTCCTACCACTTCCAAC-3′ and 5′-CGCCACCTCAAT-CACATCTC-3′; and GAPDH (Invitrogen): 5′-GCACCG-TCAAGGCTGAGAAC-3′ and 5′-TGGTGAAGACGC-CAGTGGA-3′. Quantitative RT-PCR was performed using a Taq PCR Master Mix Kit (Takara) and conducted on the ABI Prism 7500 sequence detection system (Applied Biosystems, USA) using RT Reaction Mix in a total volume of 20 μL at 25°C for 10 min, 42°C for 30 min, and 94°C for 5 min. GAPDH served as an internal control in relative RT-PCR. The relative levels of the target genes were quantified using $2^{-\Delta\Delta Ct}$ method.

2.6. Immunofluorescence Microscopy.

hCMEC/D3 cells were seeded onto circular glass coverslips in a 24-well plate and incubated for 24 h. The cells were fixed for 30 min with 4% paraformaldehyde (Solarbio, Beijing, China) on ice and permeabilized with 0.1% Triton X-100 (Beyotime) for 5 min. Samples were incubated in blocking solution of 3% bovine serum albumin (Sigma, USA) for 1 h at room temperature and in antibodies against LRP1 (1 : 200, rabbit monoclonal antibody; Abcam) and RAGE (1 : 200, rabbit polyclonal antibody; Abcam) at 4°C overnight. The secondary antibodies, Alexa Fluor-488 donkey anti-rabbit (1 : 200; Invitrogen) and Alexa Fluor 594 donkey anti-mouse (1 : 200; Invitrogen), were added and incubated for 2 h, then stained with 4′,6-diamidino-2-phenylindole (Invitrogen), and visualized using a fluorescence microscope (Nikon A1; Nikon).

2.7. Statistical Analysis.

The results are expressed as means ± standard deviation. SPSS version 17.0 (SPSS, Chicago, IL, USA) was used to perform statistical analyses. Comparisons between groups were conducted using a parametric test (one-way analysis of variance) combined with a multiple comparison test (least-squares difference or the Bonferroni post hoc test). Statistical significance was set at $p < 0.05$.

3. Results

3.1. Cell Viability.

hCMEC/D3 viability was tested using an MTT assay. HIV-1 Tat at 1 μg/mL and HF at 30 μmol/L with 24 h exposure had no significant effect on hCMEC/D3 cell viability (Figure 1).

3.2. The RhoA/ROCK Signaling Pathway Is Involved in HIV-1 Tat-Induced Changes in Occludin Expression.

To observe the effects of HIV-1 Tat on expression levels of the TJ protein occludin, hCMEC/D3 cells were exposed to 1 μg/mL HIV-1 Tat for 24 h. The protein levels of occludin were significantly lower in the HIV-1 Tat group than in the control group (Figure 2(a)). With exposure to HIV-1 Tat for 12 h, the mRNA expression of occludin, as examined by real-time RT-PCR, was consistent with the protein levels (Figure 2(b)).

To explore whether RhoA/ROCK signaling is involved in HIV-1 Tat-induced downregulation of occludin, hCMEC/D3 cells were pretreated for 2 h with 30 μmol/L HF, followed by coexposure to HF and 1 μg/mL HIV-1 Tat for 24 h (for western blotting) or 12 h (for real-time RT-PCR). Occludin protein and mRNA levels were significantly increased with coexposure to HF and HIV-1 Tat compared with HIV-1 Tat only (Figures 2(a) and 2(b)).

3.3. HIV-1 Tat-Induced Changes in LRP1 and RAGE Expression.

To observe whether HIV-1 Tat could affect the expression of Aβ transporters in hCMEC/D3 cells, the expression of LRP1 and RAGE was examined using western blotting, real-time RT-PCR, and immunoreactivity. Western blotting showed that the expression of RAGE was significantly increased compared to the control group following treatment with 1 μg/mL HIV-1 Tat, while LRP1 expression was downregulated (Figures 3(a) and 4(a)). Treatment with HIV-1 Tat also significantly decreased LRP1 mRNA and increased RAGE mRNA levels, consistent with the protein levels (Figures 3(b) and 4(b)), and resulted in markedly stronger RAGE and weaker LRP1 immunoreactivity compared with the untreated group (Figures 3(c) and 4(c)).

3.4. The RhoA/ROCK Signaling Pathway Is Involved in the HIV-1 Tat-Induced Regulation of LRP1 and RAGE Expression.

To investigate whether HF can protect against HIV-1 Tat-induced changes in LRP1 and RAGE expression, hCMEC/D3 cells were cotreated with HF and HIV-1 Tat for 24 h (for western blotting and immunofluorescence staining) or for 12 h (for real-time RT-PCR). As shown in Figures 3 and 4, HF downregulated RAGE expression and increased LRP1 protein levels. These results were consistent with those for RAGE and LRP1 mRNA levels, which significantly differed in the groups cotreated with HF and HIV-1 Tat versus HIV-1 Tat only.

4. Discussion

Although the mechanisms by which HIV invades the brain process are not fully understood, alterations of TJ protein expression can contribute, at least in part, to this phenomenon [27]. HIV-1 Tat is known to trigger oxidative stress-dependent apoptosis of neurons both in vitro and in vivo [9, 28]. Exposure to HIV-1 Tat has also been shown to disrupt the integrity of the BBB and result in endothelial hyperpermeability and increased transendothelial migration, as reported in our previous in vitro [1] and in vivo studies [28]. Tat clade B is more neuropathogenic, disrupts the integrity of the BBB to a greater extent than Tat clade C [29], and was therefore used in the current study. Our results demonstrate that HIV-1 Tat at 1 μg/mL and the Rho inhibitor HF at 30 μmol/L, with 24 h exposure, had no significant effect on hCMEC/D3 cell viability (Figure 1).

Previous reports have indicated that ROCK plays a role in ischemic stroke and edema formation [30]. Rho signaling is involved in the regulation of TJs; Rho directly phosphorylates occludin and other TJ proteins [31]; and Rho-kinase inhibitor improves cerebral integrity and function by regulating endothelial cell oxidative stress and reorganizing intercellular junctions after acute ischemic attacks [30]. In
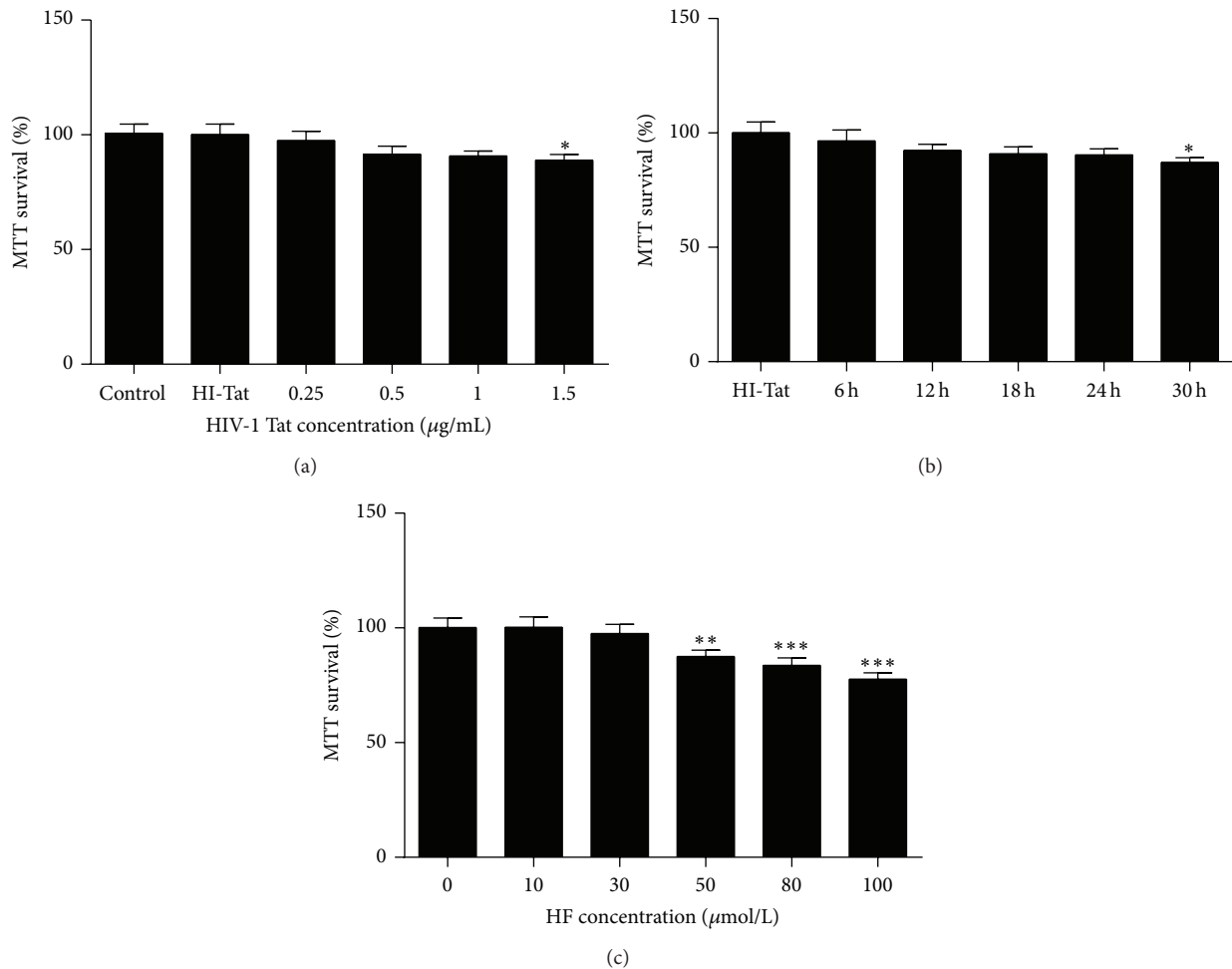
(a)

(b)

(c)

FIGURE 1: Cell viability. hCMEC/D3 cells were treated with HIV-1 Tat ((a), (b)) at different concentrations (0, 0.25, 0.5, 1, or 1.25 μg/mL) or heat-inactivated Tat or HF (0, 10, 30, 50, 80, or 100 μmol/L) (c) for different durations (0, 6, 12, 24, and 30 h), with cell viability detected using an MTT assay. Cell viability was not affected by 1 μg/mL HIV-1 Tat or 30 μmol/L HF for 24 h. Results are shown as means ± standard error of the mean ($n = 5$). $^{*}p < 0.05$, $^{**}p < 0.01$, and $^{***}p < 0.001$ versus control.

addition, inhibition of Rho activity has been reported to protect against Tat-induced alterations in total and nuclear ZO-1 protein levels [32], while ROCK inhibitor has been reported to preserve occludin and ZO-1 levels in the brain or primary human brain microvascular endothelial cells [33, 34]. In the present study, HF upregulated the protein and mRNA levels of occludin, the destruction of which was induced by HIV-1 Tat (Figures 2(a) and 2(b)). HF protected against HIV-1 Tat-mediated BBB dysfunction partly by inhibiting the RhoA/ROCK signaling pathway.

HIV-Tat is a ligand for LRP1 and it may compete with Aβ leading to decreased clearance of Aβ from the brain and promoting its deposition [35]. HIV-1 Tat has also been reported to significantly increase Aβ levels in postmortem brain samples from patients infected with HIV-1 [16]. HIV-1 exposure increases the intracellular levels of Aβ in hCMEC/D3 cells [12]. HIV-1 Tat inhibits the uptake of Aβ by primary mouse microglial cells [36]. Furthermore, the induction of HIV-1 Tat in astrocytes has been shown to increase neuronal damage, tau phosphorylation, and Aβ plaque formation in APP/presenilin-1 transgenic mice [37], suggesting an important role for HIV-1 Tat in the development of HAND. However, the molecular mechanisms involved in HIV-1 Tat-evoked Aβ deposition in the brain remain largely unknown. Neurodegeneration and dementia in Alzheimer's disease may involve similar molecular mechanisms as those involved in HIV-associated dementia [12, 38].

However, the Aβ deposition pattern in HIV appears to be distinct from that of Alzheimer's disease, in which extracellular senile plaques are a predominant feature. In the HIV-infected brain, Aβ accumulates primarily as diffuse and intraneuronal deposits [39]. Peptides and proteins generally do not cross the BBB [40], but they can be transported into the brain via specific transport systems [41]. RAGE and LRP1 remain the most interesting targets. Transport of Aβ from the bloodstream into the brain is mediated by RAGE, while Aβ transport from the brain into the bloodstream is mediated by LRP1 [42, 43]. RAGE is a multiligand receptor in IgG
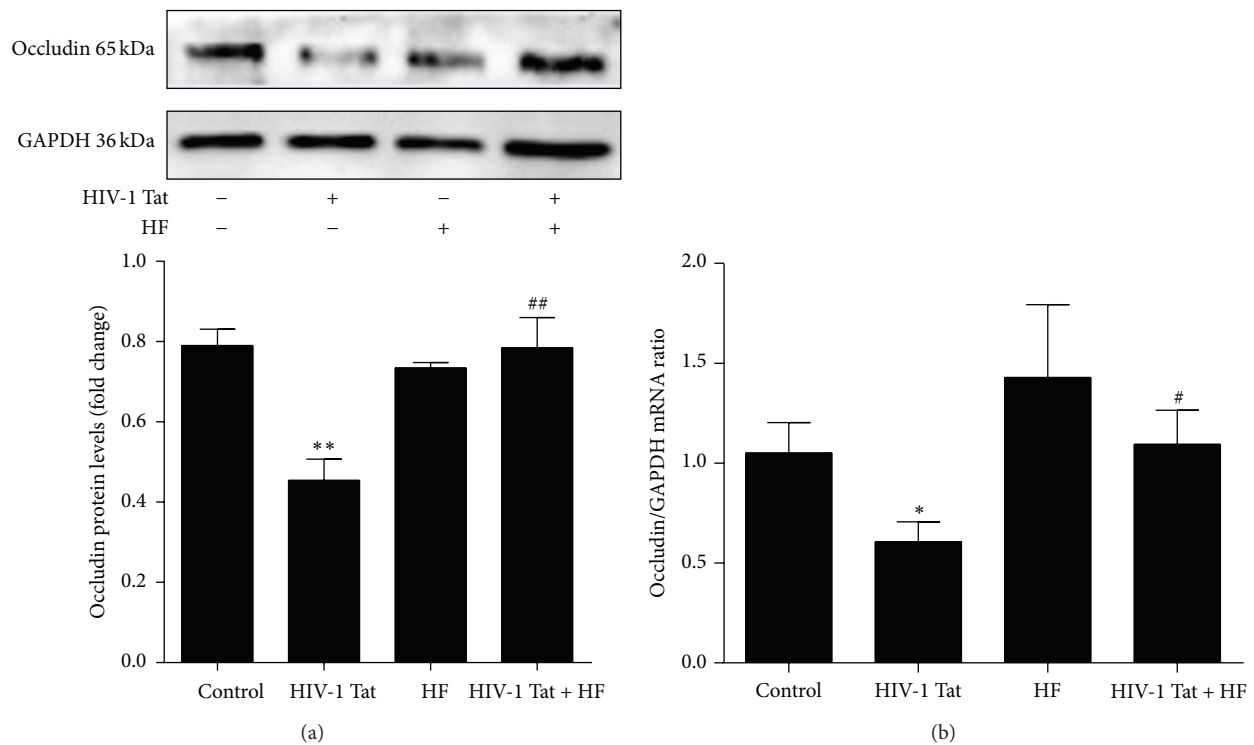
FIGURE 2: Role of RhoA/ROCK signaling in HIV-1 Tat-induced changes in occludin. hCMEC/D3 cells were pretreated with HF (30 μmol/L) 2 h prior to the addition of occludin. HIV-1 Tat treatment was continued for 24 h for western blotting (a) and for 12 h for RT-PCR (b). HIV-1 Tat exposure was associated with decreased protein and mRNA levels of occludin in hCMEC/D3 cells. With coexposure to HF and HIV-1 Tat, occludin protein and mRNA levels were significantly increased when compared with exposure to HIV-1 Tat only. Data are expressed as means ± standard error of the mean ($n = 3$, values determined by the ratio to GAPDH, for (a), $n = 5$ for (b)). $^*p < 0.05$ and $^{**}p < 0.01$ versus control; $^{\#}p < 0.05$ and $^{\#\#}p < 0.01$ versus HIV-1 Tat.

superfamily that binds soluble Aβ and mediates pathophysiologically relevant cellular responses consequent to ligation by a variety of ligands [42]. LRP1 is a multiligand lipoprotein receptor that interacts with a broad range of secreted proteins and resident cell-surface molecules, mediating their endocytosis or activating signaling pathways through multiple cytosolic adaptor and scaffold proteins [44]. Increased RAGE and decreased LRP1 immunoreactivity within the microvasculature have been found in Alzheimer's disease patients [43]. Blocking RAGE with a specific neutralizing antibody can protect against the accumulation of exogenous Aβ in HIV-1-exposed hCMEC/D3 cells [12]. In the current study, 24 h exposure to HIV-1 Tat resulted in markedly stronger RAGE immunoreactivity and increased RAGE mRNA levels compared with the control group (Figure 3). This may directly lead to increased Aβ deposition in the brain. In contrast to the alterations in RAGE expression, exposure to HIV-1 Tat attenuated LRP1 levels in hCMEC/D3 cells (Figure 4). Our data suggest that HF may prevent the movement of Aβ into the brain and stimulate brain Aβ clearance across the BBB (Figure 5). The RhoA/ROCK signaling pathway plays a favorable role in maintaining Aβ homeostasis at the level of the BBB. However, different effects of HIV-1 on LRP1 have been observed. For example, HIV-1 p24 had no effects on LRP1 levels in an *in vitro* study [12]. The reason for this might be that different HIV subtype proteins affect LRP1 via multiple signaling pathways.

5. Conclusions

In the current study, the Rho-kinase inhibitor HF significantly inhibited HIV-1 Tat-induced occludin dysfunction and regulated LRP1 and RAGE expression in hCMEC/D3 cells, suggesting a potential protective role for HF in HIV-1 Tat-mediated BBB destruction and Aβ accumulation. A better understanding of the mechanisms involved in Aβ deposition in the brain during HIV-1 infection will help with the development of new therapeutic strategies for reducing the Aβ burden in HAND.

Competing Interests

The authors declare no competing interests regarding the publication of this paper.

Acknowledgments

(a)

(b)

(c)
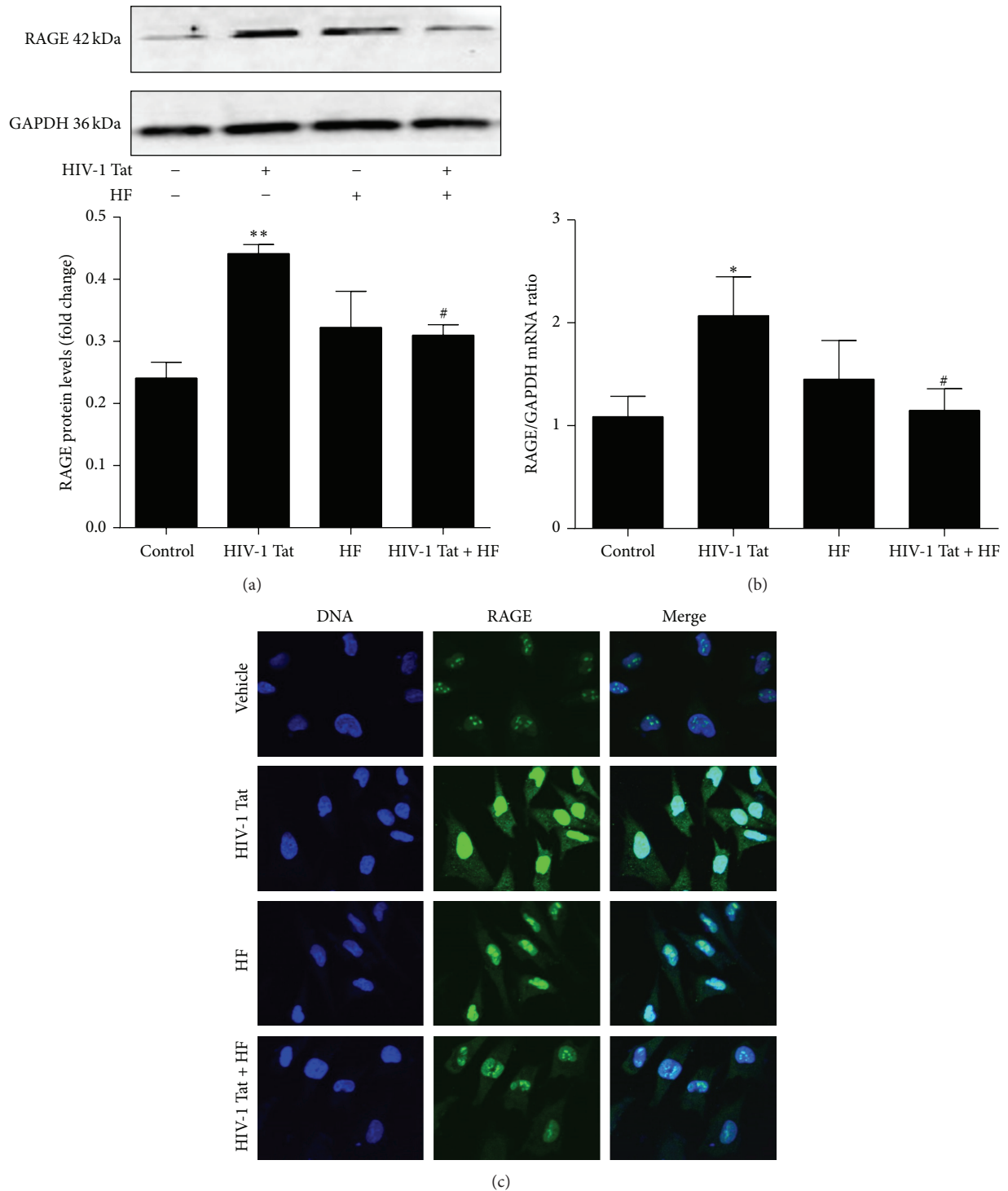
FIGURE 3: Role of RhoA/ROCK signaling in HIV-1 Tat-induced changes in RAGE. Exposure to HIV-1 Tat resulted in markedly higher levels of RAGE protein (a) and mRNA (b) and stronger immunoreactivity (c) compared with the untreated group. hCMEC/D3 cells were pretreated with HF ($30\,\mu$mol/L) 2 h prior to HIV-1 Tat treatment for 24 h. RAGE protein and mRNA levels and immunoreactivity were significantly decreased with coexposure to HF and HIV-1 Tat compared with HIV-1 Tat only. Data are expressed as means ± standard error of the mean ($n = 3$, values determined by the ratio to GAPDH, for (a), $n = 5$ for (b)). $^{*}p < 0.05$ and $^{**}p < 0.01$ versus control; $^{#}p < 0.05$ versus HIV-1 Tat.
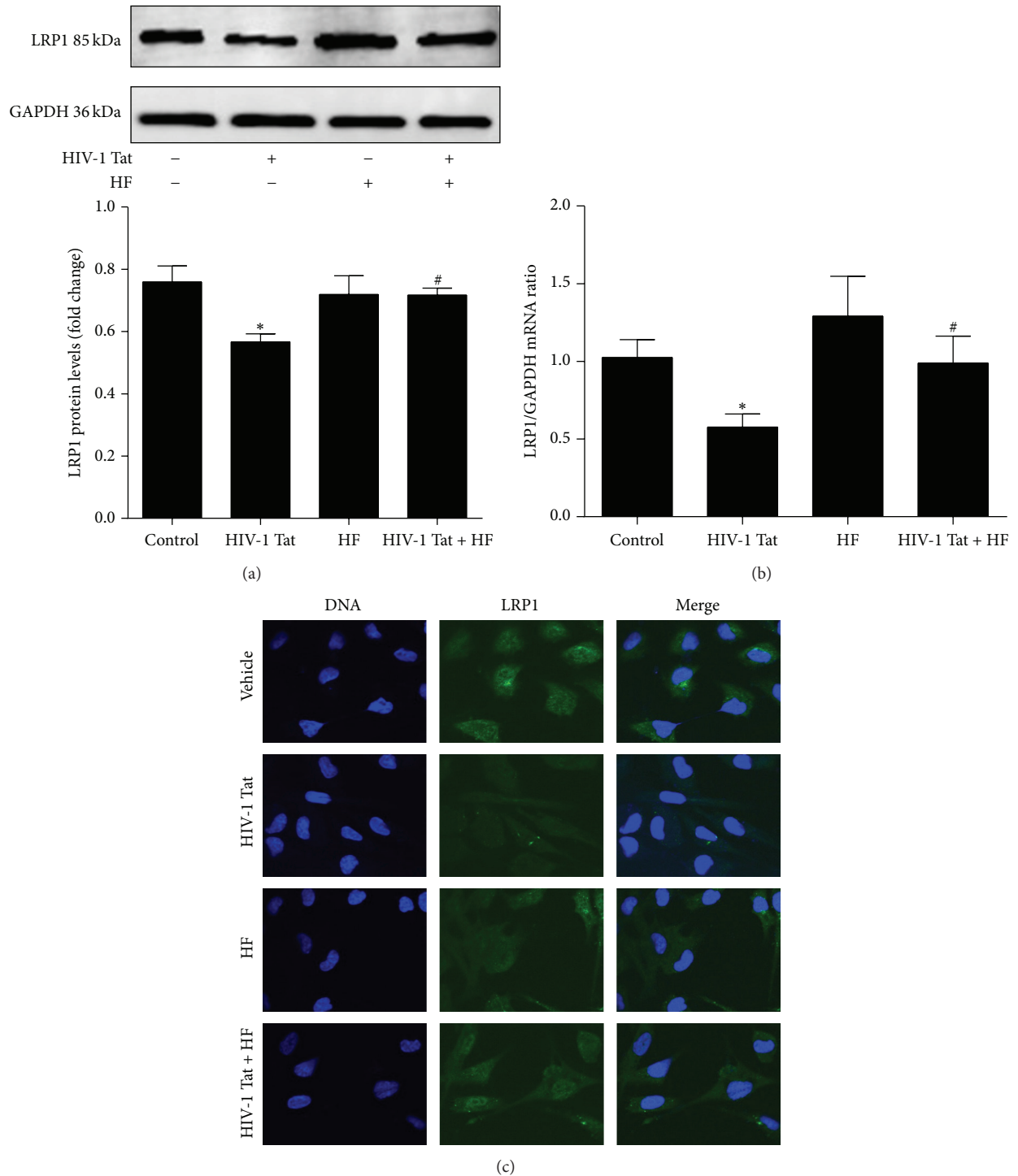
FIGURE 4: Role of RhoA/ROCK signaling in HIV-1 Tat-induced changes in LRP1. Exposure to HIV-1 Tat resulted in markedly lower levels of LRP1 protein (a) and mRNA (b) and weaker immunoreactivity (c) compared with the untreated group. hCMEC/D3 cells were pretreated with HF (30 μmol/L) 2 h prior to HIV-1 Tat treatment for 24 h. LRP1 protein and mRNA levels and immunoreactivity were significantly increased with coexposure to HF and HIV-1 Tat compared with HIV-1 Tat only. Data are expressed as means ± standard error of the mean ($n = 3$, values determined by the ratio to GAPDH, for (a), $n = 5$ for (b)). $^{*}P < 0.05$ versus control; $^{#}P < 0.05$ versus HIV-1 Tat.
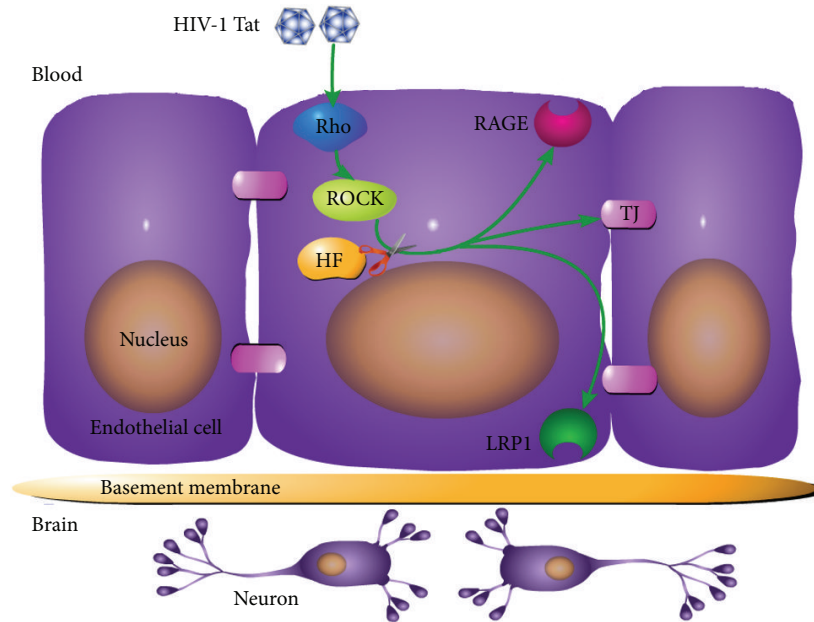
FIGURE 5: Schematic diagram illustrating the effects of HIV-1 Tat on occludin, RAGE, and LRP1 in brain endothelial cells. Exposure to HIV-1 Tat resulted in RAGE overexpression, which downregulated occludin and LRP1, stimulating the transfer of Aβ from the blood into the brain. HF protected against these effects. Exposure to HF inhibited HIV-1 Tat-induced dysregulation of occludin, RAGE, and LRP1.

References

[1] W. Huang, Y. E. Sung, I. E. András, B. Hennig, and M. Toborek, "PPARα and PPARγ attenuate HIV-induced dysregulation of tight junction proteins by modulations of matrix metalloproteinase and proteasome activities," *The FASEB Journal*, vol. 23, no. 5, pp. 1596–1606, 2009.

[2] M. Saitou, M. Furuse, H. Sasaki et al., "Complex phenotype of mice lacking occludin, a component of tight junction strands," *Molecular Biology of the Cell*, vol. 11, no. 12, pp. 4131–4142, 2000.

[3] R. D. Bell, E. A. Winkler, A. P. Sagare et al., "Pericytes control key neurovascular functions and neuronal phenotype in the adult brain and during brain aging," *Neuron*, vol. 68, no. 3, pp. 409–427, 2010.

[4] Z. Zhao, A. R. Nelson, C. Betsholtz, and B. V. Zlokovic, "Establishment and dysfunction of the blood-brain barrier," *Cell*, vol. 163, no. 5, pp. 1064–1078, 2015.

[5] M. Furuse, M. Itoh, T. Hirase et al., "Direct association of occludin with ZO-1 and its possible involvement in the localization of occludin at tight junctions," *Journal of Cell Biology*, vol. 127, no. 6, pp. 1617–1626, 1994.

[6] L.-H. Qin, W. Huang, X.-A. Mo, Y.-L. Chen, and X.-H. Wu, "LPS induces occludin dysregulation in cerebral microvascular endothelial cells via MAPK signaling and augmenting MMP-2 levels," *Oxidative Medicine and Cellular Longevity*, vol. 2015, Article ID 120641, 9 pages, 2015.

[7] I. E. András, G. Rha, W. Huang et al., "Simvastatin protects against amyloid β and HIV-1 Tat-induced promoter activities of inflammatory genes in brain endothelial cells," *Molecular Pharmacology*, vol. 73, no. 5, pp. 1424–1433, 2008.

[8] W. Kang, W. A. Marasco, H. Tong et al., "Anti-tat Hutat2:Fc mediated protection against tat-induced neurotoxicity and HIV-1 replication in human monocyte-derived macrophages," *Journal of Neuroinflammation*, vol. 11, no. 1, article 195, 2014.

[9] B. P. Irish, Z. K. Khan, P. Jain et al., "Molecular mechanisms of neurodegenerative diseases induced by human retroviruses: a review," *American Journal of Infectious Diseases*, vol. 5, no. 3, pp. 238–258, 2009.

[10] T. P. Johnson, K. Patel, K. R. Johnson et al., "Induction of IL-17 and nonclassical T-cell activation by HIV-Tat protein," *Proceedings of the National Academy of Sciences of the United States of America*, vol. 110, no. 33, pp. 13588–13593, 2013.

[11] I. E. Cisneros and A. Ghorpade, "HIV-1, Methamphetamine and astrocyte glutamate regulation: combined excitotoxic implications for neuro-AIDS," *Current HIV Research*, vol. 10, no. 5, pp. 392–406, 2012.

[12] I. E. András, S. Y. Eum, W. Huang, Y. Zhong, B. Hennig, and M. Toborek, "HIV-1-induced amyloid beta accumulation in brain endothelial cells is attenuated by simvastatin," *Molecular and Cellular Neuroscience*, vol. 43, no. 2, pp. 232–243, 2010.

[13] I. E. András and M. Toborek, "HIV-1 stimulates nuclear entry of amyloid beta via dynamin dependent EEA1 and TGF-β/Smad signaling," *Experimental Cell Research*, vol. 323, no. 1, pp. 66–76, 2014.

[14] P. Annunziata, "Blood-brain barrier changes during invasion of the central nervous system by HIV-1: old and new insights into the mechanism," *Journal of Neurology*, vol. 250, no. 8, pp. 901–906, 2003.

[15] M. A. Erickson and W. A. Banks, "Blood–brain barrier dysfunction as a cause and consequence of Alzheimer's disease," *Journal of Cerebral Blood Flow and Metabolism*, vol. 33, no. 10, pp. 1500–1513, 2013.

[16] H. C. Rempel and L. Pulliam, "HIV-1 Tat inhibits neprilysin and elevates amyloid β," *AIDS*, vol. 19, no. 2, pp. 127–135, 2005.

[17] M. Amano, Y. Fukata, and K. Kaibuchi, "Regulation and functions of Rho-associated kinase," *Experimental Cell Research*, vol. 261, no. 1, pp. 44–51, 2000.

[18] K. Liu, Z. Li, T. Wu, and S. Ding, "Role of Rho kinase in microvascular damage following cerebral ischemia reperfusion in rats," *International Journal of Molecular Sciences*, vol. 12, no. 2, pp. 1222–1231, 2011.

[19] E. Montanez, S. A. Wickström, J. Altstätter, H. Chu, and R. Fässler, "α-parvin controls vascular mural cell recruitment to vessel wall by regulating RhoA/ROCK signalling," *The EMBO Journal*, vol. 28, no. 20, pp. 3132–3144, 2009.

[20] J. Liu, H.-Y. Gao, and X.-F. Wang, "The role of the Rho/ROCK signaling pathway in inhibiting axonal regeneration in the central nervous system," *Neural Regeneration Research*, vol. 10, no. 11, pp. 1892–1896, 2015.

[21] D. Kentrup, S. Reuter, U. Schnöckel et al., "Hydroxyfasudil-mediated inhibition of ROCK1 and ROCK2 improves kidney function in rat renal acute ischemia-reperfusion injury," *PLoS ONE*, vol. 6, no. 10, Article ID e26419, 2011.

[22] M. Li, D. Yasumura, A. A. K. Ma et al., "Intravitreal administration of HA-1077, a ROCK inhibitor, improves retinal function in a mouse model of huntington disease," *PLoS ONE*, vol. 8, no. 2, Article ID e56026, 2013.

[23] Z. Zhang, A. K. Ottens, S. F. Larner et al., "Direct Rho-associated kinase inhibiton induces cofilin dephosphorylation and neurite outgrowth in PC-12 cells," *Cellular & Molecular Biology Letters*, vol. 11, no. 1, pp. 12–29, 2006.

[24] M. Dong, B. P. Yan, J. K. Liao, Y.-Y. Lam, G. W. K. Yip, and C.-M. Yu, "Rho-kinase inhibition: a novel therapeutic target for the treatment of cardiovascular diseases," *Drug Discovery Today*, vol. 15, no. 15-16, pp. 622–629, 2010.

[25] Y. Fujita and T. Yamashita, "Axon growth inhibition by RhoA/ROCK in the central nervous system," *Frontiers in Neuroscience*, vol. 8, article 338, 2014.

[26] H. Xiao, C. Neuveut, H. L. Tiffany et al., "Selective CXCR4 antagonism by Tat: implications for in vivo expansion of coreceptor use by HIV-1," *Proceedings of the National Academy of Sciences of the United States of America*, vol. 97, no. 21, pp. 11466–11471, 2000.

[27] I. E. András, H. Pu, M. A. Deli, A. Nath, B. Hennig, and M. Toborek, "HIV-1 Tat protein alters tight junction protein expression and distribution in cultured brain endothelial cells," *Journal of Neuroscience Research*, vol. 74, no. 2, pp. 255–265, 2003.

[28] W. Huang, L. Chen, B. Zhang, M. Park, and M. Toborek, "PPAR agonist-mediated protection against HIV Tat-induced cerebrovascular toxicity is enhanced in MMP-9-deficient mice," *Journal of Cerebral Blood Flow & Metabolism*, vol. 34, no. 4, pp. 646–653, 2014.

[29] N. Gandhi, Z. M. Saiyed, J. Napuri et al., "Interactive role of human immunodeficiency virus type 1 (HIV-1) clade-specific Tat protein and cocaine in blood-brain barrier dysfunction: implications for HIV-1-associated neurocognitive disorder," *Journal of Neurovirology*, vol. 16, no. 4, pp. 294–305, 2010.

[30] C. L. Gibson, K. Srivastava, N. Sprigg, P. M. W. Bath, and U. Bayraktutan, "Inhibition of Rho-kinase protects cerebral barrier from ischaemia-evoked injury through modulations of endothelial cell oxidative stress and tight junctions," *Journal of Neurochemistry*, vol. 129, no. 5, pp. 816–826, 2014.

[31] M. J. Dörfel and O. Huber, "Modulation of tight junction structure and function by kinases and phosphatases targeting occludin," *Journal of Biomedicine and Biotechnology*, vol. 2012, Article ID 807356, 14 pages, 2012.

[32] Y. Zhong, B. Zhang, S. Y. Eum, and M. Toborek, "HIV-1 Tat triggers nuclear localization of ZO-1 via Rho signaling and cAMP response element-binding protein activation," *Journal of Neuroscience*, vol. 32, no. 1, pp. 143–150, 2012.

[33] M. Fujii, K. Duris, O. Altay, Y. Soejima, P. Sherchan, and J. H. Zhang, "Inhibition of Rho kinase by hydroxyfasudil attenuates brain edema after subarachnoid hemorrhage in rats," *Neurochemistry International*, vol. 60, no. 3, pp. 327–333, 2012.

[34] R. Xu, X. Feng, X. Xie, J. Zhang, D. Wu, and L. Xu, "HIV-1 Tat protein increases the permeability of brain endothelial cells by both inhibiting occludin expression and cleaving occludin via matrix metalloproteinase-9," *Brain Research*, vol. 1436, pp. 13–19, 2012.

[35] B. V. Zlokovic, R. Deane, A. P. Sagare, R. D. Bell, and E. A. Winkler, "Low-density lipoprotein receptor-related protein-1: a serial clearance homeostatic mechanism controlling Alzheimer's amyloid β-peptide elimination from the brain," *Journal of Neurochemistry*, vol. 115, no. 5, pp. 1077–1089, 2010.

[36] B. Giunta, Y. Zhou, H. Hou et al., "HIV-1 TAT inhibits microglial phagocytosis of Abeta peptide," *International Journal of Clinical and Experimental Pathology*, vol. 1, no. 3, pp. 260–275, 2008.

[37] B. Giunta, H. Hou, Y. Zhu et al., "HIV-1 Tat contributes to Alzheimer's disease-like pathology in PSAPP mice," *International Journal of Clinical and Experimental Pathology*, vol. 2, no. 5, pp. 433–443, 2009.

[38] M. P. Mattson, "Oxidative stress, perturbed calcium homeostasis, and immune dysfunction in Alzheimer's disease," *Journal of NeuroVirology*, vol. 8, no. 6, pp. 539–550, 2002.

[39] M. Bae, N. Patel, H. Xu et al., "Activation of TRPML1 clears intraneuronal Aβ in preclinical models of HIV infection," *The Journal of Neuroscience*, vol. 34, no. 34, pp. 11485–11503, 2014.

[40] B. V. Zloković, M. B. Segal, D. J. Begley, H. Davson, and L. Rakić, "Permeability of the blood-cerebrospinal fluid and blood-brain barriers to thyrotropin-releasing hormone," *Brain Research*, vol. 358, no. 1-2, pp. 191–199, 1985.

[41] B. V. Zlokovic, M. N. Lipovac, D. J. Begley, H. Davson, and L. Rakić, "Transport of leucine-enkephalin across the blood-brain barrier in the perfused guinea pig brain," *Journal of Neurochemistry*, vol. 49, no. 1, pp. 310–315, 1987.

[42] R. Deane, Z. Wu, and B. V. Zlokovic, "RAGE (Yin) versus LRP (Yang) balance regulates Alzheimer amyloid β-peptide clearance through transport across the blood-brain barrier," *Stroke*, vol. 35, no. 11, supplement 1, pp. 2628–2631, 2004.

[43] J. E. Donahue, S. L. Flaherty, C. E. Johanson et al., "RAGE, LRP-1, and amyloid-beta protein in Alzheimer's disease," *Acta Neuropathologica*, vol. 112, no. 4, pp. 405–415, 2006.

[44] J. Herz and P. Marschang, "Coaxing the LDL receptor family into the fold," *Cell*, vol. 112, no. 3, pp. 289–292, 2003.